

**The Urothelial Glycome: Towards  
Differential Analysis of *N*- and *O*-glycans at  
the Apical Surface**

**Chung-Yao Wang**

**PhD**

**University of York**

**Chemistry**

February 2018



## Abstract

Normal mammalian urothelium lines the majority of the urinary tract performing a barrier function against penetration of toxic substances and adventitious microorganisms from the urine. These protective functions of the urothelium are dependent on the correct differentiation of urothelial cells, relying on protein expression, modification and complex assembly to regulate the basal to apical organisation of multiple cell layers, including the highly-differentiated lumen-facing superficial cell. As a poorly studied part of the urothelial differentiation programme, protein glycosylation is reported to contribute to the apical glycome, with possible roles in urothelial cancer and infection by uropathogenic *E. coli*. It is thus important to investigate the apical surface glycome of the normal superficial urothelial cell that is presumed to act in healthy urothelial function and disease.

The aim of this study was to investigate the urothelial cell apical surface glycome using MALDI-MS to analyze permethylated glycans. The first step was to define the *N*-glycome of the porcine urothelial total cell lysate using the established filter-aided *N*-glycan separation approach; this represents the first normal mammalian urothelial *N*-glycome to be defined. Moreover, this thesis presents development of a method to differentially collect the urothelial cell apical surface *N*- and *O*-glycans. An in-house designed and built device for trypsinization of the luminal urothelial surface, with subsequent  $\beta$ -elimination and PNGase F digestion was used to release apical surface *O*- and *N*-glycans. The effect of trypsinization on superficial glycoproteins was post-monitored using immunolabelling of apically-expressed uroplakin 3a protein to optimize the period of trypsinization, without compromising the integrity of the superficial urothelial layer. 47 *N*- and 12 *O*-glycan species were observed on the apical surface of porcine urothelium. The approach developed for releasing apical cell surface *N*- and *O*-glycans allowed identification of apical surface glycans as candidates implicated in urothelial barrier function.

# List of Contents

List of Figures .....	10
List of Tables.....	19
List of Appendices .....	21
Acknowledgements.....	23
Author's declaration .....	25
Chapter 1. Introduction.....	26
1.1 Urothelium .....	27
1.1.1 Urothelial <i>N</i> -glycans .....	30
1.1.2 Urothelial <i>O</i> -glycans.....	49
1.1.3 Urothelial glycosaminoglycans.....	54
1.2 Glycobiology .....	56
1.2.1 Overviews.....	56
1.2.2 Release of glycans from glycoproteins using enzymatic or chemical methods .....	67
1.3 Mass spectrometry .....	71
1.3.1 Mass spectrometry in glycobiology .....	71
1.3.2 Matrix-assisted laser desorption/ionization (MALDI).....	76
1.3.4 Fourier-transform ion-cyclotron-resonance mass spectrometry .....	86

1.3.5 Orbitrap mass analyzer .....	91
1.3.6 Mass spectrometric fragmentation of carbohydrates.....	94
1.4 Enzymatic shaving of cell surface for collection of cell surface glycans/peptides .....	98
1.5 Aim of this thesis.....	104
Chapter 2 Experimental procedures .....	106
2.1 Preparation of porcine urothelial cell lysate <i>N</i> -glycome .....	108
2.1.1 Collecting urothelial cells from porcine bladders.....	108
2.1.2 Releasing <i>N</i> -glycans from urothelial cell lysate using filter-aided <i>N</i> - glycan separation (FANGS).....	111
2.2 On-tissue trypsinization to release apical cell surface glycopeptides/peptides for subsequent sequential <i>N</i> - and <i>O</i> -glycan release.....	113
2.2.1 Device development .....	113
2.2.2 Tissue stretching process .....	115
2.2.3 On-tissue trypsinization .....	118
2.3 Fractionated <i>N</i> -glycome analysis .....	119
2.3.1 Whole cell surface shaving of CHO cells .....	119
2.4 Glycan release .....	120
2.4.1 <i>N</i> -glycan release: PNGase F digestion.....	120

2.4.2 O-glycan release: $\beta$ -elimination (applied in on-tissue trypsinization of fresh porcine bladder).....	120
2.6 Glycan sample preparation .....	121
2.6.1 C18 SPE method for separating glycans from peptides.....	121
2.6.2 C18 SPE method for purification of permethylated glycans.....	121
2.6.3 Carbon SPE method for desalting released glycans.....	122
2.6.4 Permethylation.....	122
Chapter 3. Normal mammalian urothelial <i>N</i> -glycome.....	124
3.1 The <i>N</i> -glycome of whole lysed porcine urothelium.....	125
3.1.1 Collecting urothelial cells from fresh porcine bladders.....	126
3.1.2 Porcine urothelial total cell lysate <i>N</i> -glycome .....	131
Chapter 4. Enzymatic shaving of cultured urothelial RT4 cells: fractionated <i>N</i> -glycome analysis.....	141
4.1 Method development: fractionated <i>N</i> -glycome analysis of cultured urothelial cells .....	147
4.1.1 Apical cell surface trypsinization of cultured urothelial RT4 cells ..	149
4.2 Surface <i>N</i> -glycome of cultured RT4 cells .....	156
4.2.1 Apical cell surface <i>N</i> -glycans and total cell lysate <i>N</i> -glycans released from cultured urothelial RT4 cells.....	156
4.2.2 Summary .....	160

Chapter 5. On-tissue trypsinization of fresh porcine bladders to release apical cell surface glycopeptides for subsequent <i>N</i> - and <i>O</i> -glycan release .....	161
5.1 On-tissue trypsinization on unstretched porcine bladders .....	165
5.1.1 Device development for on-tissue trypsinization.....	165
5.1.2 Exploratory on-tissue trypsinization of unstretched porcine bladders using the in-house built reaction device.....	169
5.1.3 Summary .....	170
5.2 On-tissue trypsinization of stretched porcine bladders .....	172
5.2.1 Method development for stretching porcine bladders .....	172
5.2.5 Summary .....	202
5.3 Porcine urothelial cell apical surface <i>N</i> - and <i>O</i> -glycans: towards differential glycome analysis at the apical cell surface .....	203
5.3.1 Using immunolabelling to post-monitor the luminal surface of porcine bladders after on-tissue trypsinization .....	204
5.3.2 Apical surface <i>N</i> - and <i>O</i> -glycans of superficial porcine urothelium	206
5.3.4 Comparison of the porcine urothelial total cell lysate <i>N</i> -glycome and the apical cell surface <i>N</i> -glycome .....	227
5.3.5 Product ion analysis of apical cell surface <i>N</i> - and <i>O</i> -glycans collected from porcine urothelium using on-tissue trypsinization .....	230
5.3.5 Summary .....	238

Chapter 6. Summary of results, overall conclusions and future work.....	239
References.....	271





## List of Figures

Figure 1. Multiple layers of mammalian urothelium .....	27
Figure 2. Summary of common lectin binding observed in the study of urothelial glycans. ....	32
Figure 3. Assembly of the urothelial heterotetramer UPK1a/UPK2/UPK1b/UPK3a.....	38
Figure 4. Amidation of sialic acid moiety of glycans.....	43
Figure 5. Common mammalian <i>N</i> -glycosylation pathway.....	62
Figure 6. The release of <i>N</i> -glycan from <i>N</i> -glycoproteins using PNGase F digestion.....	68
Figure 7. The release of O-glycan from O-glycoproteins by reductive $\beta$ -elimination .....	69
Figure 8. The release of O-glycan from O-glycoproteins by non-reductive $\beta$ -elimination .....	70
Figure 9. Matrix-assisted laser desorption/ionization. ....	77
Figure 10. Structures of common MALDI matrices.....	80
Figure 11. Schematic of an ESI source on a mass spectrometer .....	84
Figure 12. Models of ion production using ESI. ....	85
Figure 13. Diagram of FT-ICR mass analyzer .....	87
Figure 14. Scheme of Bruker solariX XR FTMS. ....	90

Figure 15. Cross-section of the C-trap and Orbitrap analyzer. The picture is obtained from ThermoFisher website.....	92
Figure 16. Scheme of Thermo Scientific Orbitrap Fusion™ Tribrid™. ....	94
Figure 17. Fragmentation nomenclature of oligosaccharides.....	94
Figure 18. Scheme of charge-driven dissociation by protonation, forming B ion/oxonium ion <sup>137</sup> .....	96
Figure 19. Putative structure of B ion derived from sodiated glycans .....	96
Figure 20. Porcine bladder dissection process .....	110
Figure 21. Design of on-tissue trypsinization vessel.....	114
Figure 22. Dissecting process of porcine bladders into a rectangular shape.....	116
Figure 23. The process of stretching the porcine bladder.....	117
Figure 24. H&E stained images of porcine bladder. ....	129
Figure 25. Immunolabeling of porcine bladders using anti-collagen IV antibody (Ab6586, 1/1000). ....	130
Figure 26. MALDI mass spectra of <i>N</i> -glycan profiles obtained from three individual porcine bladders, (A) Uro1, (B) Uro2 and (C) Uro3. ....	135
Figure 27. The relative percentages of <i>N</i> -glycans in three independent porcine bladders, Uro1, Uro2, and Uro3. ....	136
Figure 28. Scheme proposed for the collection of urothelial cell apical surface <i>N</i> -glycans. ....	147

Figure 29. Trypsinization for different incubation times caused appearance changes to cultured RT4 cells.....	152
Figure 30. 2 min-trypsinization caused appearance changes to RT4 cells treated with different trypsin concentrations.....	153
Figure 31. Typical MALDI mass spectrum of permethylated <i>N</i> -glycans contained in the supernatant collected after trypsinization of the RT4 cell apical surface (2 min trypsinization with 1 mL of 5 mg/mL trypsin solution). .....	154
Figure 32. MALDI mass spectra of permethylated urothelial RT4 cell apical surface <i>N</i> -glycans (A) before and (B) after spiking with permethylated GlcNAc <sub>6</sub> ([M+Na] <sup>+</sup> <i>m/z</i> 1539.7889). .....	155
Figure 33. Permethylated apical cell surface <i>N</i> -glycans released from cultured RT4 urothelial cells. ....	157
Figure 34. Permethylated total cell lysate <i>N</i> -glycans of cultured RT4 cells using FANGS without pretreated trypsinization .....	158
Figure 35. The total amount of permethylated <i>N</i> -glycans from RT4 cells released using apical cell surface trypsinization and FANGS.....	159
Figure 36. Scheme of on-tissue trypsinization to release apical surface glycopeptides/peptides followed by PNGase F digestion and β-elimination to release <i>N</i> - and <i>O</i> -glycans in one pot. ....	164
Figure 37. Design of the reaction vessel for on-tissue trypsinization.....	165
Figure 38. Porcine bladder dissection process .....	167

Figure 39. Assembly of the reaction vessel for on-tissue trypsinization .	167
Figure 40. Recovery test of trypsin solution after on-tissue trypsinization. .....	168
Figure 41. The <i>N</i> -glycan profiles obtained from unstretched porcine bladders using on-tissue trypsinization. ....	170
Figure 42. H&E stain of porcine urothelium, indicating the rugae.....	171
Figure 43. The definition of strain.....	173
Figure 44. Dissecting process of porcine bladders in a rectangular shape .....	174
Figure 45. The process of stretching the porcine bladder.....	176
Figure 46. Immunolabelling of porcine urothelium using antibody AU1 to label the superficial glycoprotein UPK3a .....	179
Figure 47. Immunolabelling of porcine urothelium trypsinized for different periods.....	180
Figure 48. Image of the whole tissue section of superficial UPK3a-labelled porcine urothelium and the sectioned images.....	183
Figure 49. The linearity of ranking scores assessing the integrity of labelled superficial UPK3a layer against different periods of trypsinization	185
Figure 50. The amount of each <i>N</i> -glycan species released from the luminal surface of porcine bladder 1 using on-tissue trypsinization for different periods.....	187

Figure 51. The amount of each <i>N</i> -glycan species released from the luminal surface of porcine bladder 2 using on-tissue trypsinization for different periods.....	187
Figure 52. The total amount of <i>N</i> -glycans released from the luminal side of porcine bladders 1 and 2 using on-tissue trypsinization for different periods.....	188
Figure 53. MALDI-MS spectra of O-glycans released from 4 µg PSM using NH <sub>4</sub> OH. ....	191
Figure 54. Product ion spectrum of m/z 1293.6246 .....	191
Figure 55. Three-stage purification reported in Hamouda’s work to purify <i>N</i> -glycans obtained from the sample matrix containing inorganic salts, using graphitized carbon and C18 SPE cartridges. ....	193
Figure 56. MALDI mass spectrum of permethylated O-glycans released from 5 µg porcine stomach mucin (PSM). ....	196
Figure 57. MALDI mass spectrum of permethylated O-glycans released from 5 µg porcine stomach mucin (PSM). ....	199
Figure 58. MALDI-MS spectrum of permethylated O-glycans released from 5 µg porcine stomach mucin using the protocol a) without or b) with two-stage SPE purification. ....	201
Figure 59. Immunolabelling of superficial UPK3a-labelled porcine bladders. ....	205

Figure 60. Representative MALDI mass spectrum of porcine urothelial cell apical surface <i>N</i> -glycan and O-glycan profiles obtained from the luminal surface of porcine bladder, <i>m/z</i> 500 to 3200. ....	208
Figure 61. Representative MALDI mass spectrum of porcine urothelial cell apical surface <i>N</i> -glycan and O-glycan profiles obtained from the luminal surface of porcine bladder, <i>m/z</i> 700 to 1500. ....	209
Figure 62. Representative MALDI mass spectrum of porcine urothelial cell apical surface <i>N</i> -glycan and O-glycan profiles obtained from the luminal surface of porcine bladder, <i>m/z</i> 1500 to 3200. ....	210
Figure 63. 55 permethylated porcine urothelial cell apical surface <i>N</i> -glycans, taking the three biological replicates together. ....	212
Figure 64. 12 permethylated porcine urothelial cell apical surface O-glycans, taking the three biological replicates together. ....	213
Figure 65. The total amounts of porcine urothelial cell apical surface <i>N</i> -glycans.....	222
Figure 66. The total amounts of porcine urothelial cell apical surface O-glycans.....	223
Figure 67. Relative percentages of the 47 porcine urothelial cell apical surface <i>N</i> -glycans that were common to the three biological replicates .....	225

Figure 68. Relative percentages of the 12 porcine urothelial cell apical surface O-glycans that were common to the three biological replicates. .... 226

Figure 69. The relative percentages of porcine urothelial total cell lysate *N*-glycan structures compared to those of porcine urothelial cell apical surface structures. .... 228

Figure 70. The percentages of oligomannose, hybrid, complex and other *N*-glycans in the porcine urothelial cell apical surface *N*-glycome of three biological replicates using the on-tissue trypsinization approach.. .... 228

Figure 71. Product ion spectrum of  $[M+Na]^+$  at  $m/z$  1141.57, in permethylated glycans collected from porcine urothelium using on-tissue trypsinization. .... 233

Figure 72. Product ion spectrum of  $[M+Na]^+$  at  $m/z$  1171.58, in permethylated glycans collected from porcine urothelium using on-tissue trypsinization. .... 234

Figure 73. Product ion spectrum of  $[M+Na]^+$  at  $m/z$  1579.79, in permethylated glycans collected from porcine urothelium using on-tissue trypsinization. .... 235

Figure 74. Product ion spectrum of  $[M+Na]^+$  at  $m/z$  1824.91, in permethylated glycans collected from porcine urothelium using on-tissue trypsinization. .... 236



Figure 75. Product ion spectrum of  $[M+Na]^+$  at  $m/z$  1835.93, in permethylated glycans collected from porcine urothelium using on-tissue trypsinization. .... 237



## List of Tables

Table 1. Putative <i>N</i> -glycan moieties of uroplakins .....	35
Table 2. Putative <i>N</i> -glycans in cultured urothelial HCV29 and KK47 cancer cells.....	44
Table 3. Putative porcine urothelial <i>N</i> -glycans reported by Skeene <i>et al.</i> <sup>68</sup> .....	50
Table 4 Putative porcine urothelial O-glycans reported by Skeene <i>et al.</i> <sup>68</sup> .....	52
Table 5. Common monosaccharides in biosynthesis <sup>78</sup> Each glycan symbol used in this text follows those described in reference <sup>78</sup> .....	57
Table 6. Three common types of mammalian <i>N</i> -glycan with linkage information based on <i>N</i> -glycosylation pathway.....	59
Table 7. Mucin type O-glycan core structures <sup>77</sup> .....	64
Table 8. Glycosaminoglycan structures <sup>79</sup> .....	66
Table 9. List of porcine urothelial total cell lysate <i>N</i> -glycans released by FANGS.....	137
Table 10. Ranking results of 18 images excised from the images of the whole superficial UPK3a-labelled porcine samples, to assess the integrity of labelled superficial UPK3a.....	184
Table 11. Medium formulation of HBSS+Ca <sup>2+</sup> /Mg <sup>2+</sup> (Gibco Cat. No. 24020) used in this study .....	189

Table 12. 47 porcine urothelial cell apical surface *N*-glycans common to the  
three biological replicates..... 214

Table 13. 12 porcine urothelial cell apical surface *O*-glycans common to the  
three biological replicates..... 219

## List of Appendices

Appendix 1. Lectins used in urothelial glycosylation .....	251
Appendix 2. Superficial UPK3a-labelled porcine urothelium.....	262
Appendix 3. Mass spectrum acquired using Thermo Orbitrap Fusion, showing dominance of background signals in the nanoESI spectrum of the permethylated urothelial glycans released together following trypsinisation of the apical surface of porcine urothelium. Hex <sub>2-4</sub> at m/z 477, 681 and 885. ....	268
Appendix 4. On-tissue formalin fixation .....	269



## Acknowledgements

I would first like to thank my thesis advisor Prof. Jane Thomas-Oates and Prof. Jenny Southgates. Jane always gave me positive and delightful suggestion helping me solve my research problem, and encouraged me when I had a hard time and nothing achieved in my first year. Jenny always patiently taught me the biological knowledge that I had totally no idea when I was doing the biological experiments. Jane and Jenny led me to the right the direction of my thesis and expanded the view of my work whenever they thought I needed it. I could not finish my Ph. D work without Jane's and Jenny's endless help.

People from the Jack Birch Unit group (JBU), Jenny Hinley, Ros Duke, Simon Baker, Jessica Jinks and Omobolanle Ayeyemi (Kemi) gave me strength to finish the biological researches in this thesis. Special thanks to Jenny Hinley who always positively and nicely taught me all the immunolabelling work since my first year, without her support, I could not obtain all the immunolabelling research results.

I would also like to acknowledge Ed Bergström supporting and advising all the mass spectrometric knowledge. Thanks to my IPMs, Daniel Ungar and Jerry Thomas, they gave me challenges in my TAP meetings, leading me to know my weakness in my work.

Thanks to everyone I worked with in the period of my study in the University of York. To my two academic mates: Emily Burn, congratulate that you have submitted your thesis. We are near the end of study. Peter Fisher, your fantastic carbohydrate work in combination with computer science is impressive. Thank you for the time we sat together in front of Solarix to explore the in-source fragmentation. Thanks to Bella Gaffney, your joining in our group made the office environment colourful and not so gloom anymore caused by other two PhD students.

Finally, sincerely thanks to my family in Taiwan and my wife Hsiu-Ching who always stays with me and looks after me. You are my soul supporter in everything I need to go to so far.





## Author's declaration

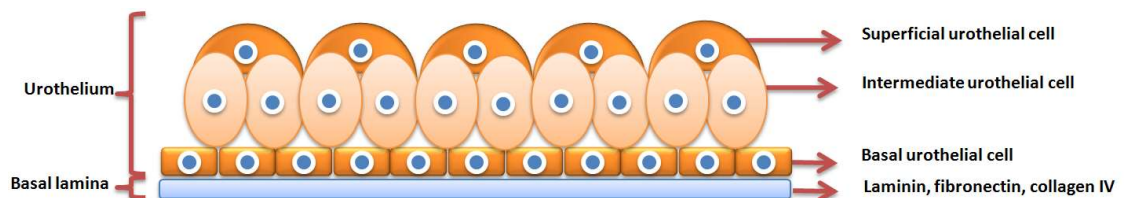
I declare that this thesis is a presentation of original work and I am the sole author.

This work has not previously been presented for an award at this, or any other, University. All sources are acknowledged as references.

# Chapter 1. Introduction

## 1.1 Urothelium

Urothelium is a stratified epithelium which lines the inner surface of mammalian urinary tract from the renal pelvis to the proximal urethra. Mammalian urothelium is stratified into basal, intermediate and superficial cells (also known as umbrella cells) (Figure 1)<sup>1,2</sup>. Normal urothelium performs a barrier function against penetration of toxic substances from the urine and also plays a role in defense against adventitious microorganisms in the urine<sup>1-4</sup>. In addition, urothelium is specialised to maintain the barrier while accommodating large changes in the inner surface area of the urinary bladder during distensions and contractions of the urinary bladder for the safe, kidney-sparing storage of urine under low pressure.



**Figure 1. Multiple layers of mammalian urothelium. A type of transitional epithelium.**

Appropriate biological functions of urothelium such as impermeability are contributed by the correct differentiation of urothelial cells, which relies on protein expression, modification and assembly. Urothelial plaques, which are formed by the assembly of a group of transmembrane proteins named uroplakins (UPs), cover much of the apical surface of fully differentiated superficial urothelium and

contribute to the barrier function and impermeability of the urothelium<sup>5-8</sup>. Proper assembly of uroplakins is linked to the protective function of urothelium<sup>9-12</sup> and is in part regulated by the glycosylation of uroplakins in the endoplasmic reticulum (ER) and the Golgi apparatus<sup>7,10,13-15</sup>.

The presence of urothelial plaques in urothelium has been demonstrated in various mammalian species including cattle, human, monkey, sheep, pig, dog, rabbit and mouse<sup>15</sup>. The urothelial plaques are composed of collections of transmembrane proteins termed uroplakins (UPs) including UPK1a (27 kDa), UPK1b (28 kDa), UPK2 (15 kDa), UPK3a (47 kDa) and UPK3b (47 kDa)<sup>15,16</sup>. The transmembrane structures of uroplakins accounts for the asymmetric appearances of the plaques because all UPs have large extracellular domains<sup>5</sup>. In the process of urothelial plaque formation, six heterotetramers composed of UPK1a/UPK2 and UPK1b/UPK3a build one single 16-nm crystal and these crystals form a unique two dimensional array covering over 90% of mammalian urothelial surface<sup>4,17</sup>. In a subset of bovine AUMs, UPK3a is substituted by UPK3b which dimerises with UPK1b to form a heterodimer<sup>5,16</sup>.

Glycosylation, a common post-translational modification of proteins is involved in the regulation of the development of urothelium barrier function<sup>4,18-20</sup>. Various glycan structures including *N*-glycans<sup>7-11,13,17,21-33</sup>, *O*-glycans<sup>34-37</sup> and glycosaminoglycans (GAGs)<sup>19,38-44</sup> have been reported in the urothelium. Anomalies in differentiation-dependent glycosylation of urothelium have been reported to be factors contributing to the development of urothelial disease such as cancer<sup>8,32,33,45,46</sup>, urinary tract

infections<sup>13,14,18,23,31</sup> and interstitial cystitis<sup>19,36,47</sup>. A full examination of mammalian urothelial glycan profiles has not yet been achieved. For *N*-glycans, to the best of my knowledge, only a few studies of *N*-glycan structural studies have been reported on mouse/bovine uroplakins<sup>7,13</sup> and cultured human urothelial cancer cells<sup>33,48</sup> using MALDI-MS. The existence of urothelial O-glycans and GAGs were inferred from lectin and antibody immunohistology studies of rabbit/donkey urothelium<sup>35,49</sup> and human/porcine urothelium<sup>44</sup>, respectively.

The knowledge of the quantitative and qualitative changes in urothelial glycans which affect the development of urothelial protective function and diseases still remains unclear. The following literature review introduces the urothelial glycans and starts with introducing the *N*-glycans and the structures of glycans identified.

### 1.1.1 Urothelial *N*-glycans

In past decades, urothelial *N*-glycans have mostly been examined on extracted uroplakins (UPK1a, UPK1b, UPK2 and UPK3)<sup>5,7–11,13,15,17,20–28,30,31</sup>, bladder tissue sections<sup>34,35,49–52</sup> and in cultured urothelial cells<sup>32,33,48</sup> using lectin histochemical examination (Figure 2)<sup>a</sup>. Lectins are glycan-binding proteins/glycoproteins that bind with differential specificity to terminal monosaccharides, including Gal, GalNAc, GlcNAc, Fuc, and NeuAc, some internal monosaccharides, glycosidic linkages, or oligosaccharides in glycans<sup>51</sup>. Lectins may be used to visualize bound glycoconjugates by conjugation to a functional group visible by light or electron microscopy. As a result, labeling with lectins reveals the distribution of bound glycoconjugates in tissues and indicates the possible terminal or internal structures of bound glycans.

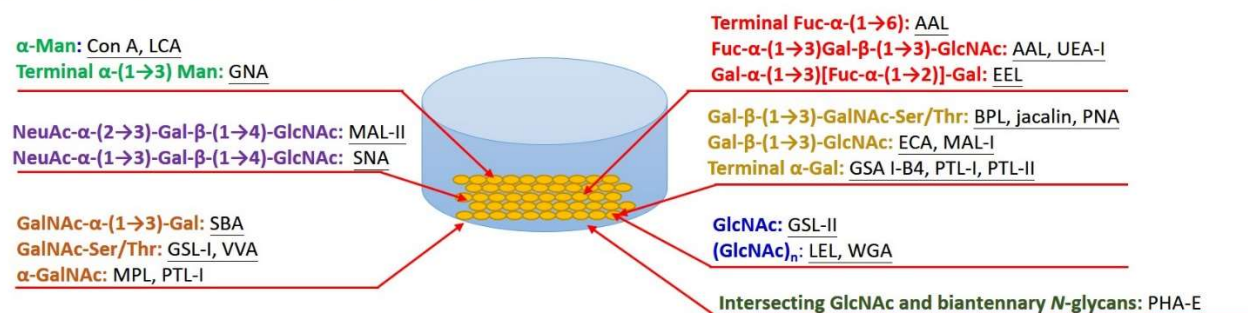
The literature describing lectin-binding studies of urothelial cells is summarized schematically in Figure 2. Cell lysates of cultured human urothelial cancer cells<sup>32,33,48</sup> have been bound by a series of lectins with differing terminal mono- or oligosaccharide specificities, including Fuc-, NeuAc-, Gal- and GlcNAc- capped glycans, oligomannose *N*-glycans and O-glycans (Figure 2A). In addition, urothelia in a range of mammalian tissues have been stained by a similar panel of lectins. The lectin-labeled glycan moieties of the isolated urothelia from bladders from five animal

---

<sup>a</sup> Some information on lectin specificity and inhibitory compounds are from this website: <http://vectorlabs.com/uk/>. The full name of lectins and their binding structure is shown in Appendix 1

species<sup>22,32,35,49,50</sup> (Figure 2B) are very similar to those recognised in the lysates of cultured human urothelial cells. This similarity appears to suggest that the urothelial glycan moieties remain highly conserved between mammalian species. However, some of the glycan structures were exclusively identified by lectin binding in one of the three differentiated urothelial layers in some animal species. Examples are the superficial layer of rat<sup>32</sup> and rabbit<sup>35</sup> urothelium were labeled with *Amaranthus caudatus* agglutinin (ACA) and jacalin, respectively, that recognized the O-glycan Gal- $\beta$ -(1 $\rightarrow$ 3)-GalNAc-Ser/Thr (T antigen). In addition, *Dolichos biflorus* agglutinin (DBA) and *Vicia villosa* agglutinin (VVA) exclusively bound the superficial layer of donkey<sup>49</sup> and rat<sup>34</sup> urothelium, respectively, recognizing the O-glycan GalNAc-Ser/Thr (Tn antigen). This result may suggest that T and Tn antigens correlate with the differentiation level of specialized urothelium in animal tissues. Labeling with *Datura stramonium* lectin (DSL) against the chitobiose moiety and concanavalin A (Con A) against the mannose moiety have revealed intense reactivity on the luminal surface of rabbit bladders and all cell surfaces of donkey urothelium, respectively<sup>35,49</sup>, suggesting that N-glycans are abundant on the urothelium<sup>53</sup>. However, limited structural information of urothelial glycans was revealed by lectin histology since most lectins recognize only terminal monosaccharides or have broad lectin-glycan binding affinities.

**(A) Cell lysates of cultured human urothelial cancer cells**



**(B) Animal tissues: rat, rabbit, donkey, bovine and porcine**

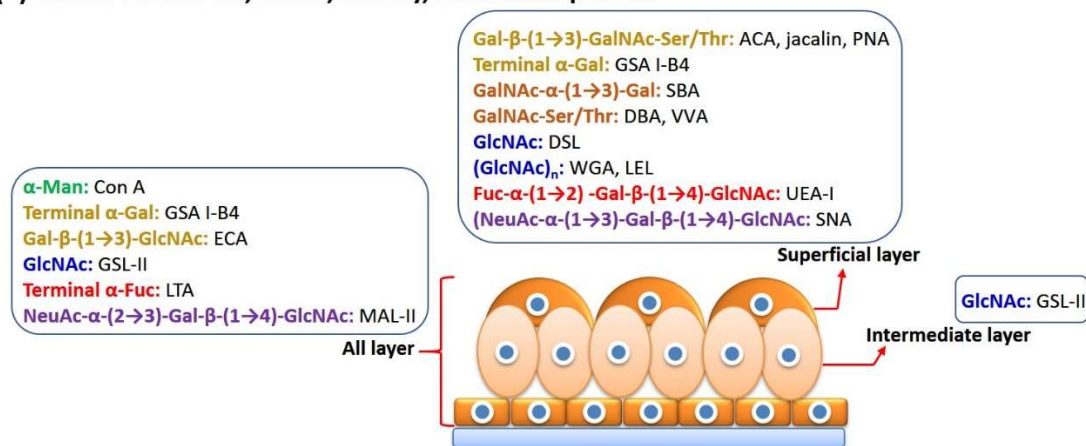


Figure 2. Summary of common lectin binding observed in the study of urothelial glycans. Colour-coding of general structural motifs recognized by the different lectins allows them to be readily identified in the two panels of the figure.



*N*-glycosylation of uroplakins in the ER and Golgi apparatus was speculated to affect the formation of urothelial plaques and has been mainly studied using urothelial plaques isolated from mouse and bovine bladders, and the cell lysates of cultured bovine urothelial cells and bovine uroplakin cDNA-transfected COS-1 cells (monkey kidney cells)<sup>9,13,28,54</sup>. The UPK1a/UPK2/UPK1b/UPK3a heterotetramer as an assembled glycosylated protein complex is an intriguing and well-studied model with which to examine the interaction of protein post-translational modification and assembly of protein complexes in the urothelium and for this reason will be discussed in detail below. Hu *et al*<sup>28</sup> postulated that the changes in *N*-glycosylation of UPKs are associated with the assembly of the heterotetramer (UPK1a/UPK2/UPK1b/UPK3a), based on a series of *in vitro* and *in vivo* studies<sup>9,28,54-57</sup>, discussed in the following paragraphs. In addition, the structural information available on urothelial glycosylation comes very largely from studies of uroplakins.

UPK1a and UPK1b belong to the tetraspanin transmembrane protein family which has been reported to commonly assemble with single transmembrane proteins<sup>58,59</sup> such as UPK2 and UPK3a. The amino acid sequences of UPK1a and UPK1b have high levels of identity and both possess one potential *N*-glycosylation site<sup>9</sup>. In addition, the amino acid sequence of UPK1a is also highly conserved between human, bovine and mouse urothelium<sup>23</sup>, suggesting that UPK1a and UPK1b may serve critical functions in the assembly of urothelial plaques. The glycoforms of UPKs identified in different animal species (Table 1) suggest that the glycoforms of urothelial *N*-glycans are species dependent. Bovine UPK1a and UPK1b appear to have oligomannose or hybrid *N*-glycans as supported by gel migration change observed

after Endo H digestion<sup>9</sup>; by contrast, bovine UPK3a appears to have complex *N*-glycans as supported by its resistance to Endo H and sensitivity to PNGase F. The glycan structures of bovine UPK1a, UPK1b and UPK3a (Table 1) have been determined using PNGase F digestion followed by permethylation prior to analysis using MALDI-MS (equipped with nitrogen laser, Reflex IV, Bruker Daltonics)<sup>13</sup>. The glycosylation sites of glycoproteins/glycopeptides and structural information from mouse UPK1a *N*-glycans was obtained using mass spectrometry in combination with chemical derivatization. In early studies, the glycosylation site of UPK1a was identified in the mouse urothelium using electrospray ionization quadrupole time-of-flight mass spectrometry (ESI-Q-TOF MS)<sup>23</sup>; mouse UPK1a was digested with PNGase F in a buffer containing 50% H<sub>2</sub><sup>18</sup>O. Deglycosylated peptides of mouse UPK1a containing a partially <sup>18</sup>O-labeled aspartic acid could be differentiated from the unlabeled glycosylation site by a mass increment of 3 Da. UPK3 is heavily *N*-glycosylated. Bovine UPK3 possesses large amounts of *N*-glycans that constitute around 50 % of the total mass of the whole glycoprotein<sup>10</sup>. Sun's group performed deglycosylation of bovine UPK3 using Endo H, PNGase F and O-glycosidase digestions. This showed that bovine UPK3 is resistant to Endo H and O-glycosidase and sensitive to PNGase F, indicating that bovine UPK3 contains dominant complex *N*-glycans<sup>10</sup>. It is worth noting that the O-glycosidase (*Diplococcus pneumoniae*) (used in Sun's study) has very tight structural specificity, and only cleaves Gal-β-(1→3)-GalNAc-Ser/Thr (T antigen); common terminal sialylation and fucosylation prevent the hydrolysis of O-glycoproteins/peptides. It requires exoglycosidases such as neuraminidases and fucosidases to remove the terminal monosaccharides prior to

the O-glycosidase digestion, in order to demonstrate the presence of O-glycans on uroplakins.

**Table 1. Reported N-glycan moieties of uroplakins**

	UPK1a	UPK1b	Immature UPK2	UPK3	References
Bovine urothelial plaques	(1)	(1)	(1) <sub>ER</sub> ->(2) <sub>Golgi</sub>	(2)	Yu <i>et al.</i> <sup>9</sup>  Lin <i>et al.</i> <sup>54</sup>  Hu <i>et al.</i> <sup>28</sup>
Mouse urothelial plaques	(1)	(1) (2) (3)	N/A	N/A	Xie <i>et al.</i> <sup>13</sup>
(1): Oligomannose, (2): Complex, and (3): Hybrid					

The transition of UPK2 from immature glycoform (pro-UPK2) to non-glycosylated mature UPK2 was reported to be associated with the formation of urothelial plaques. Immature canine UPK2, which was obtained by transcription/translation of the bovine UPK2 cDNA and translocated<sup>b</sup> to canine pancreatic microsomes<sup>c</sup>, contains a pro-peptide sequence with three potential N-glycosylation sites<sup>15,54</sup> and appears to

---

<sup>b</sup> Protein translocation is the biological mechanism of targeting, in which proteins are transported to the appropriate destinations in the cell or outside it.

<sup>c</sup> Microsomes are used to mimic the activity of the endoplasmic reticulum; it provides a way to figure out how proteins are being made on the ER in a cell by reconstituting the process in a test tube.

be modified with oligomannose *N*-glycans in the ER as evidenced by its Endo H-sensitivity<sup>28,54</sup>. The two of the three oligomannose moieties of immature UPK2 were then modified to a complex *N*-glycans in the Golgi apparatus, as evidenced by their subsequent resistance to Endo H digestion<sup>28,54</sup>. The change of glycoforms in immature UPK2, transforming oligomannose to complex *N*-glycans, was assumed to be associated with the formation of the of UPK2/UPK1a/UPK1b/UPK3a heterotetramer<sup>28</sup>. Cleavage of the glycosylated pro-peptide of UPK2 by furin<sup>d</sup> is completed in the trans-Golgi network (TGN) and produces mature UPK2 that has no glycosylation. This was evidenced by the gel migration of bovine UPK2, isolated from bovine urothelial plaques, not changing after Endo H or PNGase F digestion<sup>54</sup>.

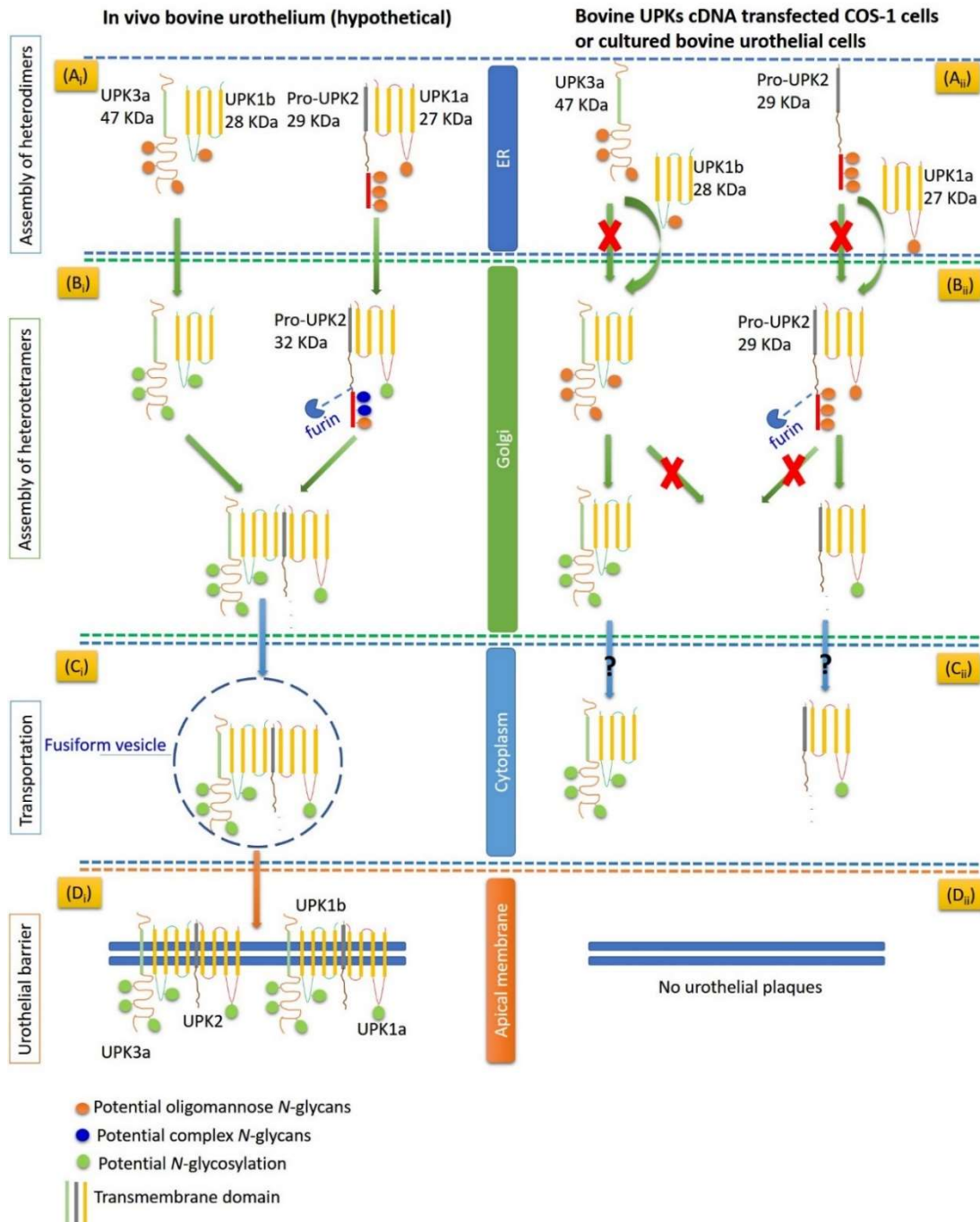
The normal expression of UPKs is critical to maintain the urothelial barrier function. Genetic ablation of mouse UPK2 or UPK3a genes resulted in no 2D crystals of urothelial plaques formed on the apical surface of urothelium, elevating the urothelium permeability<sup>11,12</sup>. Expression of UPK1a, UPK1b, UPK2 and UPK3a using cultured COS-1 cells transfected with bovine UPK cDNA, or cultured bovine urothelial cells was used to investigate the assembly of UPKs into heterodimers and heterotetramers in the ER and Golgi<sup>28</sup> (Figure 3).

In the COS-1 cells transfected only with bovine pro-UPK2-, (glycosylated) pro-UPK2 was found to fail to exit the ER (Figure 3Aii) without the presence of UPK1a. This

---

<sup>d</sup> Some proteins are inactive when they are first synthesized, and must have sections removed in order to become active. Furin cleaves these sections and activates the proteins.

observation is supported by the aggregation of pro-UPK2 which occurred on inhibition of the proteasome, the role of which is to degrade misfolded proteins in the ER. This aggregation of pro-UPK2 was visualised on immunoblotting with the antibody AE31, which binds to the epitopes of pro-UPK2<sup>28</sup>. In contrast, in COS-1 cells that were cotransfected with both UPK1a and pro-UPK2 cDNA, the presence of the UPK1a/UPK2 heterodimer in the ER was demonstrated using the antibody anti-P4 against the mature (non-glycosylated) UPK2. There was no sign of (aggregated) pro-UPK2 in the cotransfected COS-1 cells, suggesting pro-UPK2 required UPK1a to form the heterodimer and so to be able to exit the ER (Figure 3A<sub>i</sub>). In addition, after the inhibition of furin (prosequence cleavage is inhibited) the UPK1a/UPK2 heterodimer was not observed on immunoblotting with anti-P4 (no mature UPK2 is present), but was stained with AE31 (against the pro form), suggesting that furin is involved in the process of cleaving the N-terminus of pro-UPK2 to form (non-glycosylated) mature UPK2.



**Figure 3. Assembly of the urothelial heterotetramer UPK1a/UPK2/UPK1b/UPK3a.** Scheme is a summary of the information in references<sup>9,28,54-57</sup> and is modified from the origin of ref<sup>28</sup>. The left panel is a predicted model of assembly of urothelial plaques and the right panel is the experimental results of using cultured bovine urothelial cells or cultured COS-1 cells transfected with the cDNA of uroplakin family to investigate protein and glycan function.

Formation of the other uroplakin heterodimer, UPK1b/UPK3a, was also studied in the bovine cDNA-transfected COS-1 cells. UPK3a required UPK1b to leave the ER; the UPK3a, if it fails to leave the ER, aggregates, and these aggregates are stained by the antibody AU1 in the UPK3a cDNA-transfected COS-1 cells after proteasome inhibition. As a result of these observations, it was concluded that the formation of glycosylated heterodimers of UPK1a/pro-UPK2 and UPK1b/UPK3 are prerequisites for UPK components to exit the ER<sup>28,55</sup>.

The formation of the heterotetramer UPK1a/UPK2/UPK1b/UPK3a in the Golgi apparatus following the formation of the two heterodimers in the ER was suggested by Sun's group to be dependent on the modified *N*-glycosylation of pro-UPK2 in the Golgi apparatus<sup>28</sup>, because without this modification, no urothelial plaques form. However, no direct evidence for this dependence is presented in their papers.

The UPK subunit compositions of urothelial plaques isolated from fresh bovine urothelium were analyzed and compared with those of lysates of fresh bovine urothelium, the cell lysates of bovine UPK-cDNA transfected COS-1 cells and lysates of cultured bovine urothelial cells (Figure 3Bi and Bii). The 29 kDa pro-UPK2 (glycosylated with three oligomannose *N*-glycans) was identified in the transfected COS-1 cells and cultured bovine urothelial cells using the antibody AE1 against the epitopes of pro-UPK2; no complex *N*-glycans were detected on proUPK2 from either of these cultured systems. In contrast, the 29 kDa pro-UPK2 and the 32 kDa pro-UPK2 (glycosylated with two complex *N*-glycans and one oligomannose *N*-glycans)

were identified (using the same antibody) in the cell lysate of fresh bovine urothelial tissue.

Interestingly, the 15 kDa UPK2 (mature form, without the *N*-glycosylated prosequence), which is the product of Golgi-localised furin cleaving the prosequence from immature pro-UPK2, was detected in the cell lysates of bovine UPK-cDNA transfected COS-1 cells (29 kDa pro-UPK2), cultured bovine urothelial cells (29 kDa pro-UPK2) and in purified bovine urothelial plaques (29 kDa and 32 kDa pro-UPK2)<sup>28</sup>. This led these workers to suggest that the furin-mediated removal of the proglycopeptide was not affected by the glycoform of pro-UPK2 and so must recognize the epitopes on the prosequence of the peptide rather than its glycans. In addition, the enzymatic trimming of a prosequence from immature proteins was reported to be involved in the protein oligomerization<sup>(60-62)</sup>. In addition, since the prosequence of the 29 kDa form is cleaved by furin which is found in the Golgi, the 29 kDa form was also concluded to exit the ER and enter the Golgi.

Experiments using a furin inhibitor in the differentiated fresh bovine urothelium resulted in failure to form the UPK heterotetramer<sup>28</sup>. Furin-mediated cleavage of the UPK2 prosequence was thus believed to be associated with the formation of heterotetramer UPK1a/UPK2/UPK1b/UPK3a<sup>28</sup>. Export of the mature heterotetramer was proposed to be via fusiform vesicles (Figure 3Ci and ii).



Interestingly, there were no urothelial plaques observed on cultured bovine urothelial cells examined using transmission electron microscopy (Figure 3Dii), but they were positively identified on the *in vivo* fresh bovine urothelium (Figure 3Di)<sup>63</sup>. As a result, the lack of complex *N*-glycan-modified pro-UPK2 (32 kDa) was speculated to impede the formation of the heterotetramer UPK1a/UPK2/UPK1b/UPK3a in the less differentiated cultured bovine urothelial cells<sup>28</sup>. The reason for the failure of less differentiated, cultured cells to produce the 32 kDa, complex *N*-glycan-bearing form of UPK2 remains unknown.

The manipulated expression of UPKs in cultured cells and animals has shed light on the glycosylation of proteins associated with protein assembly and the urothelial barrier function, by comparing them with normal animal tissue, but the detailed mechanisms remain unclear. Hu *et al.* reported that the assembled heterodimers/heterotetramers presented altered antigenic activities to antibodies against pro-UPK2/UPK2 and UPK3a<sup>28</sup>. It was considered to be caused by the assembled protein complex having conformational changes on the assembled protein monomers, resulting in altered epitopes that were not recognized by antibodies. In addition, the failure of two heterodimers UPK1a/UPK2 and UPK1b/UPK3a to form the heterotetramer UPK1a/UPK2/UPK1b/UPK3a in the cultured bovine urothelial cells, which were described as less differentiated urothelial cells than normal well-differentiated bovine urothelium, was speculated to be associated with the glycoforms of the prosequence of UPK2 (29 kDa and 32 kDa). This observation might suggest that there are conformational changes of pro-UPK2 in the Golgi apparatus induced by modifying oligomannose *N*-glycans to complex *N*-

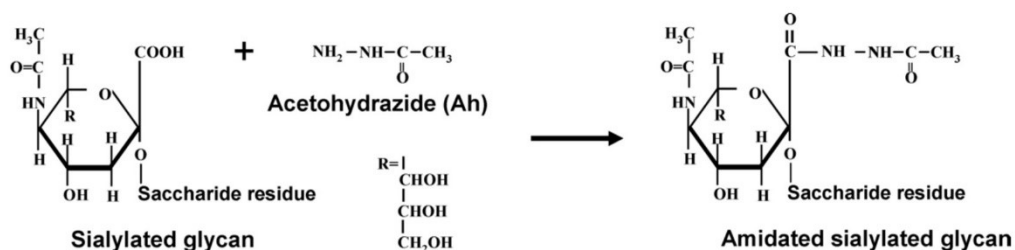
glycans prior to the furin-mediated formation of mature UPK2. Whether the furin-removed glycosylated prosequence of pro-UPK2 has a function of its own has not been investigated to the best knowledge of the author. Sun's investigations suggest that the glycosylation of UPKs is differentiation-dependent in urothelium and this clearly requires further investigation.

The cell lysate *N*-glycan profiles of cultured urothelial cells (Table 2) were examined in non-malignant bladder transitional epithelium HCV29 cells and transforming growth factor-beta-treated (TGFβ<sup>e</sup>) HCV29 cells using PNGase F digestion prior to analysis on MALDI-TOF/TOF-MS (ultrafleXtreme, Bruker Daltonics)<sup>48</sup>. 15 and 20 *N*-glycans including oligomannose, complex and hybrid *N*-glycans were identified in HCV29 cells and TGFβ-treated cells, respectively. However, sialylated glycans in Guo's study<sup>48</sup> were not chemically modified before analysis with MALDI-MS and so labile sialic acid moieties of *N*-glycans may be lost during analysis using positive mode MALDI-MS. That appears to be the reason that no sialylated *N*-glycans were identified in Guo's study. By contrast, Yang *et al.* examined cell lysate *N*-glycan profiles from HCV29 cells in comparison with nonmuscle-invasive bladder cancer KK47 cells using MALDI-MS<sup>33</sup>; the sialylated *N*-glycans were amidated using acetohydrazide before release from glycoproteins. The amidation of *N*-glycans was

---

<sup>e</sup> TGF-β is a secreted protein that controls proliferation, cellular differentiation, and other functions in most cells. In normal cells, TGF-β, acting through its signaling pathway, stops the cell cycle at the G1 stage to stop proliferation, induce differentiation, or promote apoptosis<sup>262</sup>.

aiming to neutralize the sialic acid moieties of *N*-glycans to prevent the sialic acid moieties from being lost during MS analysis (Figure 4)<sup>64,65</sup>.



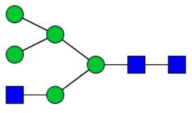
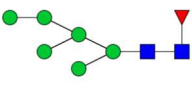
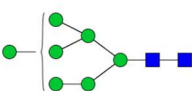
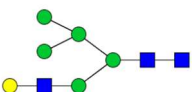
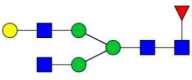
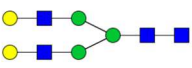
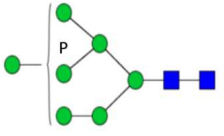
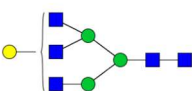
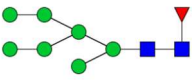
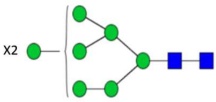
**Figure 4. Amidation of sialic acid moiety of glycans. Adapted from Gil *et al*<sup>65</sup>.**

As a result, Yang's study was capable of identifying sialylated *N*-glycans from HCV29 cells as compared with Guo's study. A total of 34 *N*-glycans were identified in both HCV29 cells and KK47 cells (Table 2). It is worth noting that all the putative *N*-glycan structures were proposed using GlycoWorkbench software in Yang's and Guo's studies. Oligomannose, sialylated and terminal Gal-bearing *N*-glycans were up-regulated in KK47 cancer cells compared with HCV29 cells. The cell lysate *N*-glycomes identified from cultured human cancer cell lines are comparable with the lectin histological results, suggesting oligomannose, sialylated/terminal Gal-bearing and multi-antennary complex *N*-glycans comprise the mammalian urothelium *N*-glycome.

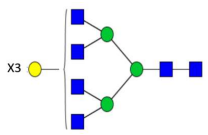
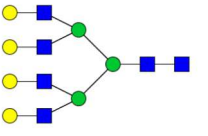
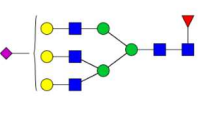
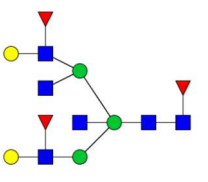
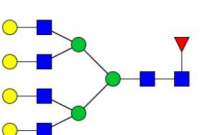
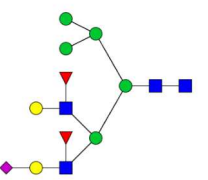
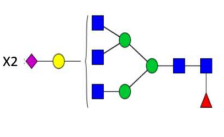
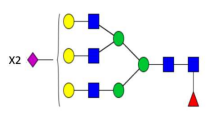
**Table 2. Putative N-glycans in cultured urothelial HCV29 and KK47 cancer cells**

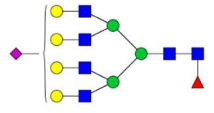
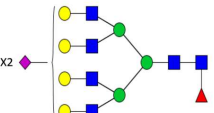
(\* These structures reported here are summarized from references<sup>33,48</sup>; \*\*  $m/z$  of  $[M+Na]^+$  with permethylation is used for this thesis, not reported in the literatures)

#	N-glycan composition	Putative structure *	$m/z$ of $[M+Na]^+$ with permethylation **
<p> <span style="color: green;">●</span> Mannose (Man)    <span style="color: blue;">■</span> N-Acetylglucosamine (GlcNAc)    <span style="color: purple;">◆</span> N-Acetylneuraminic Acid (NeuAc)  <span style="color: yellow;">●</span> Galactose (Gal)    <span style="color: yellow;">■</span> N-Acetylgalactosamine (GalNAc)    <span style="color: grey;">◇</span> N-glycolylneuraminic acid (NeuGc)  <span style="color: red;">▲</span> Fucose (Fuc)         </p>			
1	Hex <sub>3</sub> HexNAc <sub>2</sub> Fuc <sub>1</sub>		1345.6723
2	Hex <sub>5</sub> HexNAc <sub>2</sub>		1579.7826
3	Hex <sub>5</sub> HexNAc <sub>2</sub> Fuc <sub>1</sub>		1753.8718
4	Hex <sub>6</sub> HexNAc <sub>2</sub>		1783.8824

5	Hex <sub>5</sub> HexNAc <sub>3</sub>		1824.9089
6	Hex <sub>6</sub> HexNAc <sub>2</sub> Fuc <sub>1</sub>		1957.9716
7	Hex <sub>7</sub> HexNAc <sub>2</sub>		1987.9821
8	Hex <sub>6</sub> HexNAc <sub>3</sub>		2029.0087
9	Hex <sub>4</sub> HexNAc <sub>4</sub> Fuc <sub>1</sub>		2040.0247
10	Hex <sub>5</sub> HexNAc <sub>4</sub>		2070.0352
11	Hex <sub>6</sub> (pHex)HexNAc <sub>2</sub>		2081.9641
12	Hex <sub>4</sub> HexNAc <sub>5</sub>		2111.0618
13	Hex <sub>7</sub> HexNAc <sub>2</sub> Fuc <sub>1</sub>		2162.0714
14	Hex <sub>8</sub> HexNAc <sub>2</sub>		2192.0819

15	Hex <sub>5</sub> HexNAc <sub>4</sub> Fuc <sub>1</sub>		2244.1245
16	Hex <sub>7</sub> HexNAc <sub>2</sub> (pHex)		2286.0639
17	Hex <sub>9</sub> HexNAc <sub>2</sub>		2396.1817
18	Hex <sub>5</sub> HexNAc <sub>4</sub> Fuc <sub>2</sub>		2418.2137
19	Hex <sub>5</sub> HexNAc <sub>4</sub> NeuAc		2431.2089
20	Hex <sub>6</sub> HexNAc <sub>5</sub>		2519.2613
21	Hex <sub>5</sub> HexNAc <sub>6</sub>		2560.2879
22	Hex <sub>10</sub> HexNAc <sub>2</sub>		2600.2815
23	Hex <sub>4</sub> HexNAc <sub>5</sub> Fuc <sub>3</sub>		2633.3294
24	Hex <sub>6</sub> HexNAc <sub>5</sub> Fuc		2693.3506

25	Hex <sub>6</sub> HexNAc <sub>6</sub>		2764.3877
26	Hex <sub>7</sub> HexNAc <sub>6</sub>		2968.4874
27	Hex <sub>6</sub> HexNAc <sub>5</sub> NeuAc		3054.5242
28	Hex <sub>5</sub> HexNAc <sub>6</sub> Fuc <sub>3</sub>		3082.5555
29	Hex <sub>7</sub> HexNAc <sub>6</sub> Fuc		3142.5766
30	Hex <sub>7</sub> HexNAc <sub>4</sub> NeuAc		3187.5869
31	Hex <sub>5</sub> HexNAc <sub>5</sub> Fuc NeuAc <sub>2</sub>		3211.5981
32	Hex <sub>6</sub> HexNAc <sub>5</sub> Fuc NeuAc <sub>2</sub>		3415.6979

33	Hex <sub>7</sub> HexNAc <sub>6</sub> Fuc NeuAc <sub>1</sub>		3503.7503
34	Hex <sub>7</sub> HexNAc <sub>6</sub> Fuc NeuAc <sub>2</sub>		3864.9240

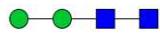
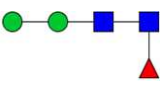
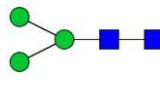
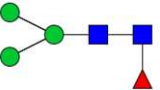
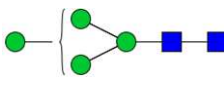
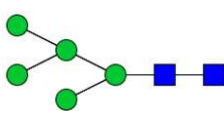
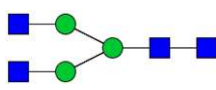
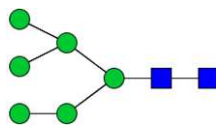
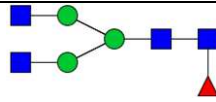
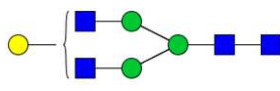


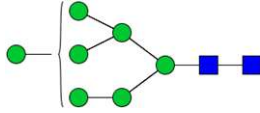
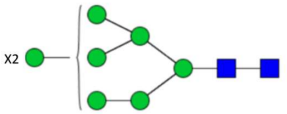
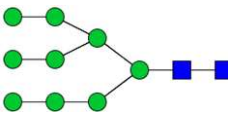
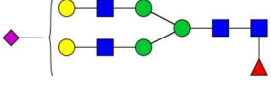
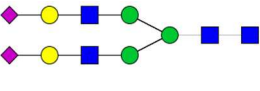
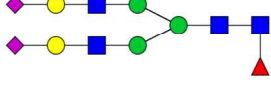
### 1.1.2 Urothelial O-glycans

Most urothelial O-glycans are reported to be mucin-type O-glycans (GalNAc-serine/threonine) following lectin histology, but there is a lack of structural information. The changes in expression levels of urothelial O-glycans was reported to be related to the stage of urothelium differentiation and cancer development using PNA and VVA for labeling T (Gal-GalNAc-serine/threonine) and Tn (GalNAc-serine/threonine) antigens<sup>34,52,66,67</sup>, supporting the studies by Buckley *et al.* and Desantis *et al.* describing mucin-type O-glycans distributed on the luminal surface of rabbit and donkey bladder examined with lectin labelling<sup>35,49</sup>.

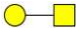
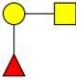
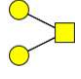
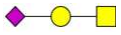
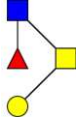
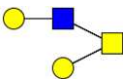
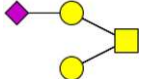
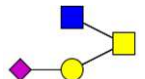
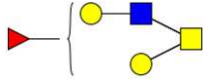
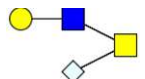
A recent study by another group member, published in Skeene *et al.*<sup>68</sup>, used porcine urothelial cells prepared as developed by the author of this thesis, using scalpel scraping, to develop a one-pot method using the established filter-aided *N*-glycans separation (FANGS) approach to sequentially release *N*- and O-glycans from cell lysates, reported 16 *N*-glycans and 17 O-glycans. The porcine urothelial *N*- and O-glycans identified by Skeene *et al.* are listed in Table 3 and Table 4, respectively, in which the porcine urothelial *N*-glycans contained major oligomannose and complex *N*-glycans; the porcine urothelial O-glycans were all mucin-type O-glycans. The structural diversities of porcine urothelial cell lysate *N*-glycans and O-glycans reported by Skeene *et al.* were in line with the results of these previous studies.

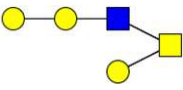
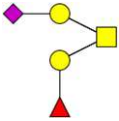
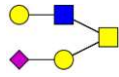
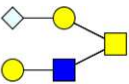
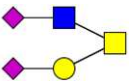
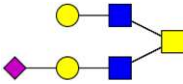
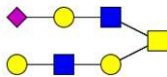
**Table 3. Putative porcine urothelial *N*-glycans reported by Skeene *et al.*<sup>68</sup>.**

#	<i>N</i> -glycan composition	Putative structure	<i>m/z</i> of [M+Na] <sup>+</sup> with permethylation
<p> <span style="color: green;">●</span> Mannose (Man)    <span style="color: blue;">■</span> <i>N</i>-Acetylglucosamine (GlcNAc)    <span style="color: purple;">◆</span> <i>N</i>-Acetylneuraminic Acid (NeuAc)  <span style="color: yellow;">●</span> Galactose (Gal)    <span style="color: yellow;">■</span> <i>N</i>-Acetylgalactosamine (GalNAc)    <span style="color: grey;">◇</span> <i>N</i>-glycolylneuraminic acid (NeuGc)  <span style="color: red;">▲</span> Fucose (Fuc)         </p>			
1	Hex <sub>2</sub> HexNAc <sub>2</sub>		967.433
2	Hex <sub>2</sub> HexNAc <sub>2</sub> Fuc		1141.570
3	Hex <sub>3</sub> HexNAc <sub>2</sub>		1171.580
4	Hex <sub>3</sub> HexNAc <sub>2</sub> Fuc		1345.645
5	Hex <sub>4</sub> HexNAc <sub>2</sub>		1375.684
6	Hex <sub>5</sub> HexNAc <sub>2</sub>		1579.781
7	Hex <sub>3</sub> HexNAc <sub>4</sub>		1661.482
8	Hex <sub>6</sub> HexNAc <sub>2</sub>		1783.883
9	Hex <sub>3</sub> HexNAc <sub>4</sub> Fuc		1835.920
10	Hex <sub>4</sub> HexNAc <sub>4</sub>		1865.921

11	Hex <sub>7</sub> HexNAc <sub>2</sub>		1987.988
12	Hex <sub>8</sub> HexNAc <sub>2</sub>		2192.065
13	Hex <sub>9</sub> HexNAc <sub>2</sub>		2396.182
14	Hex <sub>5</sub> HexNAc <sub>4</sub> FucNeuAc		2605.921
15	Hex <sub>5</sub> HexNAc <sub>4</sub> NeuAc <sub>2</sub>		2792.365
16	Hex <sub>5</sub> HexNAc <sub>4</sub> FucNeuAc <sub>2</sub>		2966.449

**Table 4 Putative porcine urothelial O-glycans reported by Skeene *et al.*<sup>68</sup>**

#	O-glycan composition	Putative structure	<i>m/z</i> of [M+Na] <sup>+</sup> with permethylation
<p> <span style="color: green;">●</span> Mannose (Man)    <span style="color: blue;">■</span> <i>N</i>-Acetylglucosamine (GlcNAc)    <span style="color: purple;">◆</span> <i>N</i>-Acetylneuraminic Acid (NeuAc)  <span style="color: yellow;">●</span> Galactose (Gal)    <span style="color: yellow;">■</span> <i>N</i>-Acetylgalactosamine (GalNAc)    <span style="color: grey;">◇</span> <i>N</i>-glycolylneuraminic acid (NeuGc)  <span style="color: red;">▲</span> Fucose (Fuc)         </p>			
1	HexHexNAc		518.257
2	HexHexNAcFuc		692.346
3	Hex <sub>2</sub> HexNAc		722.357
4	HexHexNAcNeuAc		879.430
5	HexHexNAc <sub>2</sub> Fuc		937.469
6	Hex <sub>2</sub> HexNAc <sub>2</sub>		967.483
7	Hex <sub>2</sub> HexNAcNeuAc		1083.530
8	HexHexNAc <sub>2</sub> NeuAc		1124.556
9	Hex <sub>2</sub> HexNAc <sub>2</sub> Fuc		1141.571
10	HexHexNAcNeuGc		1154.657

11	Hex <sub>3</sub> HexNAc <sub>2</sub>		1171.582
12	Hex <sub>2</sub> HexNAcFucNeuAc		1257.620
13	Hex <sub>2</sub> HexNAc <sub>2</sub> NeuAc		1328.656
14	Hex <sub>2</sub> HexNAc <sub>2</sub> NeuGc		1358.668
15	HexHexNAc <sub>2</sub> NeuAc <sub>2</sub>		1485.733
16	Hex <sub>2</sub> HexNAc <sub>3</sub> NeuAc		1573.784
17	Hex <sub>3</sub> HexNAc <sub>3</sub> NeuAc		1777.883

### 1.1.3 Urothelial glycosaminoglycans

The evidence for expression of urothelial glycosaminoglycans (GAGs) was based on using diluted acid (hydrochloric acid) to compromise the barrier function of the luminal side of bladders, that could be restored by exogenous glycosaminoglycan<sup>69-73</sup>. Hurst *et al.* used chondroitinase to digest paraffin-embedded human bladders prior to immunolabelling using an antibody that was claimed to label the epitope of chondroitin sulfate exposed after enzyme digestion<sup>74</sup>. The result reported by Hurst *et al.* suggested that human bladders collected from patients with interstitial cystitis had lower immunolabelling responses than those collected from normal subjects without interstitial cystitis<sup>74,75</sup>.

Various proteoglycans, including decorin (core protein with chondroitin sulfate or dermatan sulfate), perlecan (core protein with heparan sulfate) and syndecan-1 (core protein with heparan sulfate) were identified on the surface of normal human urothelium using immunohistochemistry using antibodies against the proteoglycan core proteins<sup>19,38</sup>. A similar distribution of different GAGs was reported by Janssen *et al* using unique GAG epitopes labelled with antibodies in human and porcine bladders, visualised using immunofluorescence<sup>44</sup>. In addition, the transepithelial electrical resistance (TEER) of cultured primary human urothelial cells, which is a well-established measure to assess epithelial paracellular permeability, decreased after treatment with chondroitinase or protamine hydrochloride, that were assumed to compromise the urothelial GAGs<sup>44</sup>.

The above research results are indirect evidence suggesting that GAGs play roles in maintaining bladder impermeability, although there remains a lack of direct evidence connecting the expression of urothelial GAGs and the location, structures, and function of different types of GAGs in the bladder.

## 1.2 Glycobiology

### 1.2.1 Overviews

Glycoproteins, formed by the covalent linkage of various glycans (oligosaccharides) at specific sites in proteins represent one subclass of glycoconjugates. The specific binding sites of the glycans to the side chains of specific amino acid residues form the basis for the categorisation of glycan linkage types. The same glycosylation site of different molecular copies of a particular protein can bear differently processed glycans, giving rise to microheterogeneity. The biological functions and identities of cell membrane glycoproteins covering most mammalian cell surfaces have received much attention in terms of their role in biological processes including immune defense, viral replication, parasitic infection, cell growth, cell-cell communication and cell-cell adhesion<sup>76</sup>.

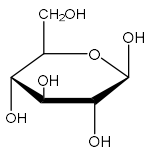

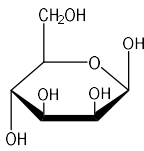

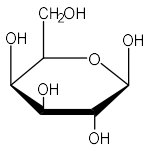

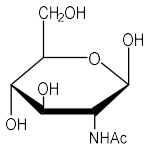

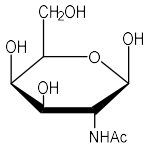

Glycosylation of a protein is a post-translational modification (PTM) which is not a templated process as is the formation of DNA. It takes place in the endoplasmic reticulum (ER) and Golgi apparatus of the cell and is the outcome of processing by enzymatic reaction via glycosyltransferases and glycosidases to carry out addition and removal of monosaccharides, respectively, from immature glycans.

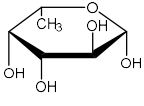

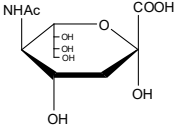

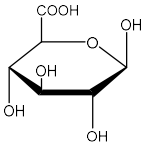

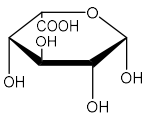

Although most monosaccharides (Table 5) have been found to form nucleotide sugars in the human body and participate in glycosylation as sugar donors<sup>77</sup>, some



monosaccharides are not directly donated from nucleotide sugars. For example,  $\beta$ -D-glucuronic acid (GlcA) is epimerized at C-5 position to form  $\alpha$ -L-iduronic acid (IdoA) via epimerization during the synthesis of chondroitin/dermatan sulfate and heparin/heparan sulfate.

**Table 5. Common monosaccharides in biosynthesis<sup>78</sup> Each glycan symbol used in this text follows those described in reference<sup>78</sup>**

Name	Structure	Symbol
$\beta$ -D-Glucose (Glc)		
$\beta$ -D-Mannose (Man)		
$\beta$ -D-Galactose (Gal)		
$\beta$ -D-N-Acetylglucosamine (GlcNAc)		
$\beta$ -D-N-Acetylgalactosamine (GalNAc)		

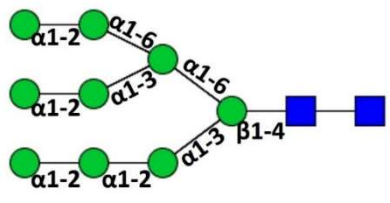
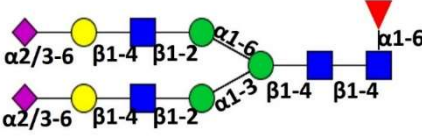
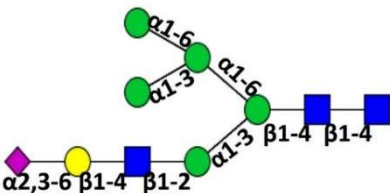
$\alpha$ -L-Fucose (Fuc)		
$\alpha$ -D-N-acetylneuraminic acid (NeuAc)		
$\beta$ -D-Glucuronic acid (GlcA)		
$\alpha$ -L-Iduronic acid (IdoA)		

During the biosynthesis of glycoprotein, two common types of covalent bonds (glycosidic bonds) are formed in a glycoprotein, the bond between each monosaccharide residues of the glycans and the bond between the glycan chains and the side chain of asparagine (*N*-linked) or to the side chain of serine or threonine (*O*-linked).

In the biosynthesis of *N*-glycoprotein, *N*-linked glycans are attached to the nitrogen atom of an asparagine (Asn) side chain in a consensus sequence Asn-Xxx-Ser/Thr, where Xxx is any amino acid except proline. It is important to note that not all such consensus sequences have to be glycosylated which means the same finished protein can be in different glycoforms as the macroheterogeneity. All *N*-glycans possess a common branched pentasaccharide core which consists of Man<sub>3</sub>GlcNAc<sub>2</sub>. All

mature mammalian *N*-glycans can be classified into three types which are oligomannose type, complex type and hybrid type (Table 6).

**Table 6. Three common types of mammalian *N*-glycan with linkage information based on *N*-glycosylation pathway.**

Type of <i>N</i> -glycans	Structures
	<p data-bbox="422 705 1380 862"> <span style="color: green;">●</span> Mannose (Man)    <span style="color: blue;">■</span> <i>N</i>-Acetylglucosamine (GlcNAc)    <span style="color: purple;">◆</span> <i>N</i>-Acetylneuraminic Acid (NeuAc)  <span style="color: yellow;">●</span> Galactose (Gal)    <span style="color: yellow;">■</span> <i>N</i>-Acetylgalactosamine (GalNAc)    <span style="color: grey;">◇</span> <i>N</i>-glycolylneuraminic acid (NeuGc)  <span style="color: red;">▲</span> Fucose (Fuc)         </p>
Oligomannose	
Complex	
Hybrid	

Protein *N*-glycosylation starts in the endoplasmic reticulum (ER) by transferring a 14-monosaccharide glycan  $\text{Glc}_3\text{Man}_9\text{GlcNAc}_2$  from dolichol phosphate to a nascent protein, catalyzed by an oligosaccharyltransferase in the luminal side of the ER membrane. The protein-bound *N*-glycan ( $\text{Glc}_3\text{Man}_9\text{GlcNAc}_2$ ) is modified by a series of removals and additions of monosaccharides catalyzed by glycosidases and glycosyltransferases in the ER and the Golgi apparatus, to form oligomannose, complex and hybrid *N*-glycans (Figure 5). In the beginning of the ER, three glucoses are removed from the  $\text{Glc}_3\text{Man}_9\text{GlcNAc}_2$  to form  $\text{Man}_9\text{GlcNAc}_2$ , catalyzed by  $\alpha$ -glucosidases I and II. The subsequent removal of the terminal  $\alpha$ 1-2 mannose of the middle arm of  $\text{Man}_9\text{GlcNAc}_2$  to form  $\text{Man}_8\text{GlcNAc}_2$  is catalyzed by the ER  $\alpha$ -mannosidase I, prior to folding of the glycoprotein and transport to the Golgi apparatus. This removal of terminal  $\alpha$ 1-2 mannose from  $\text{Man}_9\text{GlcNAc}_2$  is not necessary for all glycoproteins; the result is that  $\text{Man}_9\text{GlcNAc}_2$ - or  $\text{Man}_8\text{GlcNAc}_2$ -bound glycoproteins enter the cis-Golgi apparatus. However, if the protein fails to fold correctly at this stage, it does not pass through the ER, but is tagged with endoplasmic reticulum degradation enhancing  $\alpha$ -mannosidase-like proteins (EDEMs) and degraded by the ER degradation pathway.

Correctly folded glycoproteins in the cis-Golgi continue to undergo removal of mannoses from  $\text{Man}_9\text{GlcNAc}_2$  or  $\text{Man}_8\text{GlcNAc}_2$ , catalyzed by  $\alpha$ 1-2 mannosidases, until the *N*-glycan becomes  $\text{Man}_5\text{GlcNAc}_2$  and translocates to the medial Golgi. The removal of mannoses from  $\text{Man}_9/8\text{GlcNAc}_2$  to form  $\text{Man}_5\text{GlcNAc}_2$  is a key process in forming complex and hybrid *N*-glycans in the cis-Golgi, before translocating the  $\text{Man}_5\text{GlcNAc}_2$ -bound glycoprotein to the medial Golgi.  $\beta$ 1-2 addition of one GlcNAc

to C-2 of the mannose residue  $\alpha$ 1-3 linked in the core  $\text{Man}_5\text{GlcNAc}_2$  is catalyzed by *N*-acetylglucosaminyltransferase (GlcNAcT-I), and is the divergent step to form complex or hybrid *N*-glycans in the medial Golgi. Hybrid *N*-glycans are formed when  $\text{GlcNAcMan}_5\text{GlcNAc}_2$  is not trimmed by  $\alpha$ -mannosidase II, retaining the outermost non-reducing terminal  $\alpha$ 1-3 and  $\alpha$ 1-6 mannoses. The removal of those  $\alpha$ 1-3 and  $\alpha$ 1-6 mannoses catalyzed by  $\alpha$ -mannosidase II leads to the formation of complex *N*-glycans and is followed by the  $\beta$ 1-2 addition of one GlcNAc to the mannose residue  $\alpha$ 1-6 linked in the core  $\text{Man}_3\text{GlcNAc}_2$ . The reducing-terminal GlcNAc of the chitobiose core can be modified by  $\alpha$ 1-6 addition of fucose catalyzed by fucosyltransferase VIII, after the formation of hybrid *N*-glycans and biantennary complex *N*-glycans. Additional branching of complex *N*-glycans can be initiated with  $\beta$ 1-4 addition of one GlcNAc (GlcNAcT-IV) to the mannose residue ( $\alpha$ 1-3 linked) and  $\beta$ 1-6 addition of one GlcNAc (GlcNAcT-V) to the mannose residue ( $\alpha$ 1-6 linked) to form tri- and tetra-antennary complex *N*-glycans. The  $\beta$ 1-4 addition of galactoses, and  $\alpha$ 1-3 and  $\alpha$ 1-6 addition of sialic acids are the final capping modifications that complete *N*-glycan biosynthesis in the trans-Golgi apparatus; the mature structures are transported to their destinations via vesicle trafficking.

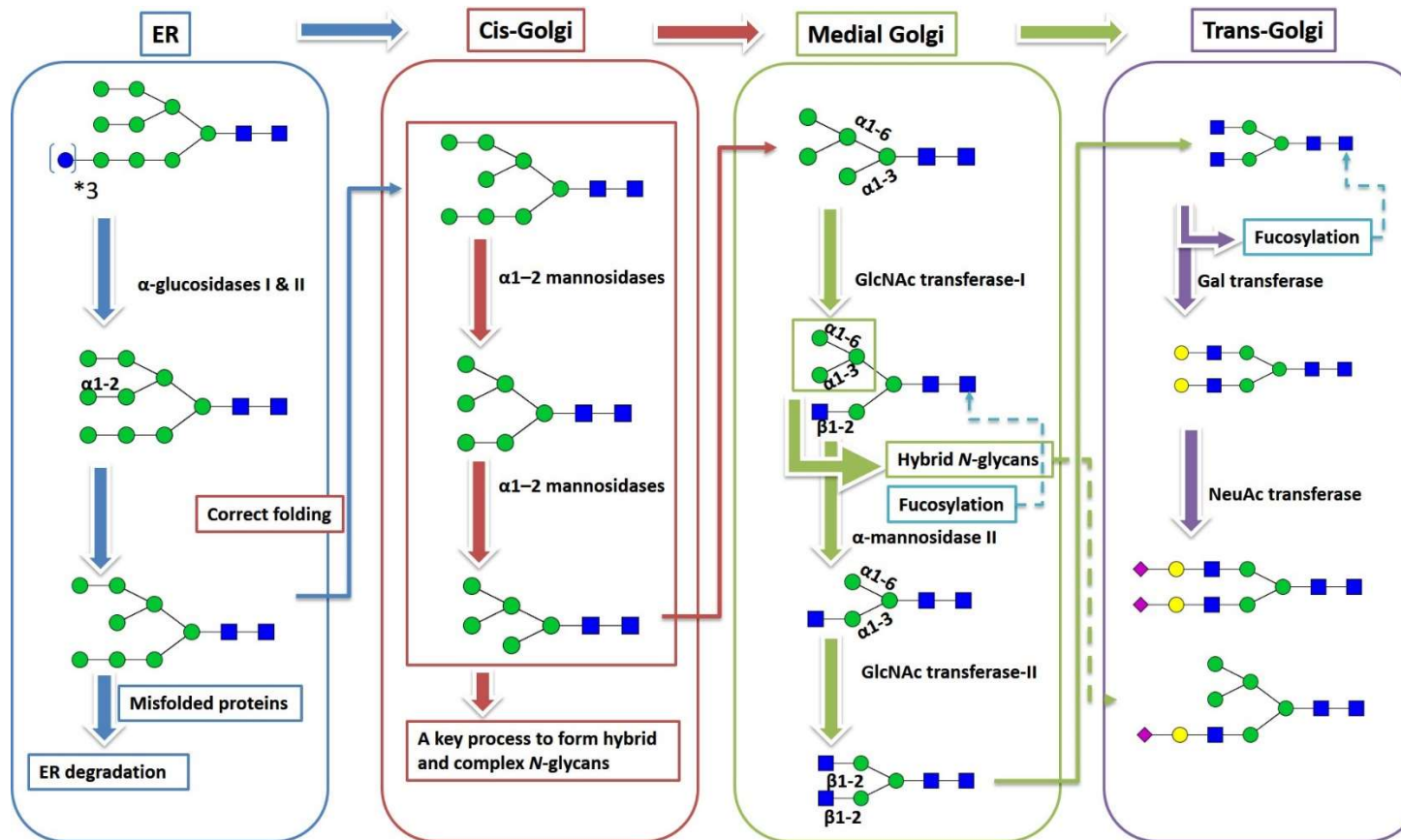
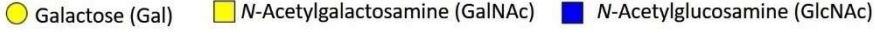
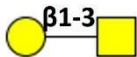
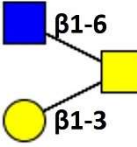

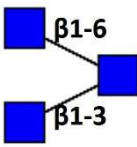
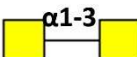

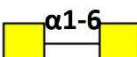
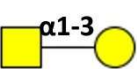


Figure 5. Common mammalian *N*-glycosylation pathway, starting with transferring a 14-monomer glycan Glc<sub>3</sub>Man<sub>9</sub>GlcNAc<sub>2</sub> from dolichol phosphate to a nascent protein in the ER.

O-glycoproteins are glycans linked to amino acid residues through the hydroxyl group of serine (Ser), threonine (Thr) or hydroxylysine (Hyl) in the protein sequence. The structures of O-glycans are much more diverse than that of *N*-glycans which have a common core structure of pentasaccharide (Man<sub>3</sub>GlcNAc<sub>2</sub>). The varieties of core structures in the O-glycan chain can be classified as the first monosaccharide bound to Ser/Thr/Hyl residues of the proteins. Several common O-glycan structures have been found in the human body shown in, in which mucin type is the most abundant type of O-glycan in the human body (Table 7)<sup>77,79</sup>.

**Table 7. Mucin type O-glycan core structures<sup>77</sup>**

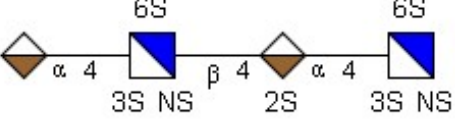
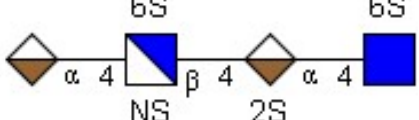
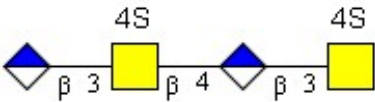
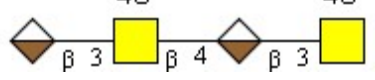
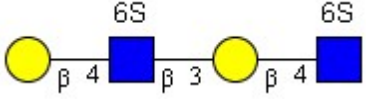
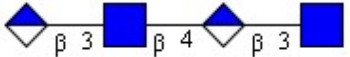
Core	Structure	Human tissue
<p>  </p>		
1		Most cells and secreted proteins
2		All blood cells
3		Colon and saliva
4		Mucin-secreting cell
5		Meconium
6		Ovarian tissue
7		Bronchus
8		



Glycosaminoglycans (GAGs) are the other common O-glycans which are unbranched and highly complex polysaccharides. GAGs are normally composed of repeating disaccharide units which often consist of aminohexoses (GlcNAc or GalNAc) linked to uronic acids (glucuronic acid or iduronic acid) or galactose. These repeating units commonly form the four types of GAGs (Table 8): 1) heparin/heparan sulfate, 2) chondroitin/dermatan sulfate, 3) keratan sulfate and 4) hyaluronic acid. These GAGs are normally modified with multiple sulfate groups (except hyaluronic acid) to exhibit the highly hydrophilic structure of GAGs.

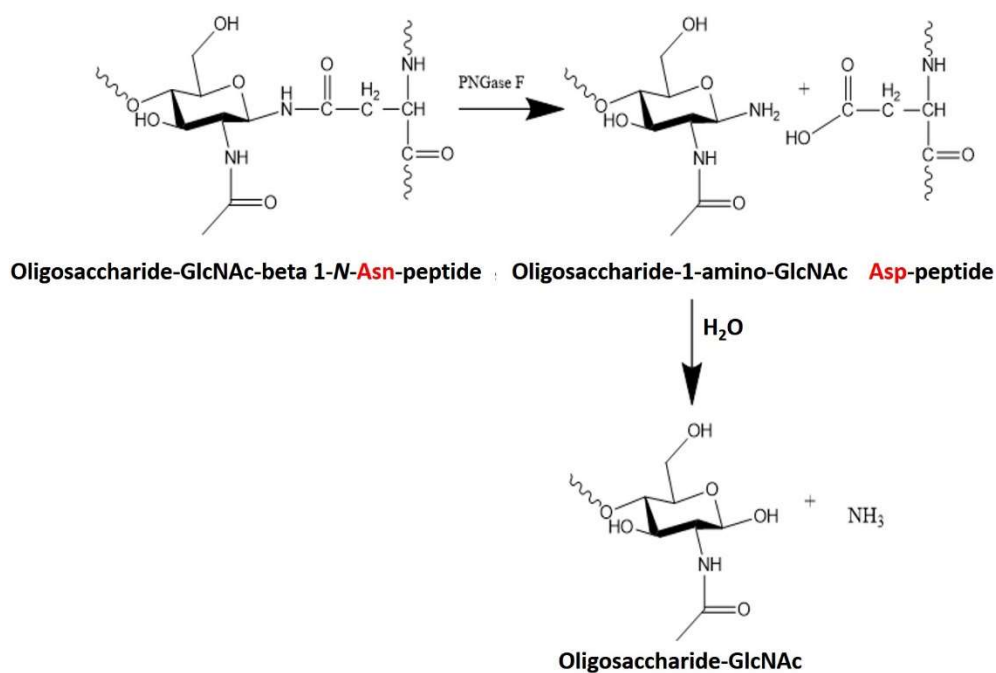
The biosynthesis of proteoglycans produces different linkages between GAGs and proteins depending on the type of GAG<sup>79</sup>. Heparin/heparan sulfate and chondroitin/dermatan sulfate possess the common tetrasaccharide GlcA-Gal-Gal-Xyl which is attached to the hydroxyl group of glycosylated serine residues in the protein. Keratan sulfate is categorized into keratan sulfate I (KS-I) and keratan sulfate II (KS-II) depending on their linkages to the protein. KS-I is *N*-linked keratan sulfate which is linked to the amide group of glycosylated Asn residues in the protein through GlcNAc<sub>2</sub>Man<sub>3</sub>. KS-II is O-linked keratan sulfate chains linked through mucin type core two structures to serine or threonine residues of the protein.

**Table 8. Glycosaminoglycan structures<sup>79</sup>**

Name of GAGs	Repeating disaccharide of GAGs
Heparin	
Heparan sulfate	
Chondroitin sulfate (CS)	
Dermatan sulfate (DS)	
Keratan sulfate (KS)	
Hyaluronic acid (HA)	
<p>XS: X is the position that may be substituted by sulfate group</p>	

### 1.2.2 Release of glycans from glycoproteins using enzymatic or chemical methods

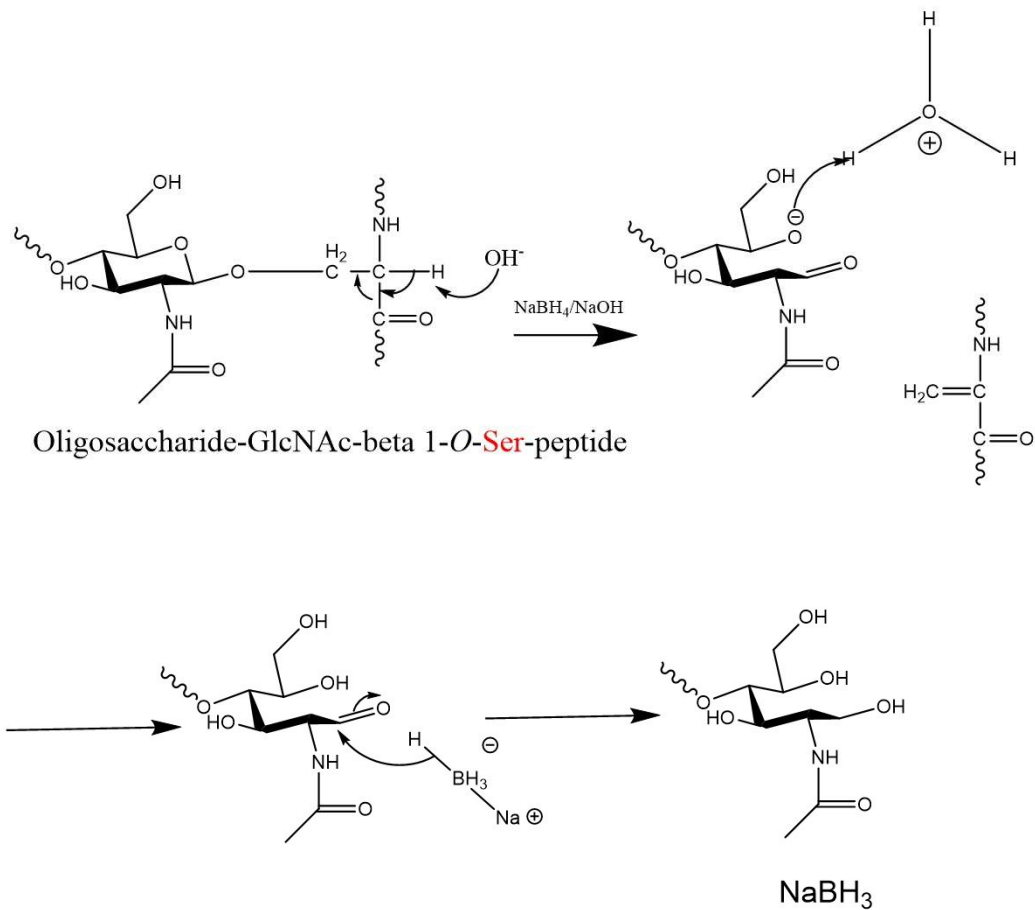
Structural identification of glycans can be achieved by enzymatic or chemical methods to liberate glycans from their bound glycoproteins prior to structure derivatization and instrumental analysis. Differences in glycan-protein linkage of *N*- and *O*-glycans require different approaches for releasing intact glycans. Enzymatic digestion of releasing *N*-glycans is the most common way to release *N*-glycans from glycoproteins<sup>80,81</sup>. Several enzymes, including peptide-*N*<sup>4</sup>-(acetyl- $\beta$ -glucosaminyl)-asparagine amidase from *Elizabethkingia meningoseptica* (previously *Flavobacterium meningosepticum*) (PNGase F) and endoglycosidase H (Endo H) are available for releasing *N*-glycans. PNGase F is an amidase that cleaves the bond between reducing terminal GlcNAc residues of *N*-glycans and asparagine residue of glycoproteins. The released *N*-glycans containing reducing terminal 1-amino GlcNAc residues are hydrolyzed to ammonia and intact glycans with chitobiose on the reducing termini (Figure 6). PNGase F has wide specificity to most of *N*-glycans with exception of *N*-glycan containing Fuc- $\alpha$ -(1 $\rightarrow$ 3)-GlcNAc on the reducing termini<sup>82</sup>. By contrast, Endo H has specificity to oligomannose and hybrid *N*-glycans; it cleaves the bond between the reducing terminal chitobiose of *N*-glycans, therefore, one GlcNAc residue remains on the digested glycoproteins and the released *N*-glycans lack one GlcNAc residue on the reducing terminus.



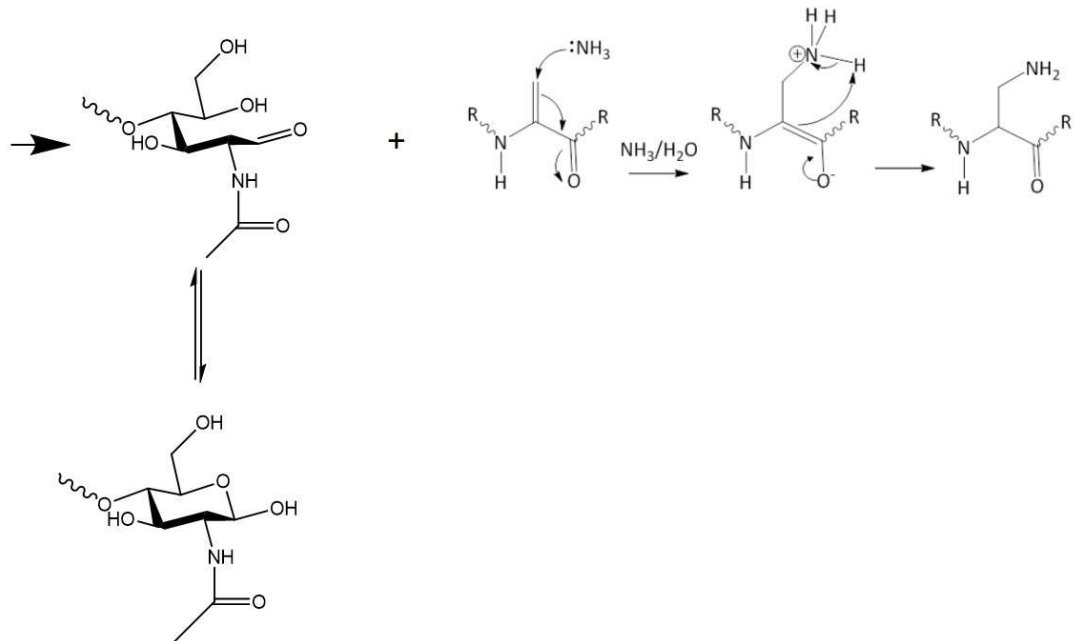
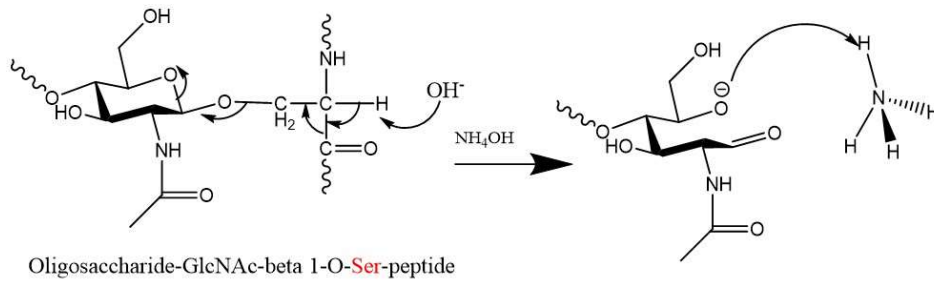
**Figure 6. The release of N-glycan from N-glycoproteins using PNGase F digestion**

The enzymatic methods of O-glycan removal are restricted by few O-glycanases with limited substrate specificities. The abundant mucin-type O-glycans are often extended with additional monosaccharides covering the epitopes that are required by O-glycanase<sup>83</sup>. The release of O-glycan from O-glycoproteins is commonly achieved using chemical methods. Alkaline  $\beta$ -elimination in the presence of high concentrations of sodium borohydride prevents peeling of the released O-glycan is the most commonly chemical method for the release of O-glycans from serine or threonine residues of proteins<sup>84</sup> (Figure 7). In addition, Rademaker *et al* reported a non-reductive  $\beta$ -elimination for O-glycan release using  $\text{NH}_4\text{OH}$  in place of  $\text{NaOH}$  as the  $\beta$ -elimination reagent<sup>85</sup> (Figure 8). The physical properties of glycoproteins such as electrophoretic mobility are altered after releasing glycans. Therefore, the gel

migration of glycoproteins before and after release of glycans provides a way to understand the properties of proteins and the types of conjugated glycans<sup>9,10,28,54</sup>.



**Figure 7. The release of O-glycan from O-glycoproteins by reductive  $\beta$ -elimination**



**Figure 8. The release of O-glycan from O-glycoproteins by non-reductive  $\beta$ -elimination**

## 1.3 Mass spectrometry

### 1.3.1 Mass spectrometry in glycobiology

Mass spectrometry (MS) has been commonly applied in glycobiology, investigating glycopeptides/glycoproteins<sup>85–90</sup>, glycolipids<sup>91–94</sup> and glycans<sup>95–98</sup>. The glycan parts of glycoproteins are commonly released chemically or enzymatically for O-glycans or N-glycans, respectively. The released glycans can be analyzed with or without prior derivatization and examined by MS which has the power, depending on the instrumentation used, of determining the accurate mass of the glycans. The acquired glycan accurate mass, together with knowledge of glycan biosynthetic routes and potentially further investigation using product ion tandem mass spectrometry, provides information on monosaccharide composition, and feasible glycan primary structures to be proposed, performing a high throughput glycome identification. However, the main challenges of carbohydrate analysis using mass spectrometry are the differentiation of structural isomers (i.e. having the same mass-to-charge ratios), defining linkage and anomericity information ( $\alpha$  /  $\beta$  form). Nuclear magnetic resonance spectroscopy (NMR) is a powerful analytical approach that requires a substantial sample amount to provide comprehensive structural information. NMR determines structural information by 1) measuring the bond correlation between all protons ( $^1\text{H}$ ) on a monosaccharide to characterize the identity of the monosaccharide (total correlation spectroscopy, TOCSY), 2) measuring single bond correlation between two different nuclei ( $^1\text{H}$  and  $^{13}\text{C}$ ) to assign the  $\alpha$  /  $\beta$  form of an anomeric carbon through its correlation with an adjacent hydrogen

(heteronuclear single quantum correlation, HSQC), and 3) measuring two different nuclear correlations ( $^1\text{H}$  and  $^{13}\text{C}$ ) across two to four bonds to assign linkage information of a glycosidic bond between two adjacent monosaccharides (heteronuclear multiple bond correlation, HMBC).

Approaches to glycan separation prior to mass spectrometric analysis offer some insights into structural information on the basis of glycan behaviour in different separation methods. An early method used for glycan separation was gel filtration on BioGel-P4; in combination with endo- and exoglycosidase digestion, observing the migration of digested glycans after the enzymatic removal of monosaccharides, offered a means to sequence glycans released for example, from urinary glycopeptides<sup>99</sup>. High-performance liquid chromatography (HPLC) offers a broad range of separation mechanisms for mono- and oligosaccharides. Traditional anion-exchange chromatography coupled with differential refractometry was used to separate native cellulose mono-, di- and oligomers<sup>100,101</sup>. In a related approach, Hardy *et al.* reported that two synthetic oligomannose nonasaccharide positional isomers (external arms terminated in GlcNAc- $\beta$ -(1  $\rightarrow$  4)-Man- $\alpha$ -(1  $\rightarrow$  3)-Man- or GlcNAc- $\beta$ -(1  $\rightarrow$  6)-Man- $\alpha$ -(1  $\rightarrow$  6)-Man-) were separated using high-performance anion-exchange chromatography with pulsed amperometric detection (HPAEC-PAD)<sup>102</sup>. Hardy *et al.* proposed that the relative acidities of the free hydroxyl groups and the accessibility of oxyanions of the oligosaccharides to the stationary phase were the factors that differentiate the structural isomers. Coupling two different separation mechanisms, such as reversed-phase chromatography (on a C18 column)



and hydrophilic interaction (on an amide column) (or the same mechanism with different chromatographic conditions) in a two-dimensional liquid chromatography (2D-LC) approach was used to examine the oligosaccharides released from glycoproteins<sup>103</sup>. Incompletely resolved compounds eluted from the first column are expected to be separated on the second column based on the two different chromatographic retention behaviors<sup>104,105</sup>. Derivatization of oligosaccharides with functional groups, such as 2-aminopyridine, prior to HPLC analysis may be required for chromatographic detection because of the general lack of natural chromophores on oligosaccharides.

Capillary electrophoresis (CE) equipped with ultraviolet (UV) or laser-induced fluorescence detectors uses an electric field to separate oligosaccharides on the basis of their differences in ionic mobility through electrolyte solutions; CE separation can be improved using modulated electrical conductivity (gradient) and/or by adjusting the electrolyte pH. Hermentin *et al.* reported that native complex *N*-glycans released from  $\alpha_1$ -acid glycoprotein using hydrazinolysis were separated by CE and detected by UV at 190 nm<sup>106</sup>. It is worth noting that UV detection at low wavelengths exploits the presence of carbonyl groups in many oligosaccharides, but is not selective for native oligosaccharides, and careful sample purification is required<sup>107</sup>.

The above-mentioned glycan separation approaches often require authentic standards for referencing known peak identities to unknown peaks identified in

glycan samples; however, the availability of authentic standards is sometimes a problem. The use of MS in conjunction with separation techniques, typically high performance liquid chromatography using porous graphitized carbon (PGC)<sup>108–112</sup> or hydrophilic interaction liquid chromatography (HILIC)<sup>113–116</sup> is capable of resolving structural isomers prior to MS analysis, allowing additional structural information to be determined.

Derivatization of native glycans has been widely conducted prior to instrumental analysis, in order to modify the retention characteristics of glycans on a chromatographic stationary phase, to stabilize labile functional groups or to improve the mass spectrometric ionisation and fragmentation characteristics of carbohydrates. Permethylation of glycans with methyl iodide catalysed by methylsulphenyl carbanion<sup>117</sup> or by sodium hydroxide<sup>118</sup> replaces exchangeable hydrogen atoms with methyl groups and so converts hydroxy groups into methyl ethers (as well as methylating amino and amido hydrogens), altering the overall hydrophobicity and surface activity of the glycans. In addition, the carboxylic acid groups of sialylated glycans, which are susceptible to rapid in-source decay in positive mode of matrix-assisted laser desorption/ionization mass spectrometry (MALDI-MS) and can affect the relative ionization efficiencies<sup>119</sup>, are protected by permethylation. The permethylated sialylated glycans act as stabilized neutral molecules and demonstrate ionization efficiencies similar to those of permethylated non-sialylated glycans<sup>94,120</sup>.

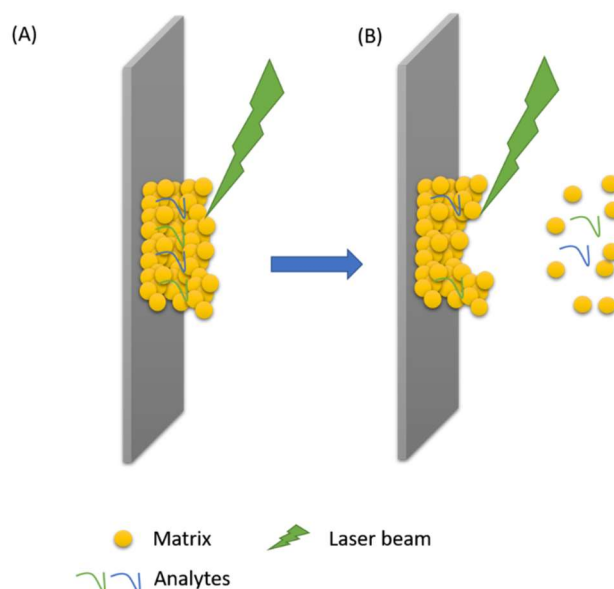
A modern mass spectrometer, which has evolved from the first invention by F. W. Aston, A. J. Dempster, E. Goldstein, J. H. E. Mattauch and J. J. Thomson in the early 20<sup>th</sup> century<sup>121</sup>, is composed of an ionization source, one or more mass analysers, vacuum systems and detectors, allowing charging analytes to be transmitted in a high-vacuum environment through electrical, electrostatic or magnetic fields in which they are separated on the basis of their  $m/z$  ratios and detected. In this thesis, positive-mode mass spectrometry has been used as a major analytical approach to identify and semi-quantify released urothelial cell glycans following permethylation. This section thus introduces the fundamentals of the MS techniques including ionization methods and mass analysers that have been applied in this study.

### 1.3.2 Matrix-assisted laser desorption/ionization (MALDI)

MALDI-MS, the most frequently applied ionization method used for the work presented in this thesis, requires sample preparation by mixing a laser-light absorbing matrix compound with the non-volatile analyte, forming dried sample spots. These are pulsed with irradiation by the MALDI laser to produce gas phase analytes (Figure 9). MALDI-MS was firstly applied to analyze amino acids by Karas and Hillenkamp, discovering that aromatic amino acids required lower laser irradiance to ionise than those amino acid without aromatic group<sup>122</sup>. In the same study, alanine in a mixture with tryptophan took a tenth lower irradiance to form protonated molecules than the irradiance required to obtain a spectrum of alanine alone. This was the first record of the use of small molecules with low-threshold irradiance (matrix) to facilitate the ionization of small molecules with high-threshold irradiance (analytes), leading to the basic concept of “matrix-assisted” laser desorption.

Following this first observation of matrix-assisted laser desorption, Karas and Hillenkamp extended their work to obtain mass spectra of a sodiated tetrasaccharide (stachyose)<sup>123</sup>, protonated peptides<sup>123</sup> and charged  $\beta$ -lactoglobulin ( $\sim m/z$  18300) and bovine albumin ( $\sim m/z$  33300)<sup>124</sup> using nicotinic acid as the MALDI matrix<sup>123,124</sup>. Due to the limited instrumental resolution at the time Karas and Hillenkamp obtained their first mass spectra of charged proteins, it was impossible to distinguish the signals of protonated and cationized proteins. A similar study by Tanaka. *et al* used cobalt powder and glycerol as the matrix to obtain mass spectra of chymotrypsinogen ( $\sim m/z$  25717)<sup>125</sup>. Sodiated stachyose, probably the first cationized oligosaccharide

recorded in a MALDI mass spectrum, was able to be ionized alone without the help of a matrix but the signal-to-noise ratio (S/N) was remarkably enhanced by the addition of nicotinic acid or tryptophan in the sample spots<sup>123</sup>.



**Figure 9. Matrix-assisted laser desorption/ionization.** The laser energy is transferred via the matrix molecules to the analytes, inducing the ionization of analytes.

The detailed mechanism of ionization in MALDI remains unclear. Multiple instrumental and experimental parameters, including wavelength and irradiance of the laser, laser length, the pressure in the ionization chamber, the condition of the dried sample spots, the species of matrix and analytes and other undiscovered parameters may all contribute to the formation of ionized compounds recorded in MALDI mass spectra. Two major MALDI ionization mechanisms, the lucky survivor model<sup>126,127</sup> and the gas phase protonation model<sup>128–130</sup>, have been reported to

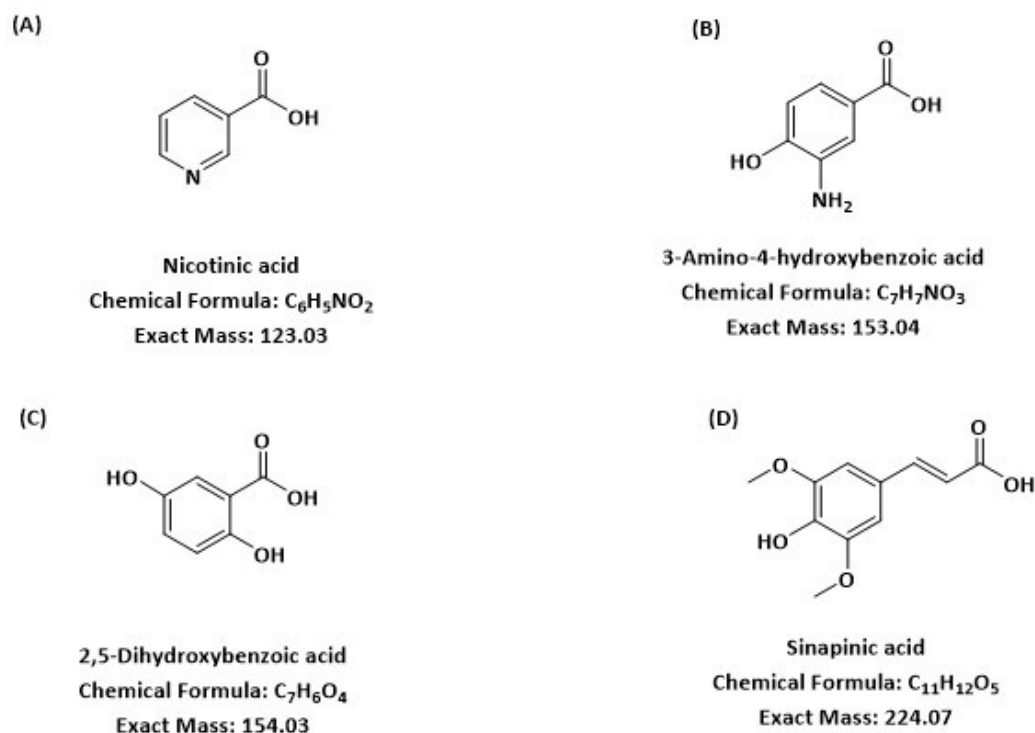
regulate MALDI ionization together to different extents depending on various parameters in sample preparation<sup>131</sup>.

The fundamental concept of the lucky survivor model is that analytes preserve their favoured solution phase charge states when dried with matrix to form MALDI spots. After the laser ablates the sample spots, two possible scenarios determine whether the ionized analytes are detected or not. In the first scenario, precharged analytes, e.g. protonated peptide  $[H\text{-Pep}]^+$ , are found with equal amounts of counterions,  $[A]^-$ , in the clusters caused by laser ablation. Following cluster dissociation, the counterions neutralize the charge-bearing species,  $[H]^+$ , on the precharged analyte, forming  $[HA]$  and  $[Pep]$  both with zero charge, neither of which is detectable mass spectrometrically. In the second scenario, so-called lucky survivors are detected; this is proposed to occur when clusters form that lack counterions to neutralize the charge-bearing species on precharged analytes, resulting in the detection of  $[H\text{-Pep}]^+$ <sup>126</sup>. The original lucky survivors model was incapable of describing the formation of negatively charged analytes because the common acidic groups on peptides or proteins have higher affinities for protons than common proton donors such as formate or acetate. A refined version of the lucky survivor model was to propose that matrix molecules may be protonated ( $[\text{matrix} + H]^+$ ) or deprotonated ( $[\text{matrix} - H]^-$ ) in the clusters, transferring protons to analytes or taking protons from analytes, respectively. MALDI matrix compounds commonly have carboxylate groups, which form anions that offer similar proton affinities to those on biomolecules, facilitating the formation of negatively charged anions.

The second model describing the MALDI mechanism is the gas phase protonation model; it suggests that analytes in dried MALDI spots can carry zero charge or may be precharged but neutralized by counterions. After ablation by the laser, neutral analytes collide with protonated or deprotonated matrix in the gas phase, forming protonated or deprotonated analytes, respectively<sup>128,130,132</sup>.

MALDI has been widely applied to analyze carbohydrates since the first MALDI spectrum of stachyose using nicotinic acid (Figure 10A) as the matrix<sup>123</sup>. The first MALDI application to glycans was reported by Mock et al. using three substituted benzoic acids (Figure 10B to D) as MALDI matrices to analyze native *N*-glycans released from glycoproteins<sup>133</sup>. Spectra of triantennary sialylated complex *N*-glycans and oligomannose *N*-glycans from bovine fetuin and ribonuclease B were obtained using 2,5-dihydroxybenzoic acid (DHB) and sinapinic acid (SA) as matrices, respectively.

DHB was originally used as a MALDI matrix for protein analysis<sup>134</sup> but has now become the most popular matrix for native and permethylated oligosaccharides. The typical appearance of dried MALDI spot using DHB in solution in a mixture of acetonitrile, or methanol, and water is long needle-like crystals that mostly radiate from the centre of the spot towards the outer edges.



**Figure 10. Structures of common MALDI matrices**

The 'sweet-spot effect' which results in high signal intensities of analytes from apparently random positions in MALDI spots, is likely to affect the reproducibility of mass spectra and so impact quantification. The homogeneity of DHB spots is often poor and results in lack of shot to shot reproducibility in replicate analysis of the same spot. Fine crystalline needles at the edges of DHB spots usually generate the best spectra, and tend to represent the sweet spots. Soltwisch and Dreisewerd introduced a binary matrix (DHB and glycerol) which provided homogeneous MALDI spots and contributed to generating reproducible MALDI mass spectra<sup>135</sup>. The binary matrix was mixed with peptides or native oligosaccharides (LNFP II) and dried with slow evaporation. High reproducibility of MALDI mass spectra was obtained



from position to position and spot to spot in MALDI spots prepared in this binary matrix.

DHB, the commonly used matrix in MALDI analysis of carbohydrates, has been suggested to be a “hotter matrix” which transfers more of the absorbed laser energy to analytes than does  $\alpha$ -cyano-4-hydroxycinnamic acid (CHCA)<sup>136</sup>. Energy transfer could be through the hydrogen bonds formed between matrix molecules and analyte in the MALDI spots<sup>136</sup>. Each DHB molecule is able to form three hydrogen bonds, while CHCA can only form two hydrogen bonds. As a result, DHB as the hotter matrix could contribute to more fragmentation of analyte ions<sup>136</sup>. It is notable that the classification of hot or cold matrix, e.g. DHB and CHCA, respectively, could also be reversed by laser energy changes and the co-crystalline structure formed between analytes and matrices<sup>136</sup>. Luo *et al.* suggested that, at low laser power, CHCA absorbed and transferred laser energy to analytes more efficiently than did DHB; as a result, CHCA could in this way be considered the hotter matrix<sup>136</sup>.

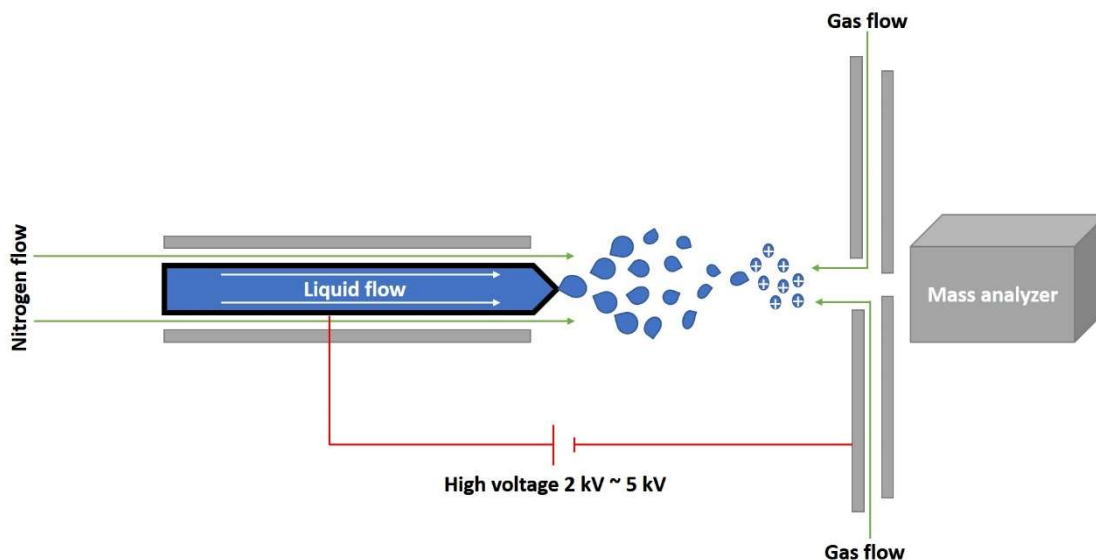
Throughout the literature on MALDI of carbohydrates, most ionized oligosaccharides are reported in the sodiated form  $[M+Na]^+$ , forming stabilized cationized oligosaccharides by the oxygen atoms of C6-hydroxyl groups and hemiketals coordinating with alkali metal ions<sup>137</sup>. Alkali metal ions have different affinities for oligosaccharides, in the order  $Cs > K > Na > Li > H$ <sup>138</sup>, although cesium is not able to ionize oligosaccharides with less than five monosaccharide units because the large size of alkali ion needs large oligosaccharides to stabilize the cationized structures<sup>137</sup>.

A good relationship between signal strength of native biantennary complex *N*-glycans and the amount of analytes on MALDI spots with DHB matrix was reported by Harvey *et al.*<sup>139</sup>. The same complex *N*-glycans analyzed using matrix 3-amino-4-hydroxy benzoic acid presented a saturation effect on signal intensity at about 30 pmol of sample amount, which implies that the species of MALDI matrix affects the ionization of glycans and DHB represents a good choice for carbohydrate analysis. Very significantly, Wada *et al.* reported an investigation assessing the robustness of relative abundance of released *N*-glycans by different derivatizations and MS techniques<sup>120</sup>. They reported that the relative abundance of signals for permethylated *N*-glycans released from transferrin or IgG analyzed using MALDI-MS presented reproducible quantification results between different labs and were comparable with the chromatographic quantification data using reductive amination for fluorescence detection. This investigation was extended to assess the relative quantification of mucin O-glycans using MS in a further study by Wada *et al.*, in which the IgA1 isolated from human serum was used for O-glycomic analysis<sup>140</sup>. The results were similar to those of the previous *N*-glycan study; permethylation of O-glycans followed by direct MALDI-MS analysis provided robust semi-quantification data. The two assessments of *N*- and O-glycans released from purified glycoproteins followed by permethylation prior to MALDI-MS analysis and compared with other analytical approaches were initiated by the Human Disease Glycomics/Proteome Initiative (HGPI) in the Human Proteome Organization (HUPO). A third HGPI study by Ito *et al.* was to compare different approaches performed by different labs for relative quantification of *N*- and O-glycans isolated from the cell lysates of three cancer cell lines (Hodgkin's lymphoma cell [L428], lymphoma cell

[U937], neuroblastoma cell [SK-N- SH])<sup>141</sup>. In this study, all cell lysate *N*-glycans were released using PNGase F digestion, and O-glycans were released by reductive or non-reductive  $\beta$ -elimination. The resulting cell lysate *N*- and O-glycans analyzed using HPLC (for 2-aminopyridine [PA] or 2-aminobenzoic acid labeled glycans), ESI-MS (for native glycans) and MALDI-MS (for permethylated glycans) gave widely varied glycan profiles, which was probably the result of differences in the sample preparation, most likely to be the preparation of cell lysate and the efficiency of chemical labeling. This study demonstrates the difficulty of analyzing the glycome in a complicate biological sample by any single analytical approach.

### 1.3.3 Electrospray ionization (ESI)

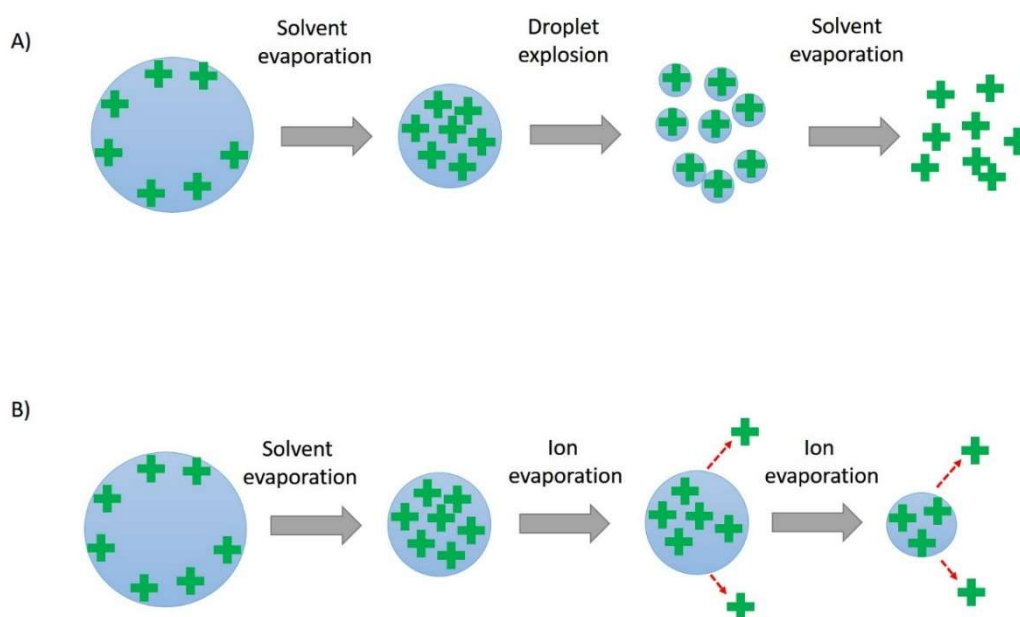
Electrospray ionization (ESI), one of the most-used soft ionization methods along with MALDI, is also commonly applied in carbohydrate analysis. ESI was invented by Dole *et al*<sup>142</sup> for ionizing negatively charged polystyrene in an evaporation chamber at atmospheric pressure with an electrical field applied on a nozzle-skimmer system, producing macromolecules multiply charged. This use of ESI (for generating charged macromolecules) was then applied to be used in conjunction with MS for analysing proteins by Fenn *et al.*<sup>143,144</sup> and is now widely applied for analysing large biomolecules as well as small molecules.



**Figure 11. Schematic of an ESI source on a mass spectrometer**

Electrospray transfers charged non-volatile analytes directly from the solution to the gas phase, which is compatible with interfacing with liquid chromatography. The process of electrospray involves spraying sample solution through a narrow capillary into an electrical field, transferring charged analytes into the gas phase with the help of a flow of gas, typically nitrogen (Figure 11). The electrical field, usually between 2 kV ~ 5 kV, polarizes the charged species in the sample solution, accumulating counter charges on the surface of liquid against the polarity of the electrical field. A conical-shaped liquid surface known as a Taylor cone is formed by this polarization, due to the repulsion of like charges accumulating at the liquid's surface. The cone is maintained as long as the surface tension of the liquid exceeds the repulsive forces between similarly charged species. However, when the charges become so concentrated at the surface that the repulsive force exceeds the surface tension (at the Rayleigh limit) the cone breaks and forms many fine charged droplets. The flow

of gas helps the desolvation of these charged droplets. There are typically two gas flows; that flowing coaxially outside the capillary (known as sheath gas) helps to nebulise the spray, while the flow from the counter direction (known as curtain gas), helps evaporate the solvent, forming smaller and smaller droplets till only charged analytes are left. This mechanism of electrospray ionization was proposed by Dole et al<sup>142</sup>, and is known as the charge residue model (Figure 12A)<sup>145</sup>. An alternative mechanism known as the ion-evaporation model, proposed by Iribarne and Thomson<sup>146</sup>, suggests that the repulsive forces caused by the concentration of similarly charged species getting higher and higher due to the loss of solvent molecules caused by evaporation eventually exceeds the surface tension of the liquid, leading to coulombic explosion and ejection of charged analytes (Figure 12B).



**Figure 12. Models of ion production using ESI. A) charge residue model and B) ion evaporation model.**

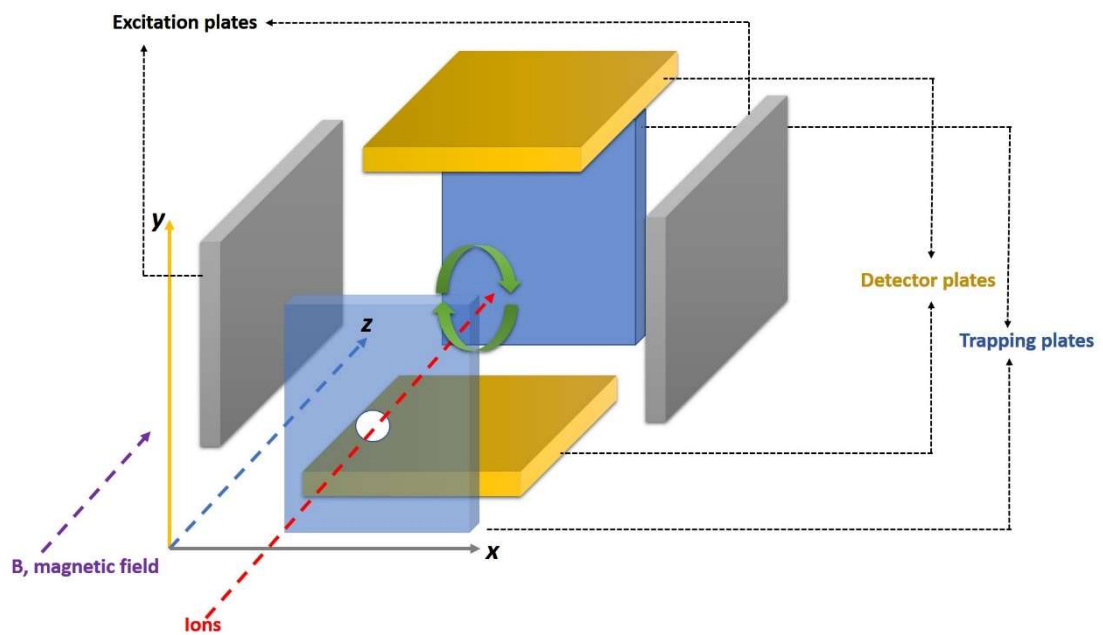
The performance of electrospray ionization can be improved by reducing the flow rates of sample solution and/or the diameters of the spray needle tip, in what has become known as nano-electrospray<sup>147</sup>. This modification of ESI can achieve lower limits of detection than regular ESI, mainly because it generates small droplets that require less solvent evaporation to generate ions. This means that salts, that can perturb the efficiency of the process become less concentrated in the droplets, and so interfere less than in regular ESI. Both ESI and nano-electrospray produce positively charged analytes via protonation or cationization, and negatively charged analytes by deprotonation or anionisation<sup>148</sup>.

#### 1.3.4 Fourier-transform ion-cyclotron-resonance mass spectrometry

Fourier-transform ion-cyclotron-resonance mass spectrometry (FT-ICR-MS) was introduced by Comisarow and Marshall<sup>149,150</sup> and offers superior mass measurement with higher signal resolution and mass accuracy than any other mass spectrometer. FT-ICR instruments are composed of four main components, including a 1) superconducting magnet, 2) an ion trapping cell known as a Penning trap, 3) an ultra-high vacuum system and 4) a complex instrument control and data acquisition system.

The charged molecules generated, typically these days using ESI or MALDI, are transmitted through multiple stages of multipoles and focusing devices to the trapping cell at a typical pressure of  $10^{-9}$  to  $10^{-10}$  Torr. The traditional design of ion trapping cell is composed of three pairs of metal plates, including trapping plates,

excitation plates and detector plates (Figure 13), which retain and excite the ions for mass analysis and detection using a combination of electrical fields and strong magnetic fields, usually between 3 T and 15 T<sup>151</sup>. The ions entering the trapping cell along the z-axis (along the axis of the magnetic field) with DC potentials applied to the pair of trapping plates, are trapped in the x-y plane, by the magnetic field. They orbit the z-axis due to the combination of the magnetic field and the voltage applied on the pair of trapping plates, resulting a circular trajectory (known as the cyclotron motion, Figure 13) of the ions between the trapping plates<sup>151,152</sup>.



**Figure 13. Diagram of FT-ICR mass analyzer. The traditional design of ion trapping cell is composed of three pairs of metal plates, including trapping plates, excitation plates and detector plates**

The resulting force,  $F$ , known as the Lorentz force (**Equation 1**) is the vector cross product of the magnitude of the magnetic field,  $B$ , and the ion's velocity,  $v$ , multiplied by the charge on the ion,  $ze$ .

**Equation 1**

$$F = ze v \times B$$

The combination of the Lorentz force and ion's initial velocity creates the cyclotron motion with the circular frequency dependent on ion's  $m/z$ . Using Newton's Second Law (**Equation 2**),

**Equation 2**

$$F = ze v \times B = m \frac{v^2}{r}$$

where  $r$  is the cyclotron radius here and  $v/r$  is the angular frequency,  $\omega$ , known here as the cyclotron frequency. As a result,

**Equation 3**

$$\frac{zeB}{m} = \omega$$



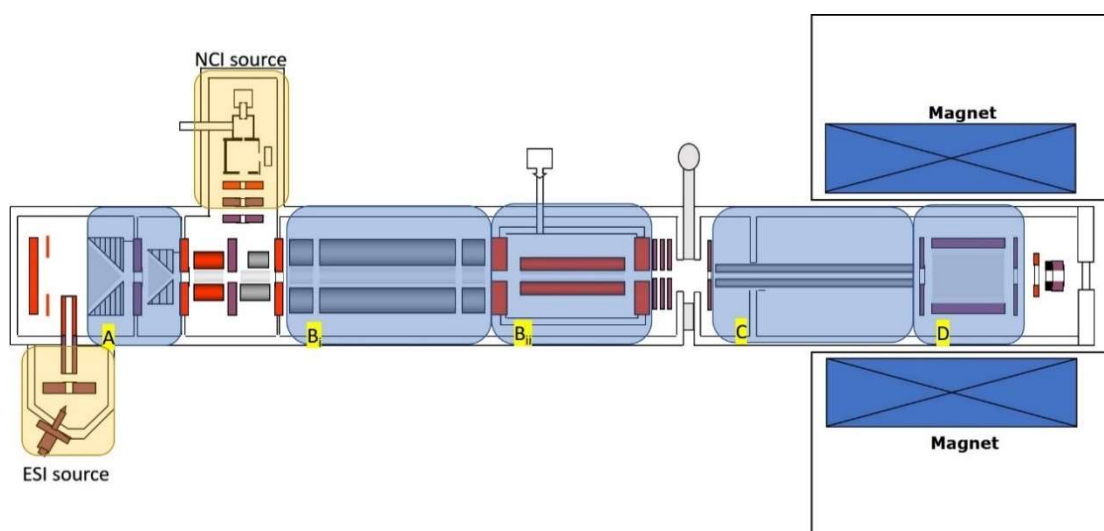
Therefore, by means of measuring the cyclotron frequency at constant magnetic,  $m/z$  can be determined using **Equation 3**, because there is no dependence on velocity, then there is no degradation of mass measurement by kinetic energy and thus velocity distribution, resulting in high mass resolution.

The cyclotron radius of an ion's motion in the initial state is usually too small for ion detection. Therefore, to determine the cyclotron frequency of ions, normally a range of frequencies are applied so that all ions over a range of  $m/z$  are excited in the measurement cycle. The energy from the RF potential only can be taken up by the ions when they have the same frequency as that of the RF. The cyclotron radius of the ions after excitation is independent of their  $m/z$  and dependent on the applied RF potential. As a result, the excited ions orbit with a larger cyclotron radius enabling detection.

The detection process in FT-ICR-MS is a non-destructive process, which means thousands or millions of measurements can be done on the same ions, enhancing the accuracy of  $m/z$  measurement. When ions orbit the z-axis, an image current is produced between the pair of detection plates and measured in time then converted into frequency by Fourier transformation. The frequency spectrum obtained is converted to a  $m/z$  spectrum by application of equation 3.

Bruker solariX XR FTMS equipped with 9.4 tesla magnet (Figure 14) was the mass spectrometer mainly used for identification of permethylated glycans in this present

thesis. The design of ICR cell (para cell) in Bruker solarix XR FTMS has been modified to equip with extra electrodes that are shaped so that the averaged electric field experienced by the ions produces a counter force to those caused by the inhomogeneous magnetic field, resulting in higher resolving power  $4 \times 10^7$  at  $m/z$  609 without the requirement for an upgrade to a higher field magnet.



**Figure 14. Scheme of Bruker solarix XR FTMS, (A) dual ion funnel source, for mass independent ion transfer, (B<sub>i</sub> and B<sub>ii</sub>) hybrid Qh-front end, a quadrupole mass analyzer (B<sub>i</sub>) hyphenated with a hexapole accumulation/collision cell (B<sub>ii</sub>) for mass dependent ion transfer/selection, conducting collisional induced dissociation, (C) hexapole ion transfer system and (D) the ICR cell.**

Bruker solarix XR FTMS equipped with a quadrupole mass analyzer hyphenated with a hexapole mass analyzer (hybrid Qh-front end) can perform the conventional collision-induced dissociation (CID) or collision-activated dissociation (CAD)<sup>153,154</sup>. Precursor ions were selected in the first quadrupole mass analyzer (Figure 14B<sub>i</sub>) and transmitted to the hexapole accumulation/collision cell (Figure 14B<sub>ii</sub>) for colliding

them with inert gas (argon) prior to the ion introduction into the ICR cell, acting as tandem-in-space mass spectrometry. In the collision process, an ions' kinetic energy is converted into internal energy, resulting in bond cleavages at weak linkages to obtain the structural information such as sequencing data.

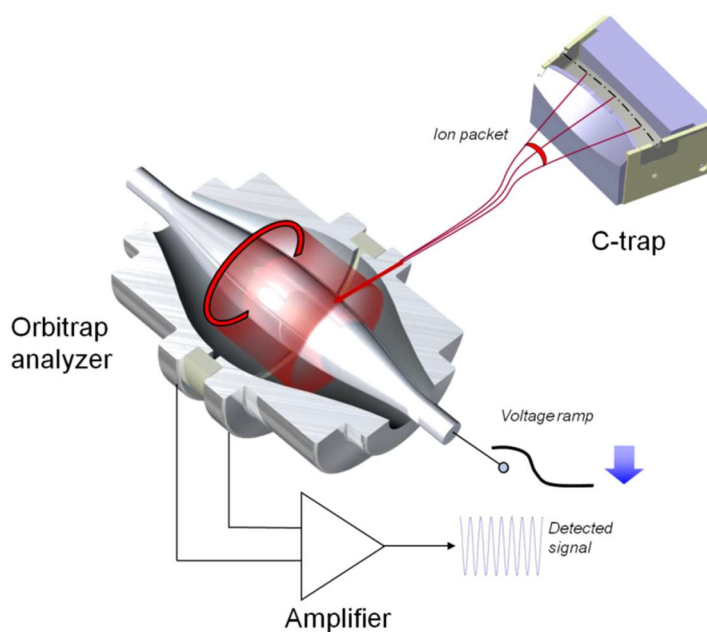
The ICR cell is also capable of performing another ion activation method for colliding precursor ions with inert gas (argon) inside the cell, so called sustained off-resonance irradiation (SORI) fragmentation. SORI is to activate precursor ions by application of an off-resonance electric pulse with a frequency slightly away from the observed ion-cyclotron frequency, typically by 300-2000 Hz<sup>155</sup>. In the duration of the pulse, the precursor ions act a series of acceleration-deceleration cycles with the presence of inert gas, results in continuous low energy collisions. The gas has to be pumped out before the detection excitation pulse is applied.

### 1.3.5 Orbitrap mass analyzer

The Orbitrap, invented by Alexander Makarov applying the concept of a Knight-style Kingdon trap<sup>121</sup>, is the registered trade mark for an ion trap mass analyzer<sup>156-159</sup>. The concept of a Knight-style Kingdon trap uses an electrostatic field for trapping ions allowing them to adopt harmonic oscillations along the z-axis<sup>157,158</sup>.

The Orbitrap consists of a spindle-like electrode covered by a coaxial barrel-like electrode, where the space between the two electrodes traps ions orbiting the inner electrode (Figure 15). The signal is measured by the detection of image current in

the time domain caused by the oscillating ions and is detected by the barrel-like electrode, the FT converts it to frequency, and equation 4 converts frequency to  $m/z$ . The induced image currents are detected over a period of time and improved by repeating the measurements or extending the measurement period.



**Figure 15. Cross-section of the C-trap and Orbitrap analyzer. The picture is obtained from ThermoFisher website<sup>6</sup>.**

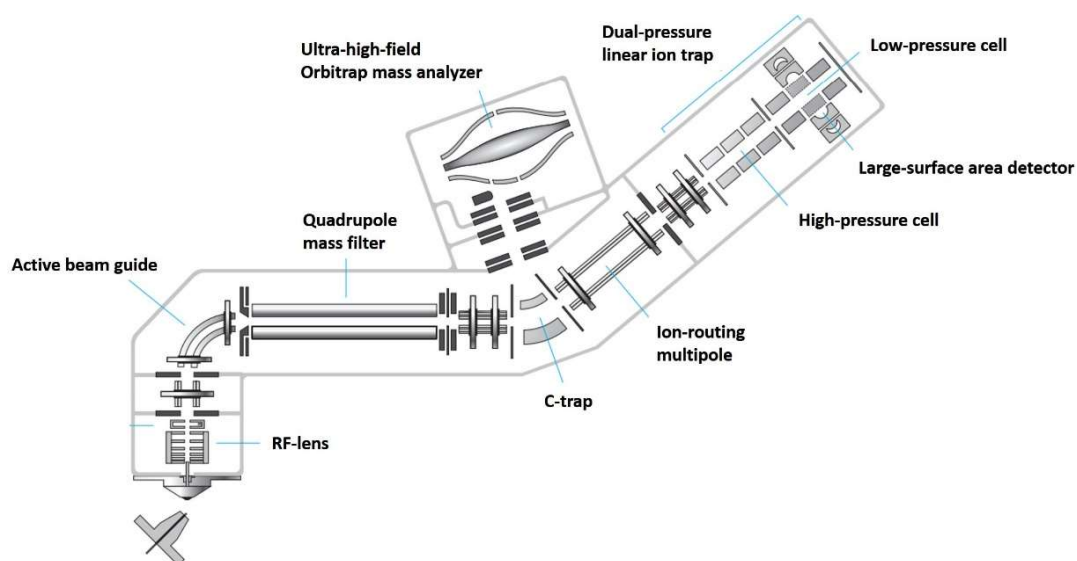
#### Equation 4

$$\omega' = \left(\frac{z}{m} k\right)^{\frac{1}{2}}$$

---

<sup>6</sup> <https://www.thermofisher.com/uk/en/home/industrial/mass-spectrometry/liquid-chromatography-mass-spectrometry-lc-ms/lc-ms-systems/orbitrap-lc-ms.html>

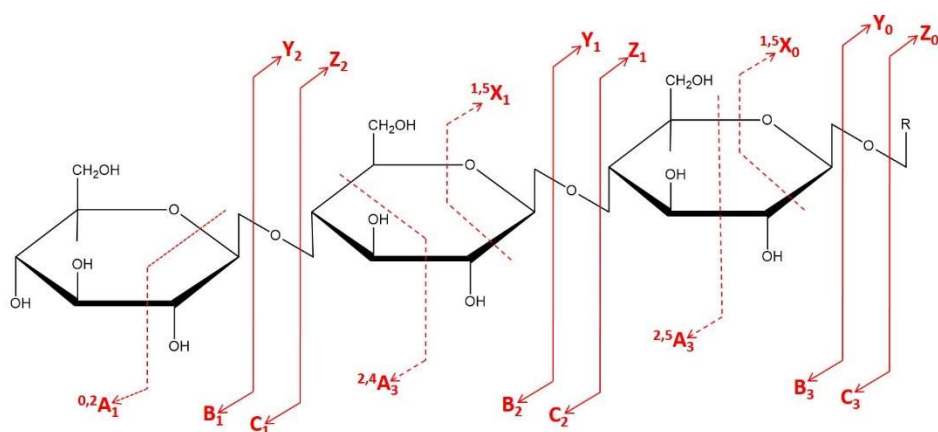
Thermo Scientific Orbitrap Fusion™ Tribrid™ is a hybrid mass spectrometer integrated with quadrupole, linear ion trap, and Orbitrap mass analyzers (Figure 16). In Orbitrap Fusion™ Tribrid™, ions are transmitted through the quadrupole mass filter into the ion-routing multipole, where the ions are stored and accumulated to be routed into a C-trap. In the C-trap, ions are collisionally cooled by gently colliding with gas molecules, to focus the ions before entering the chamber of the Orbitrap. In addition, the RF potential applied to the C-trap squeezes the ion packet in time and space, ready for injection into the Orbitrap. After a period of cooling and focusing, a DC potential from the C-trap forces the packet of ions into the Orbitrap mass analyzer, starting the harmonic oscillations to induce image currents for detection. Orbitrap Fusion™ Tribrid™ performs fragmentation of precursor ions in the ion-routing multipole for high energy collision-induced dissociation (HCD) or in the linear ion trap for CID with fragment detection in the linear ion trap or Orbitrap mass analyzers



**Figure 16. Scheme of Thermo Scientific Orbitrap Fusion™ Tribrid™. The picture is obtained from ThermoFisher website.**

### 1.3.6 Mass spectrometric fragmentation of carbohydrates

The commonly adopted nomenclature of fragmentation of carbohydrates was described by Domon and Costello (Figure 17)<sup>160</sup>. Fragmentation generally occurs on the either side of the glycosidic bond but also under more energetic conditions resulting in cross-ring cleavage.

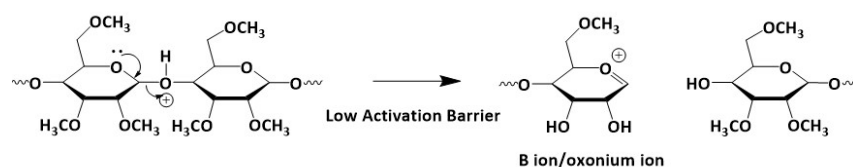


**Figure 17. Fragmentation nomenclature of oligosaccharides, recreated from Domon and Costello<sup>160</sup>**

The cleavage of glycosidic bonds, which needs the lowest energy, forms the most common non-reducing terminal B ions or reducing terminal Y ions. In the positive ion mode, single protonation of a glycosidic oxygen induces fragmentation of the glycosidic bond on the non-reducing side of the glycosidic oxygen. B ions (oxonium ions) are formed that contain the non-reducing terminus (Figure 18). Y ions,

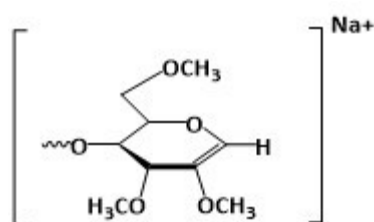
containing the reducing terminus, are produced on glycosidic cleavage with hydrogen transfer from the non-reducing portion of the molecule, to result in ions derived as summarised in Figure 17. The formation of B ions and Y ions tends to be observed even if the collision energy is too low to see other types of fragment ions. C ions and Z ions, produced by cleavage on the reducing side of the glycosidic oxygen, are less readily generated than B and Y ions. A ions and X ions are produced by cleavage across the ring, which requires the highest energy input. The subscript number indicates the number of monosaccharide residues in the fragment, e.g. B1 for the fragment of the non-reducing terminus and Y1 for the fragment of the reducing terminus.

The protonation of permethylated glycans has been described as being responsible for driving the in-source fragmentation of glycan ions<sup>161</sup>. Cancilla *et al.* suggested that protonated glycans undergo charge-driven dissociation more easily than sodiated glycans which undergo charge-remote dissociation<sup>137</sup> (Figure 18). Coordination of the proton by the oxygen of the glycosidic bond facilitates the cleavage of the glycosidic bond to form the oxonium ion, designated a B ion. In addition, from molecular simulation studies, Cancilla *et al.* reported that protonation at the glycosidic oxygen, which is the most basic site in the backbone of an oligosaccharide, would produce glycosidic bond cleavage as a result of the protonated glycosidic oxygen facilitating the delocalization of electrons on the ring oxygen<sup>137</sup>.



**Figure 18. Scheme of charge-driven dissociation by protonation, forming B ion/oxonium ion<sup>137</sup>**

The B ion is less readily formed from sodiated glycans since the sodium ion was determined to coordinate to more the ring and glycosidic oxygens and that acts as an energy barrier to the formation of the sodiated B ion<sup>137</sup>. When a B ion is derived from a sodiated glycan, possibly through charge-remote dissociation, the structure of the resulting B ion is not an oxonium ion like that derived from protonated glycans. The structure of the B ion derived from a sodiated glycan (Figure 19) is rationalized as deriving from an elimination reaction which forms a C1-C2 double bond, with the sodium ion carrying the charge<sup>162</sup>. The high energy required for fragmentation of sodiated glycan also results in cross-ring cleavages, deriving the information about linkages and functional groups' positions<sup>163,164</sup>.



**Figure 19. Putative structure of B ion derived from sodiated glycans**

Fragmentation of glycans forming rearrangement ions was reported by Kováčik *et al.*<sup>165</sup>. The internal glycosyl residues bound to both ends of other residues with glycosidic bonds are lost by CID (internal residue loss, IRL), forming the fragments



that can not be interpreted as regular  $B_i/Y_j$  glycosidic cleavage ions. Glycan fragments that are induced by IRL are hard to be identified because it requires the monosaccharide residues with different masses to compose the oligosaccharide, which is not common in *N*- and *O*-glycans. The formation of IRL was found to be independent on the linkage or the structure of the lost residue<sup>166</sup>, but dependent on the type of charge species<sup>162,167</sup>. Protonated and ammoniated oligosaccharides were found to undergo IRL by CID but not for sodiated oligosaccharides<sup>162,167</sup>.

The dissociation of carbohydrates can also be achieved in the source<sup>168,169</sup> or post-source<sup>119,170</sup> regions of a MALDI source. O'Connor's and Costello's groups have reported that elevating the pressure in the source region of a MALDI FTICR MS (IonSpec HiRes MALDI FTMS) from  $1 \times 10^{-7}$  mbar to  $1 \sim 10$  mbar during the MALDI ionization process decreased the extent of fragmentation of native sialoglycans compared to the same MALDI FTICR MS instrument with pressures less than 0.1 mbar<sup>171,172</sup>. The high background pressures in the ion source could collisionally cool the ions and result in less fragmentation of glycan ions. In addition, Soltwisch and Dreisewerd have reported that the source pressure in a UV/IR-MALDI-o-TOF mass spectrometer had influences on the types of fragment deriving from ionized peptides and native oligosaccharides (neo-lacto-*N*-fucopentaose II, LNF II)<sup>173,174</sup>.

## 1.4 Enzymatic shaving of cell surface for collection of cell surface glycans/peptides

Methods have been developed for collecting cell surface peptides/glycans for subsequent mass spectrometric analysis, with the aim of studying the biological functions and gaining structural information on cell surface molecules, exploring the mechanisms of cell-cell interactions, development of diseases, and biomarker discovery<sup>175–178</sup>. Many reports use membrane separation approaches to collect cell membrane glycans/peptides/proteins followed by mass spectrometric analysis. The cell membrane fraction containing membrane glycoproteins can be enriched using sequential centrifugation<sup>179,180</sup>. Lee *et al* reported that the cell lysate of rat liver tissue was centrifuged at  $2000 \times g$  to collect the supernatant containing the membrane fraction and followed by ultracentrifugation at  $120,000 \times g$  to collect the membrane pellets for solubilization of membrane proteins using the detergent Triton X-114. The enriched membrane protein solubilized in the detergent was partitioned into the detergent phase and the aqueous phase by incubation at  $37 \text{ }^\circ\text{C}$  for five minutes followed by centrifugation ( $300 \times g$  for five minutes), containing hydrophobic membrane proteins and GPI-anchored proteins, respectively, for following protein digestion and mass spectrometric analysis<sup>179</sup>. In a similar attempt, An *et al*. reported that the membrane (glyco)proteins of a cultured human embryonic stem cell lysate were enriched using sequential centrifugation to separate the cell membrane fraction from the nuclear and debris fractions ( $1000 \times g$ ), followed by multiple rounds of ultracentrifugation ( $200,000 \times g$ ) with the aid of  $\text{Na}_2\text{CO}_3$  to break up the microsome and collect the membrane pellets<sup>180</sup>. However, the enriched cell

membrane fraction obtained using centrifugation potentially contains membranes of other subcellular compartments, compromising the identification of cell membrane (glyco)proteins/peptides<sup>181</sup>. As a result, different approaches have been developed to collect cell membrane glycoproteins for subsequent glycan/protein analysis. Mun *et al.* reported an adhesion-based isolation of cell membranes, in which intact CHO cells were attached to a polylysine-coated glass plate prior to cell lysis using ice-cold water and washed with TBS to remove the intracellular organelles and the cell debris. The residual CHO cell membrane fraction on the glass plate was trypsinized to release glycopeptides followed by PNGase F digestion for *N*-glycan release prior to MALDI-MS analysis<sup>182</sup>. The resulting amount of oligomannose glycans was reduced, compared to those of *N*-glycans released from cell lysates (discussed in chapter 4).

The isolation of cell surface membrane proteins or glycans also can be achieved using biotin-avidin labelling or click chemistry. Non-covalent interaction with a high degree of affinity and specificity between water soluble biotin (vitamin H) and avidin/streptavidin (SA) is one of the most commonly used technique in chemistry and biology. Membrane proteins can be specifically modified with biotin-based reagents (biotinylation) for following detection with avidin-based reagents (fluorophore-, horseradish peroxidase-, or alkaline phosphatase-conjugates) or precipitation with avidin-coated solid supports. Biotinyl-*N*-hydroxy-succinimide ester (NHS-biotin), coupling of biotin and NHS, was early used to label lysines into several bacteriophages, lectins, and antibodies and has been the most popular biotinylating reagent for biotinylation of proteins<sup>183,184</sup>. Mi *et al.* reported that the membrane proteins of cultured hepatocellular carcinoma cells were labelled with

biotin groups, sequentially followed by cell lysis, centrifugation, protein extraction and tryptic digestion. The biotinylated membrane glycopeptides were enriched via affinity capture using immobilized avidin<sup>185</sup>. In a similar approach of cell surface molecule labelling, click chemistry uses biocompatible small molecule to linking substrates of membrane molecules in one pot and is not interrupted by water. Click chemistry was firstly defined by Sharpless *et al.* that the reaction needs to be modular, high yields, and generating only inoffensive byproduct in a water-only condition or solvent free condition. Carbon-heteroatom bond forming reactions comprise the foundation of click reaction by cycloaddition of unsaturated species, nucleophilic substitution, carbonyl chemistry and additions of carbon-carbon multiple bonds<sup>186-188</sup>. Wu's group reported a strategy that the cultured HEK293T cells were fed with a sugar analog containing an azido group (*N*-azidoacetylgalactosamine) to produce membrane proteins with azide groups, followed by labelling with dibenzocyclooctynesulfo-biotin using click chemistry under physiological conditions. The cultured HEK293T cells were lysed and digested to release surface glycopeptides with biotin tags for subsequent enrichment using avidin-modified beads and the release of *N*-glycans using PNGase F digestion in heavy-oxygen water. 144 *N*-glycopeptides containing 152 *N*-glycosylation sites were identified in 110 proteins in HEK293T cells<sup>189,190</sup>.

Although these methods attempted to collect/enrich the cell membrane/membrane protein, the glycans released from the enriched fraction can be from both the extracellular and intracellular domains, resulting in a glycan profile that may well not represent specifically the cell surface glycome. Moreover, these methods based on

cell membrane collection all involved the process of cell lysis and thus can not be performed on live cells or fresh tissues for the investigation of a live cell surface glycome.

Enzymatic shaving of the cell surface is an approach used to collect surface peptides/glycans while the cells remain intact, without releasing the intracellular components. The early method development of enzymatic shaving of the cell surface was to identify the surface peptides/proteins that extend beyond the cell wall and polysaccharide capsule of bacteria. Those surface peptides/proteins of bacteria are expected to play important roles in communicating and interacting with the environment and act as candidates for vaccine treatment<sup>191</sup>. The concept of using protease digestion to “shave” the cell surface was first reported by Rodríguez-Ortega *et al.*; the bacterium (*Streptococcus pyogenes*) was incubated with 20 µg trypsin or 5 µg proteinase K for 30 minutes at 37 °C to release surface peptides for peptide identification using nano-LC-MS/MS. 95% of the surface proteins identified after enzymatic shaving were predicted to belong to the categories of cell wall anchored proteins, lipoproteins, transmembrane-spanning proteins and secreted proteins using topological prediction analysis<sup>192</sup>. This treatment was reported not to impair bacterial integrity as assessed by plating the bacteria before and after protease digestion (data not reported in the paper)<sup>192</sup>. Several research groups have since applied enzymatic shaving of the cell surface, mostly using trypsinization, to study the surface proteins/peptides of bacteria<sup>193–195</sup>. In addition, Castro-Borges *et al.* reported that the live schistosome parasite was incubated with trypsin (Promega, trypsin MS, 5 mL of 10 µg/mL) or phosphatidylinositol-specific

phospholipase C to release the peptides from the parasite surface proteins or GPI-anchored proteins, respectively, for peptide identification using MALDI-MS. The membrane integrity of enzyme-treated parasites was reported to be minimally impaired, assessed visually under a dissecting microscope<sup>196</sup>.

Trypsinization is frequently applied to detach adherent cultured cells for passage to a new dish. The cells are suspended and appear rounded when trypsinization is complete. The surface proteins of cultured cells are often cleaved because of the proteolytic activity of trypsin, which leads to the approach of enzymatic shaving for the release of cell surface peptides/glycans from cultured cells. Blanchard's group reported a tryptic shaving-based method to release cell surface *N*-glycans from various cultured mammalian cell lines, followed by permethylation prior to MALDI-MS analysis, reporting a tryptic *N*-glycome released from the cell surface that was distinct from the total cell lysate *N*-glycome<sup>197</sup>. They reported that cell viability was no different for each cultured cell line tested before or after tryptic digestion, suggesting that the trypsin-aided release of *N*-glycans was mainly from the cell surface. The same approach was applied in a recent publication from Blanchard's group, comparing the cell surface *N*-glycome released from cultured human embryonic stem cells (hESCs) with cultured definitive endodermal cells (DECs), cultured hepatocyte-like cells (HLCs) and primary human hepatocytes (PHHs)<sup>198</sup>.

The authenticity of cell surface glycans/peptides released using tryptic shaving relies on the conditions used for trypsinization; there is of course a risk of releasing

intracellular (glyco)peptides if the cell membrane is compromised or damaged by trypsinization. In addition, trypsinization may induce stress on the treated cells, complicating the released surface glycans/peptides by the potential inclusion of components secreted or released from the surface by the stress.<sup>199,200</sup> Intracellular uptake of trypsin by cultured cervical cancer cells (HeLa cells) and mouse kidney cells was observed after trypsinization (37 °C) with fluorescein isothiocyanate-labelled or tritium acetyl-labelled trypsin.<sup>199</sup> Huang *et al.* reported that 36 proteins revealed a significant expression change in cultured breast cancer cells and HeLa cells after trypsinization (0.05% trypsin-EDTA for 10 min at 37 °C) followed by MALDI-MS identification<sup>200</sup>. Those findings demonstrate that the use of trypsin in cell culture practices, and for cell surface shaving may have noticeable or unnoticeable effects on cell physiology; methods for the identification of cell surface glycans/peptides following trypsinization of cells thus requires careful examination and of the effects on the cells.

## 1.5 Aim of this thesis

There is limited structural information reported on urothelial glycans; to date, only *N*-glycans have been identified on porcine urothelium and *in vitro* in cultured urothelial cells using MALDI-MS<sup>33,48,68,201</sup>. In this thesis, a comprehensive study was designed to identify urothelial glycans using fresh porcine urothelium, and analyzing with MALDI-MS for permethylated glycan identification.

In chapter 3, urothelial glycome was investigated by starting with *N*-glycans released from porcine urothelial cells collected from fresh porcine bladders using a scalpel. The scraping process was examined as an appropriate approach for the collection of urothelial cells without compromising underlying tissues using immunohistology. The collected urothelial cells were used for the release of total cell lysate *N*-glycans using the literature filter-aided *N*-glycans separation (FANGS) approach. The cell lysate *N*-glycan profile identified was the first normal mammalian urothelial *N*-glycome to be determined with molecular structural information.

In chapter 4 and 5, the subsequent work developed and demonstrated the validity of an approach to identify the apical cell surface *N*- and *O*-glycans on the luminal surface of porcine superficial urothelium using trypsinization in an in-house built reaction device. The apical cell surface *N*- and *O*-glycans identified are the products of highly polarized differentiated normal superficial urothelium, presenting a snapshot of the compositions of potential functional glycome on the urothelial cell apical surface.



Importantly, alongside the sample handling approaches and the semi-quantitative molecular analyses using MALDI-MS, histology/immunohistology approaches were used to demonstrate the origins of the collected urothelial glycans, and to demonstrate the effects of the different sample-treatment approaches on the porcine bladder urothelial cells. The results achieved in this study aimed to complement the to date only partial structural information on the urothelial glycome, and provides an insight into the polarized apical cell surface glycome that is potentially responsible for cell-cell biological functions.

## Chapter 2 Experimental procedures



## 2.1 Preparation of porcine urothelial cell lysate *N*-glycome

All fresh porcine bladders used in this thesis were obtained from a local abattoir (A. Traves & Son Ltd, Mansion House, Main Street, York, North Yorkshire, YO19 6TP) and transported in sealed plastic bags or bottles with ice bags outside. All porcine bladders were processed for collecting urothelial cells or conducting on-tissue trypsinization right after arrival in the laboratory. Autoclaved scissors and forceps were used to remove any unwanted body parts, fat and connective tissue. All animal waste was discarded in a sealed Petri dish and stored at -20°C prior to disposal.

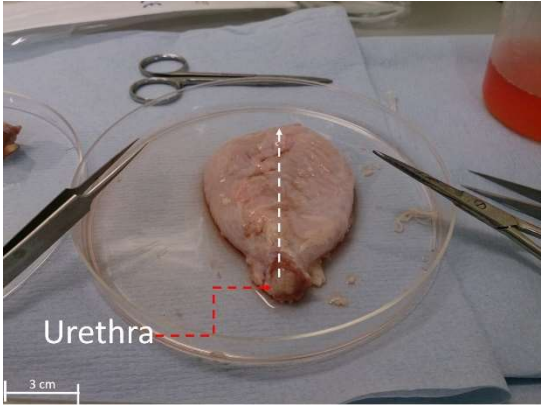

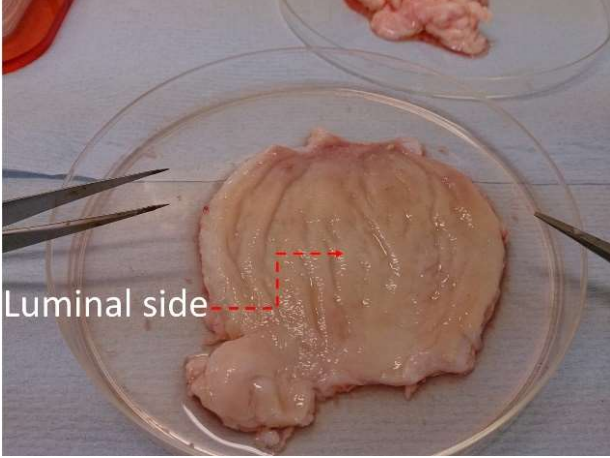
### 2.1.1 Collecting urothelial cells from porcine bladders

The porcine bladders were opened using scissors and cleaved from the urethra side (Figure 20A to C), exposing the luminal side of bladders for scraping. The luminal surface of the bladders was gently washed with 2 mL of phosphate-buffered saline (PBS).

A range of instruments including scalpels and dining knives was tested for the ability to gently scrape the luminal surface of the porcine bladders, physically detaching the urothelial cells for collection. A small amount of PBS was added onto the luminal surface of bladders to recover the urothelial cells; the collected porcine urothelial

cells from each bladder were divided into different aliquots (wet weight ~ 50 mg/vial, 16 ~ 20 vials/porcine bladder). The collected porcine urothelial cells were kept in -80 °C freezer for further processing.

**Figure 20. Porcine bladder dissection process**

A) Cutting from the urethra side	B) Open the bladder	C) Opened bladder
 <p>A photograph showing a porcine bladder in a petri dish. A vertical dashed white line indicates the cutting path. A red dashed box at the bottom is labeled "Urethra". A 3 cm scale bar is visible in the bottom left corner. Surgical instruments are present around the specimen.</p>	 <p>A photograph showing the porcine bladder being opened along the cutting line. The internal structure is partially visible.</p>	 <p>A photograph showing the fully opened porcine bladder. A red dashed box on the inner surface is labeled "Luminal side". Surgical instruments are visible on the left side.</p>

### 2.1.2 Releasing *N*-glycans from urothelial cell lysate using filter-aided *N*-glycan separation (FANGS)

The procedure of filter-aided *N*-glycan separation (FANGS) carried out for the studies described in this thesis, to release *N*-glycans from urothelial cell lysates, is based directly on the published procedure<sup>202</sup> with slightly modification. To make a cell lysate, one vial of collected porcine urothelial cells was heated in SDS lysis buffer (4% w/v sodium dodecyl sulfate, 100 mM dithiothreitol in 100 mM Tris.HCl at pH 7.6) at 95°C in a water bath or a heating block. The cell lysate was mixed well with exchange buffer (8 M urea in 100 mM Tris.HCl pH 7.6) in a ratio of 1:10 cell lysate to exchange buffer by volume. The cell lysate-exchange buffer mixture was transferred into an ultrafiltration device (one filter membrane device with one collection tube; Amicon Ultra-0.5, Ultracel-30 membrane, nominal mass cutoff 30 kDa, Millipore) for centrifugation. The centrifuge was operated at 14,000 x g for 10 min, transferring all of the mixture one x mL aliquot at a time, until all the mixture had passed through the ultrafiltration device.

The sample solution retained above the filter membrane was washed twice by the addition of 250 µL of exchange buffer and centrifugation. 300 µL of 40 mM iodoacetamide freshly prepared in exchange buffer was then mixed well with the sample solution above the filter membrane and the device left in the dark at ambient temperature for 15 min then centrifuged at 14,000 x g for 10 min. 250 µL of exchange buffer was added into the sample solution above the filter membrane and centrifuged for 10 min. The sample solution above the filter membrane was washed

four times by four successive additions of 250  $\mu$ L of 50 mM ammonium bicarbonate, followed by centrifugation at 14,000 x g for 10 min. The filter membrane device holding sample solution was transferred into a new collection tube and the sample solution above the membrane mixed with 100  $\mu$ L of 50 mM ammonium bicarbonate solution and 8 U of PNGase F (2 U/ $\mu$ L, made in Dr. Daniel Ungar's group). The whole device was sealed with Teflon tap and incubated at 37 °C overnight. After incubation, the digested sample solution was centrifuged first, then washed twice by successive addition of 250  $\mu$ L of water (HPLC grade) and centrifuged for 10 min. The released *N*-glycans were obtained in solution in the collection tube following centrifugation. The released *N*-glycan solution was dried using a vacuum centrifuge.

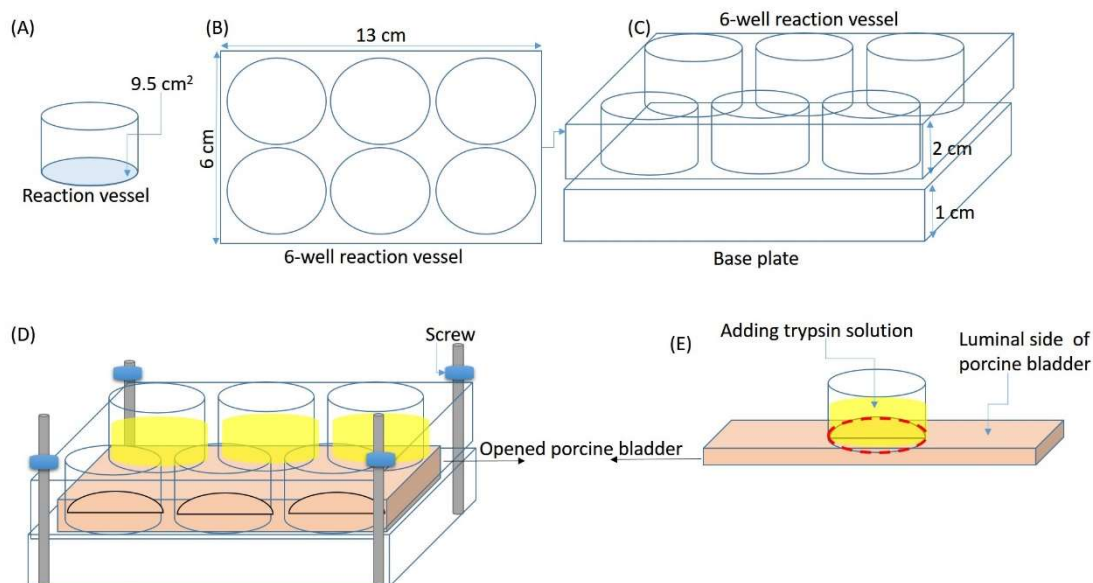


## 2.2 On-tissue trypsinization to release apical cell surface glycopeptides/peptides for subsequent sequential *N*- and *O*-glycan release

Developing methods for liberating apical cell surface glycopeptides from fresh porcine bladders was conducted using on-tissue trypsinization in an in-house built reaction device.

### 2.2.1 Device development

An in-house built reaction device (Figure 21) based on a conventional 6-well cell culture vessel was designed and made to hold firmly an opened porcine bladder and retain trypsin solution on the luminal side of porcine bladders for a period of time, to attempt to liberate apical cell surface glycopeptides/peptides from the superficial surface of the urothelium. Each of six-reaction vessels with a 9.5 cm<sup>2</sup> tissue-contact surface area (Figure 21A) in a 13 cm × 6 cm six-reaction vessel (Figure 21B) was assembled with a base plate as an on-tissue trypsinization device (Figure 21C). Porcine bladders were clamped tightly between the six-reaction vessel and the tissue holding tray (Figure 21D), preventing the leak of trypsin solution (Figure 21E). The in-house built reaction device was designed by the author and fabricated in cooperation with Timothy Ayers (Electronics Workshop, Department of Chemistry, University of York).

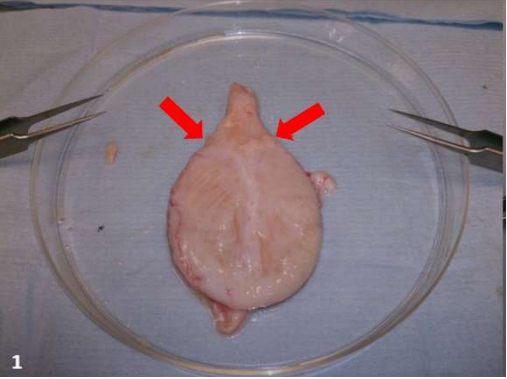
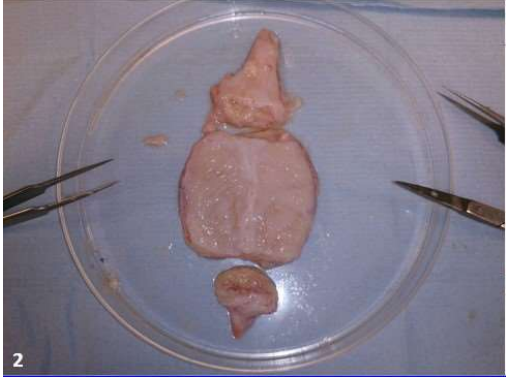
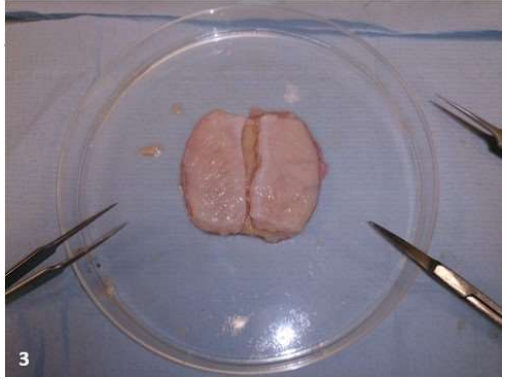
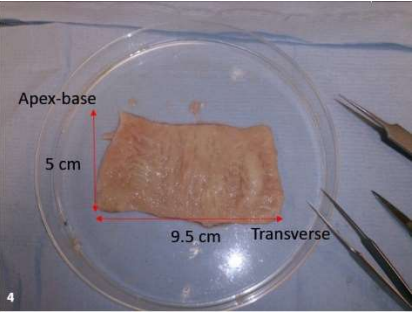


**Figure 21. Design of on-tissue trypsinization vessel. Each of six-reaction vessels with a 9.5 cm<sup>2</sup> tissue-contact surface area (A) in a 13 cm × 6 cm six-reaction vessel (B) was assembled with a base plate as an on-tissue trypsinization device (C). Porcine bladders were clamped tightly between the six-reaction vessel and the tissue holding tray (D), preventing the leak of trypsin solution (E). The in-house built reaction device was designed by the author and fabricated in cooperation with Timothy Ayers (Electronics Workshop, Department of Chemistry, University of York).**

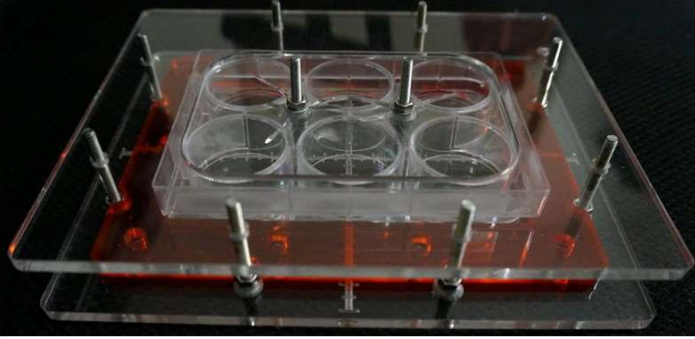
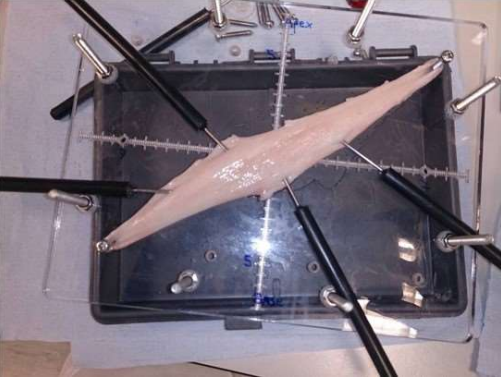


## 2.2.2 Tissue stretching process

Applying force to stretch and flatten the luminal surface of porcine bladders was attempted to expose an even luminal bladder surface for trypsin-aided glycopeptide release. A different way to dissect the porcine bladder, learned from Ashley Ward<sup>203</sup>, in order to shape the opened bladder into a rectangle is depicted in Figure 22A to D; this involves removing the top side approximately above the ureters (red arrow) and the bottom side and cutting through the vertical central line. The rectangular shape aimed to distribute the strain induced by the stretching evenly across the bladder. The process of stretching bladders using a modified reaction device is shown in Figure 23 ; this involves a modified device with a ruler-marked plate (Figure 23B) on which to fix the stretched bladders with pins and stretching the bladder slowly from two diagonally opposite corners until the whole bladder was equally expanded (Figure 23C). In order to flatten further the stretched bladder, an additional plate (the orange plastic surface seen in Figure 23D) was added. A further discussion of the stretching process is in chapter 5.

**Figure 22. Dissecting process of porcine bladders into a rectangular shape**

A) The undissected bladder	B) Removing the top and bottom	C) Cutting through the central line
 <p>1</p> <p>A photograph of a whole porcine bladder in a petri dish. Two red arrows point to the top and bottom poles of the bladder. The number '1' is in the bottom-left corner.</p>	 <p>2</p> <p>A photograph showing the bladder in a petri dish with the top and bottom portions removed. The number '2' is in the bottom-left corner.</p>	 <p>3</p> <p>A photograph showing the bladder in a petri dish, cut along its central longitudinal line. The number '3' is in the bottom-left corner.</p>
D) Rectangular opened bladder		
 <p>4</p> <p>Apex-base 5 cm 9.5 cm Transverse</p> <p>A photograph of the rectangular opened bladder in a petri dish. Red dimension lines indicate a height of 5 cm (labeled 'Apex-base') and a width of 9.5 cm (labeled 'Transverse'). The number '4' is in the bottom-left corner.</p>		

**Figure 23. The process of stretching the porcine bladder**

A) The undissected bladder	B) Removing the top and bottom	C) Cutting through the central line
 A photograph showing a porcine bladder in a clear plastic tray. The bladder is partially submerged in a red liquid. The tray has several metal pins or clamps around its perimeter.	 A photograph showing the bladder being stretched across a metal frame. The top and bottom edges are being held by clamps. A central line is visible, indicating where it will be cut.	 A photograph showing the bladder after being cut along its central line. The bladder is now a flat, rectangular sheet stretched across the metal frame.
D) Rectangular opened bladder		
 A photograph showing the final rectangular opened bladder. It is placed on a red tray with a ruler for scale. The ruler has markings in centimeters. The text "SHATTER RESISTANT" is visible on the ruler. Labels "Apex-base" and "Transverse" are present on the tray.		

### 2.2.3 On-tissue trypsinization

5 mg/mL trypsin solution used for conducting on-tissue trypsinization was prepared by diluting 25 g/L trypsin solution (Sigma, Cat#T4549, 0.9% sodium chloride solution, suitable for cell culture) with Hank's balanced salt solution (HBSS, Gibco, Cat#2402091). 1 mL of prepared 5 mg/mL trypsin solution was pre-warmed at 37 °C for 5 minutes and added into one of the six reaction vessels, covering the underlying luminal side of porcine bladders. Trypsinization was carried out for different incubation times at 37 °C. Supernatants were collected and heated to deactivate trypsin at 99 °C for 5 min. Supernatants were subjected to PNGase F digestion and  $\beta$ -elimination sequentially to release *N*- and *O*-glycans from the same sample solutions. The released glycan pools were purified using solid phase extraction (SPE) cartridges packed with graphitized carbon (Supelco, Cat#57094). The resulting *N*- and *O*-glycans were permethylated and purified with using C18 SPE cartridges (Supelco, Cat#57064) prior to MALDI-MS analysis.

## 2.3 Fractionated *N*-glycome analysis

Cultured Chinese hamster ovary (CHO) cells for method development were generated in Dr. Daniel Ungar's group in Biology and kindly provided by PhD student Peter Fisher.

CHO cells were grown in Hams F12 media (Lonza) containing 5% fetal bovine serum (life technologies) and 1% penicillin/streptomycin (life technologies).

Cultured bladder cancer RT4 cells were kindly provided by Mrs. Ros Duke from the Jack Birch Unit, Department of Biology. Bladder cancer RT4 cells were cultured in DMEM:RPMI medium prepared by adding 25 mL fetal bovine serum and 5 mL L-glutamine into 250 mL RPMI 1640 medium and 250 mL Dulbeccos modified eagles medium (DMEM).

### 2.3.1 Whole cell surface shaving of CHO cells

Approximately  $1\sim 2 \times 10^6$  CHO cells (80 – 90% confluency) cultured in a culture dish were washed four times with pre-warmed PBS (37 °C) before tryptic shaving. 1 mL of 0.5 mg/mL trypsin solution containing EDTA (Gibco, Cat#15400-054) was used to cover the surface of CHO cells in a culture dish. Trypsinization for liberating cell surface glycopeptides/peptides was carried out for different incubation times at 37 °C. Supernatants were separated from digested CHO cell pellets by centrifugation at  $20000 \times g$  at 4 °C for 15 min; recovered digested cell pellets were collected for

subsequent FANGS. Trypsin in the supernatant was deactivated at 99 °C for 5 min. *N*-glycans in supernatants were released using PNGase F and separated from cell surface peptides using C18 SPE cartridges (Supelco, Cat#57064); resulting surface *N*-glycans were permethylated and analyzed using MALDI-MS.

## 2.4 Glycan release

### 2.4.1 *N*-glycan release: PNGase F digestion

All PNGase F digestion releasing *N*-glycans from samples in this thesis were carried out with addition of 4 μL of 2 U/μL PNGase F (stored in 5 mM potassium phosphate, pH 7.5). All samples were incubated at 37 °C for at least 16 hours.

### 2.4.2 O-glycan release: β-elimination (applied in on-tissue trypsinization of fresh porcine bladder)

β-elimination to release O-glycans from urothelial cell lysates, is based largely on the published procedure<sup>68</sup>. 300 μL NH<sub>4</sub>OH (28~30%, Sigma-Aldrich) was added into vacuum-dried samples containing glycopeptides and released *N*-glycans. The resulting solution was sonicated in a sonication bath (give type and manufacturer) temperature controlled at 45 °C for 5 minutes and then left for incubation for 10 minutes. Temperature control of the sonication bath was aided by an external water circulating system maintained at 41 ~ 42 °C. The cycle of 5 minutes-



sonication/10 minutes-incubation was repeated four times to give a total 20 minutes sonication time and 40 minutes incubation time.

## 2.6 Glycan sample preparation

### 2.6.1 C18 SPE method for separating glycans from peptides

The glycans released after PNGase F digestion or  $\beta$ -elimination were retrieved using C18 SPE columns to remove the peptides. The C18 cartridges were primed with 6 mL methanol (MeOH) and followed by 6 mL of MeOH/HPLC-grade water (1 : 1, volume : volume). The C18 cartridges were conditioned with 6 mL of 100% HPLC-grade water prior to loading the sample solutions. The flowthrough containing unretained glycans was collected and dried using a vacuum centrifuge (give details – type, manufacturer, temperature used).

### 2.6.2 C18 SPE method for purification of permethylated glycans

This purification of permethylated glycans was only necessary for those glycans produced during on-tissue trypsinization, and was carried out largely as described in ref<sup>204,205</sup>. The permethylated glycans were dried and reconstituted in 200  $\mu$ L of MeOH/HPLC-grade water (1 : 1, volume : volume). The C18 cartridges were primed with 6 mL MeOH and followed by 6 mL acetonitrile (ACN). The C18 cartridges were conditioned with 6 mL 100% HPLC-grade water prior to loading the sample solutions. The sample solutions were carefully loaded onto the cartridges and sequentially

washed with 5 mL HPLC-grade water, 2 mL 15% ACN in water, 2 mL of 25% ACN in water. The samples were eluted with 2 mL 50% ACN in water and collected. The collected eluent containing the glycans were dried prior to MALDI-MS analysis.

### 2.6.3 Carbon SPE method for desalting released glycans

Underivatised glycans released using PNGase F digestion or  $\beta$ -elimination were desalted using carbon SPE cartridges<sup>206</sup>. The sample solution was dissolved in 2 mL HPLC-grade water. The carbon cartridges were sequentially primed with a) 6 mL ACN, b) 6 mL ACN with 0.1% trifluoroacetic acid (TFA), c) 6 mL of HPLC-grade water, d) 6 mL of 50% ACN in HPLC-grade water with 0.1% TFA, e) 6 mL of 5% ACN in HPLC-grade water with 0.1% TFA and f) 6 mL of HPLC-grade water. The sample solution was loaded onto the cartridge and sequentially washed with 2 mL of HPLC-grade water and 1.5 mL of 5% ACN in HPLC-grade water with 0.1% TFA. The glycan fraction was eluted with 3 mL of 50% ACN in HPLC grade water with 0.1% TFA and dried for permethylation.

### 2.6.4 Permethylation

The method of permethylation was reported by Hakomori<sup>117</sup> in which the reaction was catalysed by methylsulfinyl carbanion in dimethyl sulfoxide. An improved and shorter version of permethylation was reported by Dell *et al*<sup>205</sup> and followed here with slight modifications. All samples were vacuum dried in glass reaction tubes

prior to permethylation. 1 mL of DMSO (approximately 40 drops) was added into the reaction tube to reconstitute the dried sample. Finely ground NaOH (approximately 10 ~ 20 mg) was added to the sample solution, followed by addition of 10 drops of iodomethane (CH<sub>3</sub>I). The solution was gently shaken and left to stand for 10 minutes. Another 10 drops of iodomethane were added, vortexed and left to stand for 10 minutes. A final 20 drops of iodomethane were added to the sample solution, again gently mixed, and left to stand for 20 minutes. The reaction was quenched with the slow addition of 1 mL 100 mg/mL sodium thiosulfate solution. 1 mL dichloromethane (DCM) was added into the sample solution, and vortex mixed, to extract the permethylated glycans. The (upper)aqueous layer was removed and the organic layer was washed with 2 mL of HPLC-grade water, repeating four times. The organic layer containing the permethylated glycans was dried using vacuum centrifugation, for subsequent MS analysis.

## Chapter 3. Normal mammalian urothelial *N*-glycome

In the work described in this thesis, *N*-glycosylation in urothelium has been studied in order to better understand the contribution it makes to urothelial barrier function. Prior to this work, the *N*-glycosylation of uroplakins and the relative expression levels of various *N*-glycans in different cultured urothelial cancer cell lines are the only two studies of the *N*-glycome that have been reported in the literature. There is very limited knowledge of the normal mammalian urothelial *N*-glycome (see chapter 1.1: urothelial *N*-glycans); a full definition of the normal urothelial glycome is not available. This chapter provides a definition of the first normal mammalian urothelial cell *N*-glycome using porcine bladders as study subjects.

### 3.1 The *N*-glycome of whole lysed porcine urothelium

For biological replicates, three different fresh porcine bladders were obtained from a local abattoir (A Traves & Son Ltd, YO19 6TP). Fresh porcine bladders (biological replicates) were processed by tissue dissection and urothelial isolation immediately on return to the laboratory. The collected porcine urothelial cells from each of three bladders were divided into different aliquots (wet weight ~ 50 mg/vial, 16 ~ 20 vials/porcine bladder) side by side and designated Uro1, Uro2 or Uro3, depending on the bladder. For technical replicates, three aliquots of urothelial cells from each of the three bladders were used side by side for *N*-glycan release using established filter-aided *N*-glycan separation (FANGS). The released *N*-glycans were permethylated and analyzed on a MALDI FTICR MS (solariX XR).

### 3.1.1 Collecting urothelial cells from fresh porcine bladders

Collection of porcine urothelial cells from fresh porcine bladders was carried out using scalpels and other instruments. The histological appearance of porcine bladders before and after scraping was examined by immunohistology with haematoxylin and eosin (H&E) stain in order to collect evidence of cell removal without damage to the underlying tissue of the basal lamina. The histological appearance of the porcine bladders was considered to be acceptable if it showed removal of the porcine urothelium without damage to the underlying connective tissues.

The surface appearance of H&E stained porcine bladders showed an intact layer of urothelium before scraping (Figure 24A) and an intact stromal surface with very little damage once scraped using a scalpel (Figure 24B). By contrast, the H&E results of porcine bladders scraped using kitchen knives and lab spatulas suggested that these two types of instruments were not capable of collecting urothelial cells efficiently, with either a thin layer of residual urothelial cells remaining (Figure 24C), and almost intact layers of urothelial cells on porcine bladders (Figure 24D), respectively.

The collection of exclusively urothelial cells without including underlying connective tissues was further examined, by determining the presence of basement membrane, which sits between the urothelium and the underlying connective tissues<sup>207,208</sup>. Type IV collagen (Col IV), one of the components of the basement membrane<sup>209,210</sup>,

has been examined and found in monkey<sup>207</sup> and human bladders<sup>208</sup>, presenting a potential target to examine the basement membrane in the scraped porcine bladders.

Immunolabeling using anti-collagen IV (Abcam, Ab6586)<sup>7</sup> antibody, raised against human Col IV, was conducted on human and porcine bladders in this study. Specimens of human ureters were used to examine the immunolocalisation of anti-collagen IV antibody (kindly provided by Jessica Jinks in the Jack Birch Unit, Department of Biology, who is qualified in handling human tissues).

The results of Col IV immunolabeling of experimental and control groups show the tissue sections with (experimental) and without (control) using the primary antibody, respectively, in order to demonstrate there was no non-specific staining by the secondary antibody and staining reagents (Figure 25). An intense labeling by Col IV (red arrow) was shown between the human urothelium and the underlying connective tissues (Figure 25A), suggesting that this antibody is capable of labeling the Col IV in human basement membrane. However, less intense labeling of Col IV was shown in porcine bladder before scraping, along with light background staining in the layers of porcine urothelium and underlying connective tissues (Figure 25B). The damaged area of the porcine bladder that was noted before scraping, which was probably caused by the process of antigen retrieval and exposed the surface of the basement membrane, showed enhanced labeling of Col IV. It may suggest that the

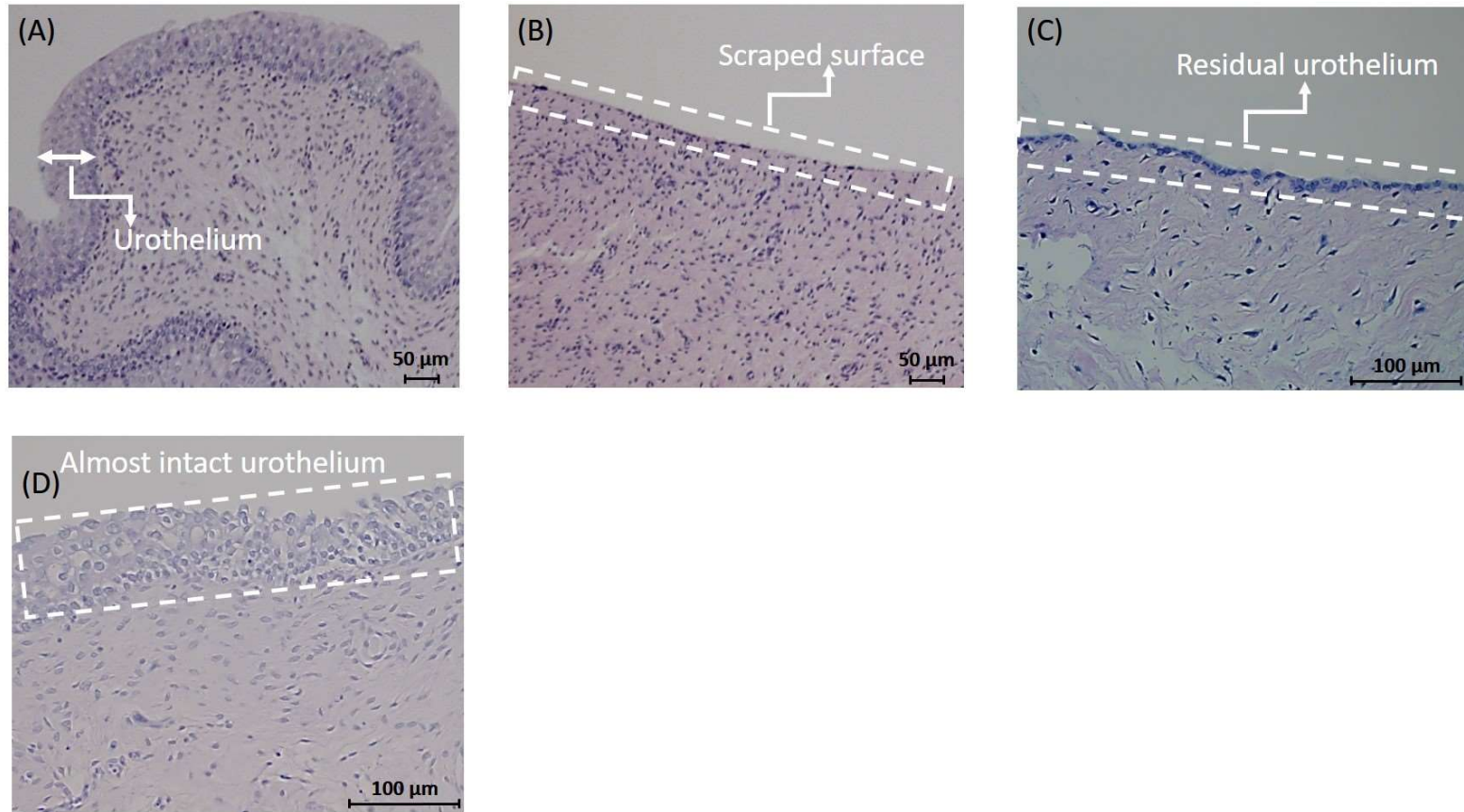
---

<sup>7</sup> Antigen retrieval was conducted by using the microwave-citric acid method and followed by using the primary antibody with a dilution factor 1 in 1000.

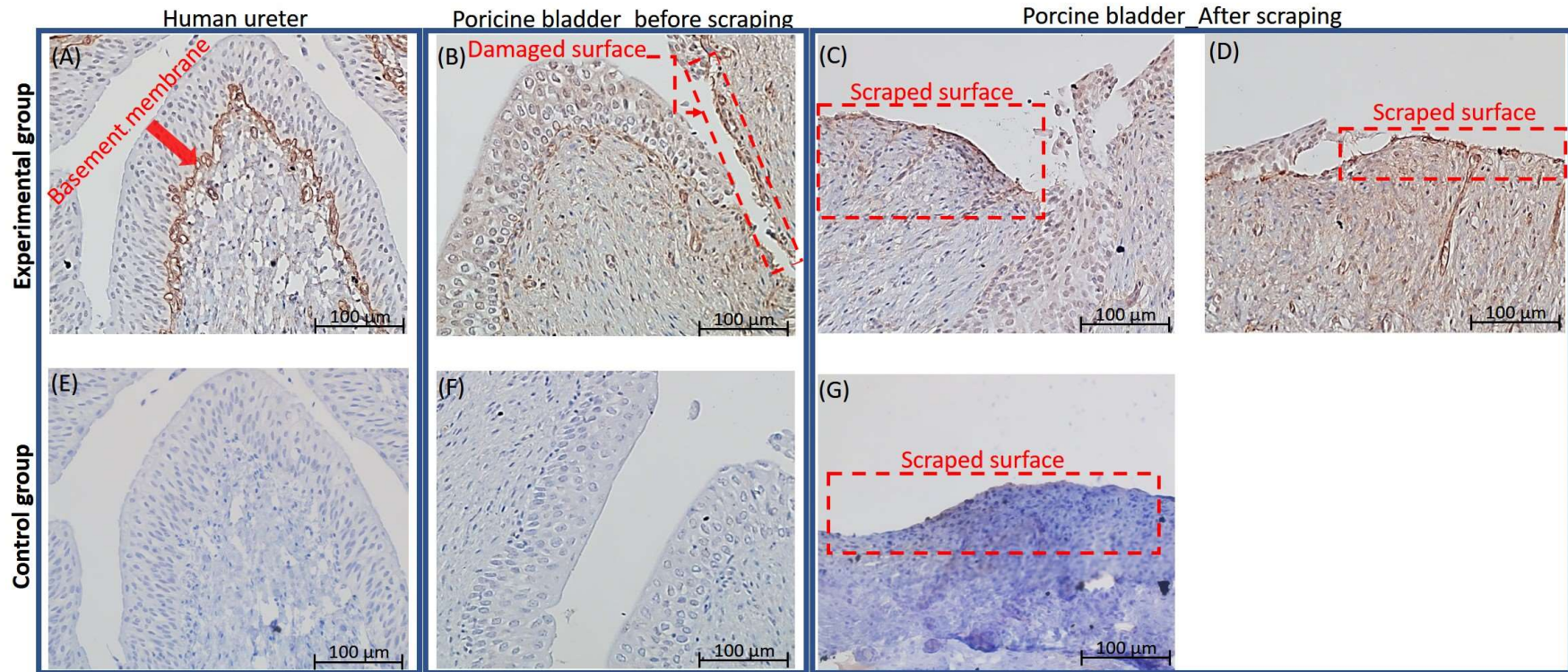
epitope of porcine Col IV required for the interaction with primary antibody is partially masked in porcine tissue.

A similar extent of positive labeling by Col IV as in the damaged area of the porcine bladder before scraping was shown in the scalpel-scraped porcine bladders (Figure 25C and D, two biological replicates), suggesting that the basement membrane still remained on the scalpel-scraped surface of porcine bladders. There was no noticeable positive labeling of Col IV in any of the control groups, suggesting that there was no false positive reaction caused by non-specific binding of the secondary antibody or adsorption of staining reagents on the scalpel-scraped surface of porcine bladders. As a result, it was concluded that the porcine urothelial cells collected using a scalpel were not compromised by inclusion of the underlying connective tissues and were thus used as the source of normal mammalian urothelial cells used for subsequent studies.





**Figure 24. H&E stained images of porcine bladder (A) before scraping, (B) after scraping using a scalpel (C) after scraping using a kitchen knife, and (D) after scraping using a lab spatula.**



**Figure 25. Immunolabeling of porcine bladders using anti-collagen IV antibody (Ab6586, 1/1000). Experimental group (using the antibody): (A) human ureter, (B) porcine bladder before scraping, (C) porcine bladder after scalpel scraping and (D) replicate of porcine bladder after scalpel scraping. Control group (without using the primary antibody): (E) human ureter, (F) porcine bladder before scalpel scraping and (G) porcine bladder after scalpel scraping.**

### 3.1.2 Porcine urothelial total cell lysate *N*-glycome

Three individual porcine bladders (Uro1, Uro2 and Uro3) were used to be the biological replicates for investigating the *N*-glycan profiles of porcine urothelium released using FANGS. Three individual aliquots of porcine urothelial cells from each biological replicate were analyzed using FANGS as technical replicates. Representative MALDI mass spectra obtained from three individual porcine bladders revealed 46 different urothelial *N*-glycans taking the three biological replicates together, and the proposed structures for the glycans represented by the most intense peaks are depicted in Figure 26. Proposed *N*-glycan structures were obtained using the GlycoWorkbench software and their mass accuracies manually checked. The total of 46 different *N*-glycans identified across the three biological replicates Uro1, Uro2 and Uro3, include oligomannose, hybrid, and complex *N*-glycans. The most intense peaks in all the mass spectra of porcine urothelial *N*-glycans can be assigned as oligomannose *N*-glycans at  $m/z$  1579.79 (Hex<sub>5</sub>HexNAc<sub>2</sub>), 1783.89 (Hex<sub>6</sub>HexNAc<sub>2</sub>), 1987.99 (Hex<sub>7</sub>HexNAc<sub>2</sub>), 2192.09 (Hex<sub>8</sub>HexNAc<sub>2</sub>) and 2396.20 (Hex<sub>9</sub>HexNAc<sub>2</sub>). In addition, an intense peak for disialylated monofucosylated biantennary complex *N*-glycan was observed at  $m/z$  2966.45 (Hex<sub>5</sub>HexNAc<sub>4</sub>FucNeuAc<sub>2</sub>).

The relative percentages of those porcine urothelial total cell lysate *N*-glycans common to all three biological replicates are shown in Figure 27. The semi-quantification of each *N*-glycan was calculated using the following method: 1) the peak intensities of the different isotopic signals with the signal-to-noise ratio > 5 from

the isotopic envelope of each *N*-glycan species were summed to generate a total signal intensity for each *N*-glycan species (denoted as  $\Sigma_i$ ), 2) the total peak intensities of all those *N*-glycan species common to all three biological replicates were summed for each spectrum (denoted as  $\Sigma_T$ ), and 3) this sum of peak intensities ( $\Sigma_T$ ) was used to normalize the intensity of the signal for each *N*-glycan species ( $\Sigma_i$ ) within the same MALDI mass spectrum. The normalized signal intensities for each *N*-glycan species from triplicate MALDI spots were averaged and the mean was used to derive the relative percentages of *N*-glycans in one technical replica. The relative percentages of *N*-glycans from three technical replicates were averaged for each biological replica and plotted using Excel; the error bars indicate standard deviation of the mean. Small standard deviations ( $n=3$ ) were obtained among technical replicates for each *N*-glycan structure, demonstrating that the FANGS approach is capable of giving high reproducibility of mass spectra which is in line with the studies by Rahman *et al.*<sup>202</sup> and Skeene *et al.*<sup>68</sup>.

The most abundant *N*-glycans in each biological replica were the complex *N*-glycans that represented 55.0%, 61.6% and 56.9% of the common *N*-glycome in Uro1, Uro2 and Uro3, respectively. The proportion of oligomannose *N*-glycans was 37.7%, 30.0% and 38.3% in Uro1, Uro2 and Uro3, respectively. The proportion of hybrid *N*-glycans was less than 5% in all samples. It is worth noting that the ~3-5 % *N*-glycan structures smaller than Hex<sub>2</sub>HexNAc<sub>5</sub> were presumed to be degraded *N*-glycans and not categorized into any groups.

Most *N*-glycan structures were highly reproducible in all three biological replicates. Of these 46 *N*-glycans, 29 were present in all biological replicates and are shown with their mass accuracies in Table 9. Seven *N*-glycans were obtained in two of the three biological replicates, with *m/z* at 1345.67 (Hex<sub>3</sub>HexNAc<sub>2</sub>Fuc), 1416.71 (Hex<sub>3</sub>HexNAc<sub>3</sub>), 1794.90 (Hex<sub>4</sub>HexNAc<sub>3</sub>Fuc), 2070.04 (Hex<sub>5</sub>HexNAc<sub>4</sub>), 2227.11 (Hex<sub>4</sub>HexNAc<sub>4</sub>NeuAc), 2489.21 (Hex<sub>5</sub>HexNAc<sub>5</sub>Fuc), and 3054.52 (Hex<sub>6</sub>HexNAc<sub>5</sub>FucNeuAc). Ten *N*-glycans were only obtained in one of the three biological replicates, with *m/z* at 1998.99 (Hex<sub>5</sub>HexNAc<sub>3</sub>Fuc), 2011.99 (Hex<sub>4</sub>HexNAc<sub>3</sub>NeuGc), 2197.10 (Hex<sub>3</sub>HexNAc<sub>4</sub>FucNeuAc), 2214.11 (Hex<sub>4</sub>HexNAc<sub>4</sub>Fuc<sub>2</sub>), 2216.09 (Hex<sub>5</sub>HexNAc<sub>3</sub>NeuGc), 2274.14 (Hex<sub>6</sub>HexNAc<sub>4</sub>), 2326.18 (Hex<sub>3</sub>HexNAc<sub>6</sub>Fuc), 2809.40 (Hex<sub>5</sub>HexNAc<sub>4</sub>FucNeuAc), 2822.39 (Hex<sub>5</sub>HexNAc<sub>4</sub>NeuAcNeuGc), 3026.49 (Hex<sub>5</sub>HexNAc<sub>4</sub>FucNeuGc<sub>2</sub>). Those seventeen *N*-glycans identified in one or two biological replicates were generally less than 1% of averaged total intensities of all *N*-glycans in each biological replicate and had low absolute signal intensities (< 10<sup>6</sup>), being considered as very low abundance of urothelial *N*-glycans in the total cell lysate *N*-glycans.

One particular monosialylated monoantennary *N*-glycan identified in the three biological replicates, Hex<sub>3</sub>HexNAc<sub>3</sub>NeuAc, was not reported in previous urothelial *N*-glycan studies but was identified in native form on human neutrophil cathepsin G (nCG)<sup>211</sup> and human bone marrow-derived mesenchymal stem cells (MSC)<sup>212</sup> using LC-MS/MS and MALDI-MS, respectively. Uro2 contains particularly low percentages of Hex<sub>5</sub>HexNAc<sub>2</sub> and Hex<sub>5</sub>HexNAc<sub>4</sub>FucNeuAc<sub>2</sub> and more different complex *N*-glycan species (Hex<sub>5</sub>HexNAc<sub>3</sub>Fuc, Hex<sub>4</sub>HexNAc<sub>3</sub>NeuGc, Hex<sub>4</sub>HexNAc<sub>4</sub>Fuc<sub>2</sub>, Hex<sub>6</sub>HexNAc<sub>4</sub>, Hex<sub>3</sub>HexNAc<sub>6</sub>Fuc, Hex<sub>5</sub>HexNAc<sub>4</sub>FucNeuAc, Hex<sub>5</sub>HexNAc<sub>4</sub>NeuAc,

Hex<sub>5</sub>HexNAc<sub>4</sub>FucNeuGc and Hex<sub>6</sub>HexNAc<sub>5</sub>FucNeuAc) when compared to Uro1 and Uro3. Since the three porcine bladders were collected and processed at the same time, this difference is likely to be caused by individual biological differences and not by sample preparation, since there is small standard deviation in technical triplicates.

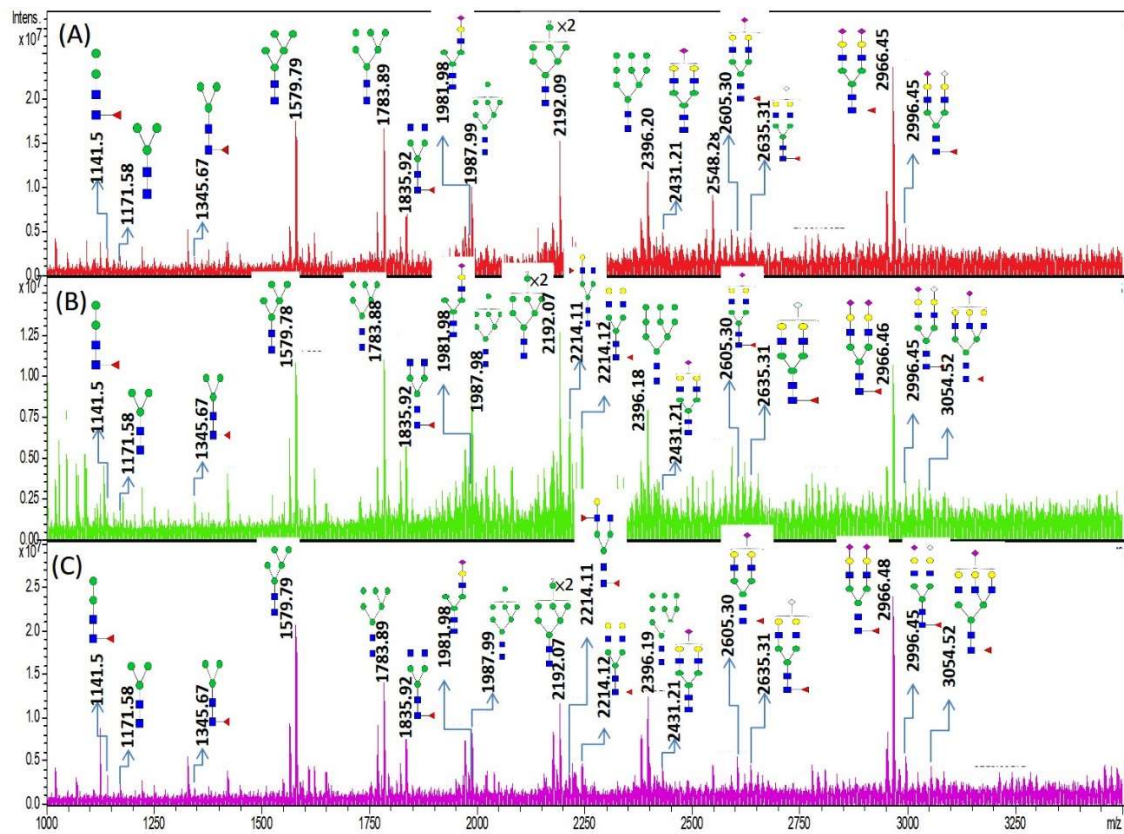


Figure 26. MALDI mass spectra of *N*-glycan profiles obtained from three individual porcine bladders, (A) Uro1, (B) Uro2 and (C) Uro3. The putative *N*-glycan structures of intense peaks are depicted.

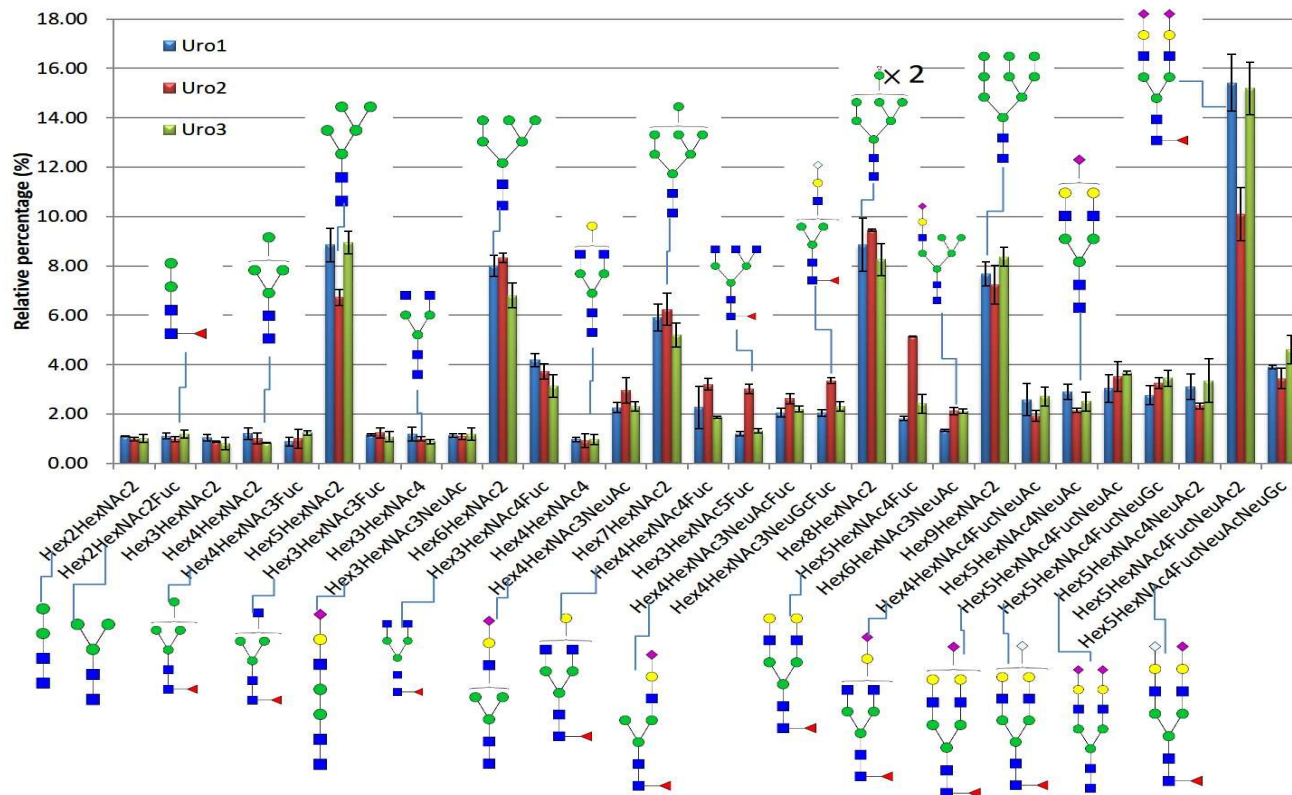


Figure 27. The relative percentages of *N*-glycans in three independent porcine bladders, Uro1, Uro2, and Uro3. The average relative percentages of 29 *N*-glycan species from analysis of technical replicates are shown ( $n = 3$ ). Error bars indicate the standard deviations of the mean for three technical replicates



**Table 9. List of porcine urothelial total cell lysate *N*-glycans released by FANGS**

Urothelial <i>N</i> -glycan list	Theoretical <i>m/z</i>	Uro1		Uro2		Uro3	
		Measured <i>m/z</i> (n=9)	Mass accuracy (ppm)	Measured <i>m/z</i> (n=9)	Mass accuracy (ppm)	Measured <i>m/z</i> (n=9)	Mass accuracy (ppm)
Hex <sub>2</sub> HexNAc <sub>2</sub>	967.4833	967.4843	0.99	967.4838	0.49	967.4846	1.36
Hex <sub>2</sub> HexNAc <sub>2</sub> Fuc	1141.5725	1141.5741	1.42	1141.5717	-0.67	1141.5739	1.19
Hex <sub>3</sub> HexNAc <sub>2</sub>	1171.5831	1171.5840	0.77	1171.5822	-0.74	1171.5841	0.87
Hex <sub>4</sub> HexNAc <sub>2</sub>	1375.6828	1375.6846	1.31	1375.6815	-0.97	1375.6809	-1.35
Hex <sub>4</sub> HexNAc <sub>3</sub> Fuc	1549.7720	1549.7381	-21.89	1549.7361	-23.16	1549.7391	-21.24
Hex <sub>5</sub> HexNAc <sub>2</sub>	1579.7826	1579.7852	1.67	1579.7811	-0.93	1579.7841	0.94
Hex <sub>3</sub> HexNAc <sub>3</sub> Fuc	1590.7986	1590.8024	2.39	1590.7980	-0.38	1590.7935	-3.23
Hex <sub>3</sub> HexNAc <sub>4</sub>	1661.8357	1661.8389	1.90	1661.8338	-1.15	1661.8353	-0.26
Hex <sub>3</sub> HexNAc <sub>3</sub> NeuAc	1777.8830	1777.8805	-1.39	1777.8760	-3.92	1777.8819	-0.63
Hex <sub>6</sub> HexNAc <sub>2</sub>	1783.8824	1783.8849	1.39	1783.8803	-1.17	1783.8851	1.51
Hex <sub>3</sub> HexNAc <sub>4</sub> Fuc	1835.9249	1835.9260	0.57	1835.9223	-1.42	1835.9248	-0.05
Hex <sub>4</sub> HexNAc <sub>4</sub>	1865.9355	1865.9251	-5.59	1865.9251	-5.57	1865.9435	4.27
Hex <sub>4</sub> HexNAc <sub>3</sub> NeuAc	1981.9828	1981.9847	0.93	1981.9783	-2.28	1981.9834	0.31
Hex <sub>7</sub> HexNAc <sub>2</sub>	1987.9821	1987.9853	1.61	1987.9791	-1.51	1987.9857	1.83
Hex <sub>4</sub> HexNAc <sub>4</sub> Fuc	2040.0247	2040.0243	-0.20	2040.0186	-3.01	2040.0249	0.12

Hex <sub>3</sub> HexNAc <sub>5</sub> Fuc	2081.0512	2081.0561	2.36	2081.0475	-1.78	2081.0553	1.97
Hex <sub>4</sub> HexNAc <sub>3</sub> NeuAcFuc	2156.0720	2156.0651	-3.18	2156.0664	-2.59	2156.0722	0.10
Hex <sub>4</sub> HexNAc <sub>3</sub> NeuGcFuc	2186.0820	2186.0842	1.00	2186.0826	0.27	2186.0792	-1.28
Hex <sub>8</sub> HexNAc <sub>2</sub>	2192.0819	2192.0794	-1.16	2192.0731	-3.99	2192.0794	-1.13
Hex <sub>5</sub> HexNAc <sub>4</sub> Fuc	2244.1245	2244.1293	2.12	2244.1178	-2.99	2244.1260	0.65
Hex <sub>6</sub> HexNAc <sub>3</sub> NeuAc	2390.1824	2390.1956	5.53	2390.1810	-0.57	2390.1907	3.48
Hex <sub>9</sub> HexNAc <sub>2</sub>	2396.1817	2396.1892	3.12	2396.1791	-1.09	2396.1875	2.41
Hex <sub>4</sub> HexNAc <sub>4</sub> FucNeuAc	2401.1983	2401.2093	4.58	2401.1997	0.58	2401.2063	3.35
Hex <sub>5</sub> HexNAc <sub>4</sub> NeuAc	2431.2089	2431.2144	2.27	2431.2066	-0.94	2431.2119	1.24
Hex <sub>5</sub> HexNAc <sub>4</sub> FucNeuAc	2605.2981	2605.3062	3.12	2605.2969	-0.44	2605.3019	1.46
Hex <sub>5</sub> HexNAc <sub>4</sub> FucNeuGc	2635.3087	2635.3163	2.90	2635.3121	1.30	2635.3204	4.42
Hex <sub>5</sub> HexNAc <sub>4</sub> NeuAc <sub>2</sub>	2792.3826	2792.3934	3.85	2792.3776	-1.79	2792.3849	0.82
Hex <sub>5</sub> HexNAc <sub>4</sub> FucNeuAc <sub>2</sub>	2966.4718	2966.4662	-1.89	2966.4575	-4.83	2966.4634	-2.85
Hex <sub>5</sub> HexNAc <sub>4</sub> FucNeuAcNeuGc	2996.4824	2996.4776	-1.61	2996.4668	-5.22	2996.4698	-4.21

Most studies of urothelial *N*-glycans that have been reported are of uroplakins and the glycoforms of *N*-glycans on uroplakins are species dependent (see chapter 1). A summary of these urothelial *N*-glycan structures identified in previous studies includes oligomannose (Hex<sub>5~9</sub>HexNAc<sub>2</sub>), hybrid, and bi-, tri-, and tetra-antennary complex glycans bearing one to four fucose and sialic acid residues in bovine and mouse uroplakins<sup>9,13,22,28,33,54,68</sup>. Human urothelial *N*-glycans have been reported to contain the structures listed above as well as proposing the presence of an intersecting GlcNAc glycoform<sup>33</sup>. The mammalian urothelial *N*-glycans identified in previous studies are in line with the *N*-glycan structures obtained from porcine urothelium in the present study. A recent study by another group member, published in Skeene *et al.*<sup>68</sup>, also used porcine urothelial cells prepared as developed by the author of this thesis, using scalpel scraping, to develop a one-pot method using FANGS to sequentially release *N*- and O-glycans from cell lysates, reported 16 *N*-glycans containing five oligomannose *N*-glycans (Hex<sub>5~9</sub>HexNAc<sub>2</sub>), six complex *N*-glycans (Hex<sub>3</sub>HexNAc<sub>4</sub>, Hex<sub>3</sub>HexNAc<sub>4</sub>Fuc, Hex<sub>4</sub>HexNAc<sub>4</sub>, Hex<sub>5</sub>HexNAc<sub>4</sub>FucNeuA, Hex<sub>5</sub>HexNAc<sub>4</sub>NeuAc<sub>2</sub>, Hex<sub>5</sub>HexNAc<sub>4</sub>FucNeuAc<sub>2</sub>) and others (Hex<sub>2</sub>HexNAc<sub>2</sub>, Hex<sub>2</sub>HexNAc<sub>2</sub>Fuc, Hex<sub>3</sub>HexNAc<sub>2</sub>, Hex<sub>4</sub>HexNAc<sub>2</sub>Fuc, Hex<sub>4</sub>HexNAc<sub>2</sub>). All 16 *N*-glycans identified in that study were also identified in the present study. High abundance of oligomannose *N*-glycans and a relatively low abundance of complex *N*-glycans were reported by Skeene *et al.* By contrast, in the present study, along with the detection of the same oligomannose *N*-glycans, many complex *N*-glycans were identified, that were at low abundance or not detected by Skeene *et al.* It is not clear what caused the difference in the relative abundances of total cell lysate *N*-glycans between the two different studies using similarly prepared urothelial cells

from the same species. A possible explanation is that the amount of urothelial cells used to release the total cell lysate *N*-glycans in this study could have been higher (approximately  $2 \sim 3 \times 10^6$  cells) than the amount of urothelial cells used (the amount was not reported) in the study by Skeene *et al.*, enhancing the detection of many low abundance complex *N*-glycans in the high *m/z* range.

### 3.1.3 Summary

To summarise, total cell lysate urothelial *N*-glycan profiles have been successfully investigated from porcine urothelial cells using FANGS approach – this is the first comprehensive study of a mammalian urothelial *N*-glycome. The source of urothelial cells used - porcine bladders –is expected to be relatively similar to human bladders. Consequently, porcine urothelial *N*-glycan profiles can be considered to act as a preview of human urothelial *N*-glycan profiles, as well as the study serving to provide a model system for subsequent studies using more precious human tissue. This approach has shown itself to be capable of determining qualitative and quantitative urothelial *N*-glycan profiles, thereby allowing the potential functional contributions of individual *N*-glycans to urothelial function and development of urothelial diseases to be studied.

Chapter 4. Enzymatic shaving of cultured urothelial  
RT4 cells: fractionated *N*-glycome analysis



In chapter 3, the urothelial *N*-glycomic pool released from the cell lysates of porcine urothelial cells was described; it is a mixture of *N*-glycans containing intra- and extracellular glycans, containing a high abundance of complex *N*-glycans and relatively low abundance of oligomannose *N*-glycans. Oligomannose *N*-glycans are generally considered as being involved in the initial steps of the *N*-glycan biosynthesis in the endoplasmic reticulum (intracellular) but also have been reported to regulate cell-cell fusion (extracellular), mediate sperm-egg fusion<sup>213,214</sup>, osteoclast formation<sup>215,216</sup> and human immunodeficiency virus (HIV) infection<sup>217,218</sup>. The oligomannose moiety of the glycoprotein on HIV is the ligand that binds to the cell surface protein CD4 on T-lymphocytes, activating cell-cell fusion between non-HIV infected cells and HIV infected cells. The binding activity of the surface glycoprotein (gp120) on HIV can be deactivated by blocking with lectin concanavalin A (ConA)<sup>217</sup> or on endoglycosidase F (Endo F) digestion<sup>218,219</sup>. By contrast, complex *N*-glycans with sialylation are thought to be the end products in *N*-glycan biosynthesis, acting as receptors on the cell membrane (extracellular) for binding viral and bacterial pathogens, such as influenza viruses<sup>220,221</sup> and *E. coli*<sup>222–224</sup> and for cell-cell recognition in the regulation of the immune response<sup>225,226</sup>. In addition, high amount of sialylated *N*-glycans on the cell surface may correlate with prognosis of human malignancies<sup>33,48,227,228</sup>, binding to selectins on platelets, immune cells and endothelium and serving to spread metastases<sup>229,230</sup>.

Recent studies have reported that the *N*-glycomic pool released from whole cell lysates (Chinese hamster ovary cells (CHO), human embryonic kidney-293 cells (HEK-293) and human liver carcinoma cells (Hep G2)) or cell membranes (HEK293T cells and human embryonic stem cells) isolated using centrifugation contain abundant oligomannose *N*-glycans<sup>68,180,197,202,231</sup>. The *N*-glycans in the above studies were all analyzed using MALDI-MS following permethylation, using the intensities of permethylated *N*-glycan signals for semi-quantification. By contrast, complex *N*-glycans were abundant in glycan pools released from cell membranes in the study by An *et al.*; *N*-glycans were released from membranes isolated from cell lysates of human fibroblast cells (55% : 45%, complex : oligomannose) and human breast epithelial cells (72% : 28%, complex: oligomannose)<sup>180</sup>, using MALDI-MS to analyse native *N*-glycans. It thus appears that the ratio of oligomannose *N*-glycans to complex *N*-glycans released from whole cell lysates or cell membranes varies between cell types. More recently, Hamouda *et al.* used tryptic shaving of the cell surface to collect cell surface *N*-glycopeptides, from which the *N*-glycans were released. The authors studied various cell lines including HEK 293 cells, AGE1.HN cells, CHO-K1 cells and Hep G2 cells<sup>197</sup>, analysing the glycans using MALDI-MS following permethylation. Using this tryptic shaving approach, and comparing the relative signal intensities, the proportion of complex *N*-glycans increased to 75% in comparison to 18% complex *N*-glycans when studying whole cell lysates. This result is in line with the study by Mun *et al.* where *N*-glycans released from isolated cell membranes of CHO-K1 cells, by washing away intracellular glycans before the release of the *N*-glycan fraction, contained about 70% of sialylated complex *N*-glycans and 30% of oligomannose *N*-glycans (Hex<sub>5-9</sub>HexNAc<sub>2</sub>)<sup>182</sup>, using MALDI-MS to analyze



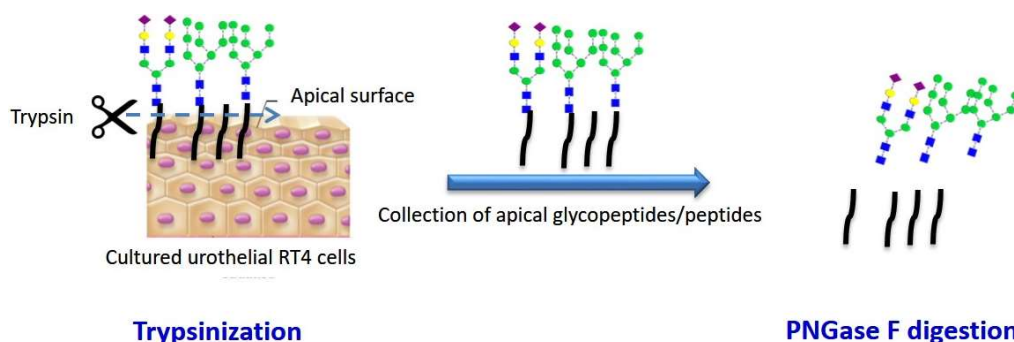
native *N*-glycans. Lin *et al.* reported enhanced detection of low abundance complex *N*-glycans by separating them from the oligomannose *N*-glycans in the cell lysate of human colon adenocarcinoma (COLO 205), using MALDI-MS to analyze permethylated *N*-glycans<sup>232</sup>. The high abundance of oligomannose *N*-glycans released from whole cell lysates were thus proposed to hinder the detection and accurate quantification of less abundant complex *N*-glycans analyzed using a mass spectrometer<sup>182,197,232</sup>.

The focus on cell surface *N*-glycans reported by other research groups<sup>182,197,232</sup> has suggested that separation of the extracellular and intracellular glycans might result in very different glycan profiles. It is also likely that a fractionated cell surface *N*-glycome is closer to the functional glycome than a total cell lysate unfractionated *N*-glycome. For example, altered cell surface glycosylation, including the enhanced expression of Tn antigen and sialylation, are reported to induce an immune response in cancer patients and facilitate the migration of cancer cells<sup>52,66,233–236</sup>, respectively. It is worth noting that approaches to extracellular glycome isolation using cellular membrane separation of a cell lysate results in a fraction that is enriched in extracellular glycans, but that this is also likely to contain some intracellular glycans because separation of the cell membrane from intracellular membranes is not complete. Collecting extracellular glycans from cells with their cell membranes intact avoids this problem, and is required to allow study of the cell surface glycome and its functions<sup>197,198</sup>.

The barrier function of normal urothelium has been reported to be dependent on the correct differentiation of polarized urothelial cells' apical surface, relying on protein expression, modification and protein complex assembly (see Chapter 1). The glycosylation of uroplakins, that form specialised plaque features on the apical cell membrane and the integrity of the proposed surface carbohydrate layer<sup>43,44,69,75</sup> on the superficial urothelium suggest a functional importance of the urothelial cell apical surface glycome. The urothelial cell apical surface glycome is proposed to contribute to a functional barrier<sup>13,23,27,66</sup>, defending the urothelium against penetration of toxic substances from the urine and also plays a role in defence against adventitious microorganisms in the urine. The aim of the work described in this chapter was thus to identify the polarized urothelial *N*-glycome on the apical surface of superficial urothelium.

## 4.1 Method development: fractionated *N*-glycome analysis of cultured urothelial cells

Development of a method for *N*-glycan release from the cell surface began with the method described by Hamouda *et al.*<sup>197</sup>, starting with CHO-K1 cells since this was one of the cell lines reported by Hamouda and colleagues; the aim was then to adapt this method for the collection of apical cell surface *N*-glycans from superficial urothelium. The plan for collecting apical cell surface *N*-glycans from the luminal surface of superficial urothelium was to expose the superficial urothelium to trypsin solution, with the intent of liberating apical surface glycopeptides/peptides. These would be isolated, and subjected to PNGase F digestion to release their *N*-glycans (Figure 28). For this approach to succeed, the superficial cell layer needed to retain its integrity under the condition of trypsinization; if trypsin were to penetrate between the cells, then release of glycopeptides/peptides from the sides of the superficial cells would occur, compromising the preparation.



**Figure 28.** Scheme proposed for the collection of urothelial cell apical surface *N*-glycans, using trypsinization to release apical glycopeptides and followed by PNGase F digestion to release *N*-glycans.

The first evaluation of a cell surface shaving approach using trypsinization was thus carried out using CHO-K1 cells and the method described by Hamouda *et al.*<sup>197</sup>. Briefly, approximately  $1 \sim 2 \times 10^6$  CHO-K1 cells grown on a cell culture dish were washed four times with pre-warmed PBS (37 °C) before tryptic shaving. 1 mL of 2.5 mg/mL trypsin solution containing EDTA (Gibco #15400-054) was used to cover the whole apical surface of the CHO cells in a cell culture dish. Trypsinization for liberating cell surface glycopeptides/peptides was carried out at 37 °C and for 15 min, which also released cells into suspension. The supernatant containing surface glycopeptides/peptides was separated from the CHO-K1 cells by centrifugation at 13200 rpm at 4 °C for 15 min; recovered digested cell pellets were examined using trypan blue to check the cell viability and membrane integrity of tryptically shaved CHO-K1 cells.

The cell viability of CHO-K1 cells before tryptic shaving was assumed to be near to 100% since a pre-wash with PBS was performed to remove dead cells before tryptic shaving. Damaged cells identified after tryptic shaving were thus probably compromised during the cell surface shaving process. The cell viabilities of tryptically shaved CHO-K1 cells after 15 minute incubation in the three experimental replicates, passaged in the same generation but in three different dishes, were above 99% (standard deviation = 0.13), which suggested that only a small fraction of CHO-K1 cells was compromised after tryptic shaving. However, visual inspection made it evident that the CHO-K1 cells started lifting from the bottom of the culture dishes after only two minutes' incubation, suggesting the trypsin solution started accessing the rest of CHO-K1 cell surface beside the apical surface and that it was thus releasing

not only apical surface glycopeptides/peptides. This result may indicate the CHO-K1 cells do not have a tight enough cell-cell attachment to retain the trypsin solution on the CHO-K1 cell apical surface, resulting in the CHO-K1 cells rapidly detaching from the dishes. In addition, it is likely that the EDTA included in the trypsin solution, also facilitated the detachment of CHO-K1 cells from the dishes by chelating  $\text{Ca}^{2+}$  and  $\text{Mg}^{2+}$  ions in the culture medium. It is worth pointing out that Hamouda *et al.* used the supernatants of their trypsin-treated cells to retrieve cells (by centrifugation) for cell viability determination, so that it is clear that their conditions must have lifted their cells too. It seems that the CHO-K1 cells, lacking the cell differentiation to form a barrier like urothelial cells, and the trypsinization conditions reported by Hamouda *et al.*<sup>197</sup> were not appropriate for application to the apical cell surface. Consequently, a further method development for collecting the apical surface glycans was conducted using cultured differentiated urothelial cancer cells, which were reported as having normal urothelial barrier function<sup>237</sup>.

#### 4.1.1 Apical cell surface trypsinization of cultured urothelial RT4 cells

A strategy aimed to isolate apical cell surface *N*-glycans using tryptic shaving was thus further developed on highly polarized urothelial RT4 cancer cells. The supernatant collected from the trypsinized RT4 cells was then further subjected to PNGase F digestion to release the apical cell surface *N*-glycans. The RT4 cell line was selected as it is reported to represent a well-differentiated non-invasive urothelial carcinoma and provides a useful source of cells that form a stratified, polarized epithelium for proof-of-concept studies prior to working with more precious normal human

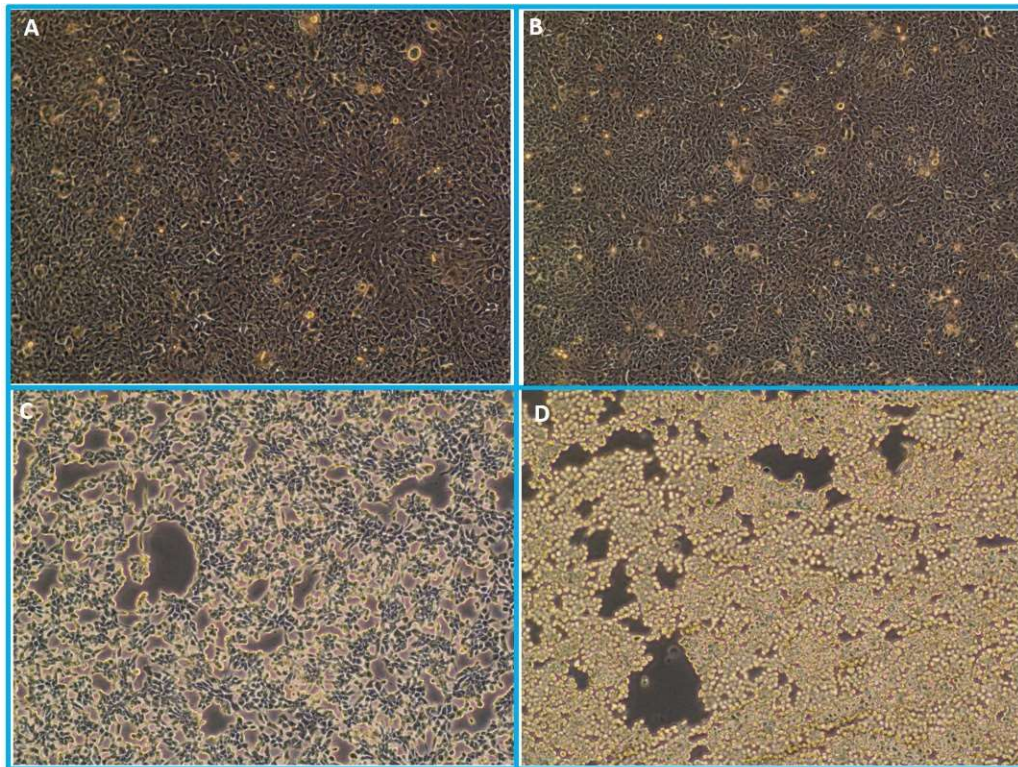
urothelial cell stocks<sup>237</sup>. It was expected that the well-differentiated RT4 cells, when fully confluent, present a barrier sufficient to retain the trypsin solution on the apical cell surface of cultured urothelial cells, releasing apical cell surface glycopeptides/peptides. In parallel, RT4 cells without prior tryptic treatment were subjected to FANGS to release total cell lysate *N*-glycans for comparison. Three experimental replicates were performed with three individual dishes of RT4 cells, passaged in the same generation, to represent one batch of urothelial cell apical surface *N*-glycans and total cell lysate *N*-glycans. All released *N*-glycans were permethylated and spiked with permethylated GlcNAc<sub>6</sub> as an internal standard at the stage of forming the sample spot on the MALDI plate, for analysis using MALDI-MS, semi-quantifying the amount of urothelial *N*-glycans.

The FANGS procedure as conducted in this chapter was optimized further compared with that used to generate the data described in Chapter 3, on the basis of new information (ref<sup>68</sup>), by diluting SDS lysis buffer, containing 4% SDS (~140 mM), 1:40 (v:v) with 8 M urea solution. The resulting concentration of SDS was 3.5 mM lower than the critical micellar concentration (CMC) of SDS (8.2 mM)<sup>238</sup> whereas in the original FANGS protocol, SDS lysis buffer was only diluted 1:10 with 8 M urea solution. In the less diluted SDS solution, it is expected that the SDS will form micelles and thus not be fully removed in the centrifugal filter (micelles being large enough to be retained above the membrane), so reducing the efficiency of PNGase F<sup>239</sup>. In contrast, the 40 times diluted SDS solution is below SDS's CMC and thus could presumably be efficiently removed using the 30 kDa-membrane filter units, enhancing PNGase F activity.

Liberating apical cell surface glycopeptides was thus attempted by incubating RT4 cells with trypsin solution for a very short time, to avoid disrupting the cell layers and so keeping the number of cells in the supernatant as close as possible to zero. The resulting supernatant is thus expected to contain apical cell surface glycopeptides/peptides and was recovered using a pipette to gently transfer it from the apical surface. The supernatant was then digested to release *N*-glycans using PNGase F. The length of time for incubation with trypsin to release RT4 cell apical surface *N*-glycans using 1 mL of 2.5 mg/mL trypsin solution at 37 °C was examined: incubation was carried out for 2, 5 and 10 minutes and cell appearance changes following these treatments are shown in Figure 29. RT4 cells started detaching from dishes and floating into the supernatant when incubation time was over 2 minutes, exposing not just the apical cell surface of the cells. At 10 minutes incubation, each RT4 cell changed from a long needle shape to a round shape, suggesting whole RT4 cells were detaching and suspending. However, no mass spectrometric signals for permethylated *N*-glycans were identified in the supernatant following incubation for 2 minutes, so increasing the concentration of trypsin was tested, to attempt to release detectable levels of *N*-glycans from the pool of glycopeptides formed on trypsinization of RT4 cell apical surfaces.

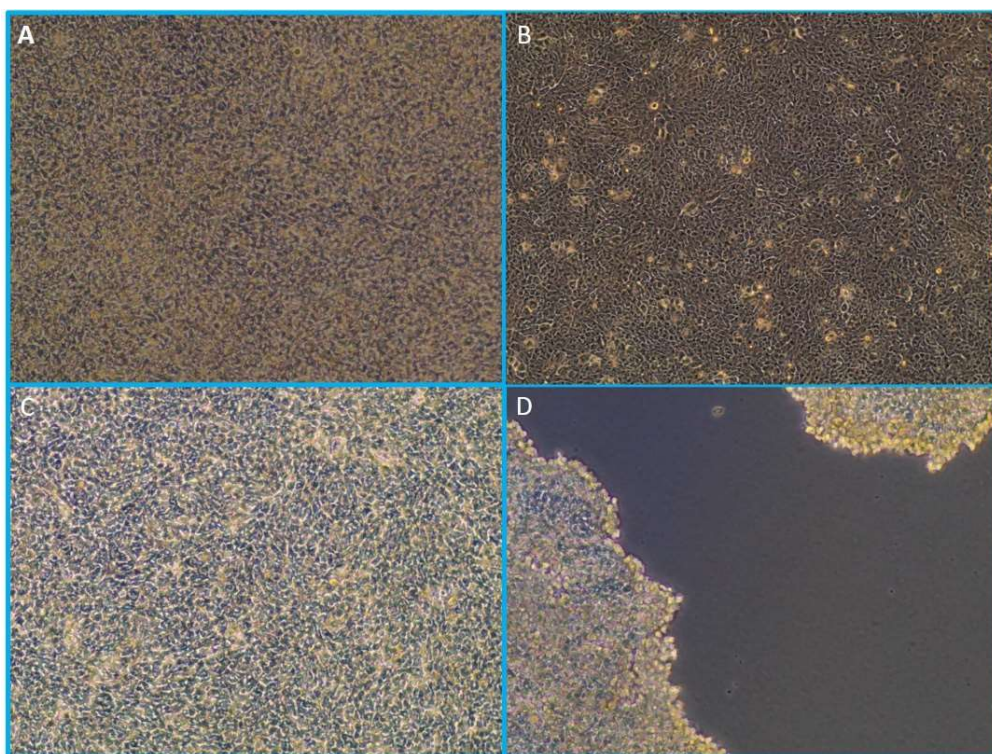
The concentrations of trypsin solutions examined were 1 mL of 2.5, 5 and 10 mg/mL for 2 min-trypsinization at 37 °C using RT4 cells passaged in the same generation but in different dishes. The cellular appearance was monitored (Figure 30B), and showed that 2.5 mg/mL-trypsin treated RT4 cells from different passages maintained consistent appearances (compare Figure 29B and Figure 29B). The surface integrity

of both the 2.5 and 5 mg/mL-trypsin treated RT4 cells (Figure 30 B and C) visually appeared to be retained. 10 mg/mL-trypsin treated RT4 cells (Figure 30D) all detached within 2 minutes of incubation. The number of cells in the supernatant of 2.5 mg/mL and 5 mg/mL-trypsin treated RT4 cells was counted using a haemocytometer, showing that less than 0.1% of fully confluent RT4 cells ( $7 \times 10^6$ ) were released into the two supernatants during apical cell surface trypsinization.



**Figure 29. Trypsinization for different incubation times caused appearance changes to cultured RT4 cells. All images of RT4 cells were recorded with 10x magnification. (A) before trypsin treatment, (B) after 2 min, (C) after 5 min and (D) after 10 min.**

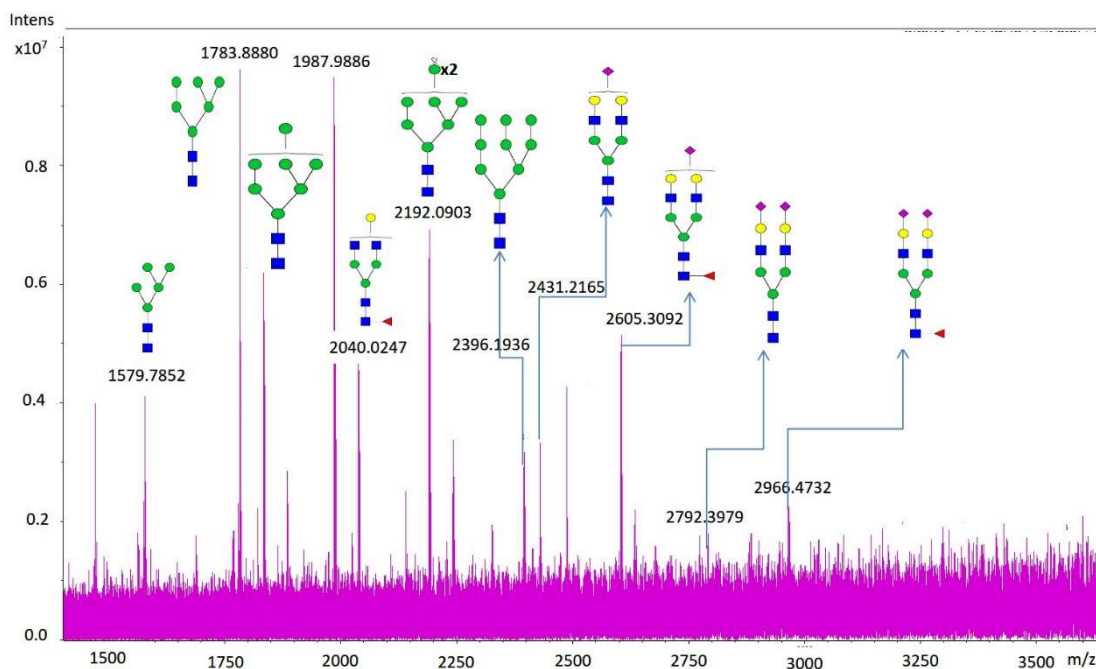




**Figure 30. 2 min-trypsinization caused appearance changes to RT4 cells treated with different trypsin concentrations. All images of RT4 cells were recorded with 10x magnification. (A) before trypsin treatment, (B) incubation with 2.5 mg/mL, (C) 5 mg/mL and (D) 10 mg/mL trypsin solution.**

The *N*-glycans released from the 2.5 mg/mL and 5 mg/mL trypsin incubation supernatants using PNGase F digestion were permethylated and analyzed using MALDI-MS. The 2.5 mg/mL trypsin-treated MALDI sample still gave no signals for permethylated *N*-glycans. The MALDI results for the 5 mg/mL trypsin-treated samples showed that oligomannose *N*-glycans from the RT4 cells were present in relatively high percentage intensity when compared with complex *N*-glycans (Figure 31). These *N*-glycans released from 5 mg/mL trypsin-treated supernatant were expected to be urothelial RT4 cell apical surface *N*-glycans, since the supernatants contained very few cells lifted as a result of trypsin treatment. Consequently this

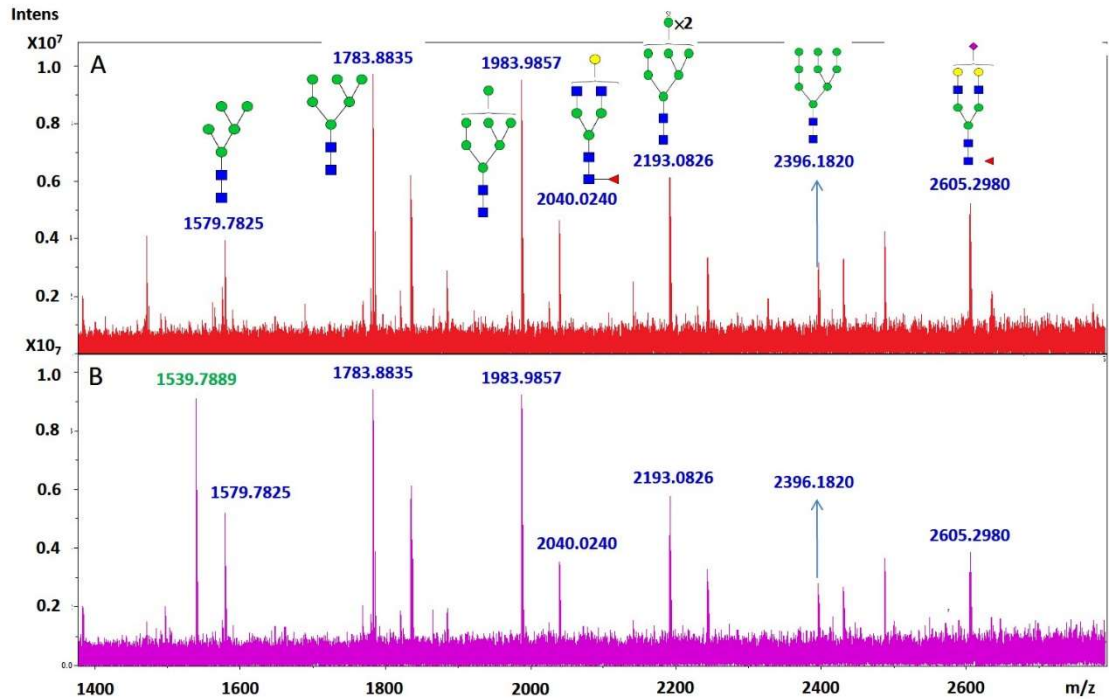
trypsinization approach was assumed to release predominantly cell apical surface glycopeptides/peptides with limited contamination with non-apical surface glycopeptides/peptides.



**Figure 31. Typical MALDI mass spectrum of permethylated *N*-glycans contained in the supernatant collected after trypsinization of the RT4 cell apical surface (2 min trypsinization with 1 mL of 5 mg/mL trypsin solution).**

Use of permethylated GlcNAc<sub>6</sub> ([M+Na]<sup>+</sup> *m/z* 1539.7889) as an internal standard spiked into permethylated *N*-glycans in the preparation of MALDI spots was conducted to enable normalisation of signals to that of the internal standard and so allowing determination of the relative amount of *N*-glycans released in the different stages. The amount of spiked permethylated GlcNAc<sub>6</sub> was adjusted on the basis of the intensity of peaks for permethylated *N*-glycans (Figure 32A) so that the intensity

of the internal standard peak was similar to that of the average sample glycan signal, and usually ranged between 1 ng to 3 ng for each sample. The addition of internal standard did not affect the signal intensity or S:N ratio of permethylated *N*-glycan signals (Figure 32B).



**Figure 32. MALDI mass spectra of permethylated urothelial RT4 cell apical surface *N*-glycans (A) before and (B) after spiking with permethylated  $\text{GlcNAc}_6$  ( $[\text{M}+\text{Na}]^+$   $m/z$  1539.7889).**

## 4.2 Surface *N*-glycome of cultured RT4 cells

### 4.2.1 Apical cell surface *N*-glycans and total cell lysate *N*-glycans released from cultured urothelial RT4 cells

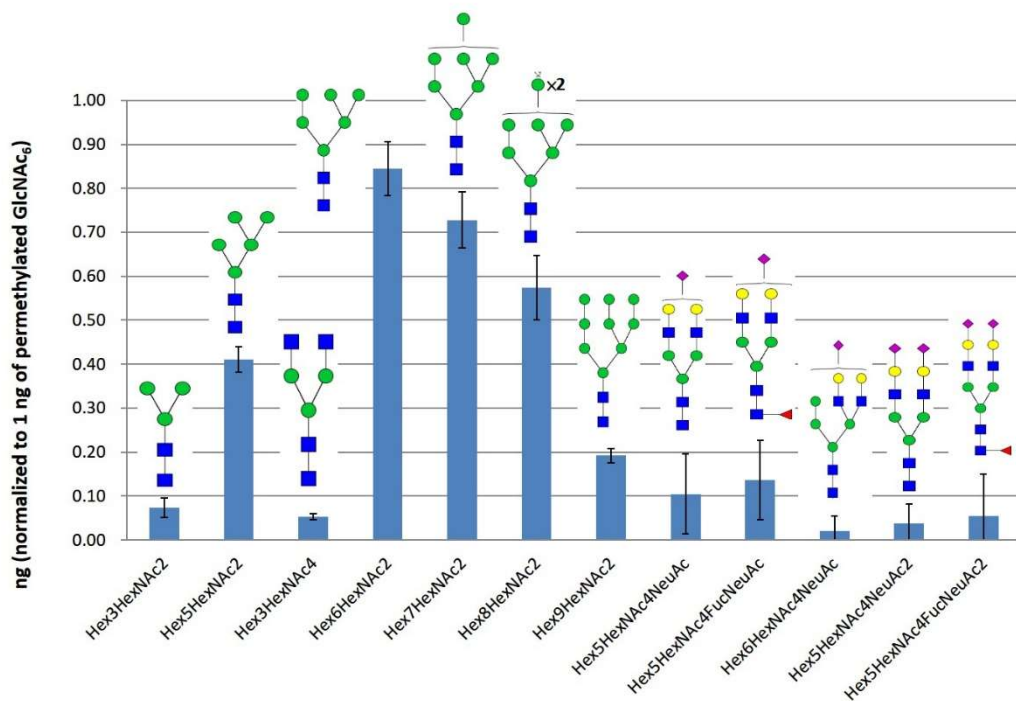
In order to determine whether the data obtained using 5 mg/mL trypsin apical surface shaving were reproducible, three experimental replicates (the same passage generation) were performed using three dishes of fully confluent RT4 cells. Three dishes of RT4 cells (one generation later than the first three) were treated with FANGS to release total cell lysate *N*-glycans as a comparison group. The normalized signal intensities for each *N*-glycan species, using the internal standard of permethylated GlcNAc<sub>6</sub>, from triplicate MALDI spots were averaged and the mean was used to derive the normalized amounts of *N*-glycans from one dish of RT4 cells. The normalized amounts of *N*-glycans from three dishes of RT4 cells were averaged for each experimental replicate and plotted using Excel; the error bars indicate standard deviation of the mean.

The compositions of the urothelial RT4 cell apical surface *N*-glycans were composed of about 86% oligomannose, 8% complex *N*-glycans, less than 1% hybrid *N*-glycans and 5% small *N*-glycan structures<sup>8</sup> (Figure 33). In contrast, the compositions of the total cell lysate *N*-glycans (without trypsinization, Figure 34) were composed of 56%

---

<sup>8</sup> These *N*-glycans are smaller than Hex<sub>5</sub>HexNAc<sub>2</sub> and could not be categorized into any of the recognised groups.

oligomannose, 26% complex, 1% hybrid and 17% small structure *N*-glycans. It is worth noting that the fractions of small glycans increased remarkably from ~5% in the cell surface trypsinization groups to ~17% in the cell lysate groups, suggesting that those small *N*-glycans might be considered as possible degradants of *N*-glycans released in the process of cell lysis.



**Figure 33.** Permethylated apical cell surface *N*-glycans released from cultured RT4 urothelial cells (n=3).

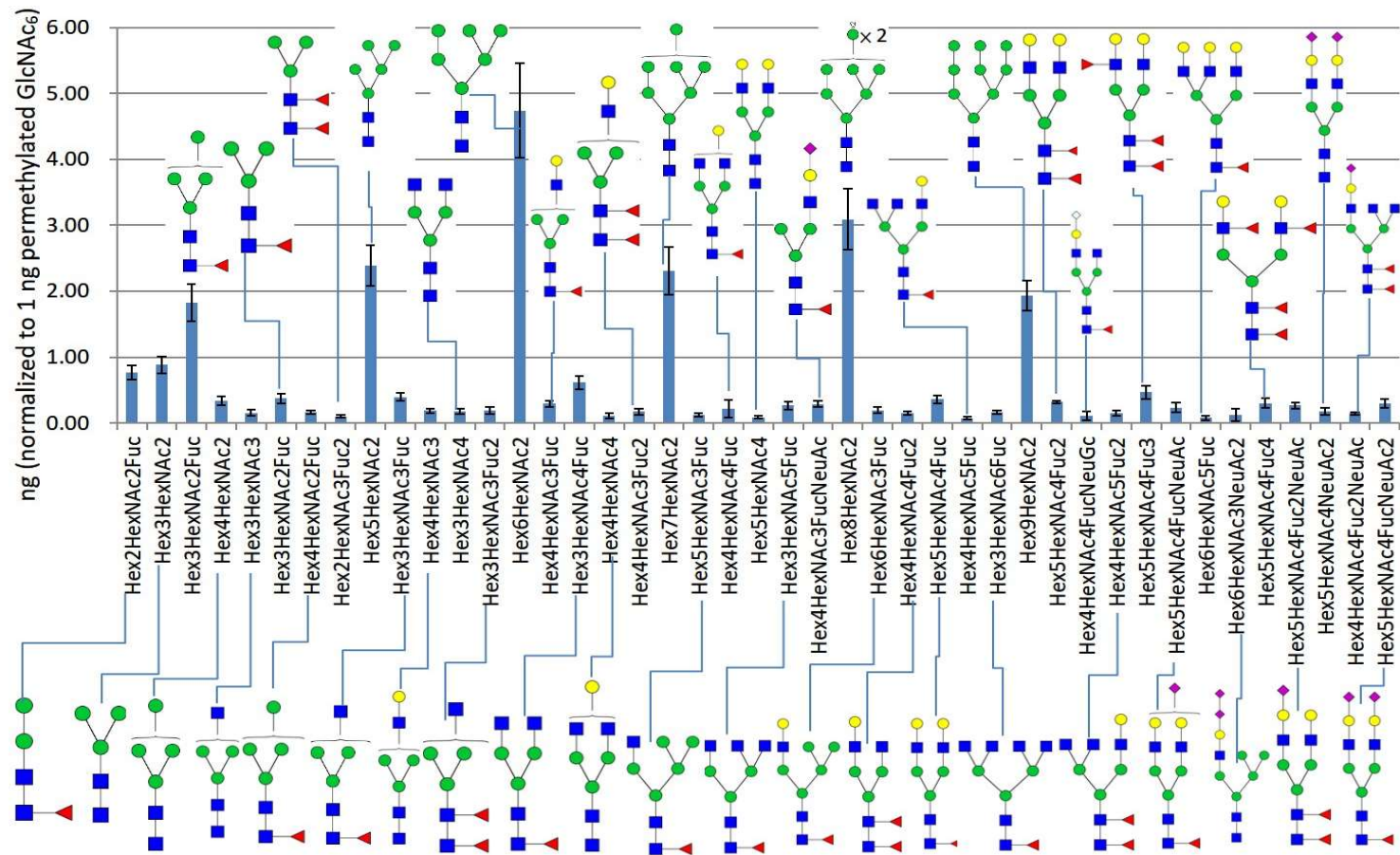
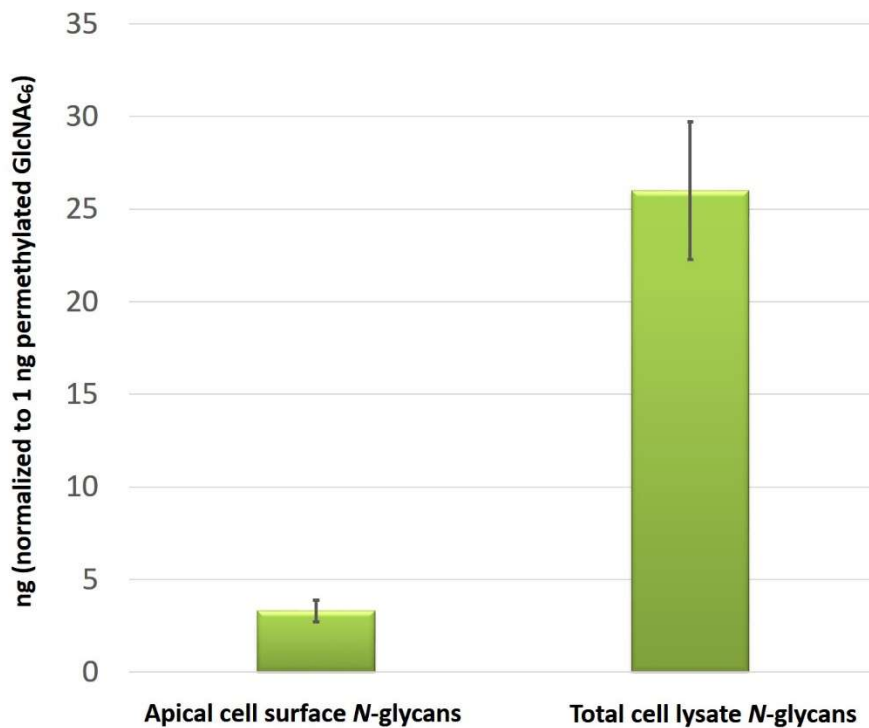


Figure 34. Permethylated total cell lysate *N*-glycans of cultured RT4 cells using FANGS without pretreated trypsinization (n=3).

The total amount of permethylated urothelial RT4 cell apical surface *N*-glycans was about one tenth of the total the amount of RT4 total cell lysate *N*-glycans (Figure 35), suggesting the apical cell surface trypsinization was not efficient in releasing all apical surface glycopeptides/peptides. The inefficient apical cell surface trypsinization could be caused by the glycocalyx, reported in the literature to be present on the superficial urothelial RT4 cells, hindering trypsin access to the apical cell surfaces for releasing glycopeptides/peptides.



**Figure 35. The total amount of permethylated *N*-glycans from RT4 cells released using apical cell surface trypsinization and FANGS (n=3, the error bars indicate standard deviation of the mean)**

Another concern had arisen during the method development studies using cultured urothelial cells: the adherent cultured RT4 cells were not capable of retaining trypsin solution on the top of cells for longer than two minutes before lifting the cells. It was suspected that the cultured RT4 cells did not form a well functioning barrier. The transepithelial electrical resistance (TEER) measurement of RT4 cells ( $\sim 150.5 \Omega \cdot \text{cm}^2$ ), done by Ros Duke (Jack Birch Unit, Department of Biology), was smaller than that of normal epithelium (above  $500 \Omega \cdot \text{cm}^2$ )<sup>44,240</sup>, suggesting that the RT4 cells do not form a proper barrier. The resulting apical cell surface glycopeptides/peptides from the urothelial RT4 cells thus may be compromised by other surface glycopeptides/peptides because the trypsin solution may penetrate between the RT4 cells.

#### 4.2.2 Summary

To summarize, the idea of identifying the apical cell surface *N*-glycans of polarized RT4 cells using trypsinization was achieved, but needs further improvement to improve efficiency and detection limits. The method for releasing apical cell surface *N*-glycans identified, with semi-quantification, following permethylation provide a way to examine the quantitative and qualitative changes in glycosylation in a comparison study of normal and cancer urothelial cells. However, due to the lack of barrier function of cultured urothelial RT4 cells, fresh and healthy porcine bladders expected to have a normal urothelial barrier function were used to complete the development of methods to release the polarized urothelial cell apical surface O- and *N*-glycans, reported in the next chapter.

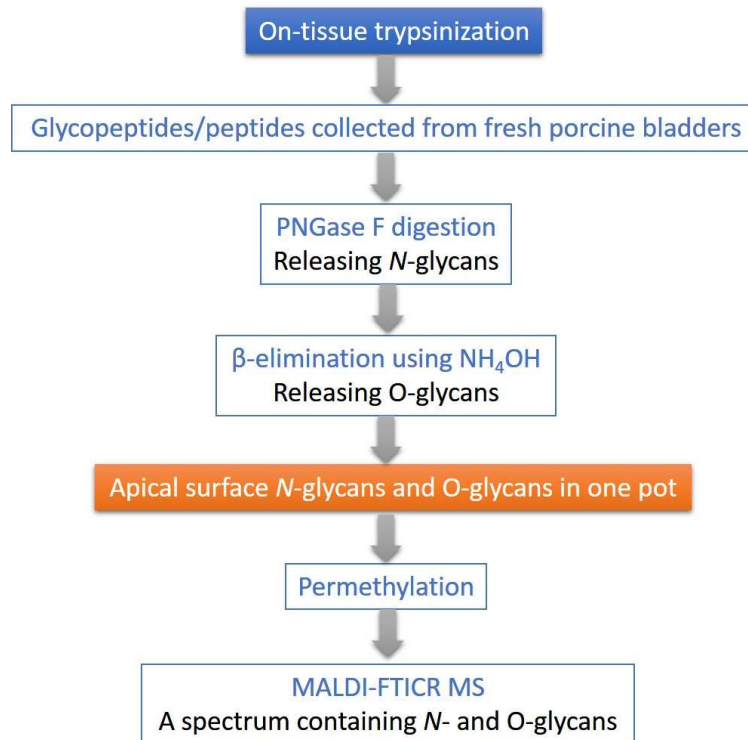


Chapter 5. On-tissue trypsinization of fresh porcine bladders to release apical cell surface glycopeptides for subsequent *N*- and O-glycan release



In chapter 4, the authenticity of the profile of apical cell surface *N*-glycans liberated from cultured polarized urothelial RT4 cells using trypsinization followed by PNGase F digestion was compromised due to the RT4 cell line's incomplete barrier function; this meant there was a potential risk of trypsin solution penetrating between the RT4 cells. In addition, the incomplete barrier function of cultured RT4 cells may be one of the factors causing the cultured RT4 cells to be unable to retain trypsin solution on their surface for longer than five minutes, resulting in poor yields of apical cell surface glycopeptides/peptides. Consequently, an alternative model, that of normal porcine urothelium (fresh from a local abattoir) with full barrier function, was used to further develop apical cell surface trypsinization to release glycopeptides/peptides from polarized superficial urothelial cells.

The aim in this chapter was thus to isolate the polarized superficial urothelial cell apical surface *N*- and *O*-glycans from fresh and healthy porcine bladders expected to have normal urothelium barrier function, in order to develop methods for the release of the polarized urothelium cell apical surface glycome (Figure 36).

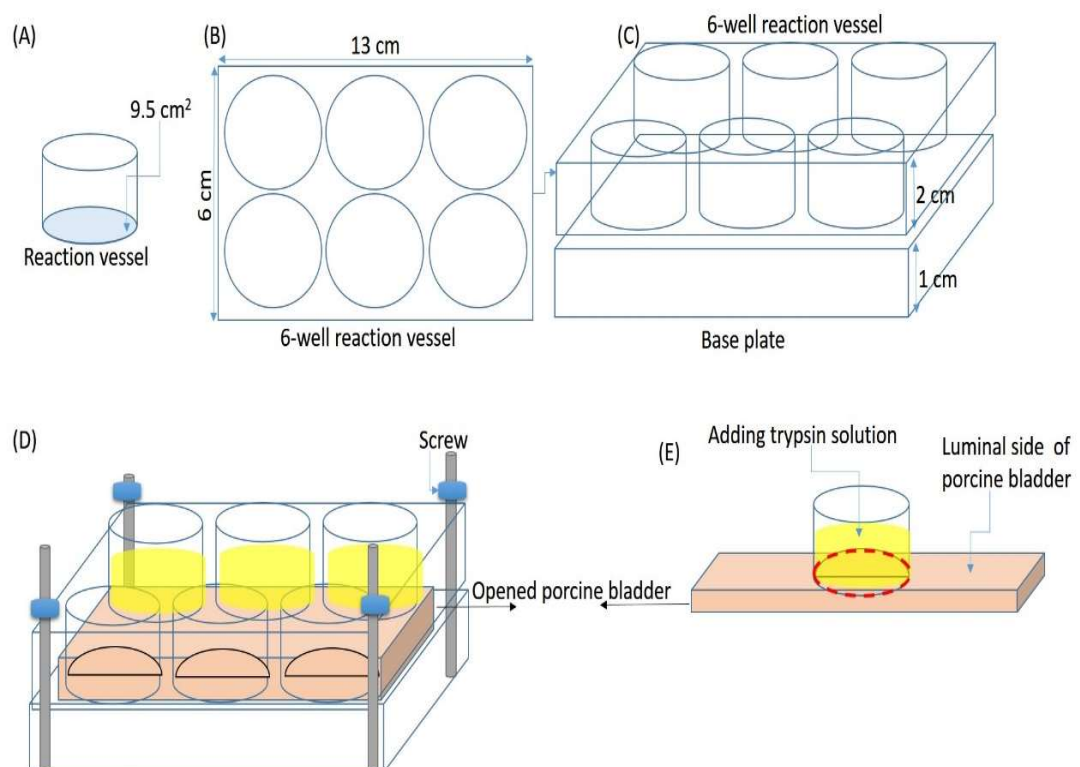


**Figure 36. Scheme of on-tissue trypsinization to release apical surface glycopeptides/peptides followed by PNGase F digestion and  $\beta$ -elimination to release N- and O-glycans in one pot.**

## 5.1 On-tissue trypsinization on unstretched porcine bladders

### 5.1.1 Device development for on-tissue trypsinization

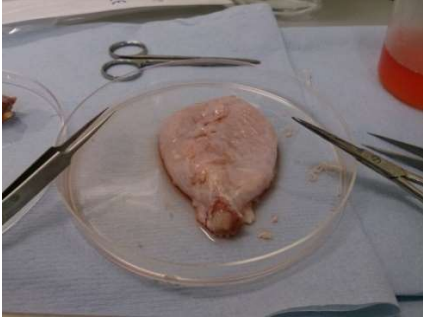

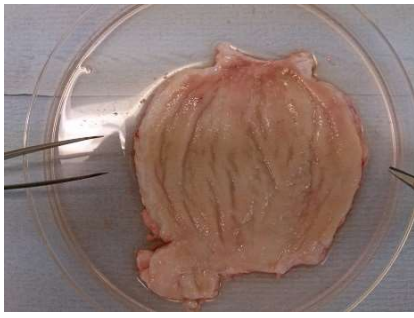
A reaction vessel (Figure 37) was produced and described in chapter 2.2.1 that was adapted from a commercial six-well cell culture plate and designed to maintain trypsin solution on the luminal sides of porcine bladders for a period of time, to attempt to liberate apical surface glycopeptides/peptides from the luminal surface of polarized superficial urothelium.



**Figure 37. Design of the reaction vessel for on-tissue trypsinization**

The porcine bladder collected fresh and dissected in order to expose its luminal side, lined with urothelium, for trypsinization (Figure 38). The luminal surface was gently washed with pre-warmed HBSS (37 °C) twice to remove residual biological waste. The reaction vessel was then assembled to hold the opened porcine bladder between the top and bottom sections of the device (Figure 39). The reaction vessel was designed by Chung-Yao Wang and made in cooperation with Timothy Ayers (Electronics Workshop, Department of Chemistry, University of York).

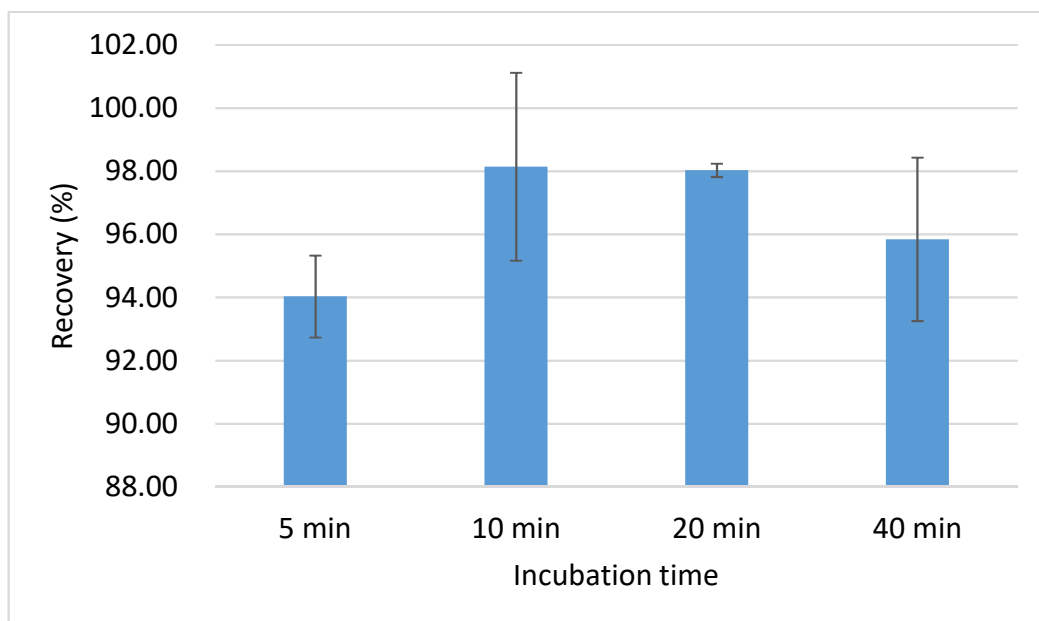
**Figure 38. Porcine bladder dissection process**

1) Cutting from the ureter side	2) Bladder opened with a Y-shaped incision	3) Opened bladder
		

**Figure 39. Assembly of the reaction vessel for on-tissue trypsinization**

1) Bladder places on base plate	2) Bladder luminal surface covered with 6-well reaction vessel	3) Device tightened using upper plates and nuts/bolts
		

A leak test was conducted in order to determine whether the trypsin solution was escaping from the reaction vessels during trypsinization, by weighing the trypsin solution before and after incubation (Figure 40). The average recovery was around 95% which suggested the device could seal the trypsin solution without obvious leaks or evaporation over the time period used for the incubation. It also suggests that solution exchange between two adjacent vessels was negligible.



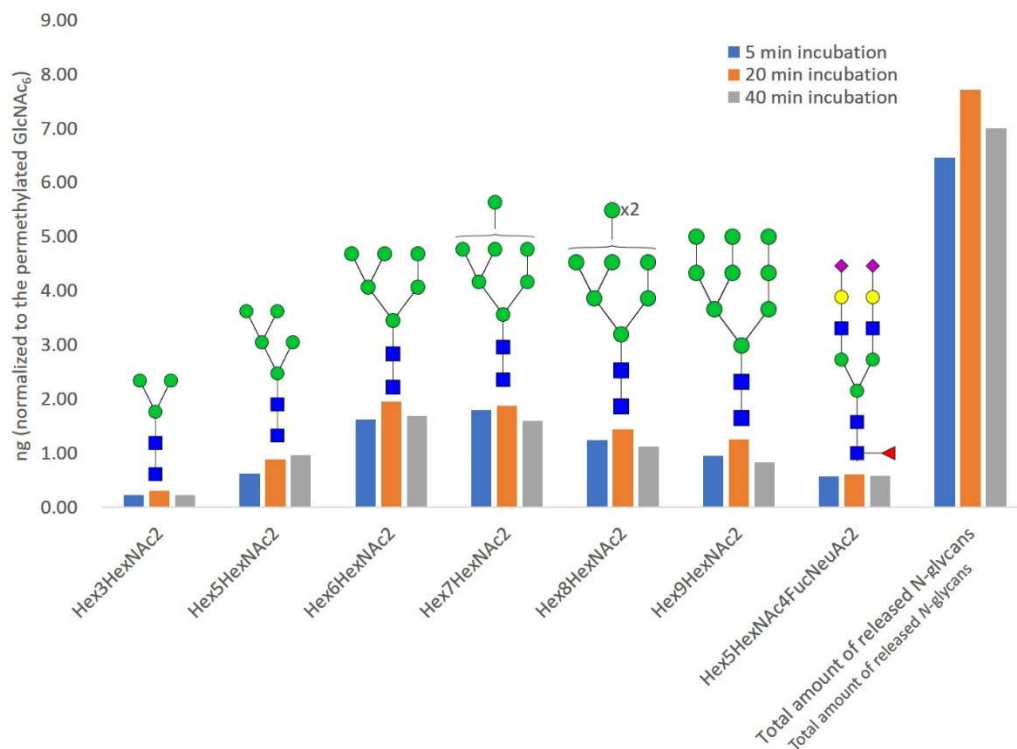
**Figure 40. Recovery test of trypsin solution after on-tissue trypsinization. Standard deviations of the mean are shown for different incubation times (n=4).**



### 5.1.2 Exploratory on-tissue trypsinization of unstretched porcine bladders using the in-house built reaction device

Fresh porcine bladders were obtained from a local abattoir and processed immediately after returning to the laboratory. On-tissue trypsinization using 5 mg/mL trypsin solution (Sigma Cat. No. T-4549) prepared in HBSS with addition of  $\text{Ca}^{2+}$  and  $\text{Mg}^{2+}$  (HBSS+ $\text{Ca}^{2+}$ / $\text{Mg}^{2+}$ , Gibco Cat. No. 24020117) was tested, with different incubation times at 37 °C. The 5 mg/mL trypsin solution concentration is the same as had been used for the early development work using the cultured RT4 cells (chapter 4). The collected supernatant after trypsinization was subjected to PNGase F digestion to release *N*-glycans, followed by purification using C18 SPE cartridges prior to permethylation, as reported in the work of Hamouda *et al*<sup>197</sup> (and also followed in the experiment reported in chapter 4). Samples of permethylated *N*-glycans were spotted with permethylated GlcNAc<sub>6</sub> as the internal standard on a MALDI plate for MALDI-MS analysis.

The *N*-glycan profiles (including semi-quantification with GlcNAc<sub>6</sub> internal standard) obtained from the process of on-tissue trypsinization on unstretched fresh porcine bladders with 5 minute, 20 minute and 40 minute incubation were analyzed (Figure 41). Only a few *N*-glycan species were observed in all three different incubations, including oligomannose *N*-glycans (Hex<sub>5~9</sub>HexnNAc<sub>2</sub>), one complex *N*-glycan (Hex<sub>5</sub>HexNAc<sub>4</sub>FucNeuAc<sub>2</sub>) and one other *N*-glycan structure (Hex<sub>3</sub>HexNAc<sub>2</sub>, smaller than Hex<sub>5</sub>HexNAc<sub>2</sub>). Increasing the incubation time (ie increasing the length of trypsin exposure) barely seemed to improve the total amount of *N*-glycans released.



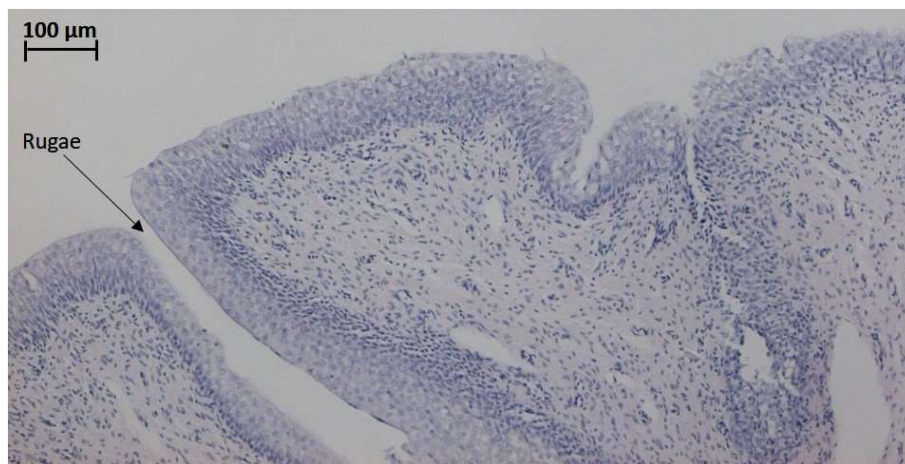
**Figure 41. The *N*-glycan profiles obtained from unstretched porcine bladders using on-tissue trypsinization. Only one bladder was used to test each different incubation time.**

### 5.1.3 Summary

The preliminary investigation of on-tissue trypsinization on fresh unstretched porcine bladders showed that it was a practical strategy for collecting glycopeptides from the luminal surface of porcine bladders using an in-house built reaction vessel, with high recovery of trypsinized supernatants.

The luminal surface of porcine bladders is covered with “rugae” (Figure 42) which are anatomical structures produced by folding of the luminal urothelium of bladders.

The rugae accommodate the storage of urine, allowing the bladder to store urine without a significant rise in internal pressure by stretching the luminal wall of the bladder. The urothelial rugae may have the effect of impeding the trypsin molecules from accessing the entire apical surface of the urothelium, compromising the efficiency of on-tissue trypsinization and making the apical surface glycan profile obtained in this way incomplete.



**Figure 42. H&E stain of porcine urothelium, indicating the rugae.**

In order to improve the efficiency of on-tissue trypsinization of fresh porcine bladders, the in-house built reaction vessel was modified in order to hold a stretched porcine bladder, with the aim of flattening the luminal surface of the urothelium. It was designed to expose an even luminal bladder surface for trypsinization, allowing the trypsin solution to access the area of the urothelium hidden in the rugae space in the unstretched samples.

## 5.2 On-tissue trypsinization of stretched porcine bladders

Applying force to stretch porcine bladders and flatten the urothelial rugae in order to improve the efficiency of on-tissue trypsinization was achieved using a modified reaction vessel. The integrity of the urothelium and apical surface glycoproteins following such stretching and trypsinization were examined using H&E staining and immunohistochemistry, respectively. Because bladders are able to expand to accommodate filling with urine, it was expected that stretching would not damage the bladder, and that trypsin treatment of the stretched urothelium would thus not result in observable damage to the urothelial surface, and that it would be possible to detect some depletion of superficial glycoproteins using immune staining following trypsin treatment.

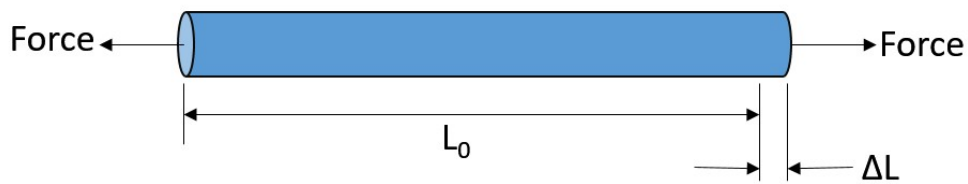
### 5.2.1 Method development for stretching porcine bladders

The force applied to stretched porcine bladders was measured in order to obtain consistent results for each stretching process. The definition of strain ( $\epsilon$ )<sup>9</sup> as the measurement of stretching force is shown in Figure 43, showing the amount of

---

<sup>9</sup> <https://www.nde-ed.org/EducationResources/CommunityCollege/Materials/Mechanical/StressStrain.htm>

deformation in the direction of the applied force divided by the initial length of the material. This results in a unitless measurement.



$$\text{Strain}(\varepsilon) = \frac{\text{Elongation}}{\text{Original Length}} = \frac{\Delta L}{L_0}$$

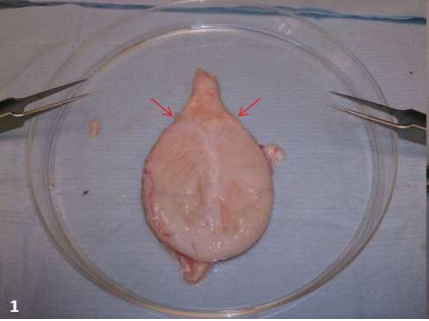
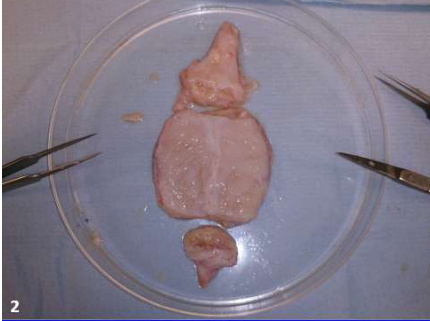
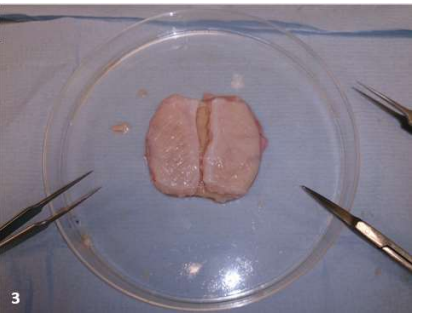
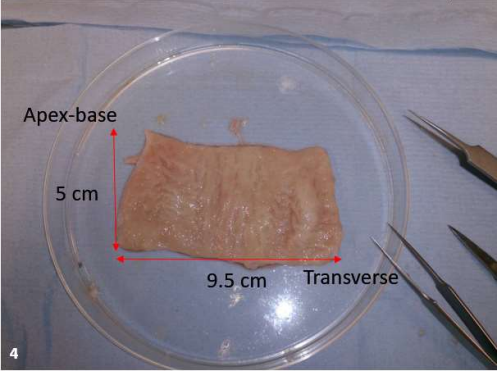
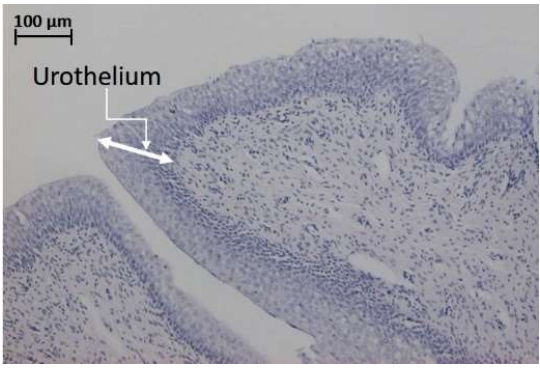
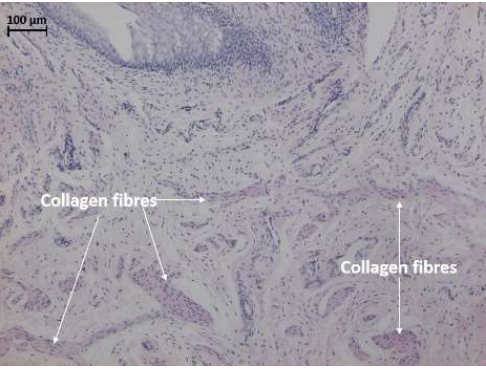
**Figure 43. The definition of strain. The definition of strain ( $\varepsilon$ )<sup>10</sup> as the measurement of the amount of deformation in the direction of the applied force divided by the initial length of the material.**

A new way to dissect the porcine bladder in order to shape the opened bladder into a rectangle for ease and uniformity of stretching is depicted in Figure 44; this involved removing the top approximately above the ureters (red line) and the bottom, and cutting through the vertical central line. The rectangular shape aimed to distribute the strain evenly across the bladder. The urothelium and its rugae examined using H&E staining show that the anatomical structures remained intact after dissection (Figure 44, 5th box). In addition, the smooth muscle collagen fibres (stained pink by H&E) were compacted together (Figure 44, 6th box), showing the bladder was not in a distended state.

---

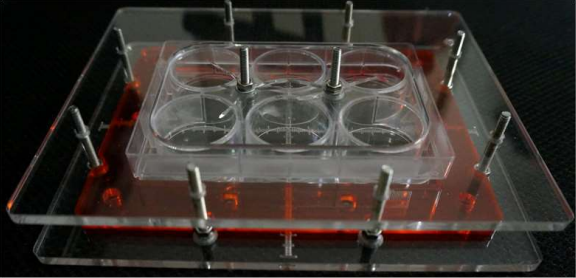
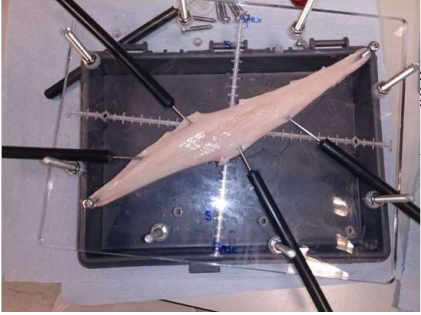

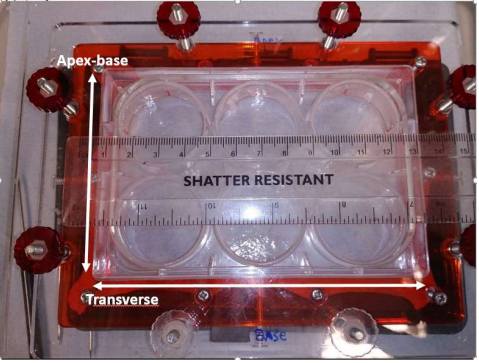
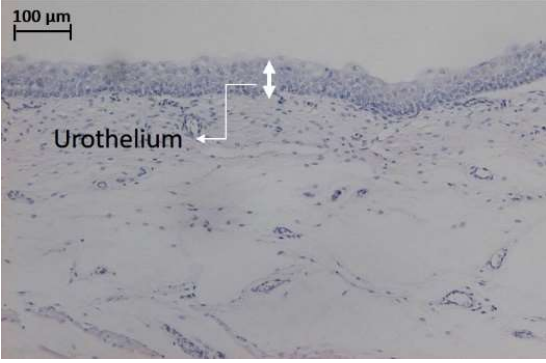
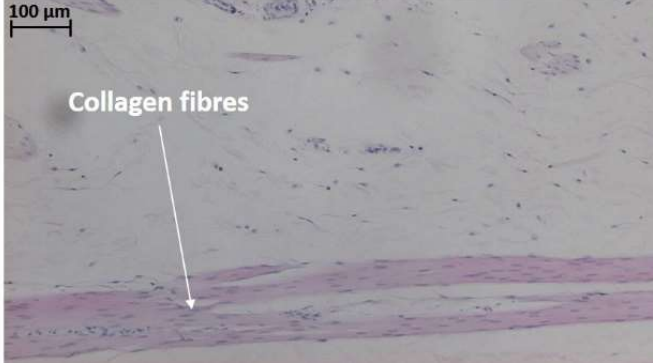
<sup>10</sup> <https://www.nde-ed.org/EducationResources/CommunityCollege/Materials/Mechanical/StressStrain.htm>

**Figure 44. Dissecting process of porcine bladders in a rectangular shape**

1. Freshly removed bladder	2. Top and bottom removed	3. Cut through central line
 <p>1</p>	 <p>2</p>	 <p>3</p>
4. Rectangular opened bladder	5. H&E of urothelium right after dissection	6. H&E of bladder muscle collagen fibres
 <p>4</p>	 <p>100 μm</p> <p>Urothelium</p>	 <p>100 μm</p> <p>Collagen fibres</p> <p>Collagen fibres</p>

It was not known how much strain would be sufficient to flatten the rugae. Following a discussion with Ashley Ward, who had experience of stretching bladders<sup>203</sup>, uncoiling the smooth muscle collagen fibres may result in flattening the rugae. He advised applying a strain of 1.5 and 2.0 to bladders in the apex-to-base and transverse directions, respectively; these values have been shown to be capable of uncoiling the smooth muscle collagen fibres<sup>241</sup>. The process of stretching bladders using a modified reaction vessel is recorded in Figure 45; this involved a ruler-marked plate (Figure 45, 2nd box) to fix the stretched bladders with pins and stretching the bladder slowly from two diagonally opposite corners until the whole bladder was equally expanded (Figure 45, 3rd box). The orange frame placed between the reaction vessel and the stretched bladder was used to improve the flatness of the stretched bladder (Figure 45, 4th box). The resulting strains of  $\epsilon_{\text{apex-to-base}}$  and  $\epsilon_{\text{transverse}}$  were 1 ( $L_{\text{original}}$  5 cm to  $L_{\text{elongation}}$  10 cm) and 1.8 ( $L_{\text{original}}$  5 cm to  $L_{\text{elongation}}$  14 cm), respectively. Tissue sections were collected from six different bladder locations (one in each of six wells in the reaction vessel); all gave identical H&E staining results (representative images shown) which suggest the bladder was expanded evenly. The results of H&E staining of the stretched bladder suggest that the urothelium was intact and the rugae (Figure 45, 5th box) flattened, with uncoiled underlying muscle collagen fibres (Figure 45, 6th box).

**Figure 45. The process of stretching the porcine bladder**

1. Modified device	2. Stretching the bladder	3. Fixing the stretched bladder on the base plate
		
4. Measuring the stretched bladder	5. H&E of stretched urothelium	6. H&E of stretched bladder muscle
		



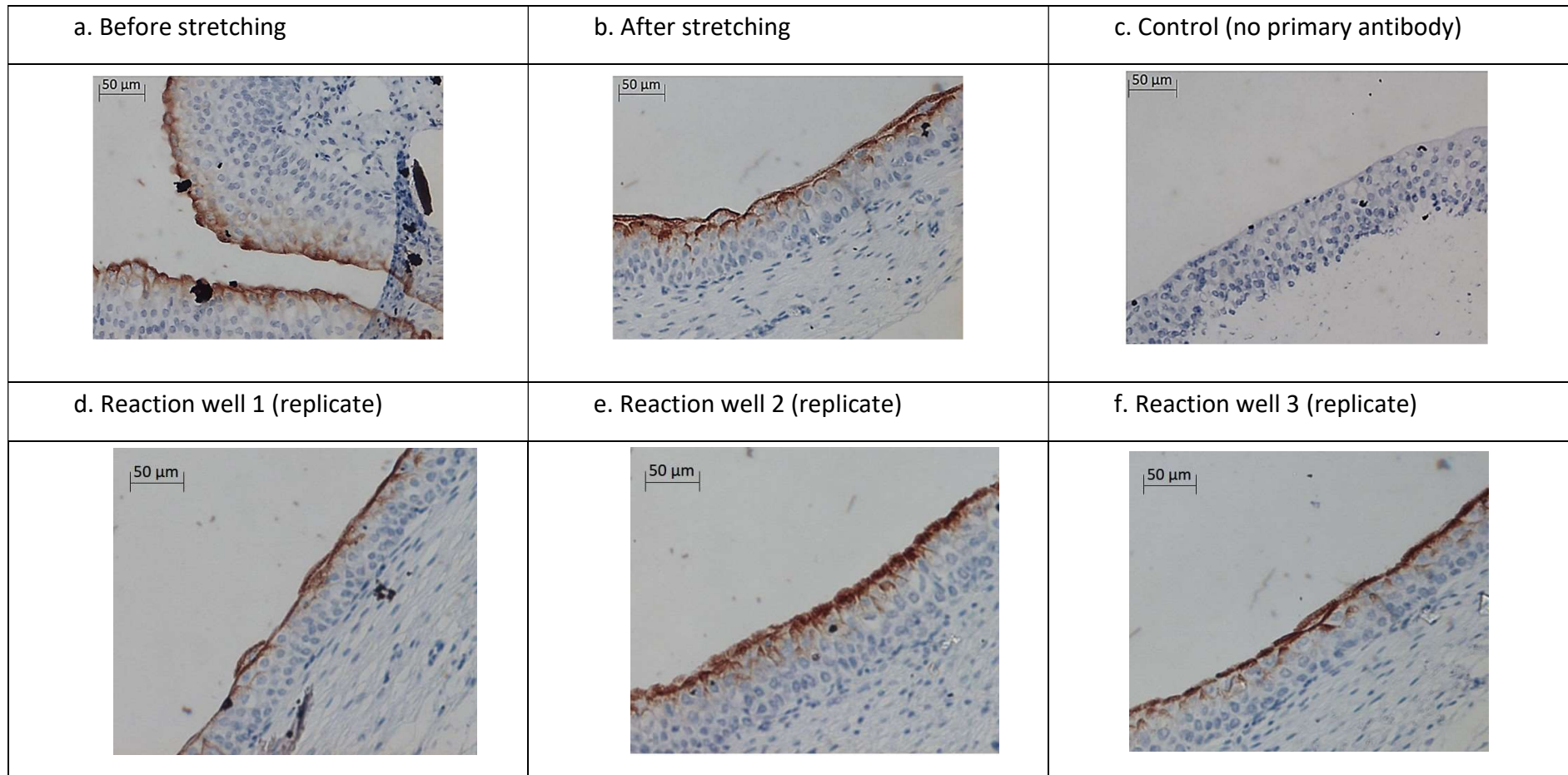
### 5.2.2 Immunolabelling of porcine urothelium using antibody AU1

The superficial (glyco)proteins before and after trypsinization were examined using immunohistochemistry in order to inform optimization of the incubation time with trypsin and obtain evidence for the depletion of cell apical surface (glyco)proteins. UPK3a, a barrier-function-related superficial glycoprotein on porcine bladders was labelled using antibody AU1 (mouse source, Progen Cat. No. 651108), showing a complete layer on the superficial layer of unstretched, untrypsinised porcine urothelium (Figure 46a, the brown coloured layer). A complete surface layer of UPK3a was retained after the bladder was stretched (Figure 46b). The control porcine urothelium without labelling with primary antibody showed no response (Figure 46c), indicating there was no non-specific reaction of the secondary antibody and dye reagent on porcine urothelium. Tissue sections collected from different bladder locations (in each of the six reaction wells); all gave identical immunolabelling results (Figure 46d-f) indicating an intact UPK3a layer on the urothelial apical surface.

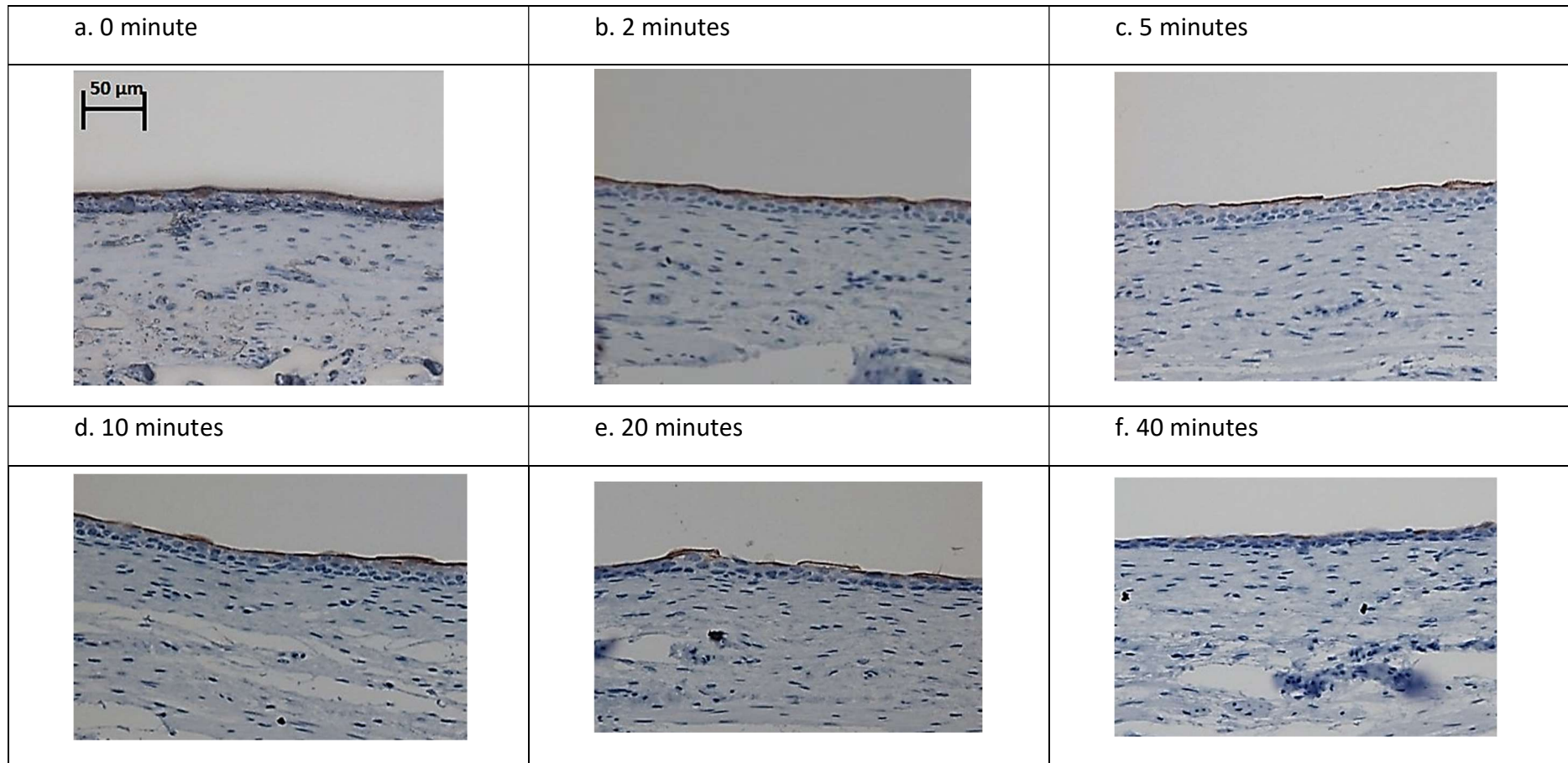
Immunolabelling of superficial UPK3a-labelled porcine urothelium was conducted on one porcine bladder trypsinized for different times; each of six reaction wells on the in-house built device was used to test a different incubation period (0, 2, 5, 10, 20, 40 minutes), in order to monitor the extent of damage to the UPK3a layer by trypsinization of the luminal surface (Figure 47). The UPK3a labelled on the superficial porcine urothelium was intact before trypsinization (Figure 47a) and started depleting after 5 minute trypsinization; it had faded almost completely after

40 minutes' trypsinization. These results suggest that the antibody AU1 is capable of revealing the damage to the labelled superficial UPK3a on increasing periods of trypsinization.

**Figure 46. Immunolabelling of porcine urothelium using antibody AU1 to label the superficial glycoprotein UPK3a**



**Figure 47. Immunolabelling of porcine urothelium trypsinized for different periods.**

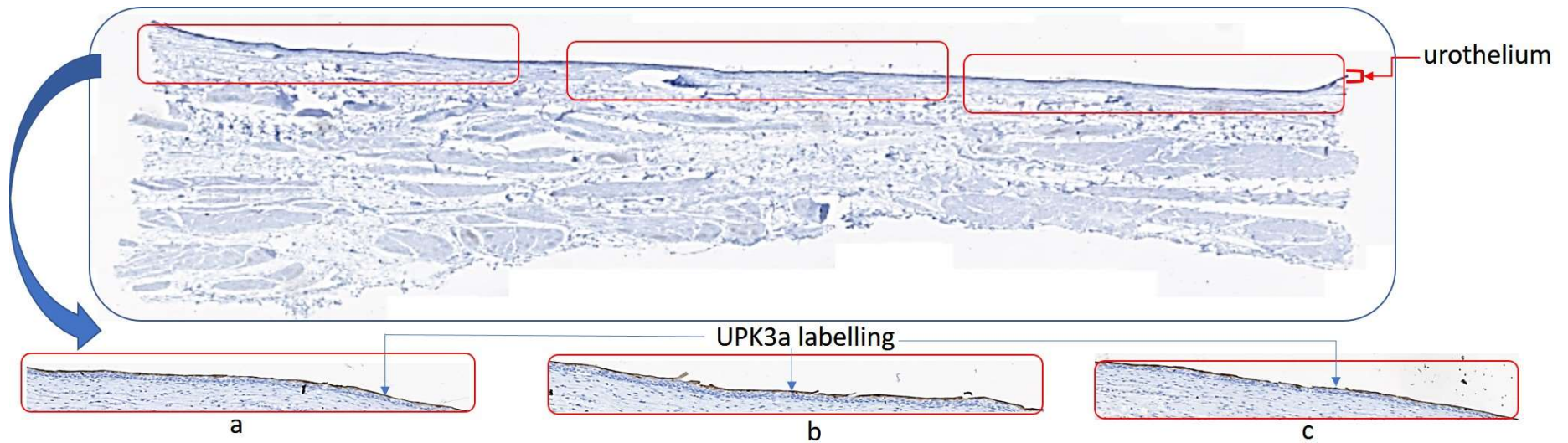


### 5.2.3 Determination of the length of incubation for on-tissue trypsinization

In order to liberate apical surface glycopeptides/peptides from the luminal surface of porcine urothelium without compromising the integrity of superficial layer of urothelium, the optimised length of incubation to conduct on-tissue trypsinization, was assessed by 1) using the immunolabelling results of superficial UPK3a-labelled porcine urothelium trypsinized for different periods, in combination with 2) the quantification of the total amount of released *N*-glycans, assessed using permethylation and spiking with the internal standard permethylated GlcNAc<sub>6</sub> prior to MALDI-MS analysis.

Porcine urothelium sections were collected from one porcine bladder trypsinized for 0 minute, 2 minute, 5 minute, 10 minute, 20, minute, 40 minute incubation (in different reaction wells), following formalin fixation, paraffin wax embedding and immunolabelling with antibody AU1 in a single batch. Each resulting slide was scanned using a ZEISS Axio Scan.Z1 slide scanner, to create an image of a whole tissue section of immunolabelled porcine urothelium. Three different regions of the urothelium layer were identified from each image of a whole tissue slide (Figure 48) and denoted a, b or c using image analysis software (Zeiss ZEN lite, blue edition). A total of 18 images (Appendix 2), three from each of six different periods of trypsinization, were randomized and provided to seven different subjects without giving any experimental information, for independent ranking the integrity of the labelled superficial UPK3a layer. The ranking criteria were based on the subject's

assessment of 1) the coverage by labelled UPK3a; if images were considered to have similar coverage, then 2) the thickness of the UPK3a layer, ranking from 1 (lowest integrity) - 18 (highest integrity). The integrity ranking results are shown in Table 10. The ranking scores for each slide were averaged and plotted against the period of trypsinization, using software GraphPad InStat, assessing the linearity between the average ranking score of each slide and the period of trypsinization (Figure 49). The slope of the line in Figure 49 was tested using linear regression (P value = 0.0005) and was significantly different from zero, suggesting that the antibody AU1 can be used to monitor on-tissue trypsinization by labelling the superficial UPK3a layer. Moreover, the integrity of the labelled superficial UPK3a layer on the luminal surface of porcine urothelium was compromised because of trypsinization; its relative reduction can be applied to monitor the trypsin shaving of the apical surface of urothelium. It is worth noting that the labelled superficial UPK3a layer seems not to evenly cover the superficial urothelium even before starting trypsinization (see Appendix 2); this is routinely observed for all urothelium examined during this thesis, and is one reason for always examining replicates. This unevenness may be the result of damage during sample handling, or to only partial antigen retrieval occurring during the process of immunolabeling, resulting in the differences in UPK3a labeling between and within slides. This may explain why the ranking scores for two of the three replicates for the 5 minute group are lower than those for the 10 minute group (Figure 49).

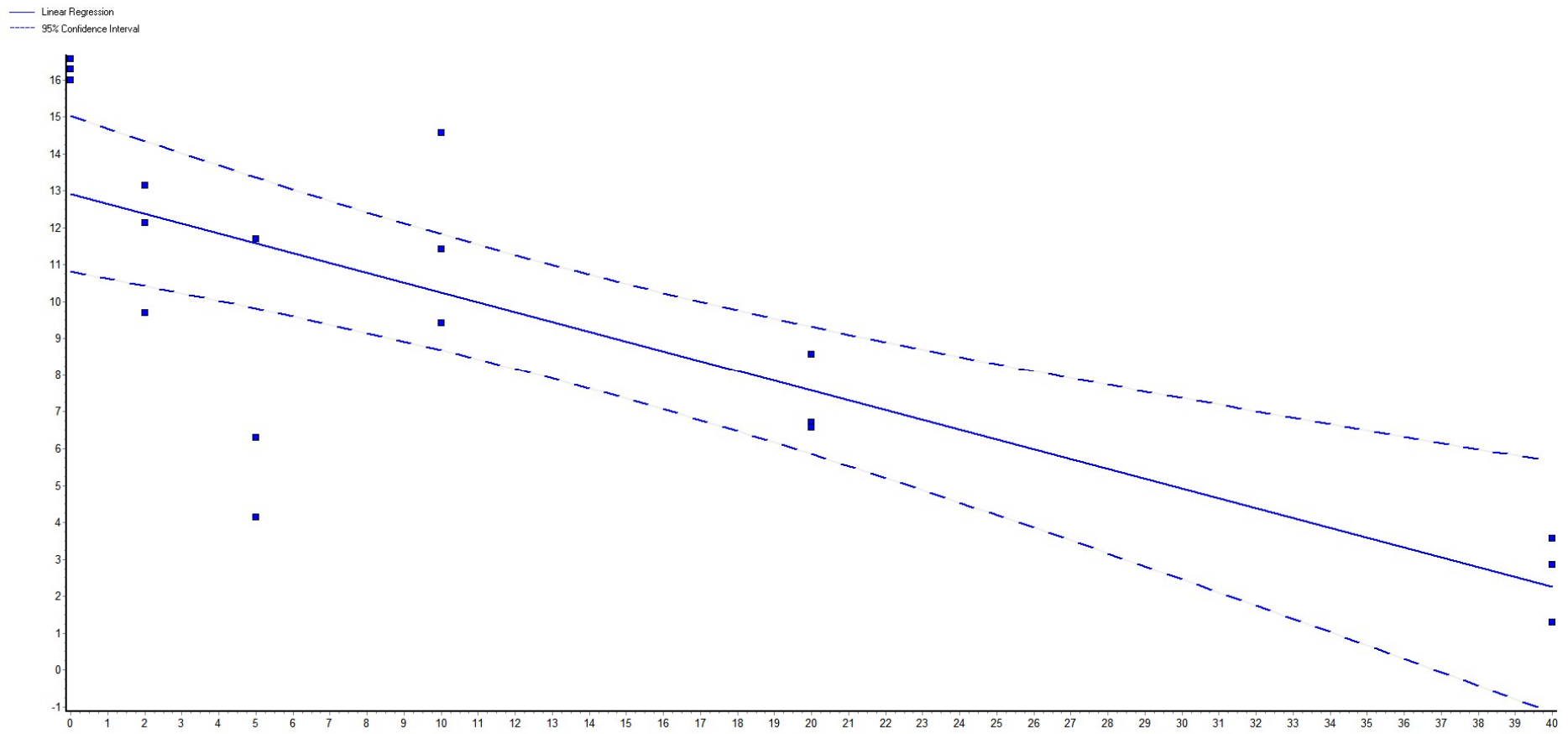


**Figure 48.** Image of the whole tissue section of superficial UPK3a-labelled porcine urothelium and the sectioned images. Three different regions of the urothelium layer were identified from each image of a whole tissue slide and denoted a, b or c using image analysis software (Zeiss ZEN lite, blue edition).

**Table 10. Ranking results of 18 images excised from the images of the whole superficial UPK3a-labelled porcine samples, to assess the integrity of labelled superficial UPK3a**

	0 min_a	0 min_b	0 min_c	2 min_a	2 min_b	2 min_c	5 min_a	5 min_b	5 min_c
Subject_1	15	17	16	10	11	14	9	5	4
Subject_2	17	18	16	8	15	13	14	2	4
Subject_3	16	18	17	14	13	8	11	9	4
Subject_4	16	18	17	5	11	13	8	6	4
Subject_5	15	18	17	10	13	16	11	6	4
Subject_6	17	16	18	10	13	14	12	6	4
Subject_7	18	7	15	11	9	14	17	10	5
Average	16.3	16.0	16.6	9.7	12.1	13.1	11.7	6.3	4.1
	10 min_a	10 min_b	10 min_c	20 min_a	20 min_b	20 min_c	40 min_a	40 min_b	40 min_c
Subject_1	18	13	6	12	7	8	3	2	1
Subject_2	12	10	9	7	5	3	1	11	6
Subject_3	15	12	10	7	6	5	1	2	3
Subject_4	15	9	14	7	12	10	1	3	2
Subject_5	14	9	12	7	8	5	1	2	3
Subject_6	15	11	9	8	5	7	1	3	2
Subject_7	13	16	6	12	4	8	1	2	3
Average	14.6	11.4	9.4	8.6	6.7	6.6	1.3	3.6	2.9

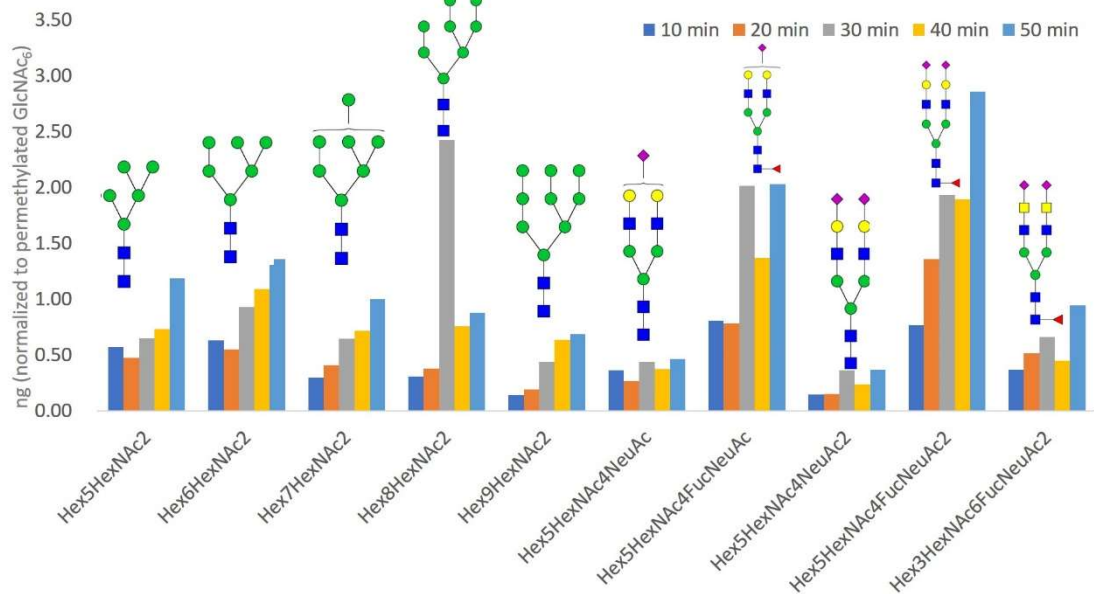




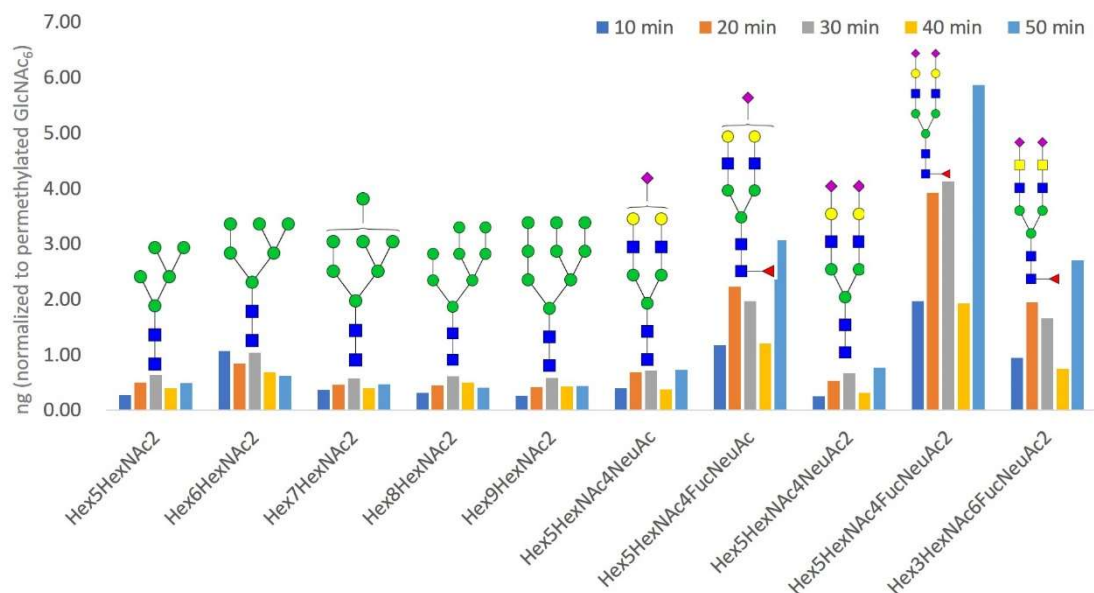
**Figure 49. The linearity of ranking scores assessing the integrity of labelled superficial UPK3a layer against different periods of trypsinization**

The amounts of *N*-glycans released from the luminal surface of two porcine bladders (bladder 1 and bladder 2) incubated with trypsin for different periods (10, 20, 30, 40, 50 minutes) were analyzed following permethylation and quantified with the internal standard permethylated GlcNAc<sub>6</sub> using MALDI-MS. The amount of each *N*-glycan species released from bladders 1 and 2 (Figure 50 and Figure 51, respectively) increased slowly after 30 minutes' trypsin treatment. However, extending the length of trypsinization did not release more different *N*-glycan species; 10 different *N*-glycans were identified in the two minute incubation group and were common to the other groups incubated for longer, without more different *N*-glycan species being identified.

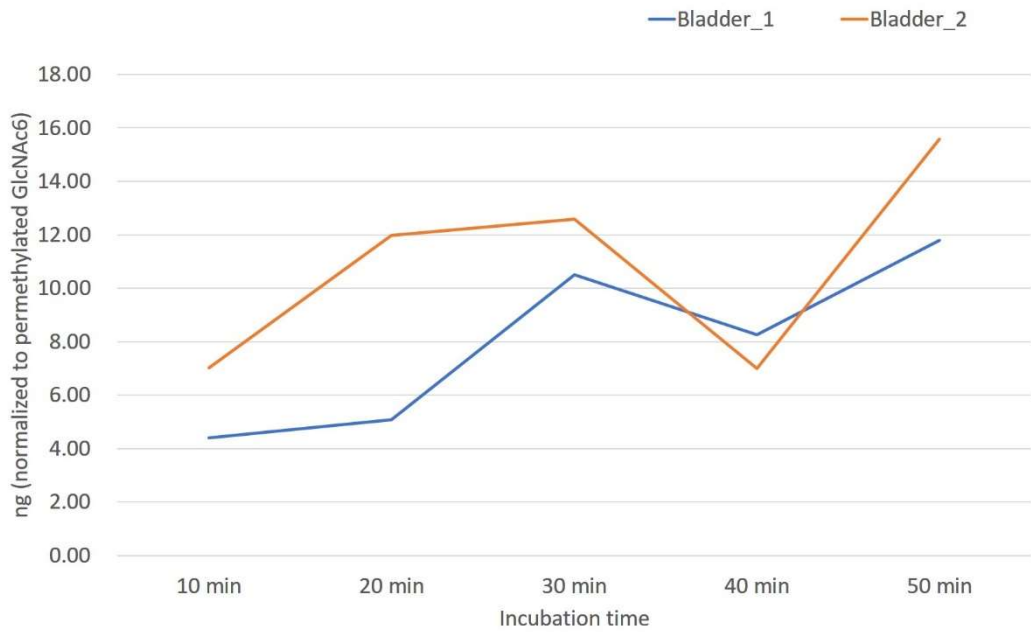
The results of using immunolabelling to post-monitor the extent of damage of superficial UPK3a on the luminal surface of porcine urothelium caused by trypsinization suggested that limited amounts of superficial UPK3a were left after incubation for 40 minutes. This may allow trypsin direct access to the surface of the superficial urothelial cell membrane, and start to compromise the integrity of urothelial apical cells, perhaps liberating glycopeptides from the sides of urothelial apical cells. In addition, extending the incubation over 30 minutes made little contribution to the total amount of apical surface *N*-glycans released (Figure 52) and the number of *N*-glycan species identified. As a result, 30 minute incubation was chosen as the trypsinization condition to be used for generating biological replicates, from which to collect the superficial urothelial cell apical surface *N*- and *O*-glycans.



**Figure 50.** The amount of each *N*-glycan species released from the luminal surface of porcine bladder 1 using on-tissue trypsinization for different periods.



**Figure 51.** The amount of each *N*-glycan species released from the luminal surface of porcine bladder 2 using on-tissue trypsinization for different periods



**Figure 52. The total amount of *N*-glycans released from the luminal side of porcine bladders 1 and 2 using on-tissue trypsinization for different periods.**

On the basis of the immunolabelling results and the mass spectrometric quantification results, the modified reaction vessel was deemed capable of holding stretched porcine bladders to expose an even luminal surface of the superficial urothelium for trypsinization.

#### 5.2.4 Sample preparation for mass spectrometric glycan analysis.

Appropriate conditions for maintaining the urothelium during trypsinisation are very far from the ideal conditions under which to carry out mass spectrometric analysis of the released cell-surface glycans. The use of HBSS containing  $\text{Ca}^{2+}/\text{Mg}^{2+}$  for the preparation of trypsin solution was chosen to be cell friendly and to minimise cell stress during trypsinization of the treated cell surface. The additional inorganic salts  $\text{Ca}^{2+}/\text{Mg}^{2+}$  (Table 11) were included to help maintain the cell-cell contacts and thus the barrier. However, the presence in particular of these inorganic salts was expected to be unfavourable for MALDI-MS analysis, there being the chance of these involatile inorganic components suppressing the ionization of permethylated glycans.

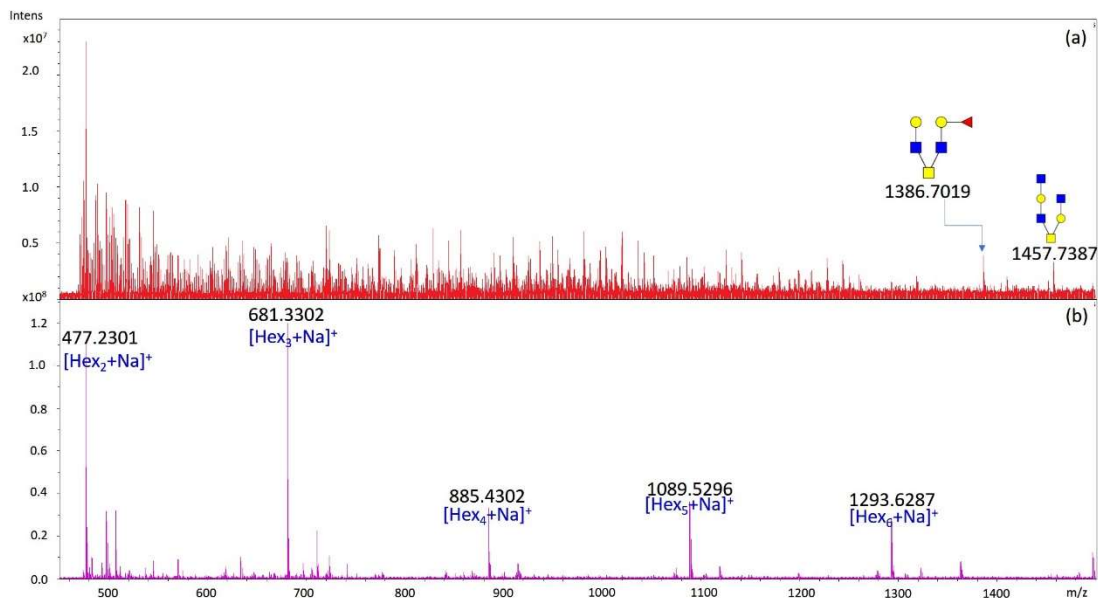
**Table 11. Medium formulation of HBSS+ $\text{Ca}^{2+}/\text{Mg}^{2+}$  (Gibco Cat. No. 24020)<sup>11</sup> used in this study**

<b>Components</b>	<b>CaCl<sub>2</sub></b>	<b>MgCl<sub>2</sub></b>	<b>MgSO<sub>4</sub></b>	<b>KCl</b>	<b>KH<sub>2</sub>PO<sub>4</sub></b>
mM	1.26	0.49	0.41	5.33	0.44
<b>Components</b>	<b>NaHCO<sub>3</sub></b>	<b>NaCl</b>	<b>Na<sub>2</sub>HPO<sub>4</sub></b>	<b>D-Glucose</b>	<b>Phenol Red</b>
mM	4.17	137.9	0.34	5.55	0.26

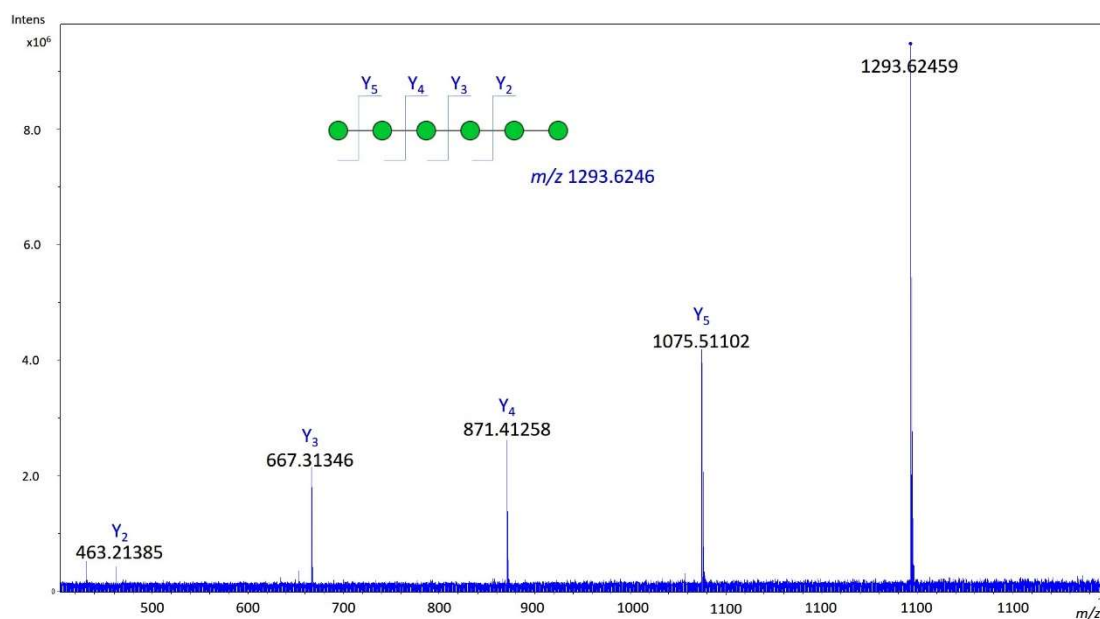
---

<sup>11</sup> <https://www.thermofisher.com/uk/en/home/technical-resources/media-formulation.152.html>

In addition, during the period of method development to release apical surface O-glycans from urothelial glycopeptides following PNGase F digestion, it was found that intense signals from polyhexoses dominated the MALDI mass spectra, compromising the detection of low abundance O-glycans. Porcine stomach mucin (PSM)<sup>68,242</sup> was thus used to investigate the influence on mass spectrometric detection of the use of HBSS+Ca<sup>2+</sup>/Mg<sup>2+</sup> (Figure 53), by comparing the mass spectra of permethylated O-glycans released from PSM dissolved in H<sub>2</sub>O or in HBSS+Ca<sup>2+</sup>/Mg<sup>2+</sup>. MS signals at *m/z* 477.2 (Hex<sub>2</sub>+Na<sup>+</sup>), 681.3 (Hex<sub>3</sub>+Na<sup>+</sup>), 885.4 (Hex<sub>4</sub>+Na<sup>+</sup>), 1089.5 (Hex<sub>5</sub>+Na<sup>+</sup>), and 1293.6 (Hex<sub>6</sub>+Na<sup>+</sup>) were obtained in the spectrum from 4 µg PSM dissolved in HBSS+Ca<sup>2+</sup>/Mg<sup>2+</sup> (Figure 53b), but not in that from the PSM dissolved in H<sub>2</sub>O (Figure 53a), suggesting that those intense signals originated in the HBSS+Ca<sup>2+</sup>/Mg<sup>2+</sup>. Product ion analysis of the signal at *m/z* 1293.6 (Figure 54) yielded a complete series of Y ions, consistent with a sodiated linear hexahexose [Hex<sub>6</sub>+Na]<sup>+</sup>. Similar results were obtained on product ion analysis of *m/z* 477.2, 681.3, 885.4 and 1089.5, indicating those were linear [Hex<sub>2</sub>+Na]<sup>+</sup>, [Hex<sub>3</sub>+Na]<sup>+</sup>, [Hex<sub>4</sub>+Na]<sup>+</sup> and [Hex<sub>5</sub>+Na]<sup>+</sup>, respectively.



**Figure 53. MALDI-MS spectra of O-glycans released from 4 µg PSM using NH<sub>4</sub>OH. PSM was dissolved in a) 2 mL H<sub>2</sub>O or b) 2 mL HBSS+Ca<sup>2+</sup>/Mg<sup>2+</sup> prior to β-elimination.**



**Figure 54. Product ion spectrum of m/z 1293.6246**

The source of these polyhexoses [Hex<sub>2~6</sub>] was most probably the D-glucose used in the HBSS+Ca<sup>2+</sup>/Mg<sup>2+</sup> (Table 11); these would be expected to be a by product of the industrial enzymatic hydrolysis of starch to produce glucose<sup>12</sup>. This suggestion is supported by the observation of similar sodiated signals for polyhexoses on analysis of native glucose (lab stock) using MALDI-MS.

The detrimental effects on detection of low abundance glycans due to the presence in the released glycan samples of components of the HBSS medium led to an investigation into how to remove these components for MALDI-MS analysis of permethylated glycans. Sample purification was investigated using SPE cartridges with different packings, e.g. those retaining on the basis of hydrophobicity (reversed phase C18) and hydrophilicity (graphitized carbon), to desalt and purify the released glycans.

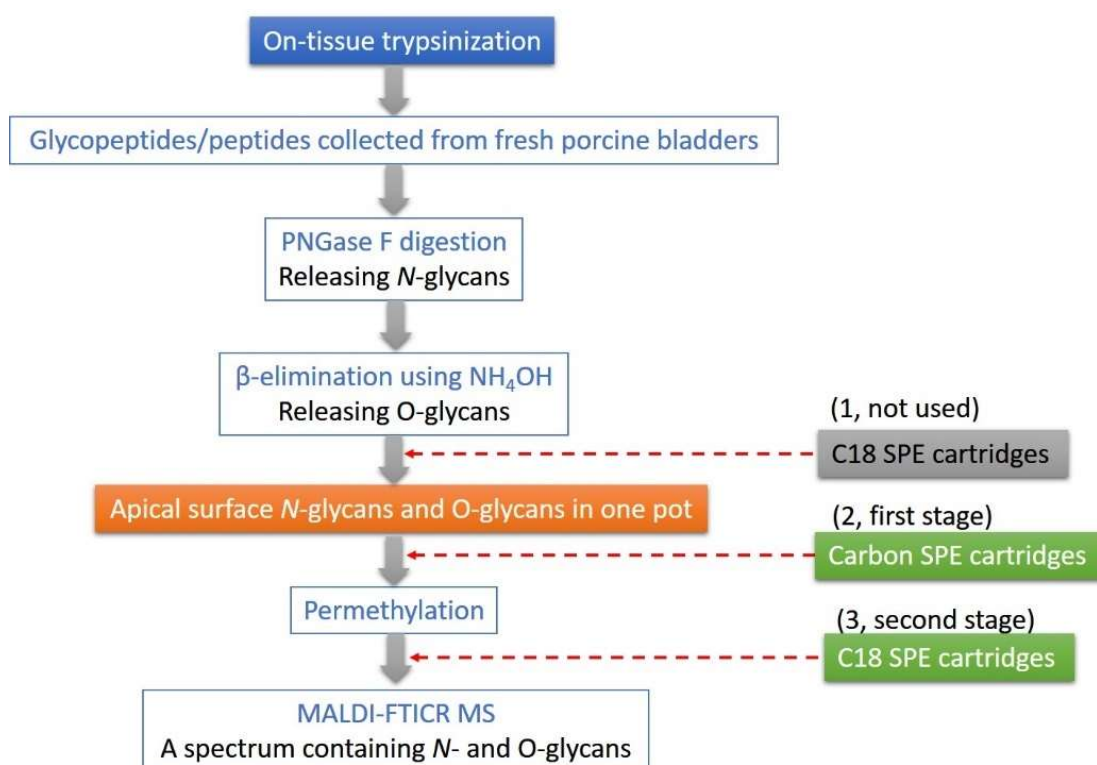
The sample purification method development was initially based on the protocol reported by Hamounda *et al.*<sup>197</sup>, in which three-stage purifications were applied to obtain the *N*-glycans released from the surface of cultured cells using trypsinization and PNGase F digestion. Briefly, 1) reversed phase C18 SPE separation was used to separate the *N*-glycans from tryptic peptides, followed by 2) graphitized carbon SPE to desalt the sample solution prior to permethylation. 3) Reversed phase C18 SPE separation was used again after permethylation to clean up the permethylated *N*-

---

<sup>12</sup> <https://en.wikipedia.org/wiki/Glucose#Commercial>



glycans before MALDI-MS analysis. The trypsin solution prepared in a biologically-friendly buffer (PBS) in Hamouda's work was not dissimilar to that (HBSS+Ca<sup>2+</sup>/Mg<sup>2+</sup>) used in the present work. Consequently, I set out to evaluate the three-stage purification (Figure 55) for the sample purification required in the work described in this chapter.

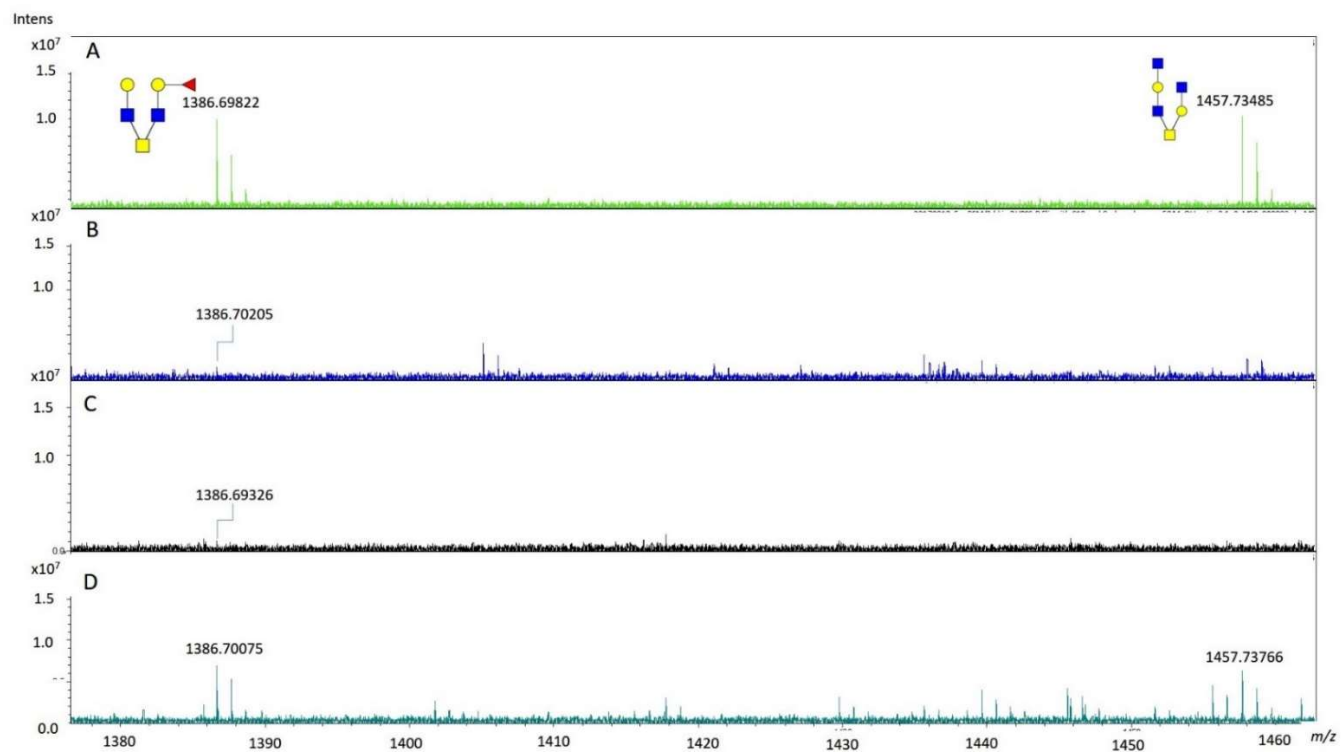


**Figure 55. Three-stage purification reported in Hamouda's work to purify N-glycans obtained from the sample matrix containing inorganic salts, using graphitized carbon and C18 SPE cartridges. The use of C18 SPE purification (grey box) before using carbon SPE cartridges was abandoned in the porcine bladder work, after method development.**

The first C18 SPE purification was assumed to facilitate the permethylation and analysis of glycans by removing the tryptic peptides from the samples. Based on long experience in the research group (e.g. ref<sup>243</sup>), the first C18 SPE purification was assumed to be important and so was retained and so the first experiments assessed the process using the second, carbon-based SPE separation and the third C18 SPE separation.

The efficiency of the use of carbon SPE cartridges to desalt the released glycans was assessed by comparing the mass spectra of 1) permethylated O-glycans released from PSM dissolved in H<sub>2</sub>O for  $\beta$ -elimination isolated either with or without carbon SPE separation (both prepared using the first C18 SPE separation). The mass spectra acquired from the two sets of glycans gave identical signal-to-noise ratios for peaks for the PSM O-glycans, suggesting the carbon SPE separation led to no remarkable sample loss on the step intended for separation of glycans from inorganic salts. The effect of the carbon SPE cartridges was further assessed by comparing the mass spectra of 2) permethylated O-glycans released from PSM dissolved in HBSS+Ca<sup>2+</sup>/Mg<sup>2+</sup> for  $\beta$ -elimination isolated either with or without carbon SPE separation (again, using the first C18 SPE separation). There were no peaks identifiable as PSM O-glycans in the HBSS+Ca<sup>2+</sup>/Mg<sup>2+</sup> sample prepared without the carbon SPE separation, while weak peaks were identified for PSM O-glycans following carbon SPE separation. The signal-to-noise ratios of peaks for PSM O-glycans identified in the samples prepared in H<sub>2</sub>O and isolated using carbon SPE separation (Figure 56A) were much higher than those of peaks from the sample prepared in

HBSS+Ca<sup>2+</sup>/Mg<sup>2+</sup> (Figure 56B), suggesting the carbon SPE separation was not enough to remove the interference from HBSS+Ca<sup>2+</sup>/Mg<sup>2+</sup>.

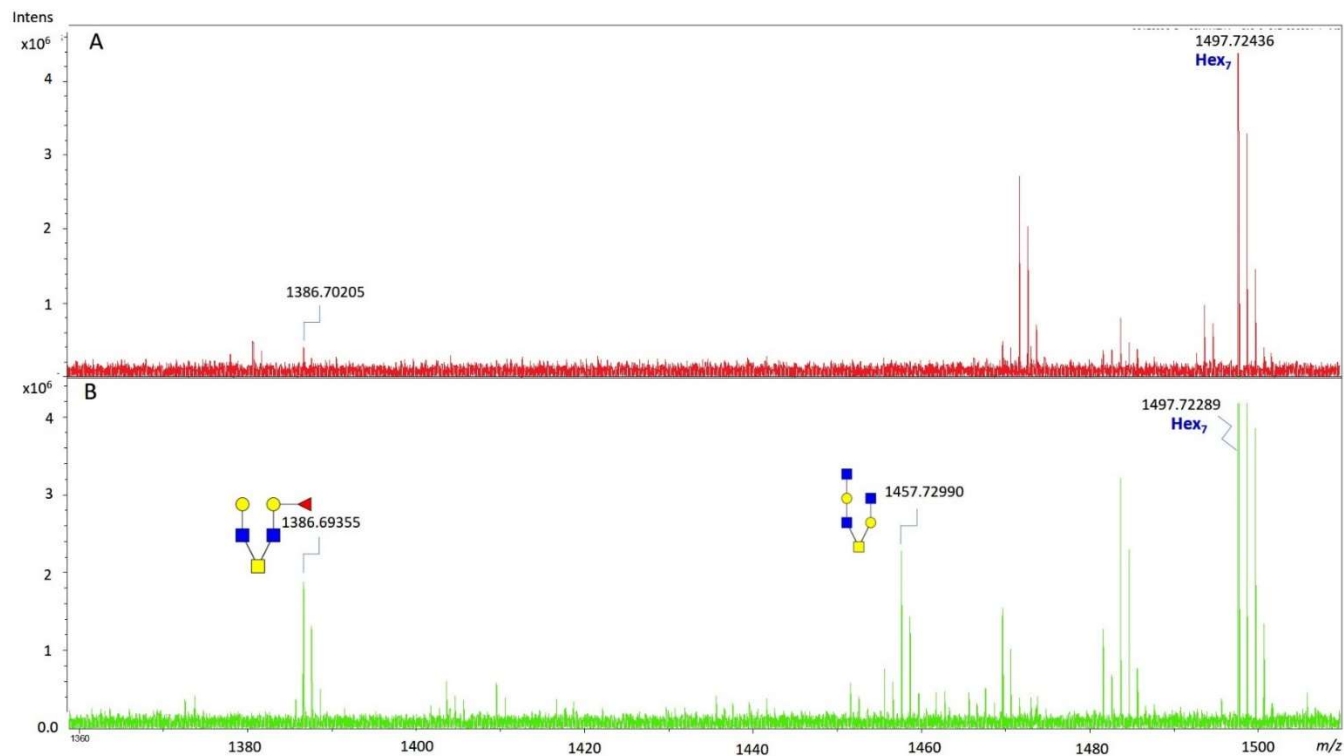


**Figure 56. MALDI mass spectrum of permethylated O-glycans released from 5  $\mu$ g porcine stomach mucin (PSM). PSM dissolved in (A)  $H_2O$  followed by 1<sup>st</sup> C18 SPE/2<sup>nd</sup> carbon SPE, (B) HBSS+ $Ca^{2+}$ / $Mg^{2+}$  followed by 1<sup>st</sup> C18 SPE/2<sup>nd</sup> carbon SPE, (C) HBSS+ $Ca^{2+}$ / $Mg^{2+}$  followed by 1<sup>st</sup> C18 SPE and 3<sup>rd</sup> C18 SPE after permethylation and (D) HBSS+ $Ca^{2+}$ / $Mg^{2+}$  followed by 1<sup>st</sup> C18 SPE/2<sup>nd</sup> carbon SPE and 3<sup>rd</sup> C18 SPE after permethylation. The scales of the Y-axis are similar, to allow comparison of the signal-to-noise ratios of peaks at  $m/z$  1386.70.**

The value of the third (C18) SPE separation was then assessed for its ability to clean up the glycans after permethylation, by comparing the mass spectra of PSM O-glycans further processed from the above experiments. The intensity of the signal at  $m/z$  1386.7, in the spectrum of the sample released from PSM in HBSS+Ca<sup>2+</sup>/Mg<sup>2+</sup> (Figure 56C), was enhanced from undetectable to weak after post-methylation C18 SPE separation, applied without prior carbon SPE separation. Moreover, the signal-to-noise ratio of the peak at  $m/z$  1386.7 in the spectrum of the sample prepared in HBSS+Ca<sup>2+</sup>/Mg<sup>2+</sup> (Figure 56D) was remarkably enhanced after post-methylation C18 SPE separation if the sample had also previously been treated with carbon SPE separation by comparing to those of peaks from the sample without post-methylation C18 separation (Figure 56B). These results suggested that the post-methylation C18 SPE separation brings an important improvement in sample purification for samples handled in HBSS+Ca<sup>2+</sup>/Mg<sup>2+</sup>. It is worth noting that the third C18 carbon separation gave negligible sample loss of permethylated glycans; a mass spectrum identical to that in Figure 56A was obtained after the third C18 SPE separation performed on the same sample.

In spite of these successes, the signal-to-noise ratios of permethylated glycans released from sample prepared in HBSS+Ca<sup>2+</sup>/Mg<sup>2+</sup> (Figure 56D) after three stages of purification were still lower than those of sample prepared in H<sub>2</sub>O treated similarly. A subsequent study was thus conducted to assess the value of the first C18 SPE separation, included to separate glycans from tryptic peptides (Figure 55, grey box). The signal-to-noise ratio for the O-glycan at  $m/z$  1386.70 released from the PSM prepared in HBSS+Ca<sup>2+</sup>/Mg<sup>2+</sup> followed by three stage purification (Figure 57A) was

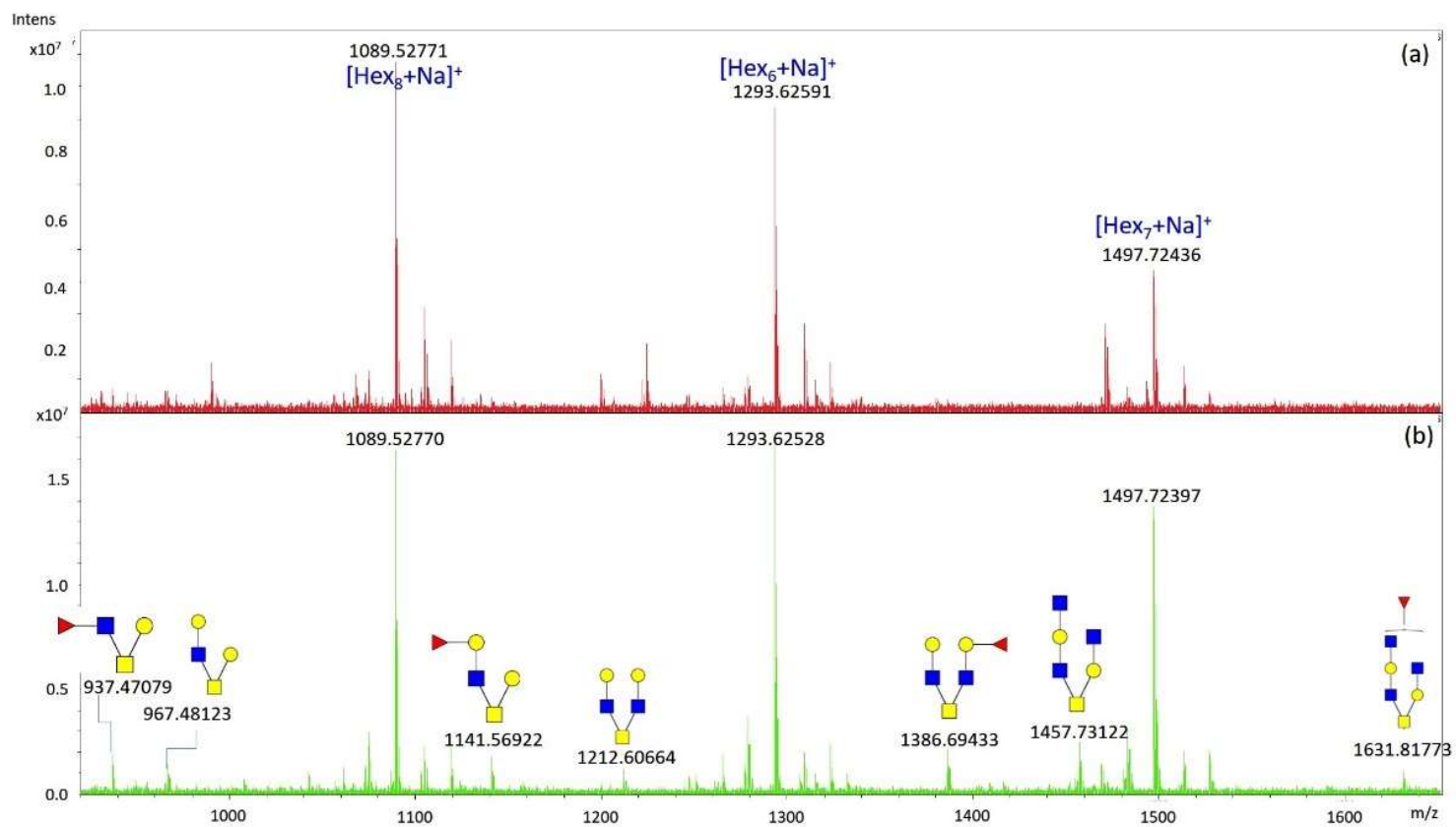
much lower than that for the same species in the sample prepared without using the first C18 SPE (Figure 57B). This suggested that substantial sample loss may be occurring during the first C18 SPE separation. In addition, the effect of sample loss affecting the detection limits for low abundance glycans using MALDI-MS may be magnified in a sample with complex ingredients, e.g. involatile inorganic components and high abundance polyhexoses, that suppress the ionization of permethylated glycans. It was thus decided to omit the first C18 SPE steps for separating glycans from tryptic peptides, but to proceed using the carbon desalting step and the post-methylation C18 SPE step.



**Figure 57. MALDI mass spectrum of permethylated O-glycans released from 5  $\mu\text{g}$  porcine stomach mucin (PSM). PSM dissolved in HBSS+Ca<sup>2+</sup>/Mg<sup>2+</sup> followed by (A) three stage purification, 1<sup>st</sup> C18 SPE / 2<sup>nd</sup> carbon SPE / 3<sup>rd</sup> C18 SPE separation or (B) two stage purification, 2<sup>nd</sup> carbon SPE / 3<sup>rd</sup> C18 SPE separation only. The scales of the Y-axis allow direct comparison of the signal-to-noise ratios of peaks at  $m/z$  1386.70.**

An optimized protocol for the release of *N*- and O-glycans from trypsinized glycopeptides/peptides, and their purification for MALDI-MS was thus developed using two stages of SPE purification (Figure 55). The first stage in the optimized protocol was conducted using graphitized carbon SPE cartridges to purify the samples containing *N*- and O-glycans, collected after PNGase F digestion and  $\beta$ -elimination. The second purification, using C18 SPE cartridges, was conducted after permethylation prior to MALD-MS analysis. A study was conducted to compare the results obtained with and without the use of these additional purification steps. 5  $\mu\text{g}$  porcine stomach mucin was prepared in 1 mL HBSS+Ca<sup>2+</sup>/Mg<sup>2+</sup> and the glycans released using NH<sub>4</sub>OH. The mass spectrum obtained from the sample prepared without the SPE purification steps had no intense peaks for permethylated O-glycans (Figure 58a). By contrast, intense peaks for permethylated O-glycans were observed at *m/z* 937.47, 967.48, 1141.57, 1212.61, 1386.69, 1457.73 and 1631.82 in the mass spectrum obtained following purification (Figure 58b).





**Figure 58. MALDI-MS spectrum of permethylated O-glycans released from 5  $\mu\text{g}$  porcine stomach mucin using the protocol a) without or b) with two-stage SPE purification. Only intense peaks are identified and labelled with putative glycan structures.**

However, intense signals for the polyhexoses in the HBSS+Ca<sup>2+</sup>/Mg<sup>2+</sup> still dominated the MALDI mass spectra. The polyhexoses are unlikely to be easily separated from the *N*- and *O*-glycans using graphitized carbon or C18 SPE cartridges with simple conditions, because of the similarities in structure of the compounds. For the future work, if it proves necessary to remove or reduce the intense signals of polyhexoses if they compromise the detection of low abundance glycans using MALDI-MS, it may be necessary to ensure that the Glc in the HBSS+Ca<sup>2+</sup>/Mg<sup>2+</sup> medium is free of the polyhexose contaminants.

### 5.2.5 Summary

The use of graphitized carbon and C18 SPE cartridges improved the protocol for on-tissue trypsinization using trypsin solution prepared in HBSS+Ca<sup>2+</sup>/Mg<sup>2+</sup> and enhanced the detection of low abundance of permethylated *O*-glycans using MALDI-MS. This optimized protocol (Figure 55) was implemented for the release of *N*- and *O*-glycans from several samples collected from fresh porcine bladders using on-tissue trypsinization and successfully contributed to the glycan profile identified using MALDI-MS. This optimized protocol was thus used to analyse the glycans released from three individual porcine bladders (biological replicates) for the identification of superficial urothelial cell apical surface *N*- and *O*-glycomes using MALDI-MS.

### 5.3 Porcine urothelial cell apical surface *N*- and *O*-glycans: towards differential glycome analysis at the apical cell surface

Three porcine bladders, denoted A, B and C, were collected and processed side-by-side as follows. Apical cell surface *N*- and *O*-glycans were attempted to be collected from the three fresh porcine bladders, using the in-house built reaction device at 37 °C using 30 minute trypsinization of the luminal surface of superficial urothelium. The trypsinized porcine bladders were subjected to formalin fixation and paraffin embedding right after trypsinization for subsequent immunolabelling using antibody AU1 to label superficial UPK3a.

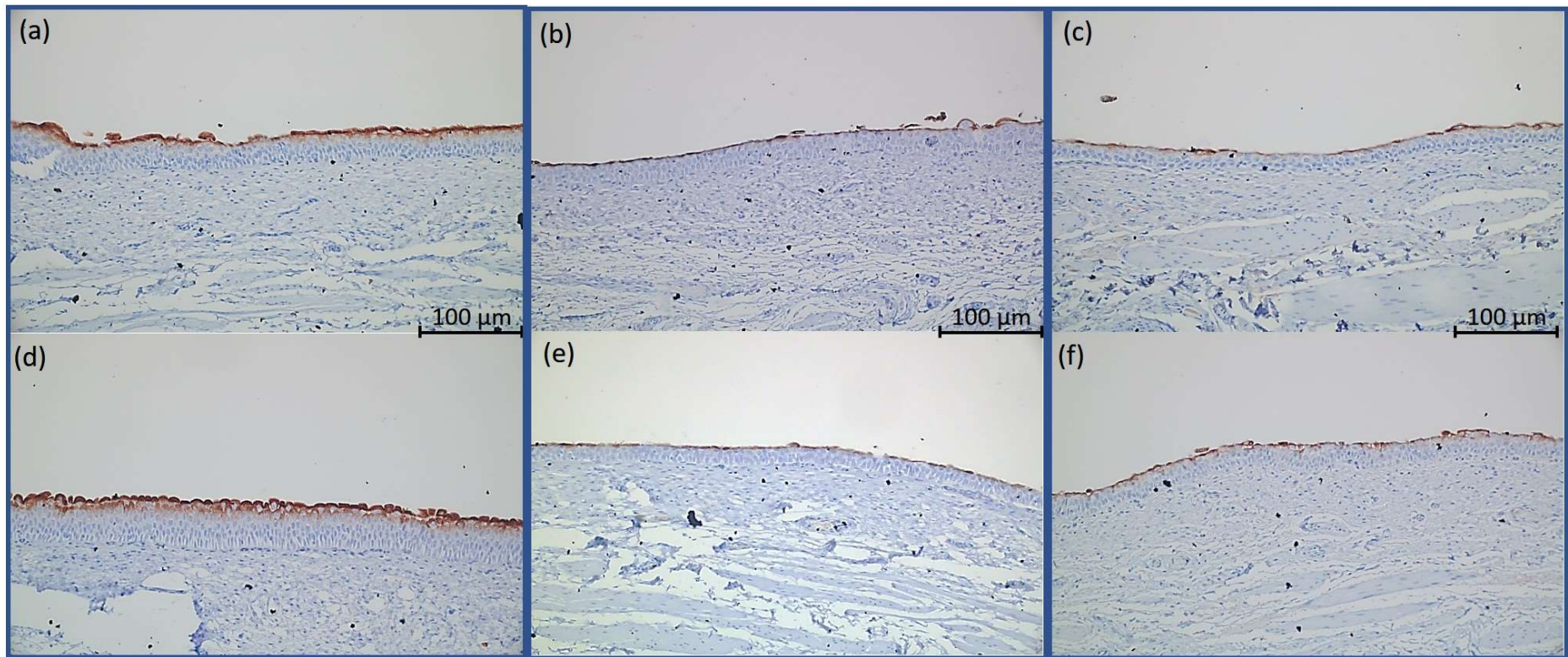
The collected trypsinized supernatants were subjected to PNGase F digestion and  $\beta$ -elimination to release *N*- and *O*-glycans that were isolated as a single pool, followed by the use of graphitized carbon before and C18 SPE separation after permethylation. Permethylated glycan samples containing *N*- and *O*-glycans, were spiked with permethylated GlcNAc<sub>6</sub> as an internal standard at the stage of forming the sample spot on the MALDI plate, for analysis using MALDI-MS, semi-quantifying the amount of urothelial glycans.

### 5.3.1 Using immunolabelling to post-monitor the luminal surface of porcine bladders after on-tissue trypsinization

The immunolabelling results of trypsinized porcine bladders using antibody AU1 to label superficial UPK3a (Figure 59) showed very good coverage of labelled UPK3a on the three porcine bladders before (Figure 59a, b and c) and after (Figure 59d, e and f) 30 minute trypsinization. The immunolabelling results of trypsinized porcine bladders were expected based on the demonstration during method development (Section 5.2.3) that 30 minute trypsinization left intact most of the superficial UPK3a on the luminal surface of porcine bladders. Moreover, the integrity of the labelled UPK3a layer remained intact after trypsinization, suggesting there was no contact between the trypsin and the lateral surfaces of the superficial urothelial cells.

It was noticed that bladder A has a thicker layer of labelled UPK3a than do bladders B and C. The difference in the thickness of the labelled UPK3a layers between the three porcine bladders was likely to be caused by individual biological differences and not by sample preparation, since all the specimens were processed together through the same IHC protocol. This assumption of individual biological differences causing the differing thicknesses of the labelled superficial UPK3a layer is also supported by the results of quantification of the released *N*- and *O*-glycans using MALDI-MS (see below).

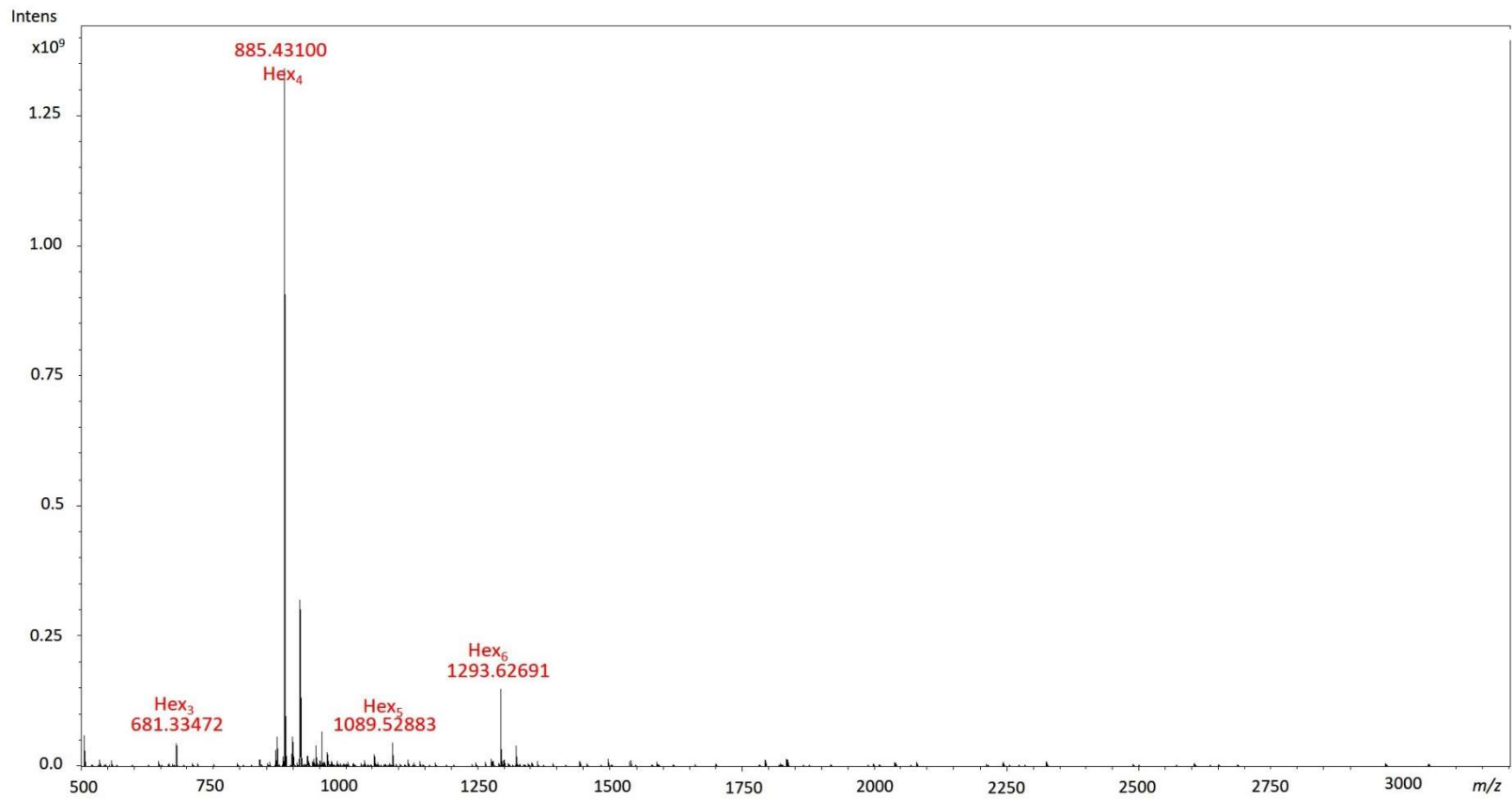
**Figure 59. Immunolabelling of superficial UPK3a-labelled porcine bladders. Bladder A: (a) and (d), bladder B: (b) and (e) and bladder C: (c) and (f) before and after 30 minute trypsinization, respectively**



### 5.3.2 Apical surface *N*- and *O*-glycans of superficial porcine urothelium

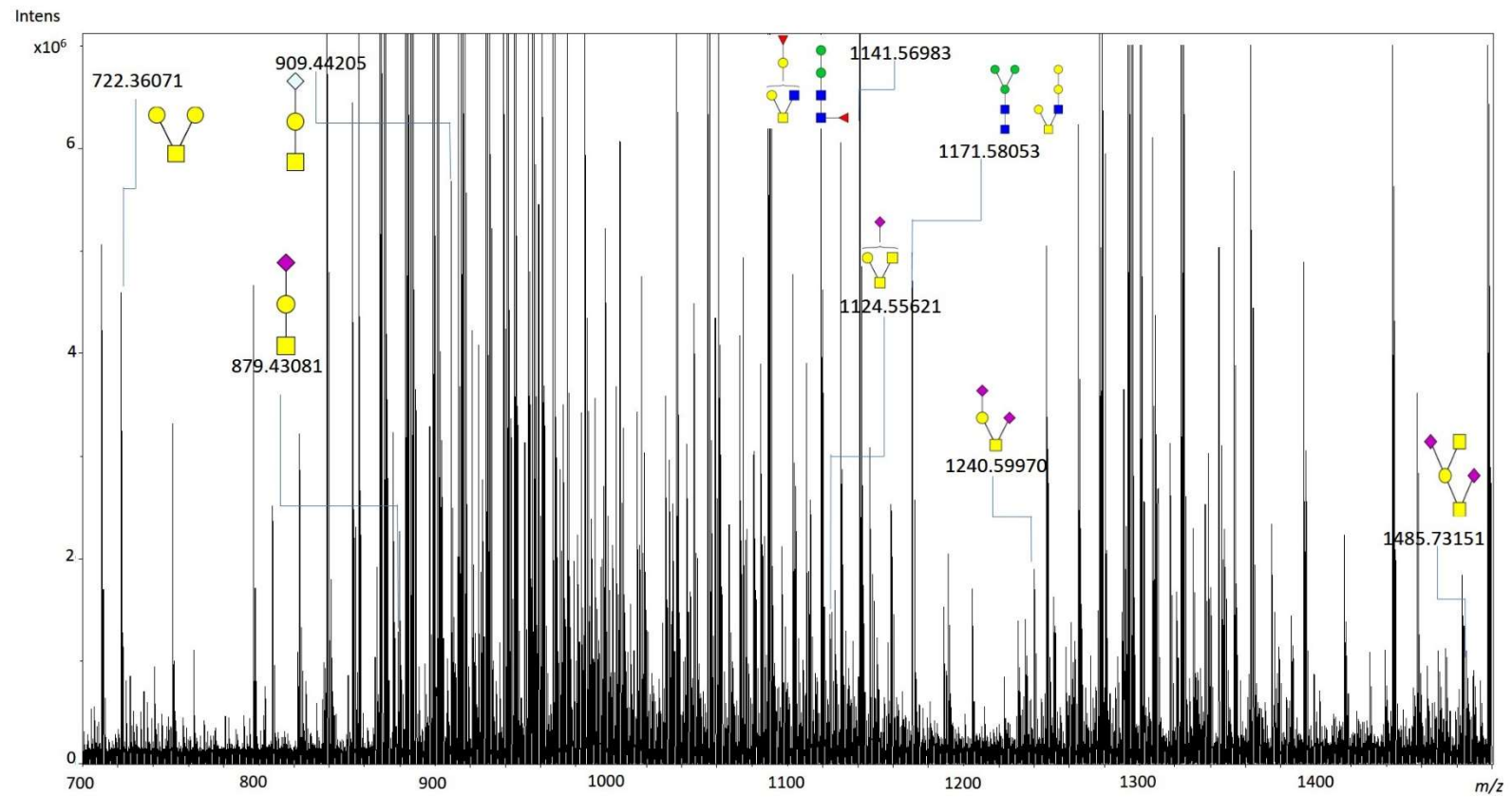
Representative MALDI mass spectra obtained from the *N*- and *O*-glycans from the three individual porcine bladders after permethylation were very similar to each other; the only main difference between each spectrum is the intensities of peak. A typical MALDI mass spectrum is shown from  $m/z$  500 to 3200 (Figure 60); intense signals from polyhexoses still dominated the MALDI mass spectrum. The MALDI mass spectrum was then plotted in two sections, the first from  $m/z$  700 to 1500 (Figure 61) and the second from  $m/z$  1500 to 3200 (Figure 62). Most of the peaks for apical cell surface *N*-glycans were much more intense than those for apical cell surface *O*-glycans. For apical cell surface *O*-glycans, the intense peaks were assigned as mucin-type *O* glycans at  $m/z$  722.36 (Hex<sub>2</sub>HexNAc), 879.43 (HexHexNAcNeuAc), 909.44 (HexHexNAcNeuGc), 1124.56 (NeuAcHexHexNAc<sub>2</sub>NeuAc), 1240.60 (HexHexNAcNeuAc<sub>2</sub>) and 1485.73 (HexHexNAc<sub>2</sub>NeuAc<sub>2</sub>). For apical cell surface *N*-glycans, the most intense peaks in all the mass spectra can be assigned to complex *N*-glycans at  $m/z$  1794.90 (Hex<sub>4</sub>HexNAc<sub>3</sub>), 1835.92 (Hex<sub>3</sub>HexNAc<sub>4</sub>Fuc), 2040.03 (Hex<sub>4</sub>HexNAc<sub>4</sub>Fuc), 2081.06 (Hex<sub>3</sub>HexNAc<sub>5</sub>), 2244.13 (Hex<sub>5</sub>HexNAc<sub>4</sub>Fuc), 2326.19 (Hex<sub>3</sub>HexNAc<sub>6</sub>Fuc), 2605.32 (Hex<sub>5</sub>HexNAc<sub>4</sub>FucNeuAc), 2652.35 (Hex<sub>7</sub>HexNAc<sub>4</sub>Fuc), 2966.51 (Hex<sub>5</sub>HexNAc<sub>4</sub>FucNeuAc<sub>2</sub>), and 3048.48 (Hex<sub>3</sub>HexNAc<sub>6</sub>FucNeuAc<sub>2</sub>). It should be noted that the peaks at  $m/z$  1141.57 (Hex<sub>2</sub>HexNAc<sub>2</sub>Fuc) and 1171.58 (Hex<sub>3</sub>HexNAc<sub>2</sub>) can be assigned as either *N*-glycans or *O*-glycans; these signals had been identified in the data generated during early method development, either solely following PNGase

F digestion or solely  $\beta$ -elimination, suggesting that the two peaks in the current data are likely to be mixtures of *N*- and *O*-glycans.



**Figure 60. Representative MALDI mass spectrum of porcine urothelial cell apical surface *N*-glycan and *O*-glycan profiles obtained from the luminal surface of porcine bladder,  $m/z$  500 to 3200. Intense signals from polyhexoses dominated the MALDI mass spectrum.**





**Figure 61. Representative MALDI mass spectrum of porcine urothelial cell apical surface *N*-glycan and *O*-glycan profiles obtained from the luminal surface of porcine bladder, *m/z* 700 to 1500. The proposed *O*-glycan structures of peaks are depicted.**

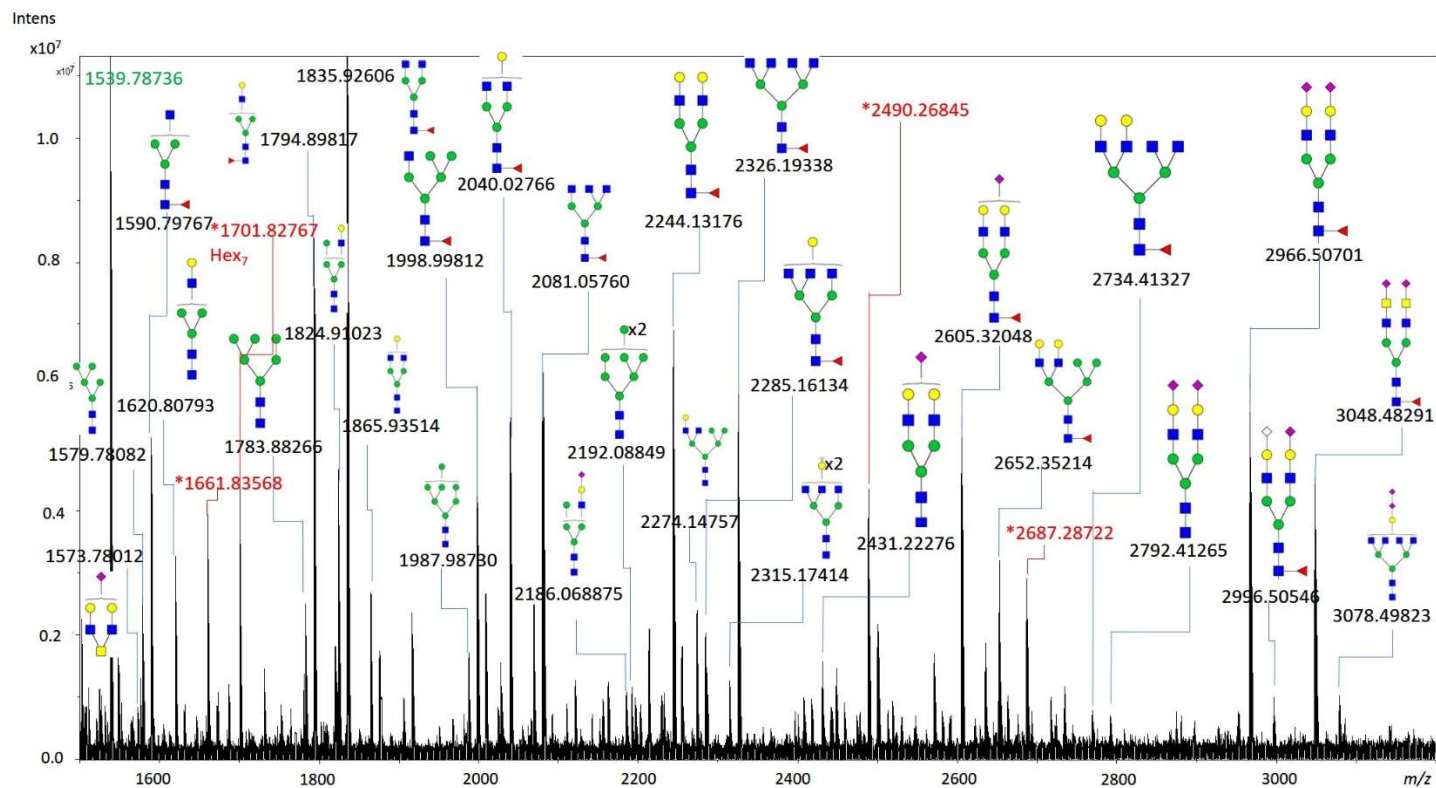


Figure 62. Representative MALDI mass spectrum of porcine urothelial cell apical surface *N*-glycan and *O*-glycan profiles obtained from the luminal surface of porcine bladder, *m/z* 1500 to 3200. The putative structures of intense peaks are depicted. Asterisks represent intense signals not to assign as *N*-glycans

In total 55 different urothelial cell apical surface *N*-glycans (Figure 63) and 12 different O-glycans (Figure 64) were identified over the three biological replicates. The normalized signal intensities for each glycan species, using permethylated GlcNAc<sub>6</sub> (*m/z* 1539.78) as an internal standard, from triplicate MALDI spots (defined as technical replicates) were averaged and the mean was used to derive the normalized amounts of glycans from one aliquot of trypsinized supernatant from each porcine bladder (defined as one experimental replicate). The normalized amounts of glycans from three experimental replicates from each porcine bladder were averaged for each biological replicate and plotted using Excel; the error bars indicate standard deviation of the mean. Small standard deviations (*n*=3, coefficient of variation (CV) less than 20%) were obtained among experimental replicates for most of the *N*- and O-glycan structures, demonstrating that the optimized protocol (Figure 55) for on-tissue trypsinization followed by sequential glycan release using PNGase F digestion followed  $\beta$ -elimination with two-stage purifications is capable of giving high reproducibility of data for apical cell surface glycan identification.

Most porcine urothelial cell apical surface glycan structures were highly reproducible across all three biological replicates. 47 of the 55 *N*-glycans were identified in all three biological replicates and are summarised with their mass accuracies in Table 12. All 12 apical cell surface O-glycan structures were common to all three biological replicates and are shown with their mass accuracies in Table 13.

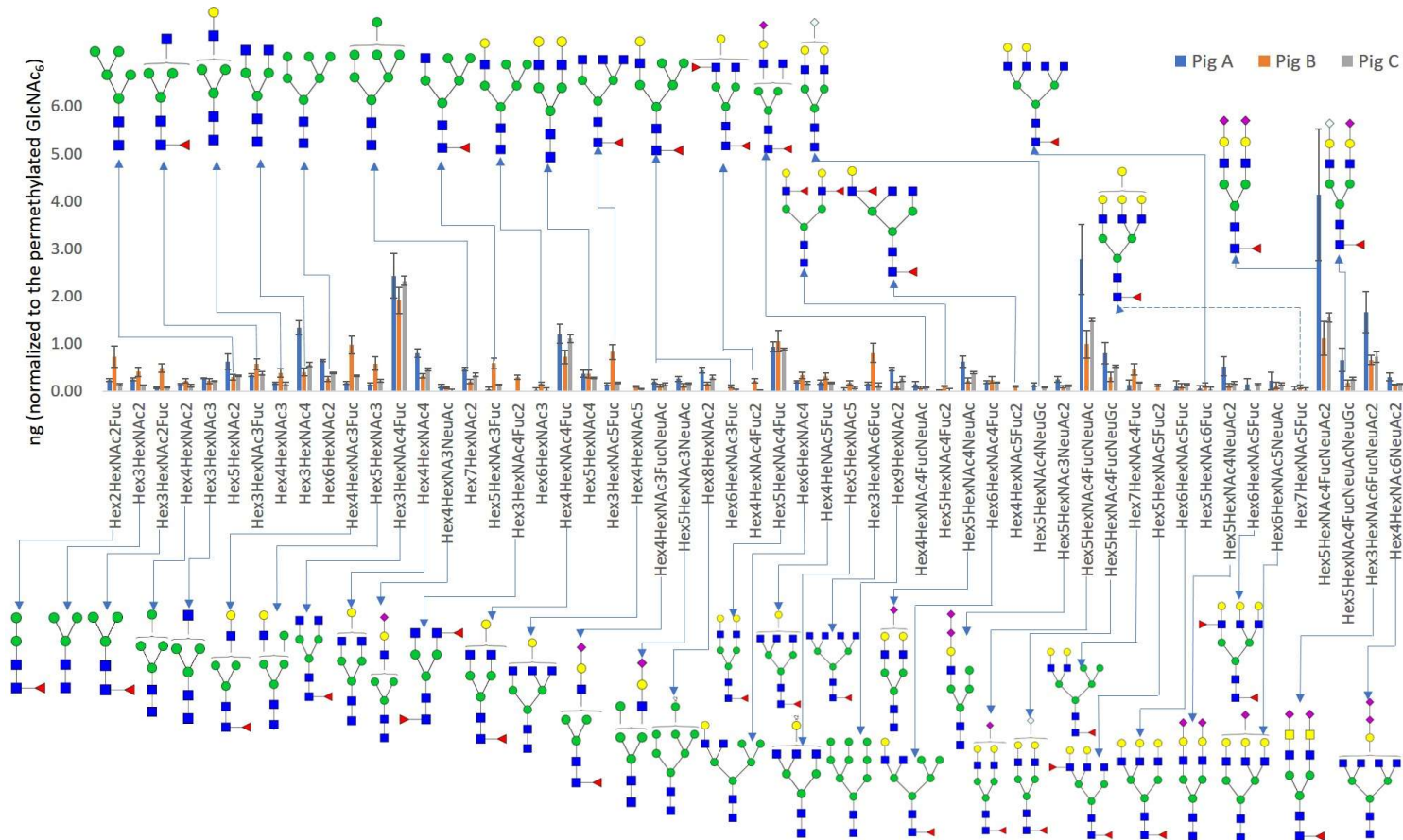


Figure 63. 55 permethylated porcine urothelial cell apical surface *N*-glycans, taking the three biological replicates together.

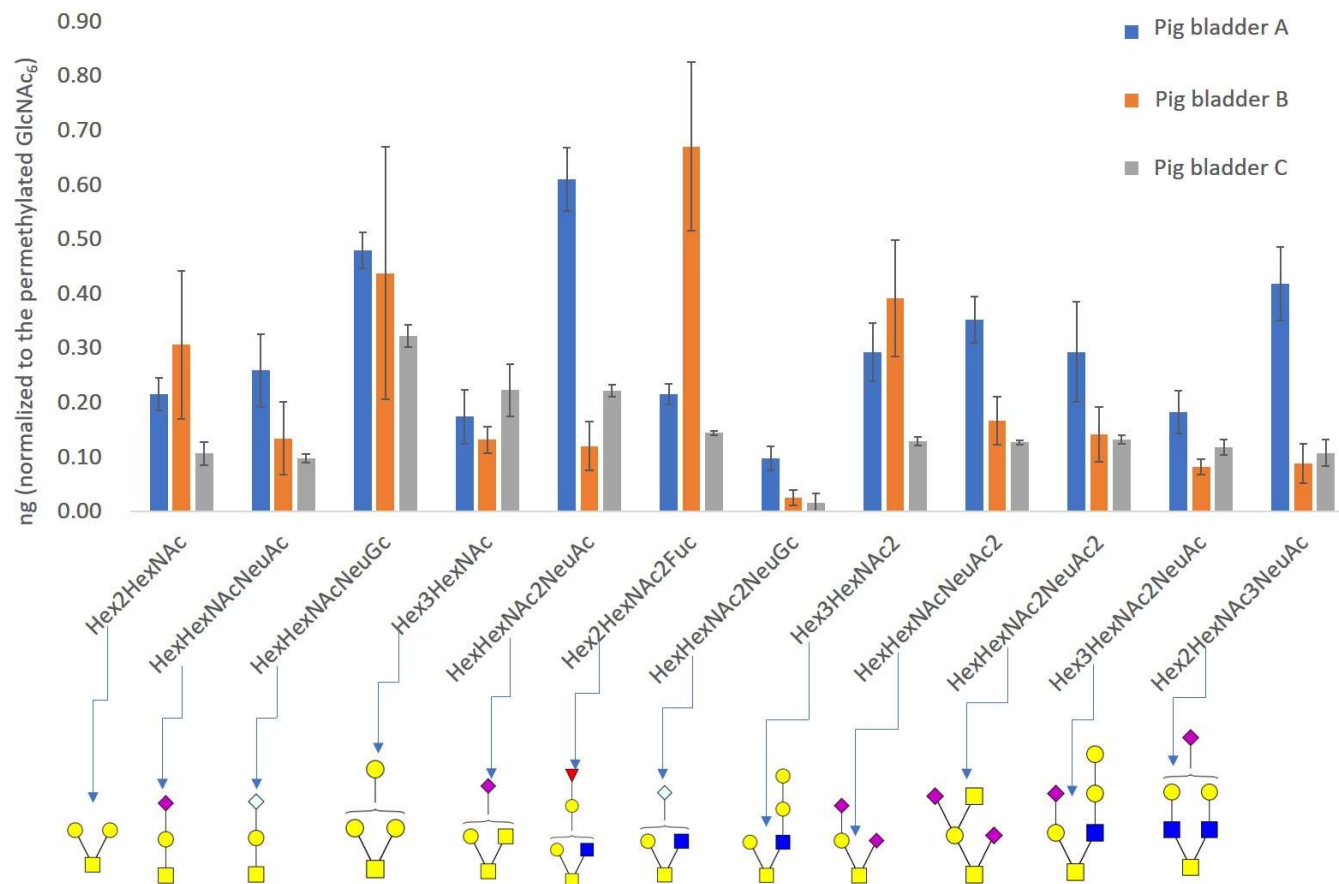


Figure 64. 12 permethylated porcine urothelial cell apical surface O-glycans, taking the three biological replicates together.

**Table 12. 47 porcine urothelial cell apical surface *N*-glycans common to the three biological replicates**

MALDI Spots		Porcine bladder A		Porcine bladder B		Porcine bladder C	
Components	theoretical m/z	Average m/z (n=9)	ppm	Average m/z (n=9)	ppm	Average m/z (n=9)	ppm
HexNAc <sub>6</sub> (Internal standard)	1539.789	1539.7905	0.96	1539.7872	-1.15	1539.7872	-1.19
Hex <sub>2</sub> HexNAc <sub>2</sub> Fuc	1141.5725	1141.5710	-1.28	1141.5699	-2.27	1141.5707	-1.57
Hex <sub>3</sub> HexNAc <sub>2</sub>	1171.5831	1171.5813	-1.56	1171.5845	1.17	1171.5809	-1.91
Hex <sub>3</sub> HexNAc <sub>2</sub> Fuc	1345.6723	1345.6710	-1.00	1345.6698	-1.89	1345.6704	-1.42
Hex <sub>4</sub> HexNAc <sub>2</sub>	1375.6828	1375.6811	-1.25	1375.6803	-1.81	1375.6855	1.96
Hex <sub>3</sub> HexNAc <sub>3</sub>	1416.7094	1416.7112	1.26	1416.7065	-2.08	1416.7074	-1.44
Hex <sub>5</sub> HexNAc <sub>2</sub>	1579.7826	1579.7828	0.16	1579.7808	-1.13	1579.7809	-1.08
Hex <sub>3</sub> HexNAc <sub>3</sub> Fuc	1590.7986	1590.7993	0.45	1590.7977	-0.57	1590.7973	-0.80
Hex <sub>4</sub> HexNAc <sub>3</sub>	1620.8091	1620.8094	0.16	1620.8076	-0.91	1620.8075	-0.98
Hex <sub>3</sub> HexNAc <sub>4</sub>	1661.8357	1661.8355	-0.12	1661.8356	-0.08	1661.8350	-0.44

<b>Components</b>	<b>theoretical m/z</b>	<b>Average m/z (n=9)</b>	<b>ppm</b>	<b>Average m/z (n=9)</b>	<b>ppm</b>	<b>Average m/z (n=9)</b>	<b>ppm</b>
Hex <sub>6</sub> HexNAc <sub>2</sub>	1783.8824	1783.8811	-0.75	1783.8821	-0.18	1783.8821	-0.15
Hex <sub>4</sub> HexNAc <sub>3</sub> Fuc	1794.8984	1794.8982	-0.13	1794.8981	-0.18	1794.8987	0.14
Hex <sub>5</sub> HexNAc <sub>3</sub>	1824.9089	1824.9091	0.10	1824.9097	0.42	1824.9085	-0.24
Hex <sub>3</sub> HexNAc <sub>4</sub> Fuc	1835.9249	1835.9243	-0.33	1835.9255	0.33	1835.9255	0.35
Hex <sub>4</sub> HexNAc <sub>4</sub>	1865.9355	1865.9342	-0.69	1865.9351	-0.23	1865.9355	0.01
Hex <sub>4</sub> HexNA <sub>3</sub> NeuAc	1981.9828	1981.9830	0.11	1981.9871	2.18	1981.9910	4.14
Hex <sub>7</sub> HexNAc <sub>2</sub>	1987.9821	1987.9831	0.48	1987.9864	2.17	1987.9857	1.79
Hex <sub>5</sub> HexNAc <sub>3</sub> Fuc	1998.9981	1998.9969	-0.61	1999.0018	1.86	1998.9998	0.85
Hex <sub>6</sub> HexNAc <sub>3</sub>	2029.0087	2029.0125	1.87	2029.0121	1.69	2029.0092	0.27
Hex <sub>4</sub> HexNAc <sub>4</sub> Fuc	2040.0247	2040.0239	-0.39	2040.0267	0.99	2040.0267	1.00
Hex <sub>5</sub> HexNAc <sub>4</sub>	2070.0352	2070.0353	0.07	2070.0386	1.62	2070.0678	15.76

<b>Components</b>	<b>theoretical m/z</b>	<b>Average m/z (n=9)</b>	<b>ppm</b>	<b>Average m/z (n=9)</b>	<b>ppm</b>	<b>Average m/z (n=9)</b>	<b>ppm</b>
Hex <sub>3</sub> HexNAc <sub>5</sub> Fuc	2081.0512	2081.0531	0.90	2081.0565	2.55	2081.0559	2.23
Hex <sub>4</sub> HexNAc <sub>3</sub> FucNeuAc	2156.072	2156.0747	1.24	2156.0763	1.99	2156.0769	2.27
Hex <sub>5</sub> HexNAc <sub>3</sub> NeuAc	2186.0826	2186.0741	-3.88	2186.0890	2.94	2186.0895	3.17
Hex <sub>8</sub> HexNAc <sub>2</sub>	2192.0819	2192.0850	1.43	2192.0890	3.24	2192.0883	2.94
Hex <sub>5</sub> HexNAc <sub>4</sub> Fuc	2244.1245	2244.1286	1.83	2244.1312	3.00	2244.1314	3.09
Hex <sub>6</sub> HexNAc <sub>4</sub>	2274.135	2274.1425	3.29	2274.1468	5.18	2274.1448	4.30
Hex <sub>4</sub> HexNAc <sub>5</sub> Fuc	2285.151	2285.1560	2.20	2285.1596	3.78	2285.1594	3.67
Hex <sub>5</sub> HexNAc <sub>5</sub>	2315.1616	2315.1766	6.46	2315.1742	5.45	2315.1770	6.63
Hex <sub>3</sub> HexNAc <sub>6</sub> Fuc	2326.1776	2326.1049	-31.24	2326.1915	5.98	2326.1306	-20.20
Hex <sub>9</sub> HexNAc <sub>2</sub>	2396.1817	2396.1932	4.80	2396.1925	4.52	2396.1947	5.42
Hex <sub>4</sub> HexNAc <sub>4</sub> FucNeuAc	2401.1983	2401.2020	1.56	2401.2121	5.75	2401.2130	6.12



<b>Components</b>	<b>theoretical m/z</b>	<b>Average m/z (n=9)</b>	<b>ppm</b>	<b>Average m/z (n=9)</b>	<b>ppm</b>	<b>Average m/z (n=9)</b>	<b>ppm</b>
Hex <sub>5</sub> HexNAc <sub>4</sub> Fuc <sub>2</sub>	2418.2137	2418.2091	-1.90	2418.2247	4.54	2418.2236	4.08
Hex <sub>5</sub> HexNAc <sub>4</sub> NeuAc	2431.2089	2431.2175	3.52	2431.2217	5.24	2431.3044	39.29
Hex <sub>6</sub> HexNAc <sub>4</sub> Fuc	2448.2242	2448.2282	1.61	2448.2427	7.54	2448.2422	7.34
Hex <sub>5</sub> HexNAc <sub>3</sub> NeuAc <sub>2</sub>	2547.2563	2547.2709	5.73	2547.2778	8.45	2547.2747	7.24
Hex <sub>5</sub> HexNAc <sub>4</sub> FucNeuAc	2605.2981	2605.3168	7.18	2605.3194	8.17	2605.3187	7.91
Hex <sub>5</sub> HexNAc <sub>4</sub> FucNeuGc	2635.3087	2635.3310	8.48	2635.3347	9.86	2635.3340	9.60
Hex <sub>7</sub> HexNAc <sub>4</sub> Fuc	2652.324	2652.3523	10.68	2652.3526	10.78	2652.3514	10.35
Hex <sub>6</sub> HexNAc <sub>5</sub> Fuc	2693.3506	2693.3726	8.17	2693.3706	7.43	2693.3750	9.04
Hex <sub>5</sub> HexNAc <sub>6</sub> Fuc	2734.3771	2734.4075	11.12	2734.4056	10.43	2734.4047	10.08
Hex <sub>5</sub> HexNAc <sub>4</sub> NeuAc <sub>2</sub>	2792.3826	2792.4105	9.99	2792.4100	9.82	2792.4083	9.20
Hex <sub>6</sub> HexNAc <sub>5</sub> NeuAc	2880.435	2880.4703	12.24	2880.4692	11.88	2880.4726	13.04

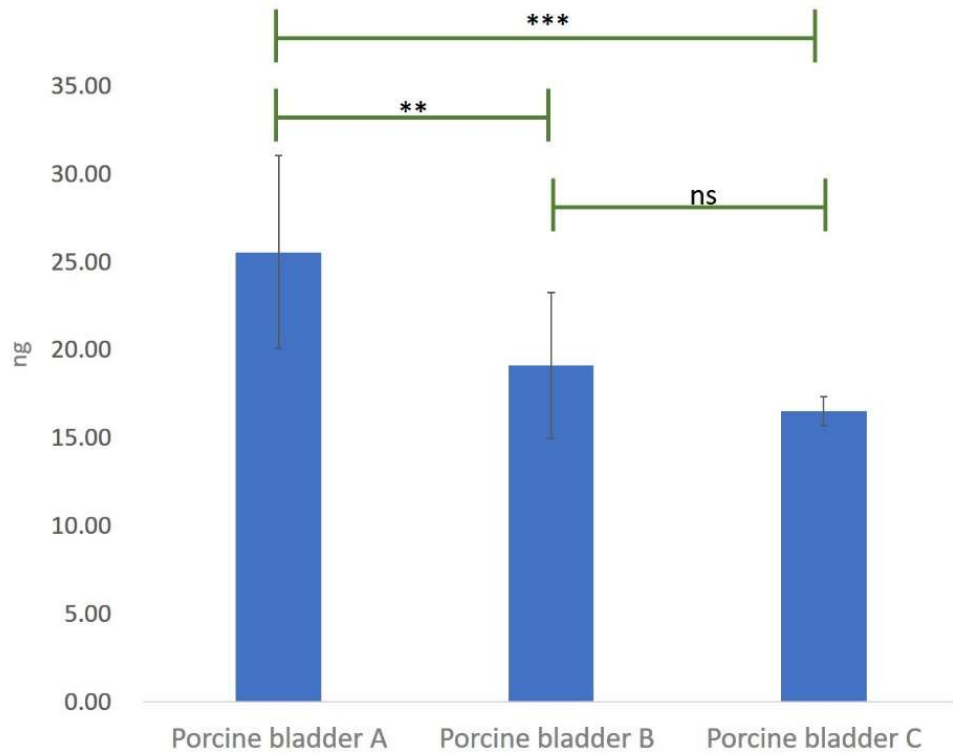
<b>Components</b>	<b>theoretical m/z</b>	<b>Average m/z (n=9)</b>	<b>ppm</b>	<b>Average m/z (n=9)</b>	<b>ppm</b>	<b>Average m/z (n=9)</b>	<b>ppm</b>
Hex <sub>7</sub> HexNAc <sub>5</sub> Fuc	2897.4503	2897.4855	12.15	2897.4898	13.62	2897.4840	11.63
Hex <sub>5</sub> HexNAc <sub>4</sub> FucNeuAc <sub>2</sub>	2966.4718	2966.5074	12.01	2966.5051	11.23	2966.5047	11.07
Hex <sub>5</sub> HexNAc <sub>4</sub> FucNeuAcNeuGc	2996.4824	2996.5178	11.81	2996.5136	10.40	2996.5185	12.03
Hex <sub>3</sub> HexNAc <sub>6</sub> FucNeuAc <sub>2</sub>	3048.5249	3048.4829	-13.76	3048.4809	-14.45	3048.4772	-15.63
Hex <sub>4</sub> HexNAc <sub>6</sub> NeuAc <sub>2</sub>	3078.5355	3078.4991	-11.83	3078.4977	-12.28	3078.4912	-14.39

**Table 13. 12 porcine urothelial cell apical surface O-glycans common to the three biological replicates**

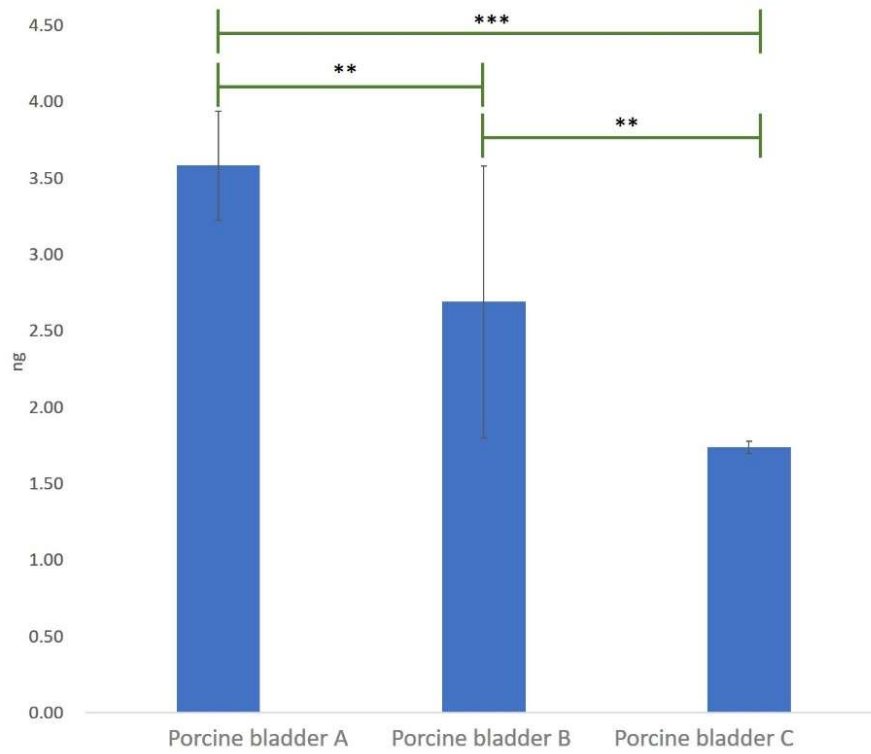
MALDI Spots		Porcine bladder A		Porcine bladder B		Porcine bladder C	
Components	theoretical m/z	Average m/z (n=9)	ppm	Average m/z (n=9)	ppm	Average m/z (n=9)	ppm
HexNAc6 (internal standard)	1539.789	1539.7905	0.96	1539.7872	-1.15	1539.7872	-1.19
Hex <sub>2</sub> HexNAc	722.357	722.3607	5.11	722.3607	5.18	722.3606	4.95
HexHexNAcNeuAc	879.4308	879.4317	1.07	879.4317	0.99	879.4325	1.92
HexHexNAcNeuGc	909.4414	909.4420	0.70	909.4421	0.79	909.4420	0.61
Hex <sub>3</sub> HexNAc	926.4567	926.4557	-1.09	926.4568	0.14	926.4570	0.36
HexHexNAc <sub>2</sub> NeuAc	1124.5572	1124.5553	-1.73	1124.5553	-1.71	1124.5554	-1.64
Hex <sub>2</sub> HexNAc <sub>2</sub> Fuc	1141.5725	1141.5707	-1.59	1141.5695	-2.64	1141.5707	-1.57
HexHexNAc <sub>2</sub> NeuGc	1154.5677	1154.5656	-1.84	1154.5652	-2.14	1154.5661	-1.43
Hex <sub>3</sub> HexNAc <sub>2</sub>	1171.5831	1171.5812	-1.64	1171.5806	-2.15	1171.5809	-1.85
HexHexNAcNeuAc <sub>2</sub>	1240.6045	1240.6017	-2.26	1240.6017	-2.26	1240.6017	-2.29
HexHexNAc <sub>2</sub> NeuAc <sub>2</sub>	1485.7308	1485.7302	-0.40	1485.7265	-2.93	1485.7311	0.17

<b>Components</b>	<b>theoretical m/z</b>	<b>Average m/z (n=9)</b>	<b>ppm</b>	<b>Average m/z (n=9)</b>	<b>ppm</b>	<b>Average m/z (n=9)</b>	<b>ppm</b>
Hex <sub>3</sub> HexNAc <sub>2</sub> NeuAc	1532.7567	1532.7539	-1.83	1532.7538	-1.88	1532.7538	-1.92
Hex <sub>2</sub> HexNAc <sub>3</sub> NeuAc	1573.7833	1573.7811	-1.38	1573.7803	-1.93	1573.7810	-1.49

The total amounts of porcine urothelial cell apical surface *N*- and *O*-glycans determined by summing the intensities of the signals for the 47 *N*-glycans and 12 *O*-glycans that were common to the three biological replicates, are shown in Figure 65 and Figure 66. The total amounts of apical surface *N*- and *O*-glycans collected from porcine bladder A were significantly higher than those collected from porcine bladders B and C ( $P < 0.001$ ), where porcine bladders B and C had very similar amounts of total apical cell surface *N*-glycans ( $P > 0.05$ ) but different amounts of apical cell surface *O*-glycans ( $P < 0.01$ ). Statistical analysis was carried out using one-way analysis of variance (ANOVA) with Tukey-Kramer multiple comparisons post-hoc test. In addition, a direct comparison was made between the amount of apical cell surface *N*-glycans compared to apical cell surface *O*-glycans, since the apical cell surface *N*- and *O*-glycans in each of technical replicates were obtained from the same MALDI mass spectrum, using the same internal standard peak for normalization. This latter analysis showed the amounts of porcine urothelial cell apical cell surface *N*-glycans in the three biological replicates to be ~ 7 to 10 times higher than the total amount of porcine urothelial cell apical cell surface *O*-glycans.



**Figure 65.** The total amounts of porcine urothelial cell apical surface *N*-glycans, determined by summing the 47 apical cell surface *N*-glycans common to all the three biological replicates, where \*\*\*:  $P < 0.001$ , \*\*:  $P < 0.01$  and ns:  $P > 0.05$



**Figure 66. The total amounts of porcine urothelial cell apical surface O-glycans, determined by summing the 12 apical cell surface *N*-glycans common to the three biological replicates, where \*\*\*:  $P < 0.001$ , and \*\*:  $P < 0.01$**

The relative percentages of glycans were calculated for the porcine urothelial cell apical surface *N*- and O-glycans of the three biological replicates, using the total amounts of the 47 apical cell surface *N*-glycans and 12 apical cell surface O-glycans, that were common to all biological replicates, to normalize individual amounts of each *N*- and O-glycan (Figure 67 and Figure 68), respectively. The compositions of apical cell surface *N*-glycomes were very similar across the three biological replicates; complex *N*-glycans Hex<sub>3</sub>HexNAc<sub>4</sub>Fuc, Hex<sub>4</sub>HexNAc<sub>4</sub>Fuc, Hex<sub>5</sub>HexNAc<sub>4</sub>Fuc, Hex<sub>5</sub>HexNAc<sub>4</sub>FucNeuAc, Hex<sub>5</sub>HexNAc<sub>4</sub>FucNeuAc<sub>2</sub> and Hex<sub>3</sub>HexNAc<sub>6</sub>FucNeuAc<sub>2</sub> were in abundance in all three biological replicates. The compositions of apical cell surface O-glycomes were also very similar across the three biological replicates; only porcine bladder B had particularly high abundance of Hex<sub>2</sub>HexNAc, Hex<sub>2</sub>HexNAc<sub>2</sub>Fuc and Hex<sub>3</sub>HexNAc<sub>2</sub>, and low abundance of HexHexNAc<sub>2</sub>NeuAc and Hex<sub>2</sub>HexNAc<sub>3</sub>NeuAc.



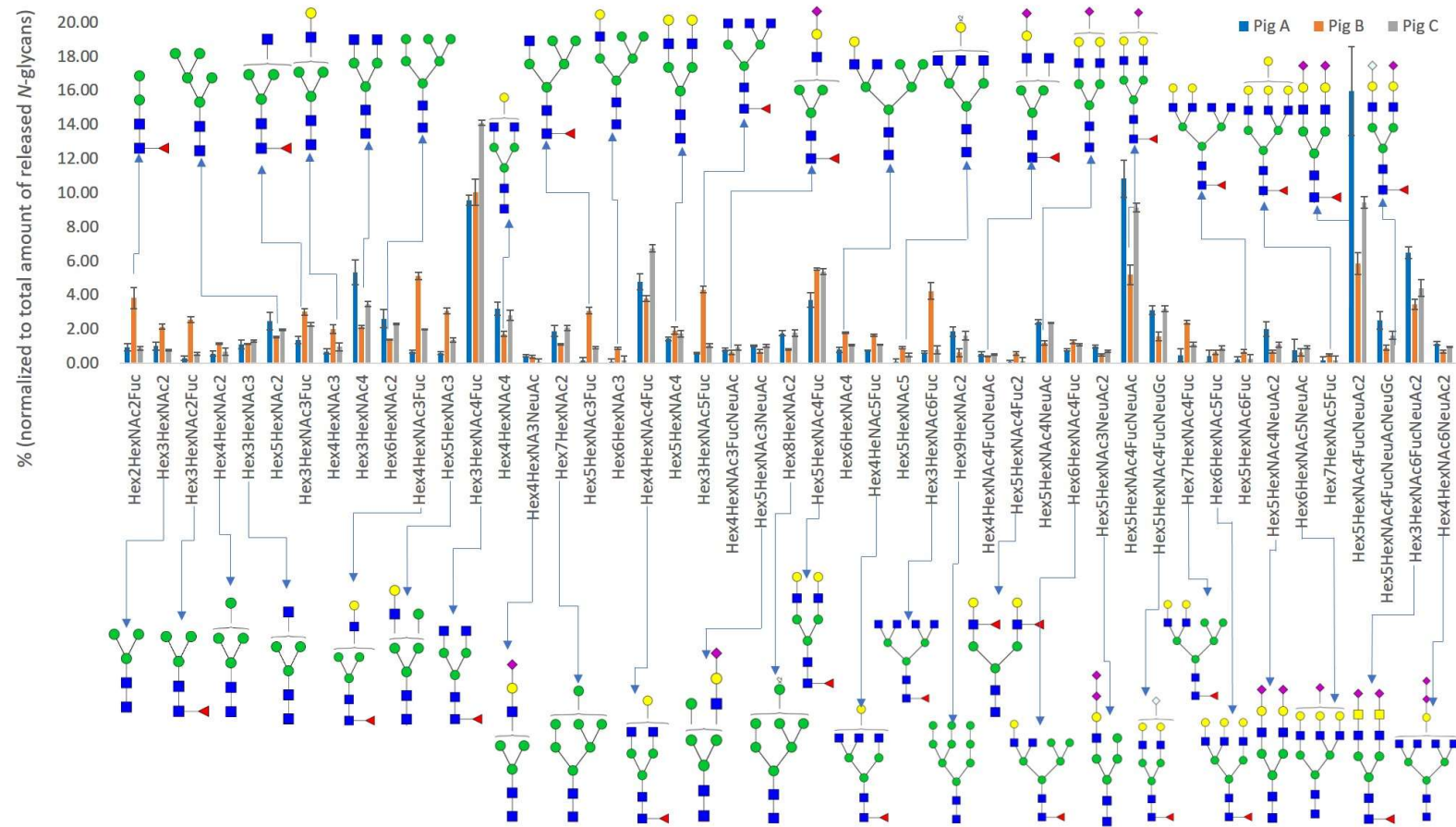


Figure 67. Relative percentages of the 47 porcine urothelial cell apical surface *N*-glycans that were common to the three biological replicates

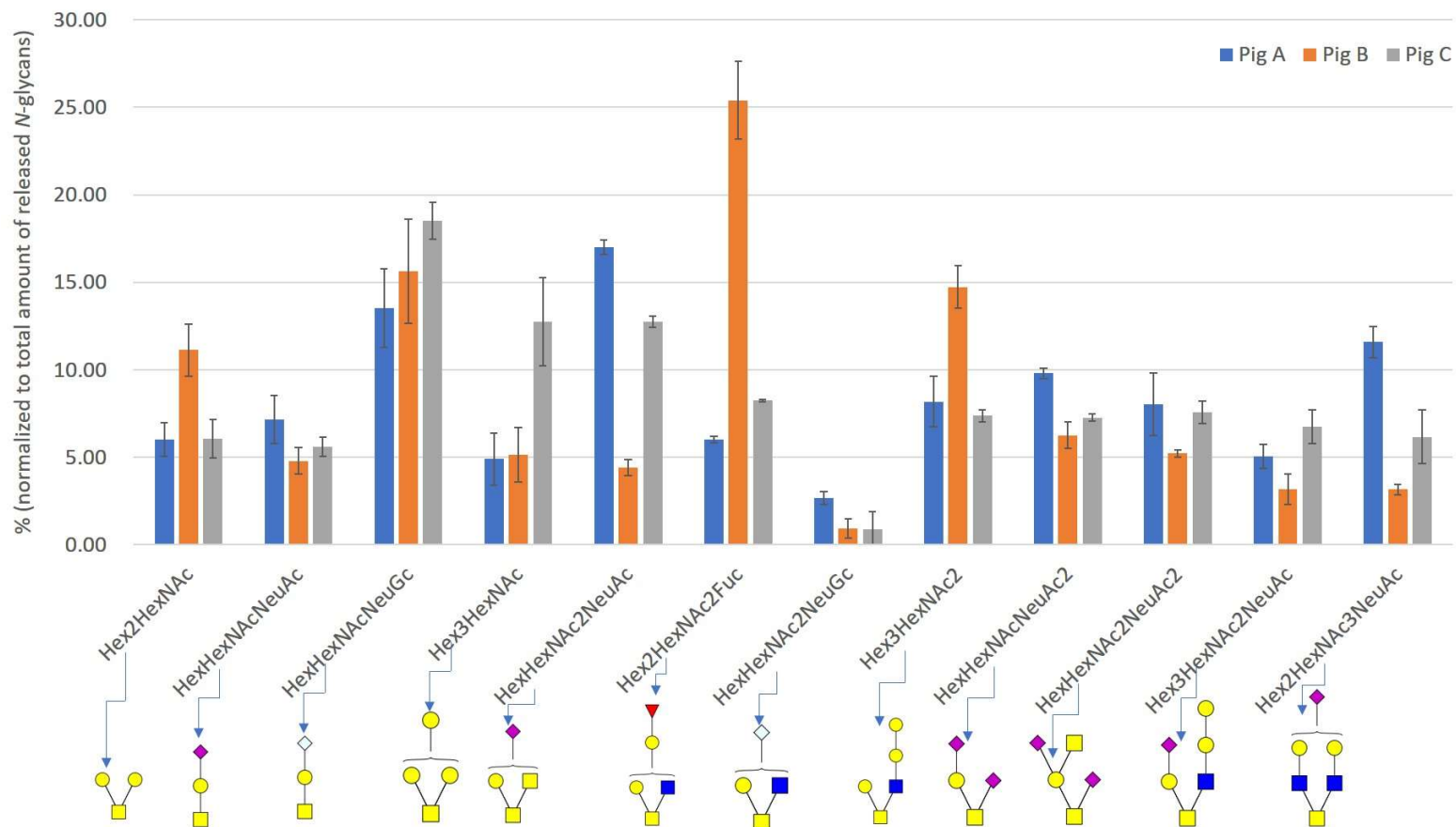


Figure 68. Relative percentages of the 12 porcine urothelial cell apical surface O-glycans that were common to the three biological replicates.

#### 5.3.4 Comparison of the porcine urothelial total cell lysate *N*-glycome and the apical cell surface *N*-glycome

The relative percentages of the 29 *N*-glycans in the porcine urothelial total cell lysate *N*-glycome, identified using the FANGS approach (chapter 3), were compared with the relative percentages of the 47 *N*-glycans in the porcine urothelial cell apical surface *N*-glycome, identified using on-tissue trypsinization (Figure 69). Each of the relative percentages obtained using the two different approaches, represent the means of the three biological replicates. 22 *N*-glycan structures were identified only in the apical cell surface *N*-glycome, of which 20 were complex *N*-glycans and two were smaller than Hex<sub>5</sub>HexNAc<sub>2</sub>. In contrast, four *N*-glycan structures were identified only in the total cell lysate *N*-glycome, of which two were complex *N*-glycans and two were smaller than Hex<sub>5</sub>HexNAc<sub>2</sub>.

The apical surface *N*-glycan structures can be divided into four structural groups (Figure 70). The most abundant apical cell surface *N*-glycans in each biological replicate were the complex *N*-glycans that represented 81.7%, 70.9% and 79.8% of the common *N*-glycome in porcine bladders A, B and C, respectively. The proportion of oligomannose *N*-glycans was 10.6%, 5.4% and 9.7% in bladders A, B and C, respectively. The proportion of hybrid *N*-glycans was 3.9%, 12.9%, 6.4% in bladders A, B and C, respectively. The proportion of other *N*-glycans, which were smaller than Hex<sub>5</sub>HexNAc<sub>2</sub>, was 3.9%, 5.4% and 4.2% in bladders A, B and C, respectively.

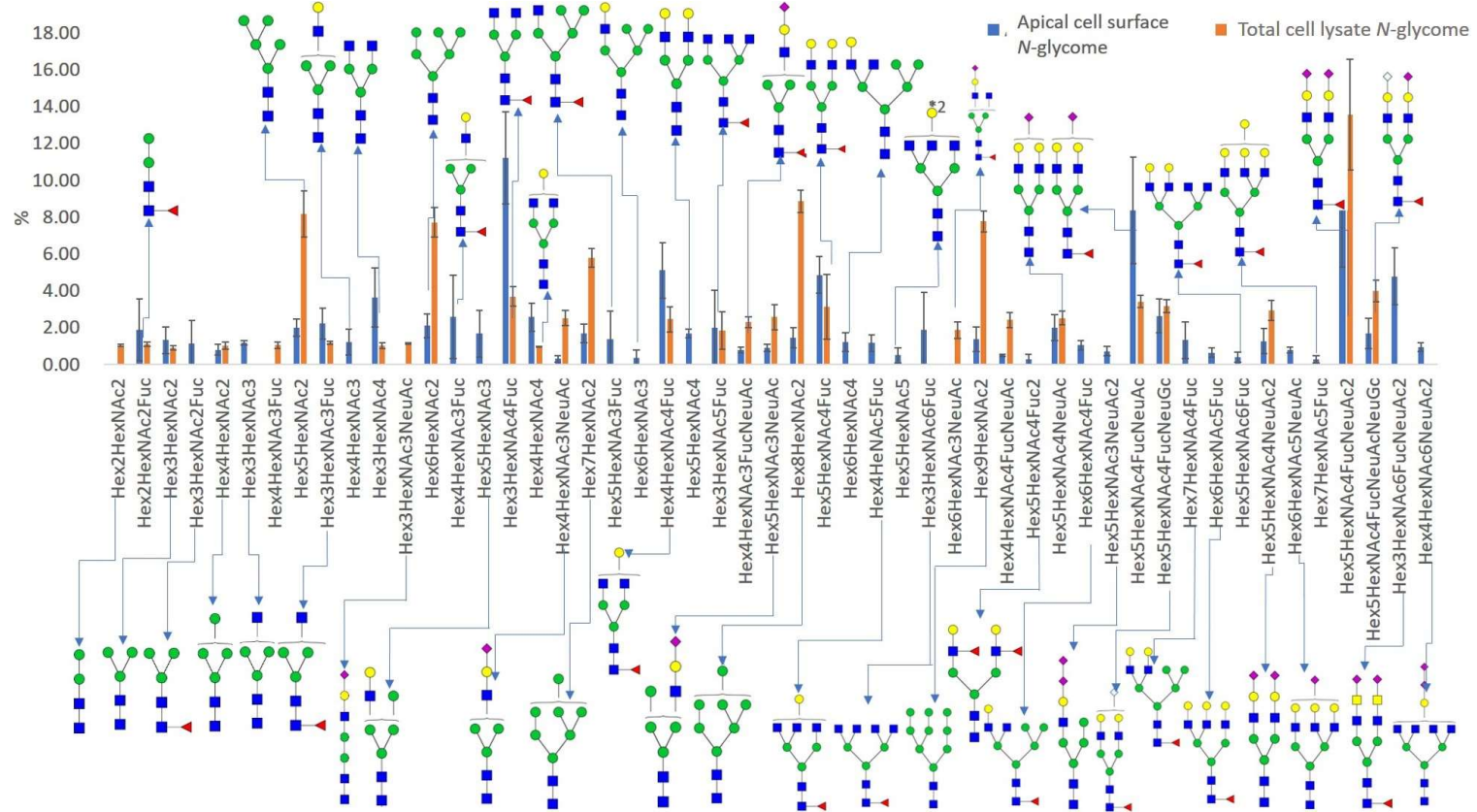
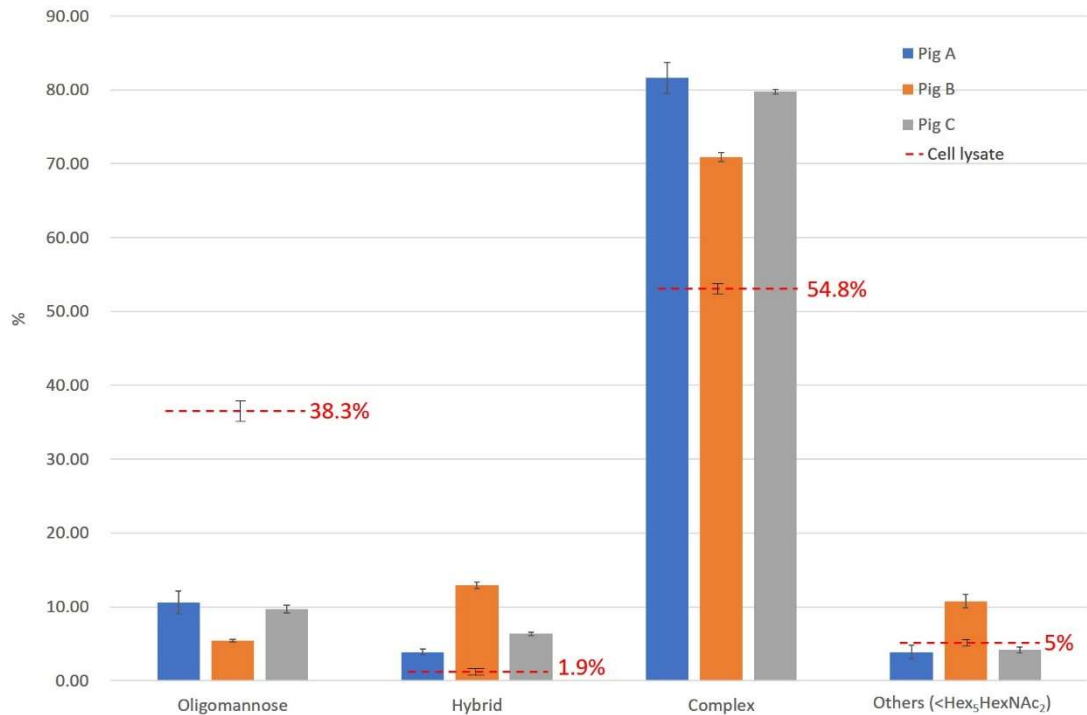


Figure 69. The relative percentages of porcine urothelial total cell lysate *N*-glycan structures compared to those of porcine urothelial cell apical surface structures.



**Figure 70. The percentages of oligomannose, hybrid, complex and other *N*-glycans in the porcine urothelial cell apical surface *N*-glycome of three biological replicates using the on-tissue trypsinization approach. The red dotted lines indicate the percentages of the different types of *N*-glycan, representing the means of the three biological replicates, in the porcine urothelial total cell lysate *N*-glycome.**

The proportion of complex *N*-glycans released from the porcine urothelial cell apical surface increased to 77.5% from 54.8% from total cell lysates. By contrast, the proportion of oligomannose *N*-glycans released from the apical cell surface reduced to 8.6% from 38.3% in the total cell lysates. In addition, 20 more complex *N*-glycans were identified only in the apical cell surface *N*-glycome. This result is in line with the results of the study by Hamouda *et al.*<sup>197</sup> discussed in chapter 4, where a reduction in the level of intracellular (immature, oligomannose) *N*-glycans may enhance the detection of low abundance mature (mostly complex) *N*-glycans.

### 5.3.5 Product ion analysis of apical cell surface *N*- and *O*-glycans collected from porcine urothelium using on-tissue trypsinization

In order to verify that the structural assignments made on the basis of composition and knowledge of biosynthesis and well established *N*- and *O*-glycan structures, the product ion analysis were conducted to investigate the of some of the more interesting apical cell surface glycans, released together as a mixture, from porcine urothelium. The candidates of glycans for product ion analysis included 1) two groups of *N*- and *O*-glycans identified at  $m/z$  1141.57 and 1171.58 , 2) basic oligomannose *N*-glycan at  $m/z$  1579.69, 3) basic hybrid *N*-glycans at  $m/z$  1824.91 and 4) basic complex *N*-glycans at  $m/z$  1835.93.

Product ion analysis was conducted using the higher energy collision mode (HCD) using the Thermo Orbitrap Fusion Tribrid, in which the precursor ions were selected in the quadrupole and collided in the ion-routing multipole followed by mass analysis in the Orbitrap. Permethylated glycan samples were dissolved in 80% methanol / 20% water / 0.1% formic acid and loaded into home-pulled emission tips to enable nano-electrospray ionisation.

A serial of intense background signals, largely corresponding to the contaminating hexose oligomers from the cell culture medium (Appendix 3), was co-selected with precursor ions; consequently these signals appear in each product ion spectrum obtained in these analyses. These background signals are labelled with asterisks in the following product ion mass spectra, and have their origins in the well-accepted

co-selection of isobaric contaminants that have led Thermo to propose Synchronous Precursor Selection workflows to minimise this limitation of their source for tandem mass tags (TMT) peptide quantification.

The on-tissue trypsinization released apical cell surface *N*- and O-glycans into one pot without separation, resulting in FucHex<sub>2</sub>HexNAc<sub>2</sub> at *m/z* 1141.57 and Hex<sub>3</sub>HexNAc<sub>2</sub> at *m/z* 1171.58 that could be assigned as *N*-glycan or O-glycan structural isomers. The product ion spectrum of *m/z* 1141.57 (Figure 71) shows a series of B/Y ions that indicate a linear structure, supported by diagnostic Y<sub>2α</sub> (FucHexNAc<sub>2</sub>) and B<sub>2α</sub> (Hex<sub>2</sub>) ions. There are no fragment ions consistent with the presence of a typical O-glycan at *m/z* 1141.57, such as the diagnostic Y<sub>1α</sub> that would be expected at *m/z* 504.24. By contrast, the product ion spectrum of Hex<sub>3</sub>HexNAc<sub>2</sub> at *m/z* 1171.58 (Figure 72) shows two sets of fragments in a chimaeric spectrum. The B<sub>3</sub> ion at *m/z* 894.43 and B<sub>2</sub> ion at *m/z* 649.31 are diagnostic peaks supporting the absence of a branching Hex linked to the reducing terminal HexNAc, suggesting those two fragments were from the *N*-glycan form of Hex<sub>3</sub>HexNAc<sub>2</sub>. In contrast, the Y<sub>1α</sub> ion at *m/z* 504.24 (see insert) indicates there is a branching Hex linked to the reducing terminal HexNAc, consistent with the O-glycan isomer of Hex<sub>3</sub>HexNAc<sub>2</sub>. The peak at *m/z* 1171.58 can derive from both the *N*- and O-glycan forms of Hex<sub>3</sub>HexNAc<sub>2</sub>.

The product ion mass spectrum of Hex<sub>5</sub>HexNAc<sub>2</sub> at *m/z* 1579.69 (Figure 73) contains signals deriving from double cleavages at *m/z* 1084.52 (Y<sub>4α</sub>'/B4) and 676.32(Y<sub>3α</sub>/B4) and a signal caused by cleavage of three bonds at *m/z* 866.40 (Y<sub>4α</sub>'/Y<sub>4α</sub>''/B4). The

fragmentation pattern is consistent with the expected Hex<sub>5</sub> oligomannose glycan structure. The product ion spectrum of Hex<sub>5</sub>HexNAc<sub>3</sub> at  $m/z$  1824.91 (Figure 74) shows two sets of fragments consistent with the presence of two isomeric hybrid *N*-glycan isomers. The Y<sub>3α</sub> ion at  $m/z$  1157.57 (green label) and Y<sub>4α</sub> ion at  $m/z$  1565.77 (blue label) must derive from different non-reducing terminal structures, suggesting the presence of two different isomeric hybrid *N*-glycans, one biantennary and the other triantennary. The product ion mass spectrum of Hex<sub>3</sub>HexNAc<sub>4</sub> at  $m/z$  1835.93 (Figure 75) also shows two sets of fragments in the same spectrum. The complex *N*-glycan with two HexNAcs on the same non-reducing terminus is evidenced by the double cleavage Y<sub>4α</sub>/B<sub>4</sub> ion at  $m/z$  880.42 (green label in the insert spectrum) and the Y<sub>4α</sub> at  $m/z$  1331.66 formed by the loss of two HexNAcs. By contrast, the double cleavage Y<sub>4α</sub>/Y<sub>4β</sub> ion at  $m/z$  1317.64 and the Y<sub>3β</sub> ion at  $m/z$  1372.69 suggest the structure of a complex *N*-glycan with one HexNAc on each of the two non-reducing termini.



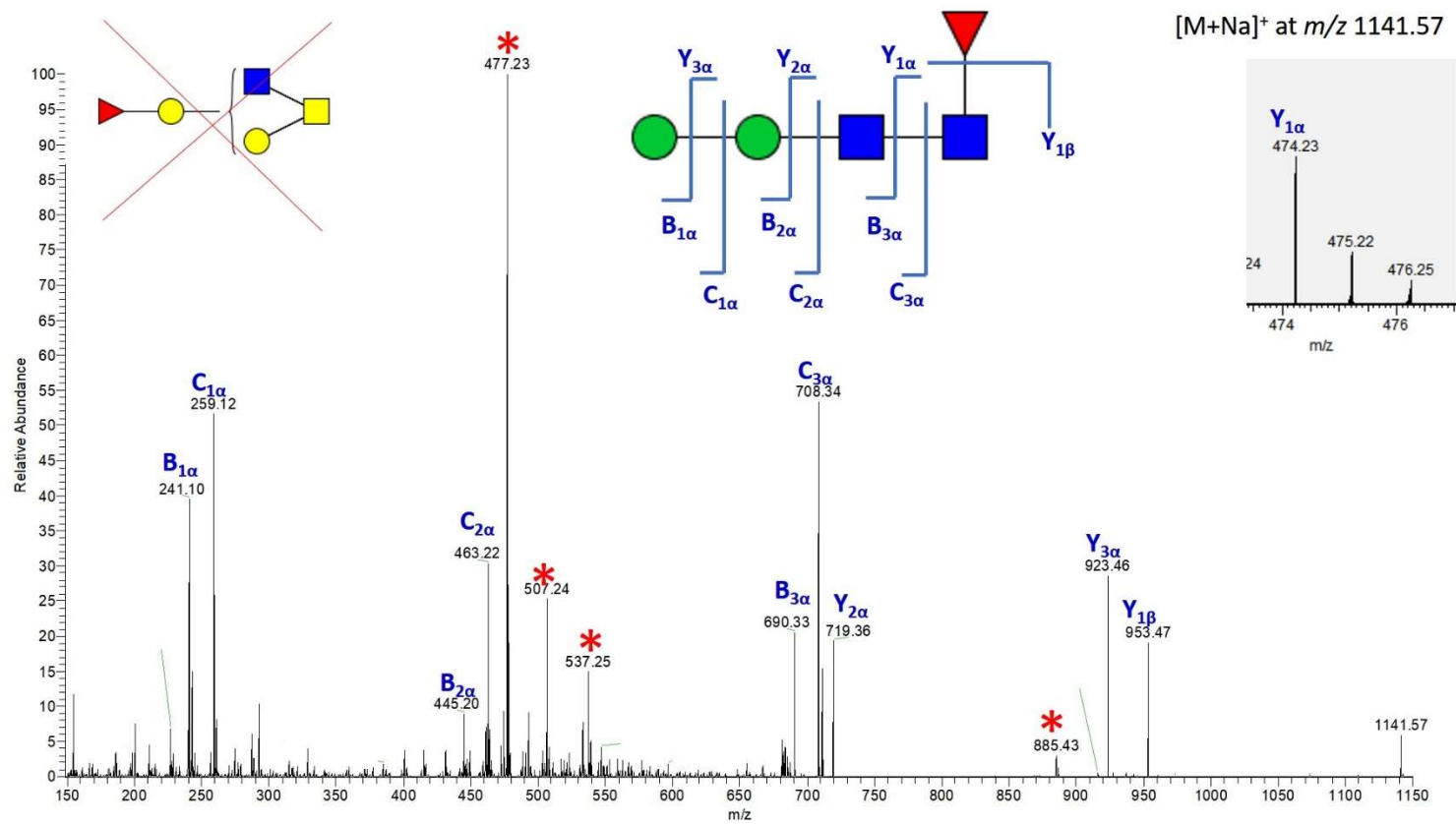


Figure 71. Product ion spectrum of  $[M+Na]^+$  at  $m/z$  1141.57, in permethylated glycans collected from porcine urothelium using on-tissue trypsinization. Asterisks mark ions derived from co-selected glucose oligomers.

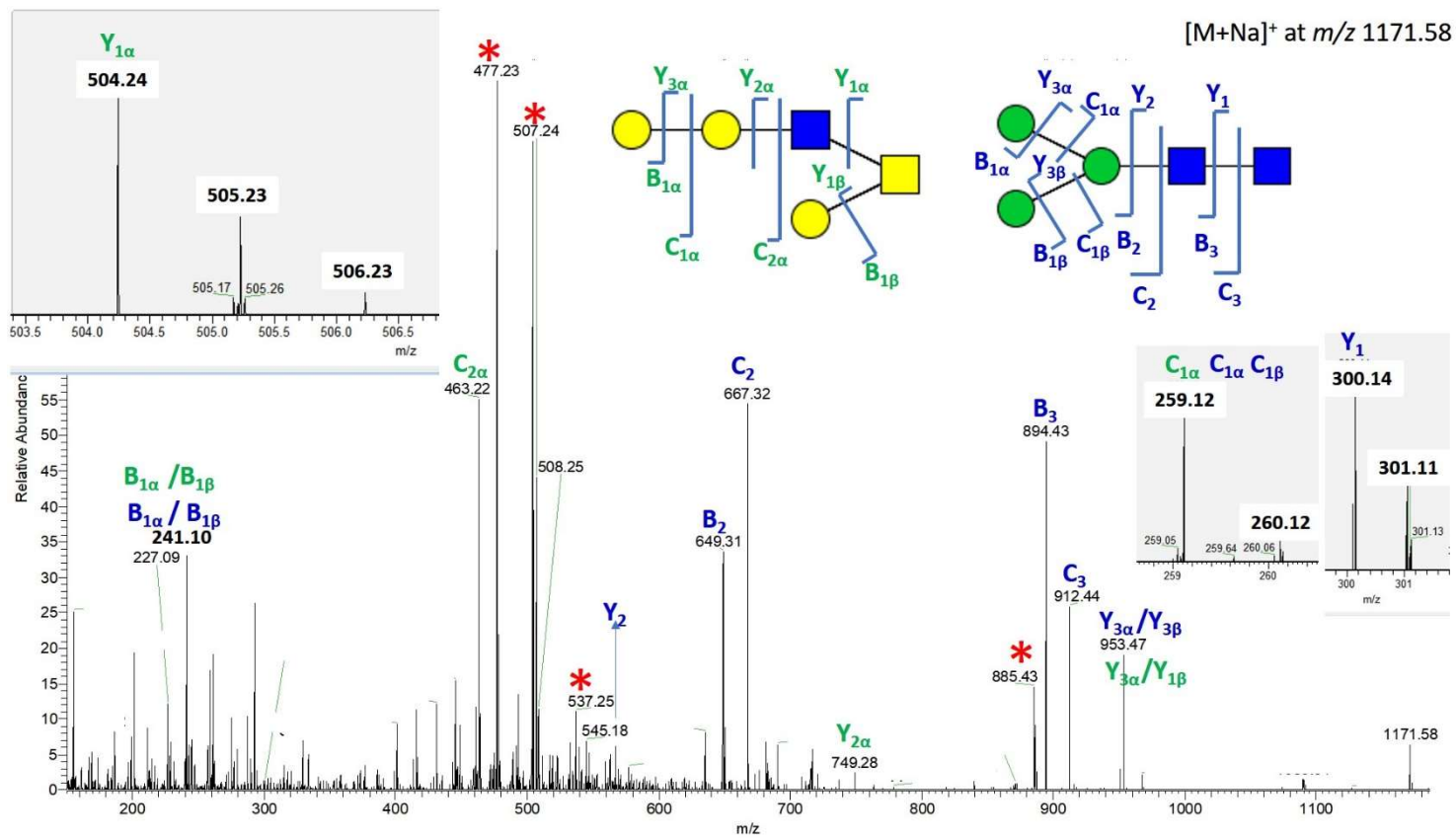


Figure 72. Product ion spectrum of  $[M+Na]^+$  at *m/z* 1171.58, in permethylated glycans collected from porcine urothelium using on-tissue trypsinization. Asterisks mark ions derived from co-selected glucose oligomers.

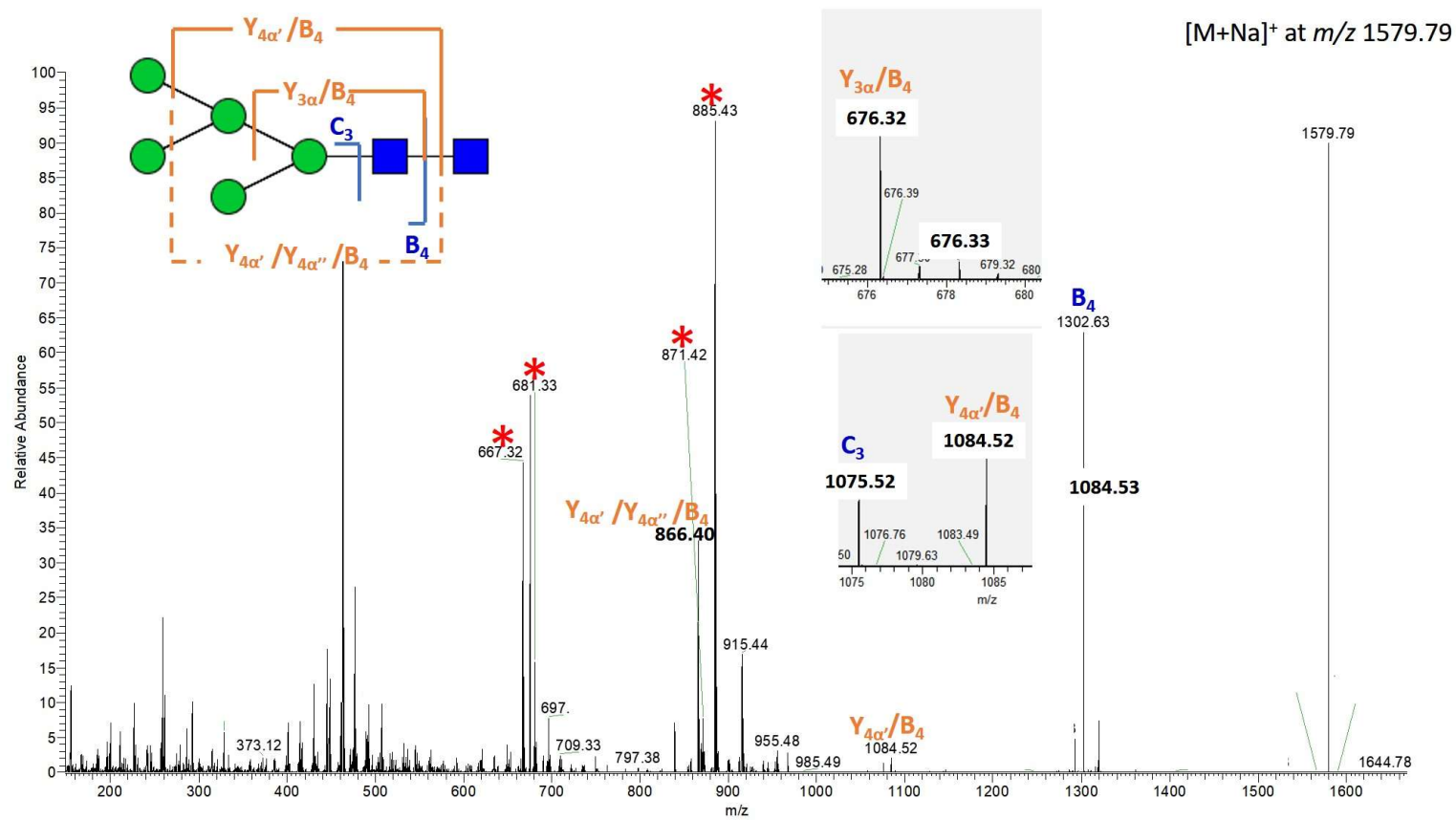


Figure 73. Product ion spectrum of  $[M+Na]^+$  at  $m/z$  1579.79, in permethylated glycans collected from porcine urothelium using on-tissue trypsinization. Asterisks mark ions derived from co-selected glucose oligomers.

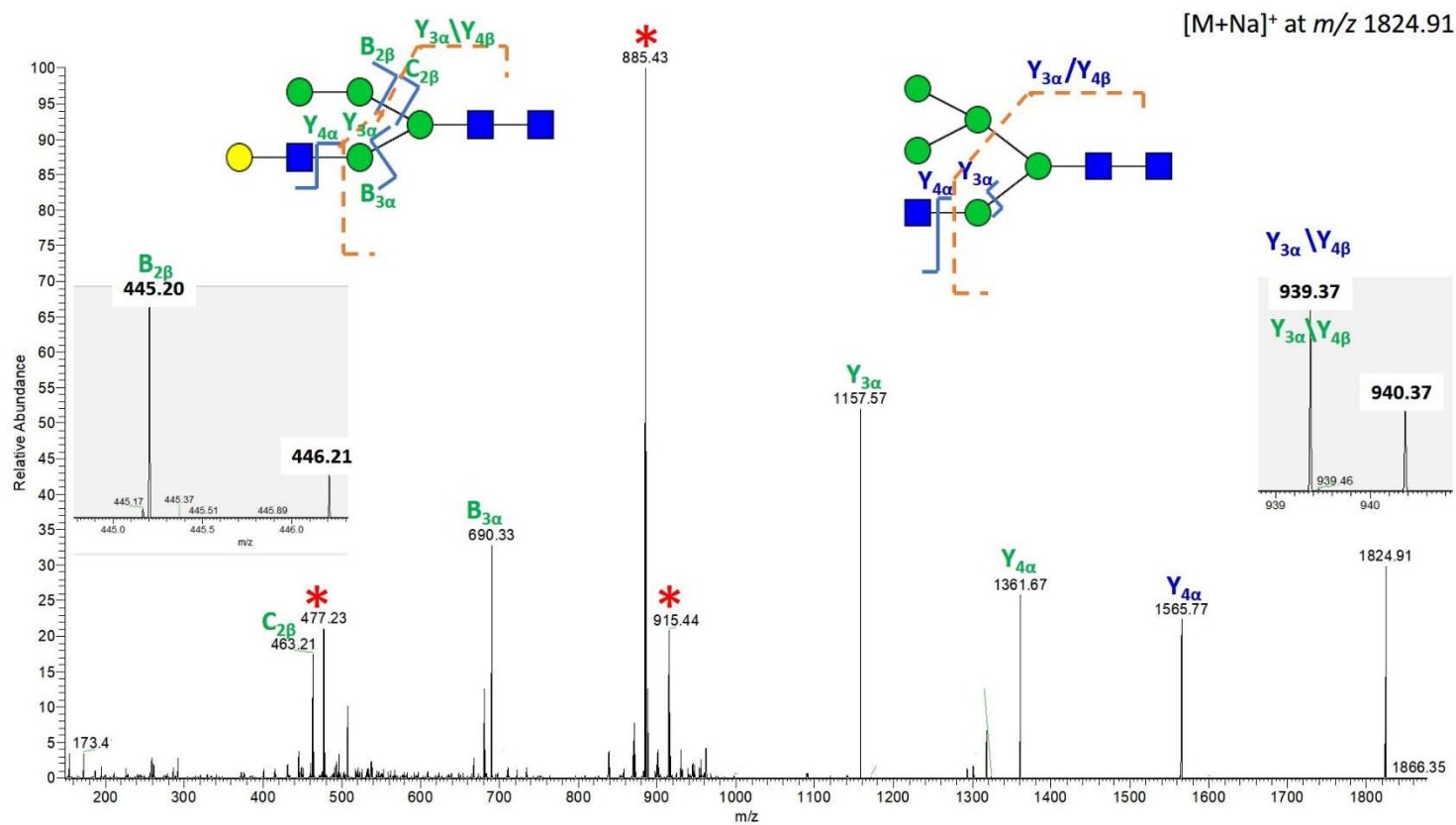


Figure 74. Product ion spectrum of [M+Na]<sup>+</sup> at *m/z* 1824.91, in permethylated glycans collected from porcine urothelium using on-tissue trypsinization. Asterisks mark ions derived from co-selected glucose oligomers.

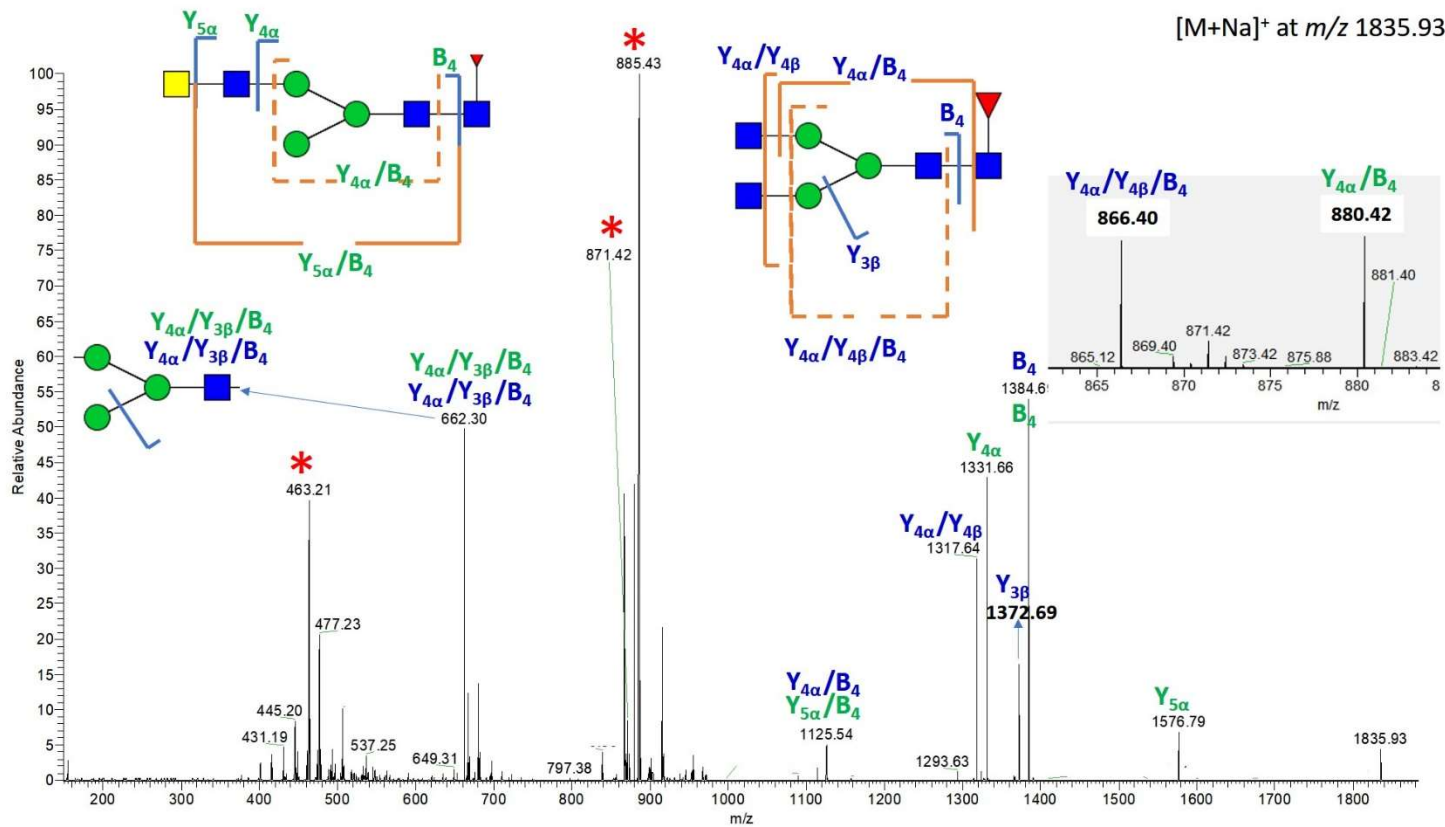


Figure 75. Product ion spectrum of [M+Na]<sup>+</sup> at *m/z* 1835.93, in permethylated glycans collected from porcine urothelium using on-tissue trypsinization. Asterisks mark ions derived from co-selected glucose oligomers.

### 5.3.5 Summary

The approach of collecting the apical cell surface *N*- and *O*-glycans from the luminal surface of fresh polarized porcine superficial urothelium using on-tissue trypsinization was achieved. The use of an in-house built reaction device with six wells enabled surface trypsinization and allowed multiple experimental replicates on the uniform luminal surface of stretched porcine bladders. Moreover, this six-well device also allowed processing of porcine bladder samples through formalin fixation immediately after trypsinization, chemically persevering the appearance of the trypsinized cell surface for subsequent immunolabelling without delay (Appendix 4).

The results generated using this approach represent the first normal mammalian superficial urothelial cell apical surface *N*- and *O*-glycomes. The apical cell surface *N*- and *O*-glycomes obtained using the on-tissue trypsinization approach showed great reproducibility between biological replicates in the amount of released glycan and the number of different glycan species detected. Although few apical cell surface *N*- and *O*-glycans differed in terms of their proportion of the total common glycans between biological replicates, those that did differ were believed to likely be caused by individual biological variation, judged by the apparent thickness of the superficial UPK3a-layer, in combination with the total amount of released glycans over the three biological replicates. It should be noted that information on the breed, age, and sex of the animals from which the bladders provided were not available from the abattoir. Such background information may very well contribute to the individual differences observed in glycan profiles.

## Chapter 6. Summary of results, overall conclusions and future work





A full examination of a mammalian urothelial *N*-glycome was achieved using an established filter-aided *N*-glycan separation approach<sup>202</sup> to investigate the total cell lysate *N*-glycans released from porcine urothelial cells scraped from fresh porcine bladders (chapter 3). The resulting data offers an insight into the entire normally differentiated urothelial *N*-glycome with structural information provided using MALDI-MS, defining a normal *N*-glycome as a foundation for comparison with abnormal (mutant, diseased, damaged, compromised) mammalian urothelial *N*-glycomes. Furthermore, this identification of the urothelial glycome evolved from defining the intracellular and extracellular *N*-glycans of whole urothelial cells into specifically the apical surface *N*- and *O*-glycome of polarized porcine superficial urothelial cells (chapter 4 and chapter 5). The polarized apical surface glycome collected from the luminal surface of stretched fresh porcine bladders using on-tissue trypsinization using an in-house built reaction device defines a potential cell surface glycome that represents the product of glycosylation of a well-differentiated urothelium with normal barrier function. These identified apical surface *N*- and *O*-glycans can form the basis for future studies of urothelial functions that are reportedly located on the apical surface of superficial layer and involve urothelial glycans, e.g. the formation of urothelial plaques, bladder impermeability, uropathogenic *E. coli* infection and the development of cancers.

The comparison between the urothelial total cell lysate *N*-glycome and the urothelial apical surface *N*-glycome revealed distinct differences in the number and proportions of *N*-glycan species identified. This observation is in line with the results of the studies by other research groups where the identification of cell surface *N*-glycomes

released from enriched cell membrane fractions<sup>180,182,231</sup> or the tryptic shaved supernatant of the cell surface<sup>197</sup> were compared to total cell lysate *N*-glycomes. In addition, the high proportion of urothelial complex *N*-glycans released from either the total cell lysate or on apical cell surface shaving may present a signature of highly differentiated cells. This is supported by the results of the study by Montacir *et al*<sup>198</sup>, in which the authors used cell surface trypsinization to collect the cell surface *N*-glycans from cultured human embryonic stem cells (hESCs) and cultured hepatocyte-like cells (HLCs, directly differentiated from the hESCs). Montacir *et al*. classified the complex *N*-glycans into several groups with sialylation or fucosylation and only reported the number of biantennary and oligomannose. The proportion of biantennary complex *N*-glycans released from the hESC-differentiated HLC increased to 49% from 11% in the hESC. By contrast, the proportion of oligomannose *N*-glycans released from the hESC-differentiated HLC reduced to 18% from 39% in the hESC.

The value of separating (apical) surface glycans from total cell lysate glycans using different approaches is to offer a glycan profile from polarized cell surface to explore those glycans that are potentially responsible for various cell-cell interactions. The in-house built reaction device presented in this thesis offers the possibility of improving on the collection of the cell surface glycome from the whole cultured cell surface. It enables the study of a more specific apical cell surface glycome from fresh animal tissues, presenting a method to examine, in real time, the expression of glycans/peptides/proteins on differentiated tissue surfaces with structural information generated by MS analysis. In addition, the exposed tissue surface

glycans could represent novel candidates for the diagnosis or treatment of diseases. The structures of the porcine urothelial glycans identified on the apical cell surface using mass spectrometry can be further elaborated, and their tissue surface location can be independently demonstrated using lectin labeling (Figure 2). Lectin binding provides linkage information that supplements the mass spectrometric data, and allows comparison of healthy and diseased tissues, to demonstrate the presence of specific oligosaccharides in particular tissues and diseases. In tissue engineering, the on-tissue trypsinization approach also offers a platform to examine the glycans released for example from the replaced tissue surface after implantation, which is important in understanding and preventing inflammatory responses by the body<sup>244</sup>.

Further application of on-tissue trypsinization using the in-house built reaction device to examine the *N*- and *O*-glycans released from the apical surface of differentiated urothelium and that of undifferentiated urothelium is required, in order to link the identities of apical surface glycans to the differentiation of urothelium. The results of the current study will form the basis to make comparisons between normal urothelium and urothelia with aberrant functions, e.g. uropathogenic bacterially infected surfaces, urothelial with compromised impermeability, and the progression of cancer. In addition, the peptide fraction may be worth collecting after *N*- and *O*-glycan release for MS identification, if urothelial apical surface proteins are of interest.

The current knowledge regarding urothelial glycans and their biological functions on urothelium has not been studied, with the sole exception of the demonstration of the function of the oligomannose glycans on UPK1a; it is therefore not possible to assign biological functions to the urothelial apical surface glycomes reported here. Nonetheless, the following discussions attempt to link the results of the present study of urothelial glycans, with speculation in the literature regarding general glycan function in the development of differentiated epithelia, reported by other researchers.

### **Urothelial *N*-glycans**

Urothelial *N*-glycans have been mainly investigated in studies of *N*-glycosylation of uroplakins, or of cell lysate glycomes of cultured urothelial cancer cells (chapter 1). In the present study, which has generated the first normal mammalian urothelial *N*-glycome, low abundance oligomannose *N*-glycans and high abundance complex *N*-glycans were observed in both apical cell surface *N*-glycomes and the total cell lysate *N*-glycome of fresh porcine urothelium. The high abundance of complex *N*-glycans observed here in urothelium is speculated to be a feature of differentiated cells as suggested by Montacir *et al*<sup>198</sup> (in hESCs), and raises intriguing prospects for the mechanism of differentiation of polarized epithelial cells, such as found in the urothelium.

*N*-glycan structures appear to determine whether an *N*-glycoprotein is directed to the apical cell surface domain or the basolateral membrane domain in

differentiated epithelia<sup>245–248</sup>. This was first exemplified in studies of glycosylated erythropoietin (Epo), which has three *N*- and one O-glycosylation site. Its expression in differentiated Madin-Darby canine kidney cells (MDCK, epithelial cells) was identified preferentially on the apical cell surface domain<sup>249</sup>. This polarized expression was found to be compromised by treatment with tunicamycin, an antibiotic that blocks *N*-glycan synthesis on dolichol phosphate (chapter 1), suggesting that *N*-glycosylation is involved in the protein sorting pathway. In addition, site specific mutation altering one or two of the three *N*-glycosylation sites of Epo indicated that it is the *N*-glycosylation site at Asn-38 that is critical to this polarized expression<sup>249</sup>. In another study, the *N*-glycan profile of Epo expressed in human lymphoblastoid cells was reported by Cointe *et al.*, using ESI-MS to analyze native glycopeptides, in which only complex *N*-glycans were identified<sup>250</sup>, most commonly with up to two fucosylations and/or one to five LacNAc (Gal-GlcNAc-) moieties at position 38 of the Epo sequence<sup>250</sup>. Whether the complex *N*-glycan structure with a large number of LacNAc moieties bears these on a multi-antennary structure or as an oligo-LacNAc was not determined from the simple mass spectrometric measurement (mass measurement only) reported in ref<sup>250</sup>.

Protein sorting-related fucosylation of *N*-glycans in epithelia was also reported by Nakagawa *et al.*<sup>248</sup> for the polarized expression of glycoproteins in liver, which produces bile glycoproteins delivered into the bile duct through the biliary epithelial cells). Higher levels of fucosylation of  $\alpha$ -fetoprotein,  $\alpha$ 1-antitrypsin,  $\alpha$ 1-acid glycoprotein and haptoglobin were identified in bile than in serum, using lectin labelling in combination with analyzing pyridylamino-modified oligosaccharides with

MALDI-MS<sup>248</sup>. The fucosylated *N*-glycans identified on these glycoproteins also bear large numbers of LacNAc moieties, meaning that the complex *N*-glycans are highly branched and/or possess multiple oligo-LacNAc, which is in line with the *N*-glycan structures reported in the glycosylated Epo studies described above<sup>249</sup>. It is worth noting that both ref<sup>248</sup> and ref<sup>249</sup> performed desialylation of *N*-glycans prior to mass spectrometric analysis, resulting in no identification of sialylated complex *N*-glycans in these two datasets; it is unfortunate to sacrifice the information on glycan sialylation, which is a common modification of *N*- and O-glycans and that has important biological functions.

The presence of sialic acids on the cell surface contributes to the negative charge of the cell surface, and is widely believed to be a vital signature for cell-cell recognition, cancer cell migration and cell surface protection against pathogenic bacteria/virus infection<sup>251–253</sup>. Sialylation of glycans was also suggested to be involved in the protein sorting pathway in differentiated MDCK cells. Sialylation of mouse soluble dipeptidyl peptidase IV (DPP IV ectodomain) expressed in MDCK cells was impaired by treatment with benzyl-2-acetamido-2-deoxy- $\alpha$ -D-galactopyranoside (BGN), a drug impairing sialylation of glycans, resulting in decreased apical secretion and increased basolateral secretion of mouse DPP IV ectodomain<sup>254</sup>.

The most well-studied biological function of urothelial cell apical *N*-glycans is the oligomannose *N*-glycans on UPK1a, which is a member of the apical cell surface urothelial plaques covering the luminal surface of superficial urothelium<sup>14,18,26</sup>

(chapter 1). Oligomannose *N*-glycans were exclusively identified on the UPK1a collected from fresh mouse and bovine urothelial plaques and human urothelial cells using PNGase F digestion followed by MALDI-MS analysis<sup>13</sup>. In addition, the oligomannose *N*-glycans (Hex<sub>6-9</sub>HexNAc<sub>2</sub>) on UPK1a are the physiological binding receptors for type 1-fimbriated *E. coli*. The binding between glycosylated UPK1a and type 1-fimbriated *E. coli* was inhibited by Endo H digestion, removing oligomannose *N*-glycans from UPK1a. By contrast, glycosylated UPK1b, nonglycosylated UPK2 and glycosylated UPK3a were not found to have binding activity with type 1-fimbriated *E. coli*<sup>13,23</sup>.

### **Urothelial O-glycans**

Urothelial O-glycans have been mainly identified as mucin-type structures in many studies, in which only O-glycan-specific lectin-stained animal tissues or cell lysates showed the distribution of limited O-glycan structures (chapter 1)<sup>37,49,52,255</sup>. Some studies state, surprisingly, that the urothelium is a type of secretory epithelium, because most glycan structures labeled by lectins were mucin-type O-glycans (T and Tn antigens) that are commonly identified in mucus secreted by mucosa<sup>49,255</sup>. However, urothelium is not classified as a mucous epithelium<sup>256</sup>. Based on the fact that the O-glycans identified in the present study required trypsinization to shave the apical cell surface prior to  $\beta$ -elimination to release O-glycans, it is proposed that the urothelial mucin-type O-glycans are unlikely to be from secreted proteins but from the membrane-bound glycoproteins present on superficial urothelium. A control on-tissue trypsinization in the present study was conducted with HBSS+Ca<sup>2+</sup>/Mg<sup>2+</sup> and without the addition of trypsin; no detectable mass

spectrometric signals of O and N-glycans were obtained on MALDI-MS. This result suggests that the porcine urothelium does not have secreted glycoproteins and is unlikely to be secretory epithelium, which is in line with the study of N'Dow *et al.*<sup>256</sup> in which the levels of bladder surface-associated glycoproteins were shown to remain constant, even though the levels of urinary glycoprotein were very variable.

The O-glycans on glycosylated transmembrane mucin glycoprotein MUC1 were reported to be the signal molecules required for sorting MUC1 to the apical surface of differentiated MDCK cells<sup>257</sup>. O-glycosylation of MUC1 in differentiated MDCK cells was significantly modified by the overexpression of  $\alpha$ 2,6-sialyltransferase-1 (ST6GalNAc-1), which resulted in very large amounts of sialylated Tn antigen (NeuAc-GalNAc-). The sialylation reaction was expected to compete with the addition of Gal to form mucin type O-glycan core 1 (Gal-GalNAc-) and the addition of GlcNAc to form core 2 (Gal-[GlcNAc]-GalNAc-) and core 3 (GlcNAc-GalNAc-), thereby preventing the synthesis of the mucin-type O-glycans. As a result of this altered O-glycan synthesis, the expression of MUC1 changed primarily to the basolateral surface of differentiated MDCK cells.

In summary, these reported protein sorting-related glycans in differentiated epithelial cells (MDCK cells), fucosylated complex N-glycans with multiple LacNAc moieties and mucin-type O-glycans, are similar to the glycan species identified in the present porcine urothelial cell apical N- and O-glycomes (chapter 5). It is thus speculated that the presence of protein sorting-related N- and O-glycans have the



effect of coating the highly polarized urothelium with a dense glycan layer on the superficial surface, contributing to barrier function. It should be noted that the impaired glycosylation resulting from gene regulation or enzymatic inhibition used in several research groups to alter the normal glycosylation pathway, may in fact cause a wide range of effects on cell function, resulting in not only an overall changed glycan profile, but potentially less predictable and even fatal consequences on cells/animals<sup>258–260</sup>. Conversely, the altered expression of glycoproteins on the polarized apical or basolateral domain may not just be caused by a single change to glycosylation.



## Appendix 1. Lectins used in urothelial glycosylation

Lectin name	Lectin abbreviation	Binding structure	Inhibitory compound <sup>261*</sup>	Labeling in urothelium/urothelial cells
<i>Aleuria aurantia</i>	AAL	Terminal Fuc- $\alpha$ -(1 $\rightarrow$ 6) Fuc- $\alpha$ -(1 $\rightarrow$ 3)Gal- $\beta$ -(1 $\rightarrow$ 3)-GlcNAc	Fucose	Cultured human urothelial cancer cells <sup>33</sup>
<i>Amaranthus caudatus</i>	ACA	Gal- $\beta$ -(1 $\rightarrow$ 3)-GalNAc-Ser/Thr	Desialylated fetuin	Superficial layer of rat urothelium <sup>32</sup>
<i>Bauhinia purpurea</i>	BPL	Gal- $\beta$ -(1 $\rightarrow$ 3)-GalNAc	lactose	Cultured human urothelial cells <sup>33</sup>
Concanavalin A	Con A	$\alpha$ -Man	Methyl- $\alpha$ -mannose	Cultured human urothelial cancer cells <sup>33</sup>

		terminal GlcNAc		Superficial layer of rabbit urothelium <sup>35</sup>  All layers of donkey urothelium <sup>49</sup>  Superficial layer of rat urothelium <sup>50</sup>
<i>Dolichos biflorus</i>	DBA	GalNAc-Ser/Thr  GalNAc- $\alpha$ -(1 $\rightarrow$ 3)-Gal	Chitin hydrolysate	Superficial layer of donkey urothelium <sup>49</sup>
<i>Datura stramonium</i>	DSL	GlcNAc	N-Acetylglucosamine	Superficial layer of rat urothelium <sup>32</sup>

<i>Erythrina cristagalli</i>	ECA	Gal- $\beta$ -(1 $\rightarrow$ 3)-GlcNAc	Lactose	Cultured human urothelial cancer cells <sup>33</sup>  All layers of rabbit urothelium <sup>35</sup>
<i>Euonymus europaeus</i>	EEL	Gal- $\alpha$ -(1 $\rightarrow$ 3)[Fuc- $\alpha$ -(1 $\rightarrow$ 2)]-Gal	Lactose	Cultured human urothelial cancer cells <sup>33</sup>
<i>Griffonia (Bandeiraea) simplicifolia</i> I	GSL-I	$\alpha$ -Gal  $\alpha$ -GalNAc  GalNAc-Ser/Thr	Galactose	Cultured human urothelial cancer cells <sup>33</sup>
<i>Griffonia (Bandeiraea)</i>	GSL-II (BSL-II)	GlcNAc	N-Acetylglucosamine	Cultured human urothelial cancer cells <sup>33</sup>

<i>simplicifolia</i> II				Intermediate layer of rabbit urothelium <sup>35</sup>  All layers of donkey urothelium <sup>49</sup>
<i>Galanthus nivalis</i>	GNA	Terminal $\alpha$ -(1 $\rightarrow$ 3) Man	Methyl- $\alpha$ -mannose	Cultured human urothelial cancer cells <sup>33</sup>
<i>Griffonia simplicifolia</i>	GSA I-B4	Terminal $\alpha$ -Gal	Galactose	Cultured human urothelial cancer cells <sup>33</sup>  Bovine UPK3 <sup>22</sup>  All layers of donkey urothelium <sup>49</sup>

Jacalin	Jacalin	Gal- $\beta$ -(1 $\rightarrow$ 3)-GalNAc-Ser/Thr  GalNAc-Ser/Thr	Galactose	Cultured human urothelial cancer cells <sup>33</sup>  Luminal surface of rabbit urothelium <sup>35</sup>
<i>Lotus tetragonolobus</i>	LTA	Terminal $\alpha$ -Fuc	Fucose	All layers of rabbit urothelium <sup>35</sup>
<i>Lycopersicon esculentum</i>	LEL	[Gal- $\beta$ -(1 $\rightarrow$ 4)-GlcNAc] <sub>n</sub>  (GlcNAc) <sub>n</sub>	Chitin hydrolysate	Cultured human urothelial cancer cells <sup>33</sup>  Luminal surface of rabbit urothelium and lamina propria <sup>35</sup>

<i>Lens culinaris</i>	LCA	$\alpha$ -Man	Methyl- $\alpha$ -mannose	Cultured human urothelial cancer cells <sup>33</sup>
<i>Maackia amurensis</i>	MAL-I	Gal- $\beta$ -(1 $\rightarrow$ 4)-GlcNAc	Lactose	Cultured human urothelial cancer cells <sup>33</sup>
<i>Maackia amurensis</i>	MAL-II	NeuAc- $\alpha$ -(2 $\rightarrow$ 3)-Gal- $\beta$ -(1 $\rightarrow$ 4)-GlcNAc	Human glycophorin	Cultured human urothelial cancer cells <sup>33</sup>  All layers of rabbit urothelium and lamina propria <sup>35</sup>  All layers of donkey urothelium <sup>49</sup>



<i>Maclura pomifera</i>	MPL	$\alpha$ -GalNAc	Galactose,	Cultured human urothelial cancer cells <sup>33</sup>
<i>Phaseolus vulgaris</i> <i>erythroagglutinin</i>	PHA-E	Intersecting GlcNAc and biantennary <i>N</i> -glycans	bovine thyroglobulin, acetic acid	Cultured human urothelial cancer cells <sup>33</sup>
<i>Psophocarpus tetragonolobus</i>	PTL-I	$\alpha$ -GalNAc and Gal	<i>N</i> -Acetylgalactosamine	Cultured human urothelial cancer cells <sup>33</sup>
<i>Psophocarpus tetragonolobus</i>	PTL-II	Gal	<i>N</i> -Acetylgalactosamine	Cultured human urothelial cancer cells <sup>33</sup>
Peanut agglutinin	PNA	Gal- $\beta$ -(1 $\rightarrow$ 3)-GalNAc-Ser/Thr	Galactose	Cultured human urothelial cancer cells <sup>33</sup>

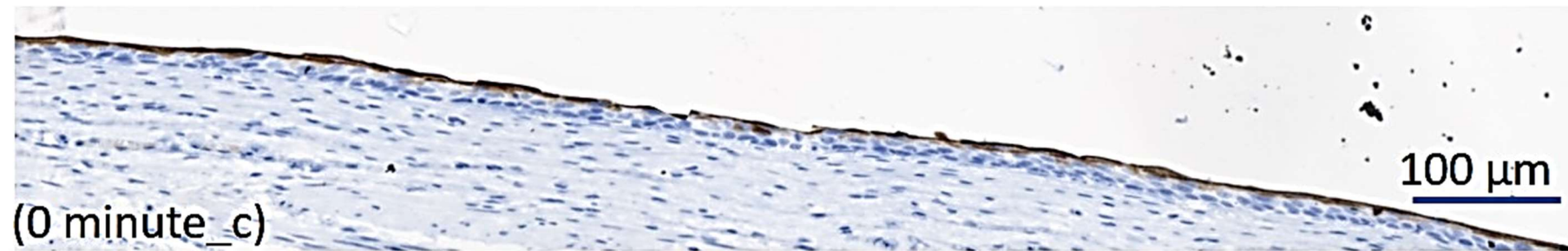
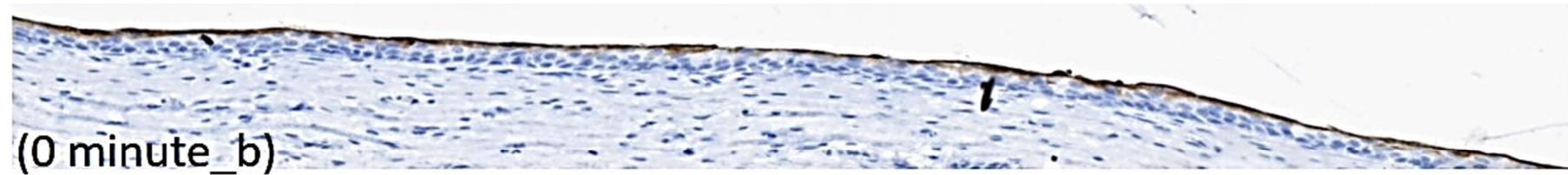
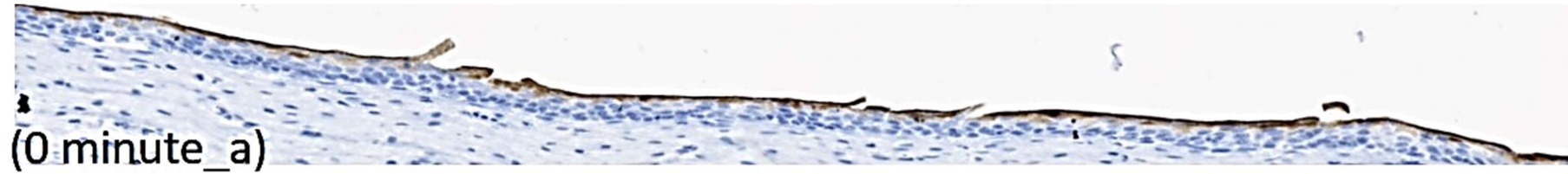
				<p>Luminal surface of rat urothelium<sup>50</sup>.</p> <p>Glycoproteins in rat bladder extracts<sup>34</sup></p> <p>Weak labeling in rabbit urothelium<sup>35</sup></p>
<p><i>Phaseolus vulgaris</i></p> <p><i>Leucoagglutinin</i></p>	PHA-L	Tetra-antennary complex <i>N</i> -glycans	bovine thyroglobulin, acetic acid	Cultured human urothelial cancer cells <sup>33</sup>
Soybean	SBA	GalNAc- $\alpha$ -(1 $\rightarrow$ 3)-Gal	<i>N</i> -Acetylgalactosamine	Cultured human urothelial cancer cells <sup>33</sup>

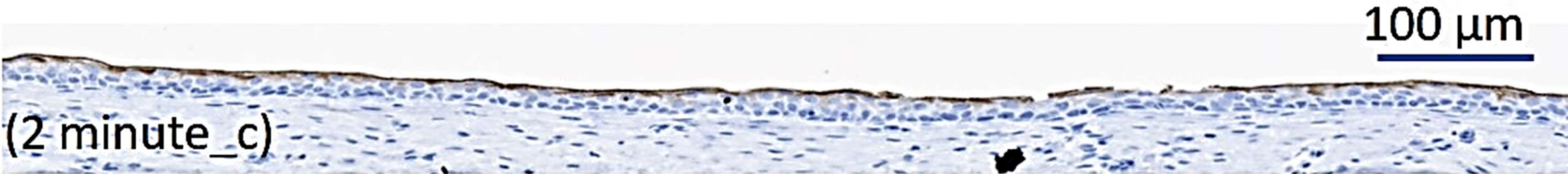
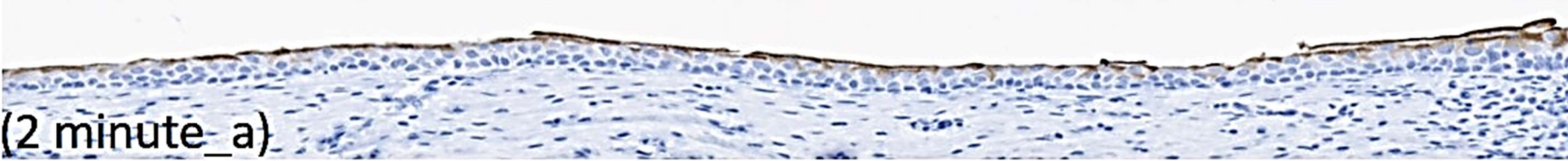
				Superficial layer of donkey urothelium <sup>49</sup>
<i>Sambucus nigra</i>	SNA	NeuAc- $\alpha$ -(1 $\rightarrow$ 3)-Gal- $\beta$ -(1 $\rightarrow$ 4)-GlcNAc	Lactose	Cultured human urothelial cancer cells <sup>33</sup> Bovine UPK3 <sup>22</sup> Underlayer of rabbit urothelium and lamina propria <sup>35</sup> Superficial layers of donkey urothelium <sup>49</sup>
<i>Ulex europaeus</i>	UEA-I	Fuc- $\alpha$ -(1 $\rightarrow$ 2) -Gal- $\beta$ -(1 $\rightarrow$ 4)-GlcNAc	Fucose	Cultured human urothelial cancer cells <sup>33</sup>

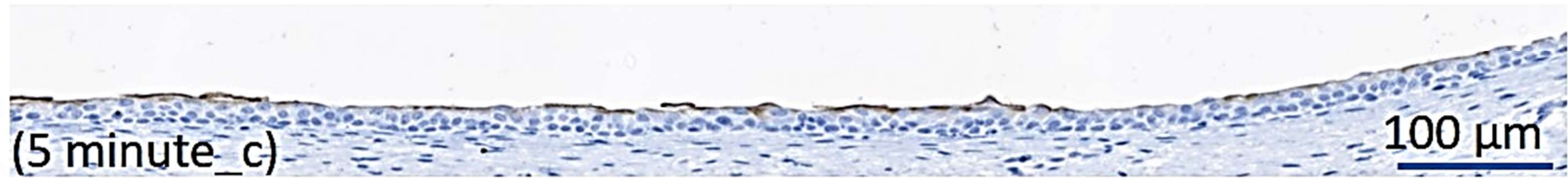
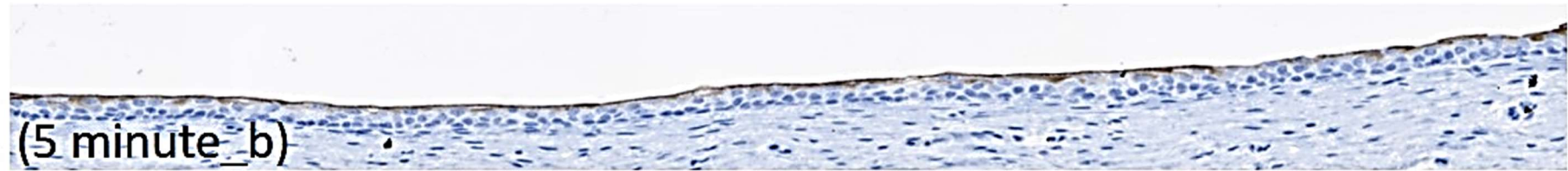
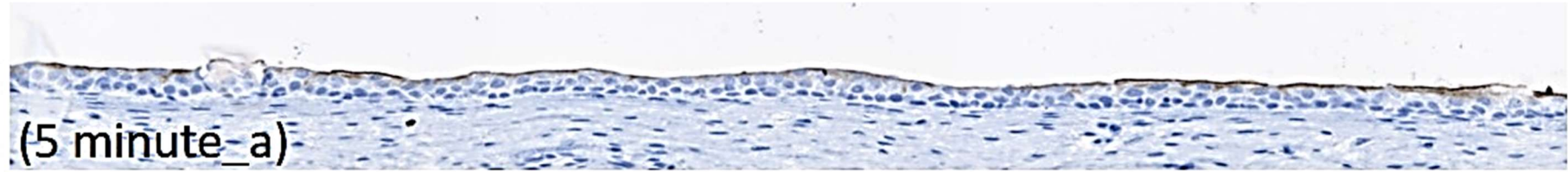
				Superficial layer of rat urothelium <sup>34</sup>
<i>Vicia villosa</i>	VVA	GalNAc GalNAc-Ser/Thr	N-Acetylgalactosamine	Cultured human urothelial cancer cells <sup>33</sup> Superficial layer of rat urothelium <sup>34</sup> Weak labeling in rabbit urothelium <sup>35</sup>
Wheat germ	WGA	(GlcNAc) <sub>n</sub>	N-Acetylglucosamine	Cultured human urothelial cancer cells <sup>33</sup> Superficial layer of rat urothelium <sup>32</sup>

				Lamina propria of rabbit urothelium <sup>35</sup>
--	--	--	--	--

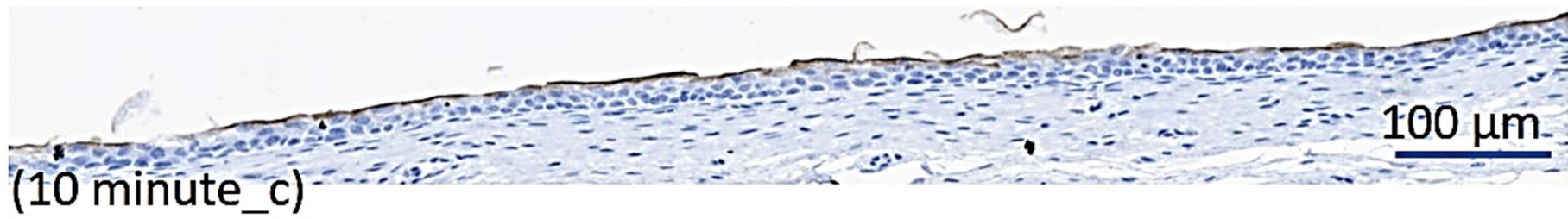
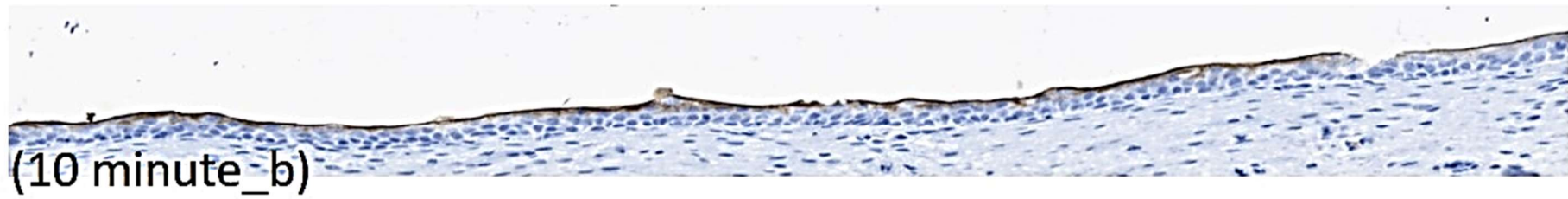
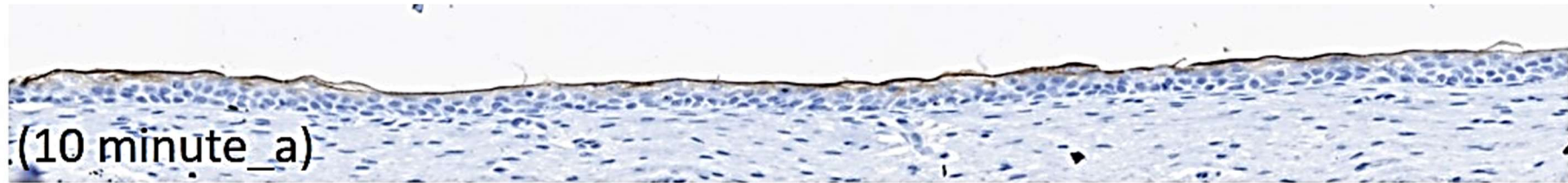
Appendix 2. Superficial UPK3a-labelled porcine urothelium

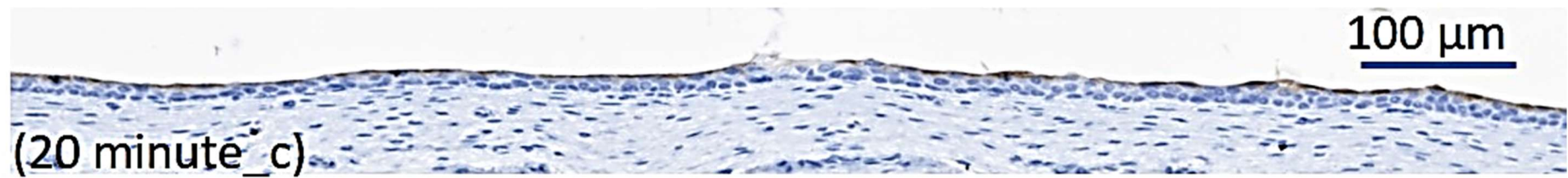
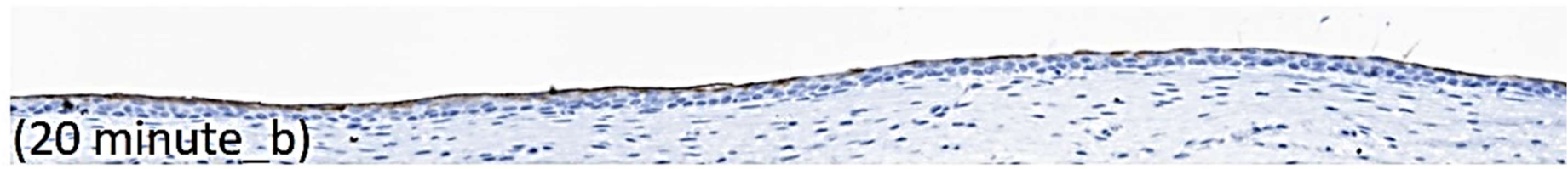
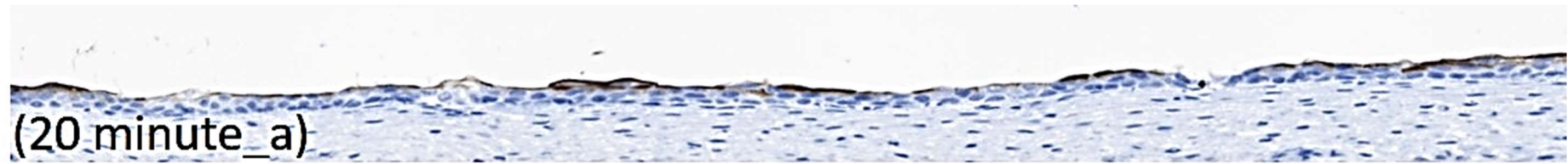


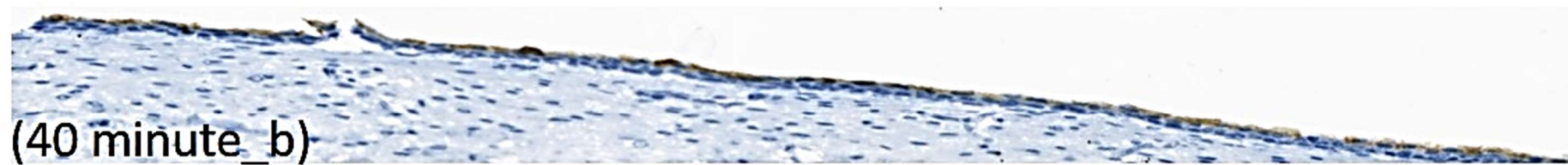
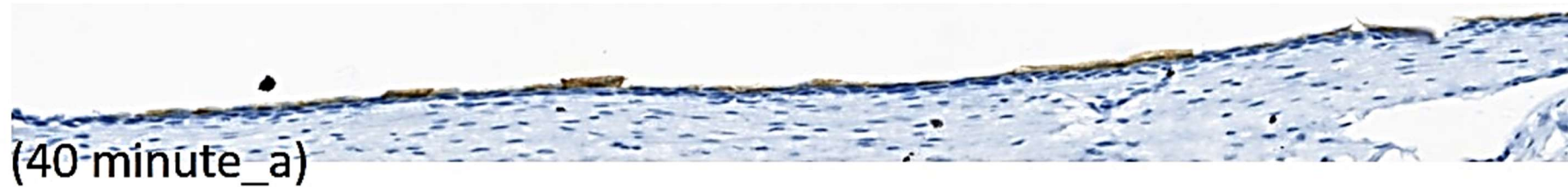




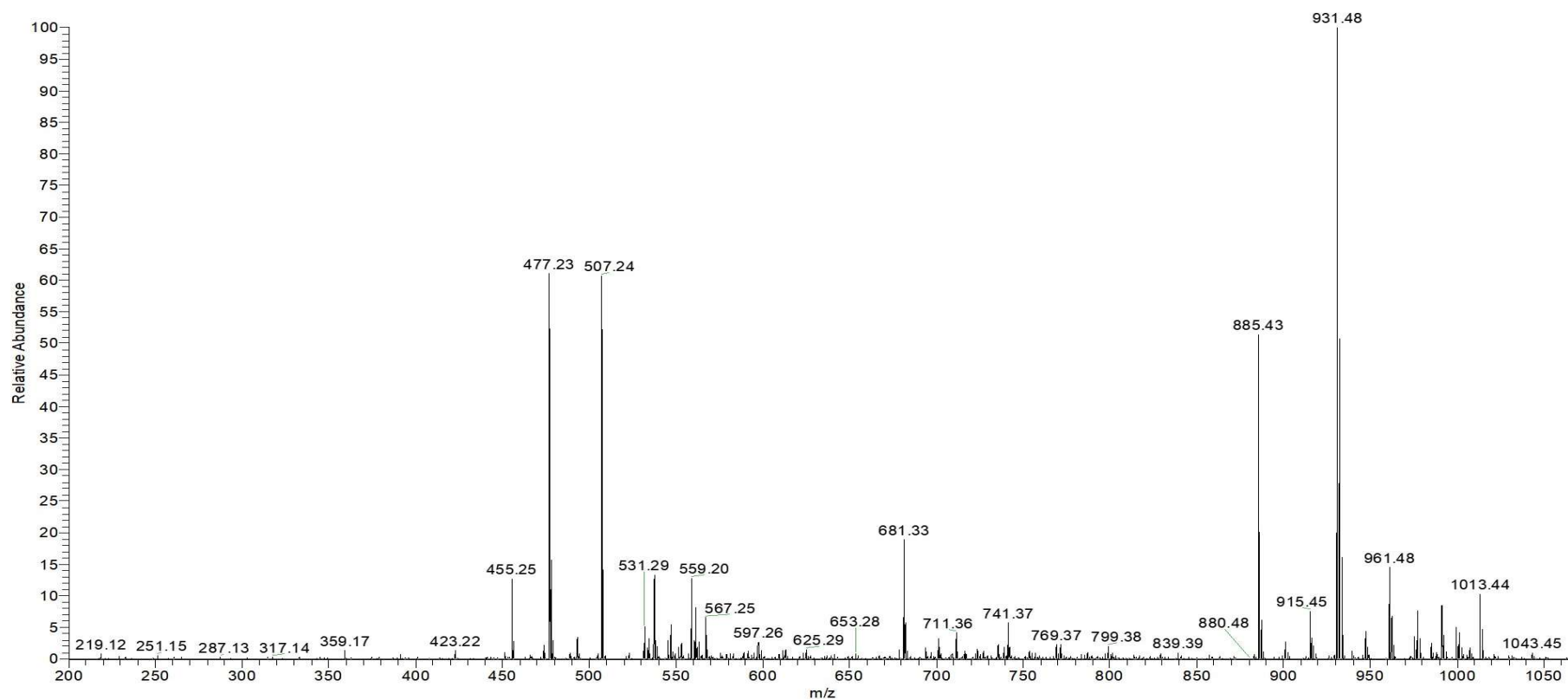








**Appendix 3. Mass spectrum acquired using Thermo Orbitrap Fusion, showing dominance of background signals in the nanoESI spectrum of the permethylated urothelial glycans released together following trypsinisation of the apical surface of porcine urothelium. Hex<sub>2-4</sub> at *m/z* 477, 681 and 885.**

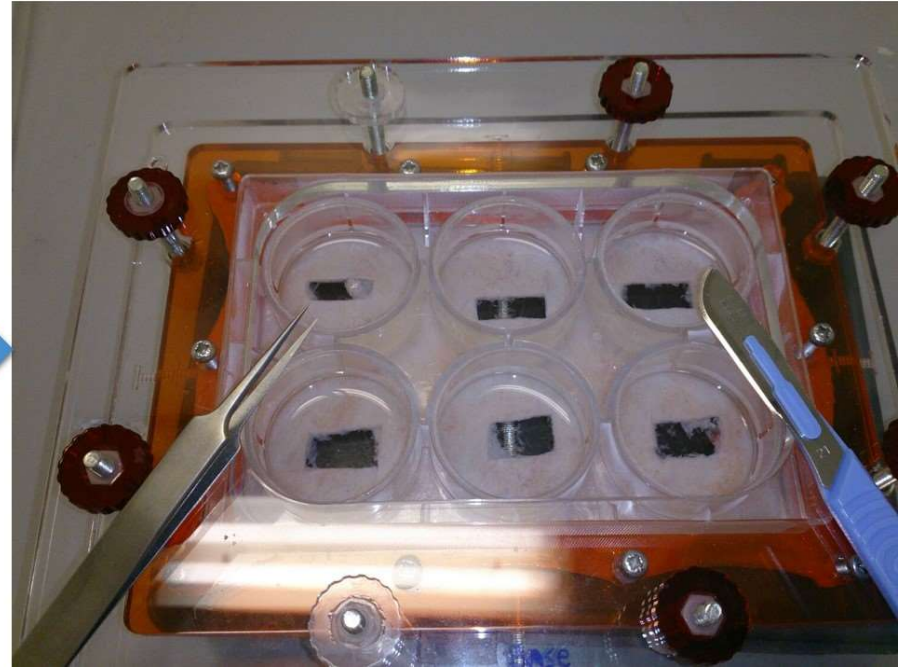


#### Appendix 4. On-tissue formalin fixation

On-tissue trypsinized porcine bladder after formalin fixation



Removing the formalin-fixed tissue sections for IHC





## References

1. Khandelwal, P., Abraham, S. N. & Apodaca, G. Cell biology and physiology of the uroepithelium. *Am. J. Physiol. Renal Physiol.* **297**, 1477–1501 (2009).
2. Lewis, S. A. Everything you wanted to know about the bladder epithelium but were afraid to ask. *Am J Physiol Ren. Physiol* **278**, 867–874 (2000).
3. Rajasekaran, M., Stein, P. & Parsons, C. L. Toxic factors in human urine that injure urothelium. *Int. J. Urol.* **13**, 409–14 (2006).
4. Apodaca, G. The uroepithelium: not just a passive barrier. *Traffic* **5**, 117–128 (2004).
5. Jenkins, D. & Woolf, A. Uroplakins: new molecular players in the biology of urinary tract malformations. *Kidney Int.* **71**, 195–200 (2007).
6. Kreplak, L., Wang, H., Aebi, U. & Kong, X. P. Atomic Force Microscopy of Mammalian Urothelial Surface. *J. Mol. Biol.* **374**, 365–373 (2007).
7. Deng, F.-M. *et al.* Uroplakin IIIb, a urothelial differentiation marker, dimerizes with uroplakin Ib as an early step of urothelial plaque assembly. *J. Cell Biol.* **159**, 685–94 (2002).
8. Sun, T.-T. Altered phenotype of cultured urothelial and other stratified epithelial cells: implications for wound healing. *Am. J. Physiol. Renal Physiol.* **291**, F9–F21 (2006).
9. Yu, J., Lin, J. H., Wu, X. R. & Sun, T.-T. Uroplakins Ia and Ib, two major differentiation products of bladder epithelium, belong to a family of four transmembrane domain (4TM) proteins. *J. Cell Biol.* **125**, 171–182 (1994).
10. Wu, X.-R. & Sun, T.-T. Molecular cloning of a 47 kDa tissue-specific and differentiation-dependent urothelial cell surface glycoprotein. *J. Cell Sci.* **106**, 31–43 (1993).
11. Hu, P. *et al.* Role of membrane proteins in permeability barrier function: uroplakin ablation elevates urothelial permeability. *Am. J. Physiol. Renal Physiol.* **283**, 1200–1207 (2002).
12. Kong, X. T. *et al.* Roles of uroplakins in plaque formation, umbrella cell enlargement, and urinary tract diseases. *J. Cell Biol.* **167**, 1195–1204 (2004).

13. Xie, B. *et al.* Distinct glycan structures of uroplakins Ia and Ib: structural basis for the selective binding of FimH adhesin to uroplakin Ia. *J. Biol. Chem.* **281**, 14644–53 (2006).
14. Wu, X.-R., Kong, X.-P., Pellicer, A., Kreibich, G. & Sun, T.-T. Uroplakins in urothelial biology, function, and disease. *Kidney Int.* **75**, 1153–1165 (2009).
15. Wu, X.-R. *et al.* Mammalian uroplakins: a group of highly conserved urothelial differentiation-related membrane proteins. *J. Biol. Chem.* **269**, 13716–13724 (1994).
16. Deng, F. M. *et al.* Uroplakin IIIb, a urothelial differentiation marker, dimerizes with uroplakin Ib as an early step of urothelial plaque assembly. *J. Cell Biol.* **159**, 685–694 (2002).
17. Hu, P. *et al.* Ablation of uroplakin III gene results in small urothelial plaques, urothelial leakage, and vesicoureteral reflux. *J. Cell Biol.* **151**, 961–971 (2000).
18. Taganna, J., Deboer, A. R., Wuhler, M. & Bouckaert, J. Glycosylation changes as important factors for the susceptibility to urinary tract infection. *Biochem. Soc. Trans.* **39**, 349–354 (2011).
19. Hauser, P. J. *et al.* Abnormal expression of differentiation related proteins and proteoglycan core proteins in the urothelium of patients with interstitial cystitis. *J. Urol.* **179**, 764–9 (2008).
20. Iwona, K., Lis, J. & Matejuk, A. Glycosylation of uroplakins . Implications for bladder physiopathology. *Glycoconj. J.* **31**, 623–636 (2014).
21. Tu, L., Kong, X.-P., Sun, T.-T. & Kreibich, G. Integrity of all four transmembrane domains of the tetraspanin uroplakin Ib is required for its exit from the ER. *J. Cell Sci.* **119**, 5077–5086 (2006).
22. Malagolini, N., Cavallone, D., Wu, X.-R. & Serafini-Cessi, F. Terminal glycosylation of bovine uroplakin III, one of the major integral-membrane glycoproteins of mammalian bladder. *Biochim. Biophys. Acta - Gen. Subj.* **1475**, 231–237 (2000).
23. Zhou, G. *et al.* Uroplakin Ia is the urothelial receptor for uropathogenic Escherichia coli: evidence from in vitro FimH binding. *J. Cell Sci.* **114**, 4095–103 (2001).



24. Wellens, A. *et al.* Intervening with urinary tract infectious using anti-adhesives based on the crystal structure of the FimH-oligomannose-3 complex. *PLoS One* **3**, 1–13 (2008).
25. Schwardt, O. *et al.* Design, synthesis and biological evaluation of mannosyl triazoles as FimH antagonists. *Bioorganic Med. Chem.* **19**, 6454–6473 (2011).
26. Bouckaert, J. *et al.* The affinity of the FimH fimbrial adhesin is receptor-driven and quasi-independent of *Escherichia coli* pathotypes. *Mol. Microbiol.* **61**, 1556–1568 (2006).
27. Wu, X.-R., Sun, T.-T. & Medina, J. J. In vitro binding of type 1-fimbriated *Escherichia coli* to uroplakins Ia and Ib: relation to urinary tract infections. *Proc. Natl. Acad. Sci. U. S. A.* **93**, 9630–9635 (1996).
28. Hu, C.-C. A. *et al.* Assembly of urothelial plaques: tetraspanin function in membrane protein trafficking. *Mol. Biol. Cell* **16**, 3937–3950 (2005).
29. Jenkins, D. & Woolf, A. S. Uroplakins: new molecular players in the biology of urinary tract malformations. *Kidney Int.* **71**, 195–200 (2007).
30. Kreft, M. E., Hudoklin, S., Jezernik, K. & Romih, R. Formation and maintenance of blood-urine barrier in urothelium. *Protoplasma* **246**, 3–14 (2010).
31. Thumbikat, P., Berry, R. E., Schaeffer, A. J. & Klumpp, D. J. Differentiation-induced uroplakin III expression promotes urothelial cell death in response to uropathogenic *E. coli*. *Microbes Infect.* **11**, 57–65 (2009).
32. Zupancic, D., Kreft, M. E. & Romih, R. Selective binding of lectins to normal and neoplastic urothelium in rat and mouse bladder carcinogenesis models. *Protoplasma* 49–59 (2014).
33. Yang, G. *et al.* Quantitative glycome analysis of N-glycan patterns in bladder cancer vs normal bladder cells using an integrated strategy. *J. Proteome Res.* **14**, 639–653 (2015).
34. Vinter-Jensen, L. & Ørntoft, T. F. Glycoproteins in the urothelium and in the urine of the epidermal growth factor induced growing urinary tract in rats. *Urol. Res.* **26**, 97–103 (1998).
35. Buckley, M. *et al.* Lectin histochemical examination of rabbit bladder glycoproteins and characterization of a mucin isolated from the bladder mucosa. *Arch. Biochem. Biophys.* **375**, 270–7 (2000).

36. Buckley, M. S., Washington, S., Laurent, C., Erickson, D. R. & Bhavanandan, V. P. Characterization and immunohistochemical localization of the glycoconjugates of the rabbit bladder mucosa. *Arch. Biochem. Biophys.* **330**, 163–73 (1996).
37. Higuchi, T., Xin, P., Buckley, M. S., Erickson, D. R. & Bhavanandan, V. P. Characterization of the rabbit homolog of human MUC1 glycoprotein isolated from bladder by affinity chromatography on immobilized jacalin. *Glycobiology* **10**, 659–67 (2000).
38. Hurst, R. E., Moldwin, R. M. & Mulholland, S. G. Bladder defense molecules, urothelial differentiation, urinary biomarkers, and interstitial cystitis. *Urology* **69**, 17–23 (2007).
39. Nickel, J. C. *et al.* A real-life multicentre clinical practice study to evaluate the efficacy and safety of intravesical chondroitin sulphate for the treatment of interstitial cystitis. *BJU Int.* **103**, 56–60 (2009).
40. Birder, L. A. Urinary bladder, cystitis and nerve/urothelial interactions. *Auton. Neurosci. Basic Clin.* **182**, 89–94 (2014).
41. Huygens, A. *et al.* Influence of the glycosaminoglycan layer on the permeation of hypericin in rat bladders in vivo. *BJU Int.* **100**, 1176–81 (2007).
42. Tyagi, P., Wu, P., Chancellor, M., Yoshimura, N. & Huang, L. Recent Advance In Intravesical Drug/Gene Delivery. *Mol Pharm* **3**, 369–379 (2006).
43. Lv, Y. S. *et al.* Intravesical hyaluronidase causes chronic cystitis in a rat model: a potential model of bladder pain syndrome/interstitial cystitis. *Int. J. Urol.* **21**, 601–7 (2014).
44. Janssen, D. A. W. *et al.* The distribution and function of chondroitin sulfate and other sulfated glycosaminoglycans in the human bladder and their contribution to the protective bladder barrier. *J. Urol.* **189**, 336–342 (2013).
45. Ferreira, J. A. *et al.* Overexpression of tumour-associated carbohydrate antigen sialyl-Tn in advanced bladder tumours. *Mol. Oncol.* **7**, 719–731 (2013).
46. Lima, L. *et al.* Response of high-risk of recurrence/progression bladder tumours expressing sialyl-Tn and sialyl-6-T to BCG immunotherapy. *Br. J. Cancer* 1–9 (2013).

47. Keay, S. K. *et al.* An antiproliferative factor from interstitial cystitis patients is a frizzled 8 protein-related sialoglycopeptide. *Proc. Natl. Acad. Sci. U. S. A.* **101**, 11803–11808 (2004).
48. Guo, J. *et al.* Alteration of N-glycans and expression of their related glyco genes in the epithelial-mesenchymal transition of HCV29 bladder epithelial cells. *Molecules* **19**, 20073–20090 (2014).
49. Desantis, S., Accogli, G., Zizza, S. & Arrighi, S. In situ characterization of glycans in the urothelium of donkey bladder: evidence of secretion of sialomucins. *Acta Histochem.* **115**, 712–718 (2013).
50. Hodges, G. M., Smolira, M. A. & Trejdosiewicz, L. K. Urothelium-specific antibody and lectin surface mapping of bladder urothelium. *Histochem. J.* **14**, 755–766 (1982).
51. Spicer, S. S. & Schulte, B. A. Diversity of cell glycoconjugates shown histochemically: a perspective. *J. Histochem. Cytochem.* **40**, 1–38 (1992).
52. Catherine, L. & Lange, P. T-antigen in normal and neoplastic urothelium. *Cancer* **58**, 1236–1245 (1986).
53. Debray, H., Decout, D., Strecker, G., Spik, G. & Montreuil, J. Specificity of twelve lectins towards oligosaccharides and glycopeptides related to N-glycosylproteins. *Eur. J. Biochem.* **117**, 41–55 (1981).
54. Lin, J. H., Wu, X. R., Kreibich, G. & Sun, T.-T. T. Precursor sequence, processing, and urothelium-specific expression of a major 15-kDa protein subunit of asymmetric unit membrane. *J. Biol. Chem.* **269**, 1775–1784 (1994).
55. Wu, X. R., Medina, J. J. & Sun, T.-T. Selective interactions of UPIa and UPIb, two members of the transmembrane 4 superfamily, with distinct single transmembrane-domained proteins in differentiated urothelial cells. *J. Biol. Chem.* **270**, 29752–29759 (1995).
56. Tu, L., Sun, T.-T. & Kreibich, G. Specific heterodimer formation is a prerequisite for uroplakins to exit from the endoplasmic reticulum. *Mol. Biol. Cell* **13**, 4221–4230 (2002).
57. Surya, B., Yu, J., & Sun T.-T. Assessing the differentiation state of cultured bovine urothelial cells: elevated synthesis of stratification-related K5 and K6 keratins and persistent expression of uroplakin I. 419–432 (1987).

58. Hemler, M. E. Tetraspanin proteins mediate cellular penetration, invasion, and fusion events and define a novel type of membrane microdomain. *Annu. Rev. Cell Dev. Biol.* **19**, 397–422 (2003).
59. Boucheix, C. & Rubinstein, E. Tetraspanins. *Cell. Mol. Life Sci.* **58**, 1189–205 (2001).
60. Sellman, B. R., Mourez, M. & Collier, R. J. Dominant-negative mutants of a toxin subunit: An approach to therapy of anthrax. *Science (80-. )*. **292**, 695–697 (2001).
61. Petosa, C., Collier, R. J., Klimpel, K. R., Leppla, S. H. & Liddington, R. C. Crystal structure of the anthrax toxin protective antigen. *Nature* **385**, 833–838 (1997).
62. Ballard, J., Sokolov, Y., Yuan, W. & Kagan, B. L. Activation and mechanism of Clostridium septicum alpha toxin. **10**, 627–634 (1993).
63. Wu, X.-R. *et al.* Large Scale Purification Uroplakins I , II , and III of Bovine. *J. Biol. Chem.* **265**, 19170–19179 (1990).
64. Toyoda, M., Ito, H., Matsuno, Y. K., Narimatsu, H. & Kameyama, A. Quantitative derivatization of sialic acids for the detection of sialoglycans by MALDI MS. *Anal. Chem.* **80**, 5211–5218 (2008).
65. Gil, G.-C., Lliff, B., Cerny, R., Velander, W. H. & VanCott, K. E. High throughput quantification of N-glycans using one-pot sialic acid modification and matrix assisted laser desorption ionization time-of-flight mass spectrometry. *Anal. Chem.* **82**, 6613–6620 (2010).
66. Nishiyama, T., Matsumoto, Y., Watanabe, H., Fujiwara, M. & Sato, S. Detection of Tn antigen with Vicia villosa agglutinin in urinary bladder cancer: its relevance to the patient's clinical course. *J Natl Cancer Inst* **78**, 1113–1118 (1987).
67. Häuselmann, I. & Borsig, L. Altered tumor-cell glycosylation promotes metastasis. *Front. Oncol.* **4**, 28 (2014).
68. Skeene, K. *et al.* One filter, One sample, and the N- and O-glyco(proteo)me: toward a system to study disorders of protein glycosylation. *Anal. Chem.* **89**, 5840–5849 (2017).
69. Hauser, P. J. *et al.* Restoring barrier function to acid damaged bladder by intravesical chondroitin sulfate. *J. Urol.* **182**, 2477–2482 (2009).

70. Engles, C. D., Hauser, P. J., Abdullah, S. N., Culkin, D. J. & Hurst, R. E. Intravesical chondroitin sulfate inhibits recruitment of inflammatory cells in an acute acid damage 'leaky bladder' model of cystitis. *Urology* **79**, 483.e13-7 (2012).
71. Parsons, C. L., Stauffer, C. & Schmidt, J. D. Bladder-surface glycosaminoglycans: an efficient mechanism of environmental adaptation. *Science*. **2081**, 605–608 (1980).
72. Hurst, R. E. Structure, function, and pathology of proteoglycans and glycosaminoglycans in the urinary tract. *World J. Urol.* **12**, 3–10 (1994).
73. Nickel, J. C. *et al.* Relative efficacy of various exogenous glycosaminoglycans in providing a bladder surface permeability barrier. *J. Urol.* **160**, 612–614 (1998).
74. Hurst, R. *et al.* A deficit of chondroitin sulfate proteoglycans on the bladder urothelium in interstitial cystitis. *Urology* **4295**, 817–821 (1996).
75. Hurst, R. *et al.* Deficit of proteoglycans on the bladder uroepithelium in interstitial cystitis. *Eur. Urol. Suppl.* **2**, 10–13 (2003).
76. Voet, D. & Voet, J. G. in *Biochemistry* 379–383 (2011).
77. Wopereis, S., Lefeber, D., Morava, E. & Wevers, R. Mechanisms in protein O-glycan biosynthesis and clinical and molecular aspects of protein O-glycan biosynthesis defects : A review. *Clin. Chem.* **52**, 574–600 (2006).
78. Varki, A. *et al.* Symbol nomenclature for glycan representation. *Proteomics* **9**, 5398–5399 (2009).
79. Varki, A. *et al.* in *Essentials of Glycobiology* (2009). at <<http://www.ncbi.nlm.nih.gov/books/NBK1908/>>
80. Ruhaak, L. R. *et al.* Glycan labeling strategies and their use in identification and quantification. *Anal. Bioanal. Chem.* **397**, 3457–81 (2010).
81. Morelle, W. & Michalski, J.-C. Analysis of protein glycosylation by mass spectrometry. *Nat. Protoc.* **2**, 1585–602 (2007).
82. Tretter, V., Altmann, F. & März, L. Peptide-N4-(N-acetyl-beta-glucosaminyl)asparagine amidase F cannot release glycans with fucose attached alpha 1-3 to the asparagine-linked N-acetylglucosamine residue. *Eur. J. Biochem.* **199**, 647–52 (1991).

83. Hart, G. Glycosylation in the nucleus and cytoplasm. *Annu. Rev. Biochem.* **58**, 841–874 (1989).
84. Carlson, D. M. & Blackwell, C. Structures and immunochemical isolated from pig submaxillary properties mucins. *J. Biol. Chem.* **243**, 616–626 (1968).
85. Rademaker, G. J. *et al.* Mass spectrometric determination of the sites of O-glycan attachment with low picomolar sensitivity. *Anal. Biochem.* **257**, 149–160 (1998).
86. Rademaker, G. J., Haverkamp, J. & Thomas-Oates, J. Determination of glycosylation sites in O-linked glycopeptides: a sensitive mass spectrometric protocol. *Org. mass Spectrom.* **28**, 1536–1541 (1993).
87. Mirgorodskaya, E., Hassan, H., Clausen, H. & Roepstorff, P. Mass spectrometric determination of O-glycosylation sites using  $\beta$ -elimination and partial acid hydrolysis. *Anal. Chem.* **73**, 1263–1269 (2001).
88. Huang, Y., Mechref, Y. & Novotny, M.V. Microscale nonreductive release of O-linked glycans for subsequent analysis through MALDI mass spectrometry and capillary electrophoresis. *Anal. Chem.* **73**, 6063–9 (2001).
89. Wilson, N. L., Schulz, B. L., Karlsson, N. G. & Packer, N. H. Sequential analysis of N- and O-linked glycosylation of 2D-PAGE separated glycoproteins. *J. Proteome Res.* **1**, 521–529 (2002).
90. Schulz, B. L., Oxley, D., Packer, N. H. & Karlsson, N. G. Identification of two highly sialylated human tear-fluid DMBT1 isoforms: the major high-molecular-mass glycoproteins in human tears. *Biochem. J.* **366**, 511–520 (2002).
91. Juhasz, P. & Costello, C. E. Matrix-assisted laser desorption ionization time-of-flight mass spectrometry of underivatized and permethylated gangliosides. *Am. Soc. mass Spectrom.* **2**, 785–796 (1992).
92. Siuzdak, G. *et al.* Evidence of Ca<sup>2+</sup>-dependent carbohydrate association through ion spray mass spectrometry. *J. Am. Chem. Soc.* **115**, 2877–2881 (1993).
93. Harvey, D. J. Matrix-assisted laser desorption/ionization mass spectrometry of sphingo- and glycosphingo-lipids. *J. Mass Spectrom.* **30**, 1311–1324 (1995).
94. Powell, A. K. & Harvey, D. J. Stabilization of sialic acids in N-linked oligosaccharides and gangliosides for analysis by positive ion matrix-assisted

- laser desorption/ionization mass spectrometry. *Rapid Commun. Mass Spectrom.* **10**, 1027–1032 (1996).
95. Taylor, A. M., Holst, O. & Thomas-Oates, J. Mass spectrometric profiling of O-linked glycans released directly from glycoproteins in gels using in-gel reductive beta-elimination. *Proteomics* **6**, 2936–46 (2006).
  96. Charlwood, J., Skehel, J. M. & Camilleri, P. Analysis of N-linked oligosaccharides released from glycoproteins separated by two-dimensional gel electrophoresis. *Anal. Biochem.* **284**, 49–59 (2000).
  97. Küster, B., Wheeler, S. F., Hunter, A. P., Dwek, R. A. & Harvey, D. J. Sequencing of N-linked oligosaccharides directly from protein gels: in-gel deglycosylation followed by matrix-assisted laser desorption/ionization mass spectrometry and normal-phase high-performance liquid chromatography. *Anal. Biochem.* **250**, 82–101 (1997).
  98. Schulz, B. L., Packer, N. H. & Karlsson, N. G. Small-scale analysis of O-linked oligosaccharides from glycoproteins and mucins separated by gel electrophoresis. *Anal. Chem.* **74**, 6088–6097 (2002).
  99. Kobata, A. Use of endo- and exoglycosidases for structural studies of glycoconjugates. *Anal. Biochem.* **100**, 1–14 (1979).
  100. Linden, J. C. & Lawhead, C. L. Liquid chromatography of saccharides. *J. Chromatogr. A* **105**, 125–133 (1975).
  101. Palmer, J. K. A versatile system for sugar analysis via liquid chromatography. *Anal. Lett.* **8**, 215–224 (1975).
  102. Hardy, M. R. & Townsend, R. R. Separation of positional isomers of oligosaccharides and glycopeptides by high-performance anion-exchange chromatography with pulsed amperometric detection. *Proc. Natl. Acad. Sci. U. S. A.* **85**, 3289–3293 (1988).
  103. Tomiya, N. *et al.* Calculated two-dimensional sugar map of pyridylaminated oligosaccharides: elucidation of the jack bean alpha-mannosidase digestion pathway of Man9GlcNAc2. *Anal. Biochem.* **100**, 90–100 (1991).
  104. Hase, S., Ibuki, T. & Ikenaka, T. Reexamination of the pyridylation used for fluorescence labeling of oligosaccharides and its application to glycoproteins. *J Biochem* **95**, 197–203 (1984).

105. Takahashi, N. *et al.* Enzymatic sialylation of N-linked oligosaccharides using an alpha-(2,3)-specific trans-sialidase from *Trypanosoma cruzi*: structural identification using a three-dimensional elution mapping technique. 333–342 (1995).
106. Hermentin, P. *et al.* The mapping by high-pH anion-exchange chromatography with pulsed amperometric detection and capillary electrophoresis of the carbohydrate moieties of human plasma alpha 1-acid glycoprotein. *Anal. Biochem.* **206**, 419–29 (1992).
107. Kakehi, K. & Honda, S. Analysis of glycoproteins, glycopeptides and glycoprotein-derived oligosaccharides by high-performance capillary electrophoresis. *J. Chromatogr. A* **720**, 377–393 (1996).
108. Davies, M. J. *et al.* Use of a porous graphitised carbon column for the high-performance liquid chromatography of oligosaccharides, alditols and glycopeptides with subsequent mass spectrometry analysis. *J. Chromatogr. A* **646**, 317–326 (1993).
109. Koizumi, K., Okada, Y. & Fukuda, M. High-performance liquid chromatography of mono- and oligo-saccharides on a graphitized carbon column. *Carbohydr. Res.* **215**, 67–80 (1991).
110. Ruhaak, L. R., Deelder, A. M. & Wuhrer, M. Oligosaccharide analysis by graphitized carbon liquid chromatography-mass spectrometry. *Anal. Bioanal. Chem.* **394**, 163–174 (2009).
111. Davies, M., Smith, K. D., Harbin, A.-M. & Hounsell, E. F. High-performance liquid chromatography of oligosaccharide alditols and glycopeptides on a graphitized carbon column. *J. Chromatogr.* **609**, 125131 (1992).
112. Robinson, S., Bergström, E., Seymour, M. & Thomas-Oates, J. Screening of underivatized oligosaccharides extracted from the stems of *Triticum aestivum* using porous graphitized carbon liquid chromatography-mass spectrometry. *Anal. Chem.* **79**, 2437–2445 (2007).
113. Ahn, J., Bones, J., Yu, Y. Q., Rudd, P. M. & Gilar, M. Separation of 2-aminobenzamide labeled glycans using hydrophilic interaction chromatography columns packed with 1.7  $\mu\text{m}$  sorbent. *J. Chromatogr. B Anal. Technol. Biomed. Life Sci.* **878**, 403–408 (2010).



114. Churms, S. C. Recent progress in carbohydrate separation by high-performance liquid chromatography based on hydrophilic interaction. *J. Chromatogr. A* **720**, 75–91 (1996).
115. Wuhrer, M., DeBoer, A. R. & Deelder, A. M. Structural glycomics using hydrophilic interaction chromatography (HILIC) with mass spectrometry. *Indian J. Exp. Biol.* **47**, 987–992 (2009).
116. Alpert, A. J. Hydrophilic-interaction chromatography for the separation of peptides, nucleic acids and other polar compounds. *J. Chromatogr. A* **499**, 177–196 (1990).
117. Hakomori, S. A rapid permethylation of glycolipid, and polysaccharide catalyzed by methylsulfinyl carbanion in dimethyl sulfoxide. *J Biol Chem* **55**, 205–208 (1964).
118. Ciucanu, I. & Kerek, F. A simple and rapid method for the permethylation of carbohydrates. *Carbohydr. Res.* **131**, 209–217 (1984).
119. Huberty, M. C., Vath, J. E., Yu, W. & Martin, S. A. Site-specific carbohydrate identification in recombinant proteins using MALD-TOF MS. *Anal. Chem.* **65**, 2791–800 (1993).
120. Wada, Y. *et al.* Comparison of the methods for profiling glycoprotein glycans — HUPO Human Disease Glycomics / Proteome Initiative multi-institutional study. *Glycobiology* **17**, 411–422 (2007).
121. Waston, J. T. & Sparkman, O. D. *Introduction to mass spectrometry.* (Wiley, 2008).
122. Karas, M., Bachmann, D. & Hillenkamp, F. Influence of the Wavelength in High-Irradiance Ultraviolet Laser Desorption Mass Spectrometry of Organic Molecules. *Anal. Chem.* **57**, 2935–2939 (1985).
123. Karas, M., Bachmann, D., Bahr, U. & Hillenkamp, F. Matrix-assisted ultraviolet laser desorption of non-volatile compounds. *Int. J. Mass Spectrom. Ion Process.* **78**, 53–68 (1987).
124. Karas, M. & Hillenkamp, F. Laser desorption ionization of proteins with molecular masses exceeding 10 000 daltons. *Anal. Chem.* **60**, 2299–2301 (1988).

125. Tanaka, K. *et al.* Protein and polymer analyses up to  $m/z$  100000 by laser ionization time-of-flight mass spectrometry. *Rapid Commun. Mass Spectrom.* **2**, 151–153 (1988).
126. Karas, M., Glückmann, M. & Schäfer, J. Ionization in matrix-assisted laser desorption/ionization: Singly charged molecular ions are the lucky survivors. *J. Mass Spectrom.* **35**, 1–12 (2000).
127. Karas, M. & Krüger, R. Ion formation in MALDI: The cluster ionization mechanism. *Chem. Rev.* **103**, 427–439 (2003).
128. Zenobi, R. & Knochenmuss, R. Ion formation in MALDI mass spectrometry. *Mass Spectrom. Rev.* **17**, 337–366 (1998).
129. Ehring, H., Karas, M. & Hillenkamp, F. Role of photoionization and photochemistry in ionization processes of organic molecules and relevance for matrix-assisted laser desorption ionization mass spectrometry. *Org. Mass Spectrom.* **27**, 472–480 (1992).
130. Knochenmuss, R. Ion formation mechanisms in UV-MALDI. *Analyst* **131**, 966 (2006).
131. Jaskolla, T. W. & Karas, M. Compelling evidence for lucky survivor and gas phase protonation: The unified MALDI analyte protonation mechanism. *J. Am. Soc. Mass Spectrom.* **22**, 976–988 (2011).
132. Knochenmuss, R. & Zenobi, R. MALDI ionization: The role of in-plume processes. *Chem. Rev.* **103**, 441–452 (2003).
133. Mock, K. K., Davey, M. & Cotrell, J. S. The analysis of underivatized oligosaccharides by matrix-assisted laser desorption mass spectrometry. *Biochem. Biophys. Res. Commun.* **177**, 644–651 (1991).
134. Strupat, K., Karas, M. & Hillenkamp, F. 2,5-Dihydroxybenzoic acid: a new matrix for laser desorption—ionization mass spectrometry. *Int. J. Mass Spectrom. Ion Process.* **111**, 89–102 (1991).
135. Soltwisch, J., Berkenkamp, S. & Dreisewerd, K. A binary matrix of 2,5-dihydroxybenzoic acid and glycerol produces homogenous sample preparations for matrix-assisted laser desorption/ionization mass spectrometry. *Rapid Commun. Mass Spectrom.* **22**, 59–66 (2008).

136. Luo, G., Marginean, I. & Vertes, A. Internal energy of ions generated by matrix-assisted laser desorption/ionization. *Anal. Chem.* **74**, 6185–90 (2002).
137. Cancilla, M. T., Penn, S. G., Carroll, J. A. & Lebrilla, C. B. Coordination of alkali metals to oligosaccharides dictates fragmentation behavior in matrix assisted laser desorption ionization / fourier transform mass spectrometry. *J. Am. Chem. Soc.* **118**, 6736–6745 (1996).
138. Mohr, M. D., Börnsen, K. O. & Widmer, H. M. Matrix-assisted laser desorption/ionization mass spectrometry: improved matrix for oligosaccharides. *Rapid Commun. Mass Spectrom.* **9**, 809–14 (1995).
139. Harvey, D. Quantitative aspects of the matrix-assisted laser desorption mass spectrometry of complex oligosaccharides. *Rapid Commun. mass Spectrom.* **7**, 614–619 (1993).
140. Wada, Y. *et al.* Comparison of methods for profiling O -glycosylation. *Mol. Cell. Proteomics* **9**, 719–727 (2010).
141. Ito, H. *et al.* Comparison of analytical methods for profiling N- and O-linked glycans from cultured cell lines: HUPO Human Disease Glycomics/Proteome Initiative multi-institutional study. *Glycoconj. J.* **33**, 405–415 (2016).
142. Dole, M., Mack, L. L. & Hines, R. L. Molecular Beams of Macroions. *J. Chem. Phys.* **49**, 2240 (1968).
143. Yamashita, M. & Fenn, J. B. Electrospray ion source. Another variation on the free-jet theme. *J. Phys. Chem.* **88**, 4451–4459 (1984).
144. Fenn, J. B., Mann, M., Wong, S. & Whitehouse, C. Electrospray ionization for mass spectrometry of large biomolecules. *Science (80-. ).* **246**, 64–71 (1989).
145. Kebarle, P. A brief overview of the present status of the mechanisms involved in electrospray mass spectrometry. *J. Mass Spectrom.* **35**, 804–817 (2000).
146. Iribarne, J.V. On the evaporation of small ions from charged droplets. *J. Chem. Phys.* **64**, 2287 (1976).
147. Wilm, M. & Mann, M. Analytical properties of the nanoelectrospray ion Source. *Anal. Chem.* **68**, 1–8 (1996).

148. Juraschek, R., Dulcks, T. & Karas, M. Nanoelectrospray — More than just a minimized-flow electrospray ionization source. *J. Am. Soc. Mass Spectrometry* **305**, 300–308 (1999).
149. Comisarow, M. B. & Marshall, A. G. Fourier transform ion cyclotron resonance spectroscopy. *Chem. Phys. Lett.* **25**, 282–283 (1974).
150. Comisarow, M. B. & Marshall, A. G. Frequency-sweep fourier transform ion cyclotron resonance spectroscopy. *Chem. Phys. Lett.* **26**, 489–490 (1974).
151. Amster, I. J. Fourier transform mass spectrometry. *J. Mass Spectrom.* **31**, 1325–1337 (1996).
152. Marshall, A. G., Hendrickson, C. L. & Jackson, G. S. Fourier transform ion cyclotron resonance mass spectrometry: a primer. *Mass Spectrom. Rev.* **17**, 1–35 (1998).
153. Jennings, K. R. Collision-induced decompositions of aromatic molecular ions. *Int. J. mass Spectrom. ion Phys.* **1**, 227–235 (1968).
154. Shukla, A. K. & Futrell, J. H. Tandem mass spectrometry: Dissociation of ions by collisional activation. *J. Mass Spectrom.* **35**, 1069–1090 (2000).
155. Gauthier, J. W., Trautman, T. R. & Jacobson, D. B. Sustained off-resonance irradiation for collision-activated dissociation involving Fourier transform mass spectrometry. Collision-activated dissociation technique that emulates infrared multiphoton dissociation. *Anal. Chim. Acta* **246**, 211–225 (1991).
156. March, R. E. Quadrupole ion trap mass spectrometry: Theory, simulation, recent developments and applications. *Rapid Commun. Mass Spectrom.* **12**, 1543–1554 (1998).
157. Makarov, A. Electrostatic axially harmonic orbital trapping: A high-performance technique of mass analysis. *Anal. Chem.* **72**, 1156–1162 (2000).
158. Hu, Q. *et al.* The Orbitrap: A new mass spectrometer. *J. Mass Spectrom.* **40**, 430–443 (2005).
159. Makarov, A. *et al.* Performance evaluation of a hybrid linear ion trap/orbitrap mass spectrometer. *Anal. Chem.* **78**, 2113–2120 (2006).

160. Domon, B. & Costello, C. E. A systematic nomenclature for carbohydrate fragmentations in FAB-MS/MS spectra of glycoconjugates. *Glycoconj. J.* **5**, 397–409 (1988).
161. Smargiasso, N. & De Pauw, E. Optimization of matrix conditions for the control of MALDI in-source decay of permethylated glycans. *Anal. Chem.* **82**, 9248–53 (2010).
162. Brüll, L. P., Kováčik, V., Thomas-Oates, J. E., Heerma, W. & Haverkamp, J. Sodium-cationized oligosaccharides do not appear to undergo 'internal residue loss' rearrangement processes on tandem mass spectrometry. *Rapid Commun. Mass Spectrom.* **12**, 1520–1532 (1998).
163. Orlando, R., Bush, C. A. & Fenselau, C. Structural analysis of oligosaccharides by tandem mass spectrometry: collisional activation of sodium adduct ions. *Biomed. Environ. Mass.* **19**, 747–754 (1990).
164. Lemoine, J. *et al.* Collision-induced dissociation of alkali metal cationized and permethylated oligosaccharides: Influence of the collision energy and of the collision gas for the assignment of linkage position. *J. Am. Soc. Mass Spectrom.* **4**, 197–203 (1993).
165. Kováčik, V. *et al.* Oligosaccharide characterization using collision-induced dissociation fast-atom-bombardment mass spectrometry - evidence for internal monosaccharide residue Loss. *J. Mass Spectrom.* **30**, 949–958 (1995).
166. Brüll, L. P., Heerma, W., Haverkamp, J., Kovacik, V. & Kovac, P. Loss of internal 1 → 6 substituted monosaccharide residues from underivatized and per-O-methylated trisaccharides. *Am. Soc. mass Spectrom.* **8**, 43–49 (1997).
167. Ernst, B., Mtiller, D. R. & Richter, W. J. Mass spectrometry false sugar sequence ions in electrospray tandem mass spectrometry of underivatized sialyl-Lewis-type oligosaccharides. *Int. J. Mass Spectrom. Ion Process.* **160**, 283–290 (1997).
168. Harvey, D. J. *et al.* Comparison of fragmentation modes for the structural determination of complex oligosaccharides ionized by matrix-assisted laser desorption/ionization mass spectrometry. *Rapid Commun. Mass Spectrom.* **9**, 1556–1561 (1995).
169. Harvey, D. J. *et al.* Examination of complex oligosaccharides by matrix-assisted laser desorption/ionization mass spectrometry on time-of-flight and magnetic sector instruments. *Org. Mass Spectrom.* **29**, 753–766 (1994).

170. Spengler, B., Kirsch, D., Kaufmann, R. & Lemoine, J. Structure analysis of branched oligosaccharides using post-source decay in matrix-assisted laser desorption ionization mass spectrometry. *Org. Mass Spectrom.* **29**, 782–787 (1994).
171. O'Connor, P. B. & Costello, C. E. A high pressure matrix-assisted laser desorption/ionization Fourier transform mass spectrometry ion source for thermal stabilization of labile biomolecules. *Rapid Commun. Mass Spectrom.* **15**, 1862–1868 (2001).
172. Connor, P. B. O., Mirgorodskaya, E. & Costello, C. E. High pressure matrix-assisted laser desorption/ionization Fourier transform mass spectrometry for minimization of ganglioside fragmentation. *Am. Soc. mass Spectrom.* **13**, 402–407 (2002).
173. Soltwisch, J., Souady, J., Berkenkamp, S. & Dreisewerd, K. Effect of gas pressure and gas type on the fragmentation of peptide and oligosaccharide ions generated in an elevated pressure UV/IR-MALDI ion source coupled to an orthogonal time-of-flight mass spectrometer. *Anal. Chem.* **81**, 2921–34 (2009).
174. Soltwisch, J. & Dreisewerd, K. Discrimination of isobaric leucine and isoleucine residues and analysis of post-translational modifications in peptides by MALDI in-source decay mass spectrometry combined with collisional cooling. *Anal. Chem.* **82**, 5628–35 (2010).
175. Dube, D. H. & Bertozzi, C. R. Glycans in cancer and inflammation--potential for therapeutics and diagnostics. *Nat. Rev. Drug Discov.* **4**, 477–488 (2005).
176. Ohtsubo, K. & Marth, J. D. Glycosylation in Cellular Mechanisms of Health and Disease. *Cell* **126**, 855–867 (2006).
177. An, H. J., Kronewitter, S. R., De Leoz, M. L. A. & Lebrilla, C. B. Glycomics and disease markers. *Curr. Opin. Chem. Biol.* **13**, 601–607 (2009).
178. Brooks, S. A *et al.* Altered glycosylation of proteins in cancer: what is the potential for new anti-tumour strategies. *Anticancer. Agents Med. Chem.* **8**, 2–21 (2008).
179. Lee, A. *et al.* Rat liver membrane glycoproteome: Enrichment by phase partitioning and glycoprotein capture. *J. Proteome Res.* **8**, 770–781 (2009).

180. An, H. J. *et al.* Extensive determination of glycan heterogeneity reveals an unusual abundance of high mannose glycans in enriched plasma membranes of human embryonic stem cells. *Mol. Cell. Proteomics* **11**, 1–13 (2012).
181. Pasquali, C., Fialka, I. & Huber, L. A. Subcellular fractionation, electromigration analysis and mapping of organelles. *J. Chromatogr. B Biomed. Sci. Appl.* **722**, 89–102 (1999).
182. Mun, J. *et al.* Efficient adhesion-based plasma membrane isolation for cell surface N-glycan analysis. *Anal. Chem.* **85**, 7462–7470 (2013).
183. Becker, J. M. & Wilchek, M. Inactivation by avidin of biotin-modified bacteriophage. *BBA - Gen. Subj.* **264**, 165–170 (1972).
184. Bayer, E. A., Skutelsky, E. & Wilchek, M. The avidin-biotin complex in affinity cytochemistry. *Methods Enzymol.* **62**, 308–315 (1979).
185. Mi, W. *et al.* Surface glycoproteomic analysis of hepatocellular carcinoma cells by affinity enrichment and mass spectrometric identification. *Glycoconj. J.* **29**, 411–424 (2012).
186. Kolb, H. C., Finn, M. G. & Sharpless, K. B. Click chemistry: diverse chemical function from a few good reactions. *Angew. Chemie - Int. Ed.* **40**, 2004–2021 (2001).
187. Jewett, J. C. & Bertozzi, C. R. Cu-free click cycloaddition reactions in chemical biology. *Chem Soc Rev* **29**, 1883–1889 (2008).
188. Sletten, E. M. & Bertozzi, C. R. Bioorthogonal chemistry: Fishing for selectivity in a sea of functionality. *Angew. Chemie - Int. Ed.* **48**, 6974–6998 (2009).
189. Smeekens, J. M., Chen, W. & Wu, R. Mass spectrometric analysis of the cell surface n-glycoproteome by combining metabolic labeling and click chemistry. *J. Am. Soc. Mass Spectrom.* **26**, 604–614 (2015).
190. Xiao, H., Tang, G. X. & Wu, R. Site-specific quantification of surface N-glycoproteins in statin-treated kiver cells. *Anal. Chem.* **88**, 3324–3332 (2016).
191. Pizza, M. *et al.* Identification of vaccine candidates against serogroup B meningococcus by whole-genome Sequencing. *Science.* **287**, 1816–1821 (2000).

192. Rodríguez-ortega, M. J. *et al.* Characterization and identification of vaccine candidate proteins through analysis of the group A Streptococcus surface proteome. *Nat. Biotechnol.* **24**, 191–197 (2006).
193. Severin, A. *et al.* Proteomic analysis and Identification of Streptococcus pyogenes surface-associated proteins. *J. Bacteriol.* **189**, 1514–1522 (2007).
194. Tjalsma, H., Lambooy, L., Hermans, P. W. & Swinkels, D. W. Shedding & shaving: Disclosure of proteomic expressions on a bacterial face. *Proteomics* **8**, 1415–1428 (2008).
195. Solis, N., Larsen, M. R. & Cordwell, S. J. Improved accuracy of cell surface shaving proteomics in Staphylococcus aureus using a false-positive control. *Proteomics* **10**, 2037–2049 (2010).
196. Castro-Borges, W., Dowle, A., Curwen, R. S., Thomas-Oates, J. & Wilson, R. A. Enzymatic shaving of the tegument surface of live schistosomes for proteomic analysis: A rational approach to select vaccine candidates. *PLoS Negl. Trop. Dis.* **5**, 1–11 (2011).
197. Hamouda, H. *et al.* Rapid analysis of cell surface N-glycosylation from living cells using mass spectrometry. *J. Proteome Res.* **13**, 6144–6151 (2014).
198. Montacir, H. *et al.* The cell-surface N-Glycome of human embryonic stem cells and differentiated hepatic cells thereof. *ChemBioCehm* 1234–1241 (2017).
199. Hodges, G. M., Livingston, D. C. & Franks, L. M. The localization of trypsin in cultured mammalian cells. *J. Cell Sci.* **12**, 887–902 (1973).
200. Huang, H. *et al.* Trypsin-induced proteome alteration during cell subculture in mammalian cells. *J. Biomed. Sci.* (2010).
201. Yang, G. *et al.* Global identification and differential distribution analysis of glycans in subcellular fractions of bladder cells. *Int. J. Biol. Sci.* **12**, 799–811 (2016).
202. Rahman, S. A. *et al.* Filter-aided N-glycan separation (FANGS): a convenient sample preparation method for mass spectrometric N-glycan profiling. *J. Proteome Res.* **13**, 1167–1176 (2014).
203. Ward, A. J. PhD thesis: engineering of decellularised porcine bladder patches. (2017).



204. Dell, A. & Thomas-Oates, J. E. *FAB-MS: Sample preparation and analytical strategies*. (1988).
205. Dell, A. *et al.* Fast-atom-bombardment mass-spectrometric strategies for sequencing sulphated oligosaccharides. *Carbohydr. Res.* **179**, 7–19 (1988).
206. Gil, G.-C. C., Velander, W. H. & VanCott, K. E. N-glycosylation microheterogeneity and site occupancy of an Asn-X-Cys sequon in plasma-derived and recombinant protein C. *Proteomics* **9**, 2555–2567 (2009).
207. Abrams, G. A., Murphy, C. J., Wang, Z. Y., Nealey, P. F. & Bjorling, D. E. Ultrastructural basement membrane topography of the bladder epithelium. *Urol. Res.* **31**, 341–346 (2003).
208. Daher, N., Abourachid, H., Bove, N., Petit, J. & Burtin, P. Collagen IV staining pattern in bladder carcinomas: Relationship to prognosis. *Br. J. Cancer* **55**, 665–671 (1987).
209. Weber, M. Basement membrane proteins. *Kidney Int.* **41**, 620–628 (1992).
210. Kefalides, N. A. Basement membranes: structural and biosynthetic considerations. *J. Invest. Dermatol.* **65**, 85–92 (1975).
211. Loke, I., Packer, N. & Thaysen-Andersen, M. Complementary LC-MS/MS-Based N-Glycan, N-Glycopeptide, and Intact N-Glycoprotein Profiling Reveals Unconventional Asn71-Glycosylation of Human Neutrophil Cathepsin G. *Biomolecules* **5**, 1832–1854 (2015).
212. Heiskanen, A. *et al.* Glycomics of bone marrow-derived mesenchymal stem cells can be used to evaluate their cellular differentiation stage. *Glycoconj. J.* **26**, 367–384 (2009).
213. Blobel, C. P., Myles, D. G., Primakoff, P. & White, J. M. Proteolytic processing of a protein involved in sperm-egg fusion correlates with acquisition of fertilization competence. *J. Cell. Biol.* **111**, 69–77 (1990).
214. Blobel, C. P. *et al.* A potential fusion peptide and an integrin ligand domain in a protein active in sperm-egg fusion. *Nature* **356**, 248–252 (1992).
215. Morishima, S. *et al.* Expression and role of mannose receptor/terminal high-mannose type oligosaccharide on osteoclast precursors during osteoclast formation. *J. Endocrinol.* **176**, 285–292 (2003).

216. Kurachi, T. *et al.* Expression on outer membranes of mannose residues, which are involved in osteoclast formation via cellular fusion events. *J. Biol. Chem.* **269**, 17572–17576 (1994).
217. Lifson, J., Coutré, S., Huang, E. & Engleman, E. Role of envelope glycoprotein carbohydrate in human immunodeficiency virus (HIV) infectivity and virus-induced cell fusion. *J. Exp. Med.* **164**, 2101–2106 (1986).
218. Matthews, T. J. *et al.* Interaction between the human T-cell lymphotropic virus type IIIB envelope glycoprotein gp120 and the surface antigen CD4: Role of carbohydrate in binding and cell fusion. *Med. Sci.* **84**, 5424–5428 (1987).
219. Scanlan, C. N. *et al.* The broadly neutralizing anti-human immunodeficiency virus type 1 antibody 2G12 recognizes a cluster of  $\alpha$ 1 $\rightarrow$ 2 mannose residues a cluster of  $\alpha$ 1 $\rightarrow$ 2 mannose residues on the outer face of gp120. *J. Virol.* **76**, 7306–7321 (2002).
220. Suzuki, Y. *et al.* Sialic acid species as a determinant of the host range of influenza A viruses. *J. Virol.* **74**, 11825–31 (2000).
221. Shinya, K. *et al.* Avian flu: influenza virus receptors in the human airway. *Nature* **440**, 435–436 (2006).
222. Moch, T., Hoschotzky, H., Hackert, J. & Jann, K. specific adhesin from Isolation and characterization of the alpha-sialyl-beta-2,3-galactosyl-specific adhesin from fimbriated Escherichia coli. *Proc, Natl. Acad. Sci. USA* **84**, 3462–3466 (1987).
223. Sharon, N. Bacterial lectins, cell-cell recognition and infectious disease. *Fed. Eur. Biochem. Soc. Lett.* **217**, 145–157 (1987).
224. Ilver, D. *et al.* Bacterium-host protein-carbohydrate interactions. *Methods Enzymol.* **363**, 134–157 (2003).
225. Ley, K. The role of selectins in inflammation and disease. *Trends Mol. Med.* **9**, 263–268 (2003).
226. McEver, R. P. Selectins: Lectins that initiate cell adhesion under flow. *Curr. Opin. Cell Biol.* **14**, 581–586 (2002).
227. Seales, E. C. *et al.* Hypersialylation of beta1 integrins, observed in colon adenocarcinoma, may contribute to cancer progression by up-regulating cell motility. *Cancer Res.* **65**, 4645–4652 (2005).

228. Zupančič, D., Kreft, M. E. & Romih, R. Selective binding of lectins to normal and neoplastic urothelium in rat and mouse bladder carcinogenesis models. *Protoplasma* **251**, 49–59 (2014).
229. Läubli, H., Stevenson, J. L., Varki, A., Varki, N. M. & Borsig, L. L-selectin facilitation of metastasis involves temporal induction of Fut7-dependent ligands at sites of tumor cell arrest. *Cancer Res.* **66**, 1536–1542 (2006).
230. Matsusako, T., Muramatsu, H., Shirahama, T., Muramatsu, T. & Ohi, Y. Expression of a carbohydrate signal, sialyl dimeric Le(x) antigen, is associated with metastatic potential of transitional cell carcinoma of the human urinary bladder. *Biochem. Biophys. Res. Commun.* **181**, 1218–1222 (1991).
231. Reinke, S. O., Bayer, M., Berger, M., Blanchard, V. & Hinderlich, S. Analysis of Cell Surface N-glycosylation of the Human Embryonic Kidney 293T Cell Line. *J. Carbohydr. Chem.* **30**, 218–232 (2011).
232. Lin, C.-H., Kuo, C.-W., Jarvis, D. L. & Khoo, K.-H. Facile removal of high mannose structures prior to extracting complex type N-glycans from de-N-glycosylated peptides retained by C18 solid phase to allow more efficient glycomic mapping. *Proteomics* **14**, 87–92 (2014).
233. Reutter, W., Köttgen, E., Bauer, C. & Gerok, W. Biological significance of sialic acids. *ell Biol. Monogr.* **10**, 263–305 (1982).
234. Freire, T., Bay, S., von Mensdorff-Pouilly, S. & Osinaga, E. Molecular basis of incomplete O-glycan synthesis in MCF-7 breast cancer cells: Putative role of MUC6 in Tn antigen expression. *Cancer Res.* **65**, 7880–7887 (2005).
235. Julien, S. *et al.* ST6GalNAc I expression in MDA-MB-231 breast cancer cells greatly modifies their O-glycosylation pattern and enhances their tumourigenicity. *Glycobiology* **16**, 54–64 (2006).
236. Julien, S. *et al.* Stable expression of sialyl-Tn antigen in T47-D cells induces a decrease of cell adhesion and an increase of cell migration. *Breast Cancer Res. Treat.* **90**, 77–84 (2005).
237. Booth, C. *et al.* Stromal and vascular invasion in an human in vitro bladder cancer model. *Lab Invest* **76**, 843–857 (1997).
238. Mukerjee, P. & Mysels, K. Critical micelle concentrations of aqueous surfactant systems. *J. Pharm. Sci.* **61**, 319 (1972).

239. Szabo, Z., Guttman, A. & Karger, B. L. Rapid release of N-linked glycans from glycoproteins by pressure-cycling technology. *Anal. Chem.* **82**, 2588–2593 (2010).
240. Fromter, E. & Diamond, J. Route of passive ion permeation in epithelia. *Nat. New Biol.* **235**, 9–13 (1972).
241. Korossis, S., Bolland, F., Southgate, J., Ingham, E. & Fisher, J. Regional biomechanical and histological characterisation of the passive porcine urinary bladder: Implications for augmentation and tissue engineering strategies. *Biomaterials* **30**, 266–275 (2009).
242. Wang, C., Fan, W., Zhang, P., Wang, Z. & Huang, L. One-pot nonreductive O-glycan release and labeling with 1-phenyl-3-methyl-5-pyrazolone followed by ESI-MS analysis. *Proteomics* **11**, 4229–4242 (2012).
243. Dell, A., Thomas-Oates, J. E., Rogers, M. E. & Tiller, P. R. Novel fast atom bombardment mass spectrometric procedures for glycoprotein analysis. *Biochimie* **70**, 1435–1444 (1988).
244. O'Brien, F. J. Biomaterials & scaffolds for tissue engineering. *Mater. Today* **14**, 88–95 (2011).
245. Potter, B. A., Hughey, R. P. & Weisz, O. A. Role of N- and O-glycans in polarized biosynthetic sorting. *Am. J. Physiol. Physiol.* **290**, C1–C10 (2006).
246. Prydz, K., Fagereng, G. L. & Tveit, H. The role of glycans in apical sorting of proteins in polarized epithelial cells. *Glycosylation* 301–326 (2012).
247. Scheiffele, P., Peränen, J. & Simons, K. N-glycans as apical sorting signals in epithelial cells. *Nature* **378**, 96–98 (1995).
248. Nakagawa, T. *et al.* Fucosylation of N-glycans regulates the secretion of hepatic glycoproteins into bile ducts. *J. Biol. Chem.* **281**, 29797–29806 (2006).
249. Kitagawa, Y. *et al.* N-Glycosylation of erythropoietin is critical for apical secretion by Madin-Darby canine kidney cells. *Exp. Cell Res.* **213**, 449–457 (1994).
250. Cointe, D. *et al.* Unusual N-glycosylation of a recombinant human erythropoietin expressed in a human lymphoblastoid cell line does not alter its biological properties. *Glycobiology* **10**, 511–519 (2000).

251. Schauer, R. Sialic acids and their role as biological masks. *Trends Biochem. Sci.* **10**, 357–360 (1985).
252. Quaggin, S. E. Sizing up sialic acid in glomerular disease. *J. Clin. Invest.* **117**, 1480–1483 (2007).
253. Varki, A. Biological roles of glycans. *Glycobiology* **27**, 3–49 (2017).
254. Aït Slimane, T., Lenoir, C., Sapin, C., Maurice, M. & Trugnan, G. Apical secretion and sialylation of soluble dipeptidyl peptidase IV are two related events. *Exp. Cell Res.* **258**, 184–194 (2000).
255. Mastrodonato, M., Mentino, D., Lopedota, A., Cutrignelli, A. & Scillitani, G. A histochemical approach to glycan diversity in the urothelium of pig urinary bladder. *Microsc. Res. Tech.* 1–11 (2016). doi:10.1002/jemt.22794
256. N'dow, J. *et al.* The bladder does not appear to have a dynamic secreted continuous mucous gel layer. *J. Urol.* **173**, 2025–2031 (2005).
257. Kinlough, C. L. *et al.* Core-glycosylated mucin-like repeats from MUC1 are an apical targeting signal. *J. Biol. Chem.* **286**, 39072–39081 (2011).
258. Freeze, H. H. Genetic defects in the human glycome. *Nat. Rev. Genet.* **7**, 537–551 (2006).
259. Lübbehusen, J. *et al.* Fatal outcome due to deficiency of subunit 6 of the conserved oligomeric Golgi complex leading to a new type of congenital disorders of glycosylation. *Hum. Mol. Genet.* **19**, 3623–3633 (2010).
260. Ma, B., Simala-Grant, J. L. & Taylor, D. E. Fucosylation in prokaryotes and eukaryotes. *Glycobiology* **16**, (2006).
261. Donczo, B., Kerekgyarto, J., Szurmai, Z. & Guttman, A. Glycan microarrays: new angles and new strategies. *Analyst* **139**, 2650–2657 (2014).
262. Gordon, K. J. & Blobel, G. C. Role of transforming growth factor- $\beta$  superfamily signaling pathways in human disease. *Biochim. Biophys. Acta - Mol. Basis Dis.* **1782**, 197–228 (2008).

